AD-A034 035 AIR FORCE INST OF TECH WRIGHT-PATTERSON AFB OHIO SCH--ETC F/G 20/8
EMISSION CROSS-SECTION MEASUREMENTS OF LOW ENERGY HE(+) IONS WI--ETC(U)
SEP 76 K E SIEGENTHALER

UNCLASSIFIED DS/PH/76-2 NL

1 OF 4
AD
A034035

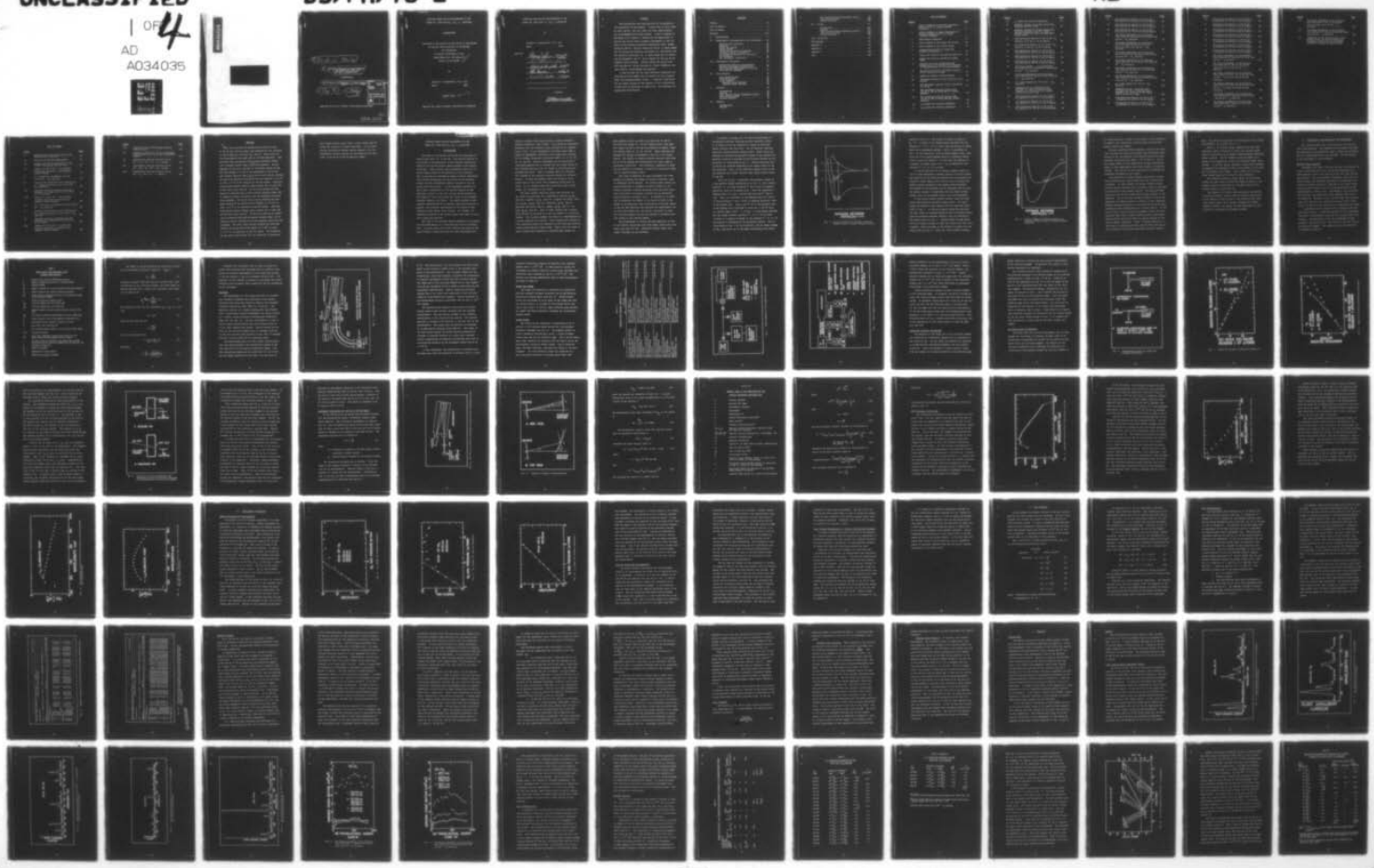


F4
4035

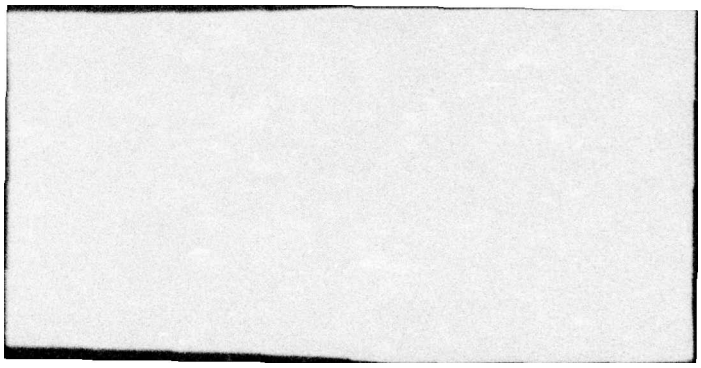

(9) Doctoral thesis,

(6) EMISSION CROSS-SECTION MEASUREMENTS OF LOW ENERGY He^+ IONS WITH Cl_2^-, Br_2^-, I_2^- REACTIONS.

DISSERTATION

(14) DS/PH/76-2 (10) Kenneth E. Siegenthaler
Major USAF

(11) Sep 76 (12) 302p.

Approved for public release; distribution unlimited.

dn

012 225

DS/PH/76-2

EMISSION CROSS-SECTION MEASUREMENTS OF LOW ENERGY He^+ IONS WITH Cl_2, Br_2, I_2 REACTIONS

DISSERTATION

Presented to the Faculty of the School of Engineering
of the Air Force Institute of Technology
Air University
in Partial Fulfillment of the
Requirements for the Degree of
Doctor of Philosophy

by

Kenneth E. Siegenthaler, B.S., M.S.
Major USAF

August 1976

EMISSION CROSS-SECTION MEASUREMENTS OF LOW ENERGY He^+ IONS WITH Cl_2, Br_2, I_2 REACTIONS

by

Kenneth E. Siegenthaler, B.S., M.S.
Major USAF

Approved:

George John 23 Aug '76
Chairman

[illegible] 23 AUG 76

Robert L Hengehold 23 Aug '76

[illegible] 23 Aug '76.

Ernest A. Parks 24 Aug 76

Accepted.

J S Przemieniecki
Dean, School of Engineering

Preface

This dissertation was made possible by the generosity and cooperation of many people. I would like to first thank my wife, Phyllis, and son, John, for their understanding and encouragement during this period. I wish to express my gratitude to Dr. Thomas O. Tiernan for the opportunity to work in one of the finest research environments in the Air Force at the Aerospace Research Laboratories (ARL), Wright-Patterson AFB OH. Special thanks are due Dr. B. Mason Hughes for his advice and technical assistance, Mr. Dean Miller for his technical assistance, Dr. E. Grant Jones for his advice and encouragement, and Dr. Darrel Hopper for the use of his computer search program. Sincere thanks are given to my AFIT advisors, Dr. George John and Dr. Robert Hengehold, for their advice, encouragement and guidance.

I wish to thank the Air Force Materials Laboratory for providing me with support for my analysis of this research after the disestablishment of ARL. I thank Mr. John Dryen for his expert drawing of the figures in this dissertation. A final debt of gratitude is owed to Mrs. Jane Manemann for typing this dissertation.

Contents

List of Figures

List of Tables

Abstract

The cross sections for production of emission lines in the 60 nm to 870 nm region were measured for the collision of 100 eV $He_{\sqcup}^{(+)}$ ions with $Cl_2^{\sqcap}$, $Br_2^{\sqcap}$, and $I_2^{\sqcap}$. These cross section measurements were made with an ion beam apparatus. Only emissions from transitions from excited electronic states with lifetimes shorter than a μsec were measured. The dependence of the cross sections on the kinetic energy of the $He_{\sqcup}^{(+)}$ ions between 2 to 170 eV was determined by use of the more intense emission lines. The total cross section obtained for emissions between 90 nm and 870 nm for chlorine is 5.0 A^2; of this, 3.8 A^2 is for emission in the VUV region. Emissions from excited neutral chlorine atoms account for at least 85% of the total cross section. Of the cross section for production of emission from excited neutral chlorine atoms, 80% is caused by direct excitation with the remainder resulting from cascading. The total cross section obtained for emissions between 80 nm and 870 nm for bromine is 14.9 A^2; of this, 11.9 A^2 is for emission in the VUV region. Emissions from excited neutral bromine atoms account for at least 85% of the total cross section. Of the cross section for production of emission from excited neutral bromine atoms, 75% is caused by direct excitation with the remainder resulting from cascading. The total cross section obtained for emissions between 100 nm and 870 nm for iodine is 15.9A^2; of this, 14.4 A^2 is for emissions in the VUV region. The proportion of the total cross section for the production of emissions

from singly-ionized iodine atoms is much larger than for either the chlorine or bromine reactions. In all three systems dissociative charge transfer appears to be the predominant reaction process for the production of emissions in the 60 nm to 870 nm spectral region.

EMISSION CROSS-SECTION MEASUREMENTS OF LOW ENERGY He^+ IONS WITH Cl_2, Br_2, I_2 REACTIONS

I. Introduction

The study of ion-neutral collisions has mushroomed in recent years (Refs 13, 23 and 46). One area of interest in this field is the examination of the emission spectra produced by the excited product species formed in ion-neutral collisions. These studies yield information about the internal energy states of the products of such reactions. This is the type of information needed to better understand the collision mechanisms and the nature of the potential surface for the intermediate complex involved in the low energy collision process. In the experiment discussed in this thesis, examination of the emission spectra of the reactions is used to study the excited states produced by low energy He^+ ions interacting with three of the halogens; chlorine, bromine, and iodine. The results produce a more complete understanding of ion-neutral collision processes in general, with possible applications in the design of more efficient plasma and/or laser systems. For example, the competing processes in the helium iodine laser might be more fully understood (Ref 62).

The study of the emission spectra produced in low energy ion-beam experiments is a relatively new area of investigation. The main reason that little interest was shown in the early studies of these processes was that experimentalists

tended to explain these interactions in terms of Massey's adiabatic hypothesis (Ref 44:261). This adiabatic hypothesis predicted very low radiative cross sections at ion energies below 10 keV. It was considered a startling result when a number of experiments resulted in very large cross sections for low energy ion-neutral collisions (Refs 5, 8, 9, 24, 39, 53, 65, and 69). Massey's hypothesis was of course only a crude approximation and it assumed that the energy levels of the colliding particles did not change as the particles approached each other. Such a treatment makes no allowance for a change in the electron structure during the collision process. At high ion energies where the collision interaction time is very short, this assumption yields good results. At low energies where the interaction time is much longer, the assumption is not valid.

The early studies reporting large cross sections for low energy ion reactions were conducted by Pretzer, et al. (Ref 53), Stebbins, et al. (Ref 65), Lippeles and Novick (Ref 39), Jaecks, et al. (Ref 24), Dworetsky, et al. (Ref 9), Dworetsky and Novick (Ref 8), DeHeer, et al. (Ref 5), and Tolk, et al. (Ref 69). Most of these studies used a system which focused an ion beam on a rare gas target in a collision chamber. The collision chamber was mated to a monochromator or a photon detector with filters. These studies were limited to total emissions within the bandwidth of the filtering system or within narrow spectral region scans. Some of the ion beams in these studies were produced by a modified high energy ion

beam apparatus which was able to go down only to 300 eV. The first low energy (0 - 170 eV) studies over a wide spectral region (50 nm to 870 nm) were reported by Hughes, Jones, and Tiernan (Refs 18, 19, 20, and 28). Their apparatus was designed for optimal performance in the 100 eV ion energy region. The ability to observe resolved spectral lines from 50 to 870 nm enabled the investigation of a wide range of electronic transitions. This provided a capability to examine the effects of cascading in relation to the direct formation of specific energy states.

This type of apparatus has many advantages over other methods of studying low energy ion-neutral reactions, such as afterglows and discharges. The latter plasma studies are usually difficult to interpret in detail because of the several concurrent reaction processes which may yield radiation (ion-neutral collisions, electron-ion recombination, neutral-neutral collisions, etc.). In addition it is difficult to determine the effect of the electric field in the plasma on the emissions seen, particularly in the VUV region. In the ion beam apparatus the pressures are sufficiently low to allow only bimolecular ion-neutral collisions to occur. The collision chamber can also be shielded to minimize electric fields in the reaction region.

One disadvantage of such an ion beam apparatus is that it can observe transitions only from energy states with lifetimes less than 10^{-6} sec. Metastable energy states with longer lifetimes are not observed.

To obtain an insight into the detailed mechanisms of ion-neutral reactions involving excited electronic states, it is useful to use the theoretical concept of potential energy surfaces (Ref 34:19-45). For two particle reactions these are called potential energy curves. These curves are obtained by plotting the potential energy of the combined two particle system as a function of the distance between the two particles, as illustrated in Fig. 1. Various potential energy curves are obtained depending on the energy states of the two particles. Thus, as the electronic energy states of the two particles are varied, various other curves results (Refs 15 and 45).

Curve (a) in Fig. 1 represents the potential energy of a two particle system consisting of an ion, A^+, and a neutral particle, B. At large distances A^+ and B exist as separate particles, each in the ground state. Curve (b) represents a bonding state of A (now a neutral particle) and B^+ (now an ion). Curve (c) represents an antibonding state of A and B^+. At large distances A and B^+ exist as separate particles, each in the ground state. When A and B^+ are in the potential well of the bonding state described by curve (b), A and B^+ exist as a bound complex $(AB)^+$.. E' in Fig. 1 is the energy required for the charge transfer reaction $A^+ + B \rightarrow A + B^+$ to occur. If there is a surplus of energy in the reaction $A^+ + B \rightarrow A + B^+$ the process is designated as an exothermic process. This is illustrated in Fig. 1 by the transition, with an energy change of ΔE_1, from curve (a) to the upper antibonding state repre-

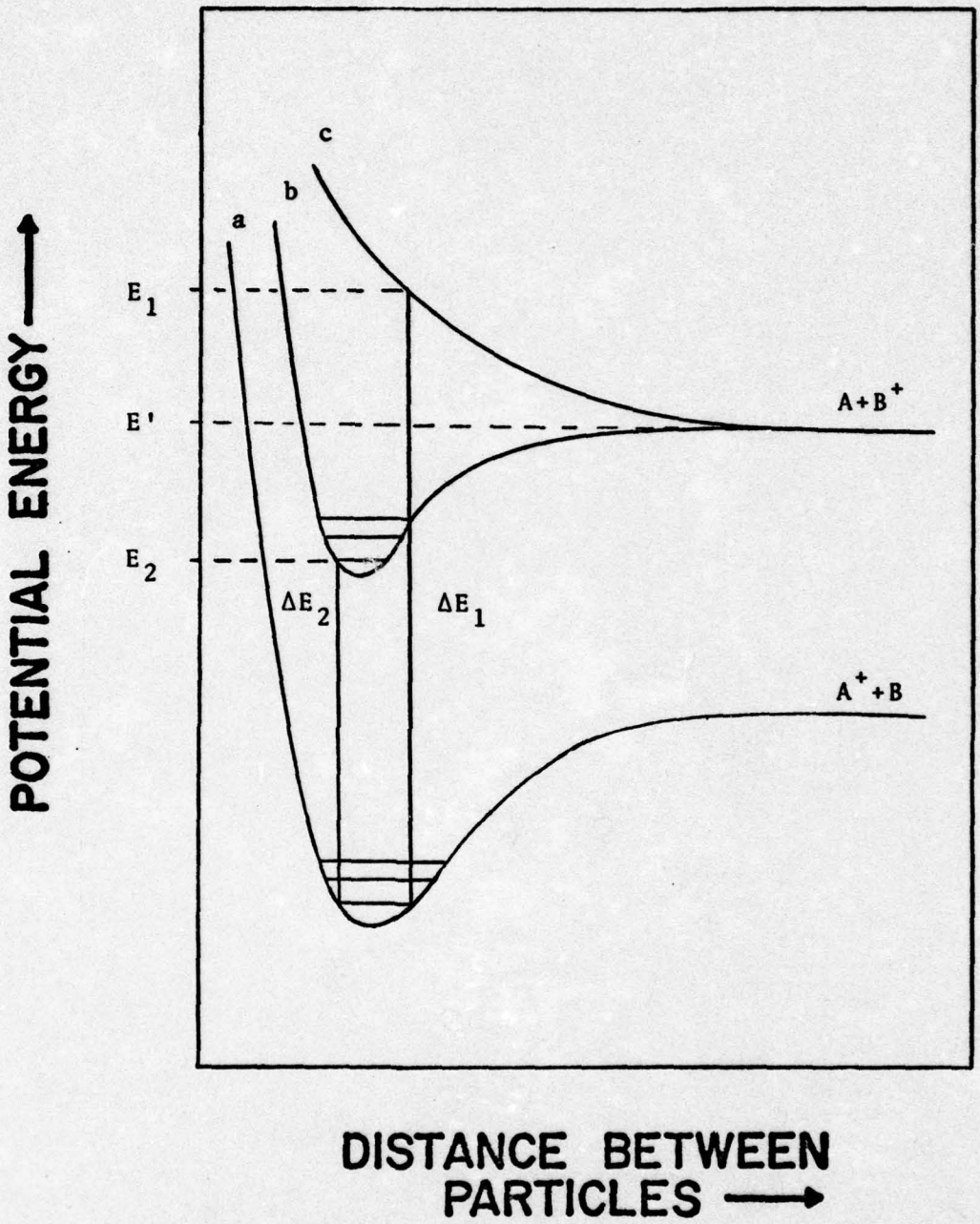

Fig. 1. Typical Examples of Possible Potential Energy Curves in Charge Transfer Process.

sented by curve (c). The surplus of energy is equal to $E_1 - E'$. If there is not enough energy available for the reaction $A^+ + B \rightarrow A + B^+$ to occur, then the process is designated as an endothermic process. This is illustrated in Fig. 1 by the transition, with an energy change of ΔE_2, from curve (a) to the upper bonding state at a potential energy value on curve (b) below E'. In this case the addition of a quantity of energy equal to $E' - E_2$ is required for the reaction $A^+ + B \rightarrow A + B^+$ to occur.

It can be seen that if the charge transfer process results in the production of product species in excited states, the detection of the emissions produced by the decaying transitions to lower energy levels can be used to identify the product species produced in the charge transfer process. This method of investigation has the advantage that not only the product species is identified, but the actual excited energy levels of the product species are also determined.

In the actual charge transfer process, there are many curves describing the possible energy states. The curve shapes are generally more complex than the idealized curves shown in Fig. 1. In the more complex system the particles are most likely to exchange energy in their collision process when the potential energies actually cross as indicated by the dashed curves in Fig. 2. Another region of high probability of energy exchange is where the curves come very close together, nearly crossing, as for example in region R of the solid curves in Fig. 2. These are called pseudo-crossings.

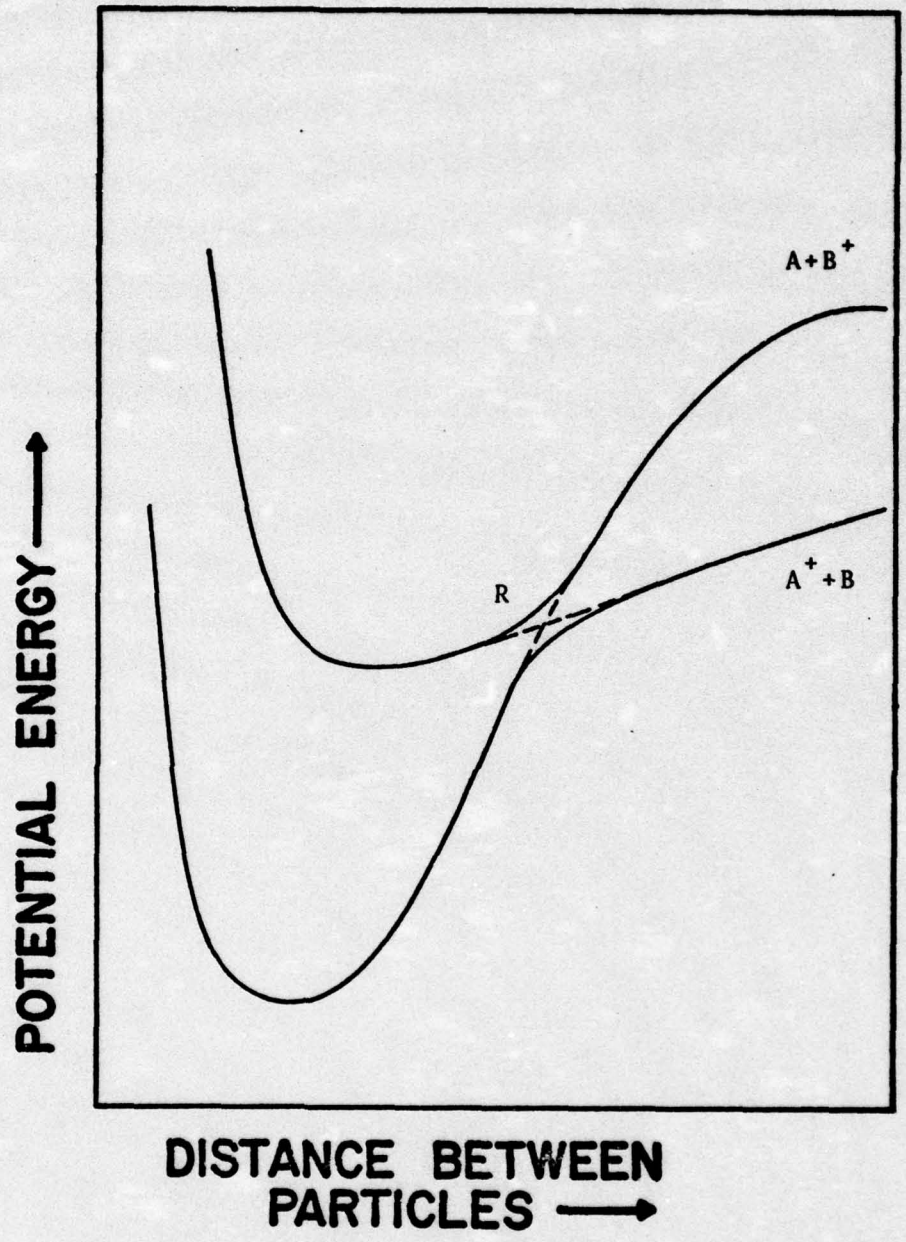

Fig. 2. Typical Example of Pseudo-Crossings of Potential Energy Curves in Charge Transfer Processes.

If a third particle is added to the system, a third dimension is added to the theoretical collision model and potential energy surfaces are formed.

The most promising theory proposed to explain the large cross sections for radiation emission from ion-neutral interactions at low ion energies is the pseudo-crossing of these potential energy surfaces (Refs 1, 59, 60 and 73). One of the primary needs for the formulation of better theoretical models is more experimental data from a number of different systems. This was one of the incentives for performing the experiment presented in this thesis.

The potential of charge transfer processes as an excitation mechanism for laser systems has only recently been considered. In some systems, the charge transfer process releases several electron volts of energy, which is available for excitation of the product species. Helium-metal-vapor lasers are some of the systems where charge transfer is very important. One of the most extensive studies to assess the importance of charge transfer in relation to the competing Penning ionization process for the He-Cd and He-Zn ion laser systems has been accomplished by G. Collins (Ref 4). On the basis of this study, Collins has proposed several new rare-gas-metal-vapor laser systems emitting lines in the region between 200 nm and 400 nm which use charge transfer as the primary pumping mechanism. (NOTE: Penning ionization is the process of producing excited ions and free electrons by the collision of an excited metastable atom and a neutral

atom. For the He-Cd system this is described by the relationship $He(2^3S) + Cd \rightarrow (Cd^+)^* + He + e^-$.)

Later, C. B. Collins, et al. proposed that very high efficiency lasers of from 50 to 10% in the visible region could be constructed using charge transfer pumping mechanisms (Refs 3 and 50). The He^+ formed by electron impact in a plasma is the pumping ion in most rare-gas-metal-vapor laser systems. C. Collins, et al. proposed a system which promises to approach the theoretical limit of one photon out for every He^+ ion formed in the plasma. Their studies of a He_2^+-N_2 laser system lasing at 427.8 nm are very promising.

The afterglow studies by Shay, et al. of the sixteen iodine ion laser lines indicate that charge transfer is the primary source of excitation for the upper levels of the helium iodine ion laser (Ref 63).

The interest in a better understanding of ion-neutral collision processes, coupled with the possible application of the results of such studies to the design of more efficient plasma and/or laser systems, prompted the present studies in which a low energy ion beam experiment has been utilized to investigate He^+/halogen systems.

II. Experimental Instrumentation and Calibration

This chapter begins with a discussion of the cross sections being measured. The remainder of the chapter describes the experimental instrumentation used to obtain the necessary data for determining these cross sections. The calibration of the instrument is also discussed.

Emission Cross Sections

Throughout this thesis the term emission cross section or cross section means the cross section for production of a given emission line by the reaction of He^+ ions with the target molecule. Due to instrument limitations, this cross section includes only emissions attributed to transitions from electronic energy states with lifetimes of less than a μsec. Excited product species move out of the focal point of the monochromator in about a μsec. Nonradiative decay processes and radiation from long lived states (greater than a μsec) are neglected. Whenever a cross section other than the emission cross section of an individual emission line is referenced, the type of cross section will be explicitly described.

A derivation of the relations for calculating the emission cross section, σ, from data measured in this experiment illustrates the parameters necessary for obtaining the cross sections. The derivation is for the monochromator whose diagram is shown in Fig. 11. The source is the exit slit of the collision chamber. The symbols used in the derivation are defined in Table I.

Table I

Symbols Used in the Derivation of the Emission Cross Section σ

σ	Emission Cross Section (cm^2/neutral particle)
n	Number of target gas particles in radiating volume
N_A	Avogadros number
N_R	Number of photons per second recorded by SSRI Photon Counter
N_S	Number of photons per second striking the grating
N_T	Total number of radiating particles in the radiating volume of the collision chamber
V	Volume of target gas radiating (cm^3)
S_{CH}	Collision chamber exit slit height (cm)
S_{CW}	Collision chamber exit slit width (cm)
ℓ	Distance between collision chamber entrance and exit slits (cm)
S_{DW}	Slit width of detector (Monochromator exit slit width) (cm)
D	Linear Dispersion (cm of wavelength/cm of detector slit)
$d\lambda$	Wavelength interval focused on detector slit (cm)
f	Flux of He^+ ions (ions/sec-cm^2)
I	He^+ ion-beam current incident on the collision volume (amps)
$F(\lambda)$	Instrument function
$\Omega_{g_\perp}$	Solid angle subtended by grating when parallel to the plane of the collision chamber exit slit (ster)
γ	Horizontal angle of rotation of the grating from parallel to the plane of the collision chamber exit slit (see Fig. 10)
P	Pressure of target gas
R_o	Ideal Gas constant
T_o	Temperature of target gas(°K)
e	Charge of an electron (coulomb)

The number of photons striking the grating per second in the wavelength interval $d\lambda$ (where $d\lambda - DS_{DW}$) is

$$N_S = \frac{N_R}{F(\lambda)} \tag{1}$$

Assuming isotropic radiation from the excited atoms, ions, or molecules in the collision chamber, the total number of photons radiated into a sphere [4π steradians solid angle] can be shown to be

$$\frac{4\pi}{\Omega_{g_\perp} \cos \gamma} \frac{N_R}{\frac{F(\lambda)}{\cos \gamma}} = N_T \tag{2}$$

The radiating volume has the dimensions $S_{CH} \times S_{CW} \times \ell$. But also

$$N_T \equiv nf\sigma \tag{3}$$

where by the ideal gas law

$$n = \frac{PVN_A}{R_o T_o} \tag{4}$$

and f can be expressed as

$$f = \frac{I}{S_{CH} \times S_{CW} \times e} \tag{5}$$

Therefore

$$\sigma = \frac{N_T}{nf} = \frac{4\pi R_o T_o N_R}{P\ell N_A I \Omega_{g_\perp} F(\lambda)} \tag{6}$$

Equation (6) illustrates that in order to obtain accurate cross sections the instrument must be carefully calibrated for accurate measurements of the target gas pressure P, the ion current I, and the instrument function $F(\lambda)$. The remainder of this chapter is devoted to describing the instrumentation used to measure these quantities and the calibration of the instrument.

Apparatus

The measurements in this study were made on an instrument originally designed and constructed by the Gaseous Excitation and Ionization Processes Group at the Aerospace Research Laboratories (ARL) (Refs 19, 20 and 21). The apparatus consists of a single-focusing mass spectrometer with a conventional electron bombardment ion source coupled to a 1-meter vacuum ultraviolet monochromator [McPherson Model 225 (see Fig. 3)]. The mass spectrometer is used to select singly-ionized helium ions and accelerate them to 170 eV (lab) translational energy. Typical helium ion currents in the collision chamber were 0.1 nanoamps with the 0.1 mm slit used for high resolution scans, and 1.0 nanoamps with the 1 mm slit used for low resolution scans.

The decelerating lens is a four element electrostatic slot lens which decreases the translational energy of the ions from 170 eV to the desired interaction energy. The beam interaction energy can be varied from 2 eV to 170 eV, and the energy resolution of the beam is on the order of

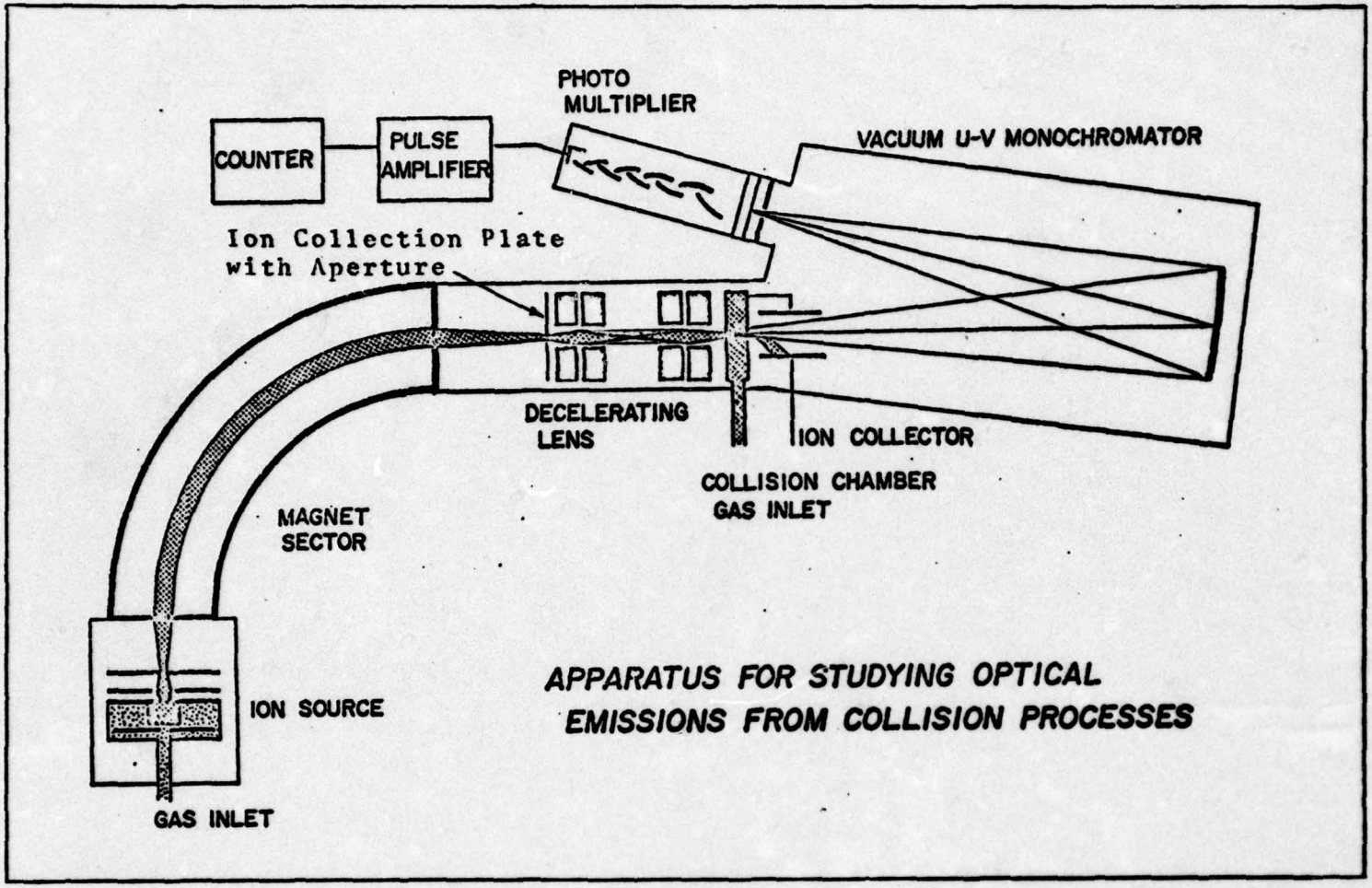

Fig. 3. Experimental Apparatus.

±1 eV. The electrostatic lens also focuses the ions at the point in the collision chamber which is the entrance focal point of the monochromator. The collision chamber and the electrostatic lens were designed to minimize the penetration of electric and magnetic fields into the collision region. The target gas in the collision chamber was at room temperature and was considered to be at thermal equilibrium for the experiments reported here. Typical target gas pressures ranging from 2 to 4 mTorr were maintained in the collision region by using differential pumping. Typical pressures in the monochromator during an experiment were in the 1×10^{-6} Torr region.

The emissions from radiative transitions of excited product species were directly observed with the scanning monochromator. The only optical element in the scanning monochromator is the concave blazed grating. The resolved spectrum is focused on the detector at the exit slit of the monochromator. The signal from the detector was measured by an SSRI photon counting system (Ref 64). The output of the SSRI photon counter was either visually observed and recorded or recorded directly on a strip chart recorder. Various combinations of detectors and gratings were used in investigating emission in the wavelength region from 50 nm to 870 nm.

In this experiment, the combinations of detectors and gratings used limit the detection of emission lines to those

radiative transitions produced by reaction cross sections greater than 1×10^{-17} cm^2. In some spectral regions the instrument can measure radiation arising from reactions with excitation cross sections as low as 7×10^{-19} cm^2. The detector and grating combinations used in these measurements are shown in Table II.

Target Gas System

The target gas pressure is controlled by a Granville Phillips Automatic Pressure Controller and an MKS Baratron Capacitance Pressure Meter (see Fig. 4). Several manual valves are positioned to allow entry of the target gas into the storage bottle, or to pump out the storage bottle and source lines with a 2" CVC oil vapor diffusion pump attached to a Model 1400 Welch mechanical forepump (25 liter/minute pumping speed).

Vacuum System

The vacuum in the instrument is maintained by two 4" and one 6" oil diffusion pumps and one 500 liters/minute mechanical forepump (see Fig. 5). The pumping systems include a pneumatic actuated gate valve, a liquid nitrogen cooled trap, and the oil diffusion pump. The 4" Norton pumps, Model 0183, maintain the vacuum in the ion source and at the electrostatic collision chamber region. The 6" diffusion pump, (CVC Model PAS-63C), maintains the vacuum in the monochromator. All three diffusion pumps are connected to a 500 liter/minute mechanical forepump, Welch Model 1397.

Table II

Detector and Grating Combinations

Detector	Grating (995.4 mm Concave Radius)	Wavelength Region
RCA C31034A Photomultiplier Cooled with Dry Ice to -78°C GaAs Photocathode UV-Transmitting Glass Window	Bausch & Lomb #2662-1-1 700 nm Blazed Wavelength 300 Grooves/mm Aluminum Coated BSC2 Glass	300 nm to 870 nm
EMR 541F-08-18-03900 Photomultiplier SN 15245 CsTe Photocathode LiF Window	Bausch & Lomb #2571-5-3 200 nm Blazed Wavelength 600 Grooves/mm MgF_2 Overcoated Aluminum on BSC2 Glass	105 nm to 350 nm
EMR 541F-08-18-03900 Photomultiplier SN 15245 CsTe Photocathode LiF Window	Bausch & Lomb #2478-19-6-1 90 nm Blaxed Wavelength 600 Grooves/mm Platinum Coated BSC2 Glass	105 nm to 190 nm
EMR 541F-09-18-03900 Photomultiplier SN 17891 CsTe Photocathode MgF_2 Window	Bausch & Lomb #2571-5-3 200 nm Blazed Wavelength 600 Grooves/mm MgF_2 Overcoated Aluminum on BSC2 Glass	115 nm to 350 nm
EMR 541F-09-18-03900 Photomultiplier CsTe Photocathode MgF_2 Window	Bausch & Lomb #2478-19-6-1 90 nm Blazed Wavelength 600 Grooves/mm Platinum Coated BSC2 Glass	115 nm to 190 nm
Bendix CEM-4028 Channeltron Photon Counter Tube	Bausch & Lomb #2478-19-6-1 90 nm Blazed Wavelength 600 Grooves/mm Platinum Coated BSC2 Glass	50 nm to 130 nm

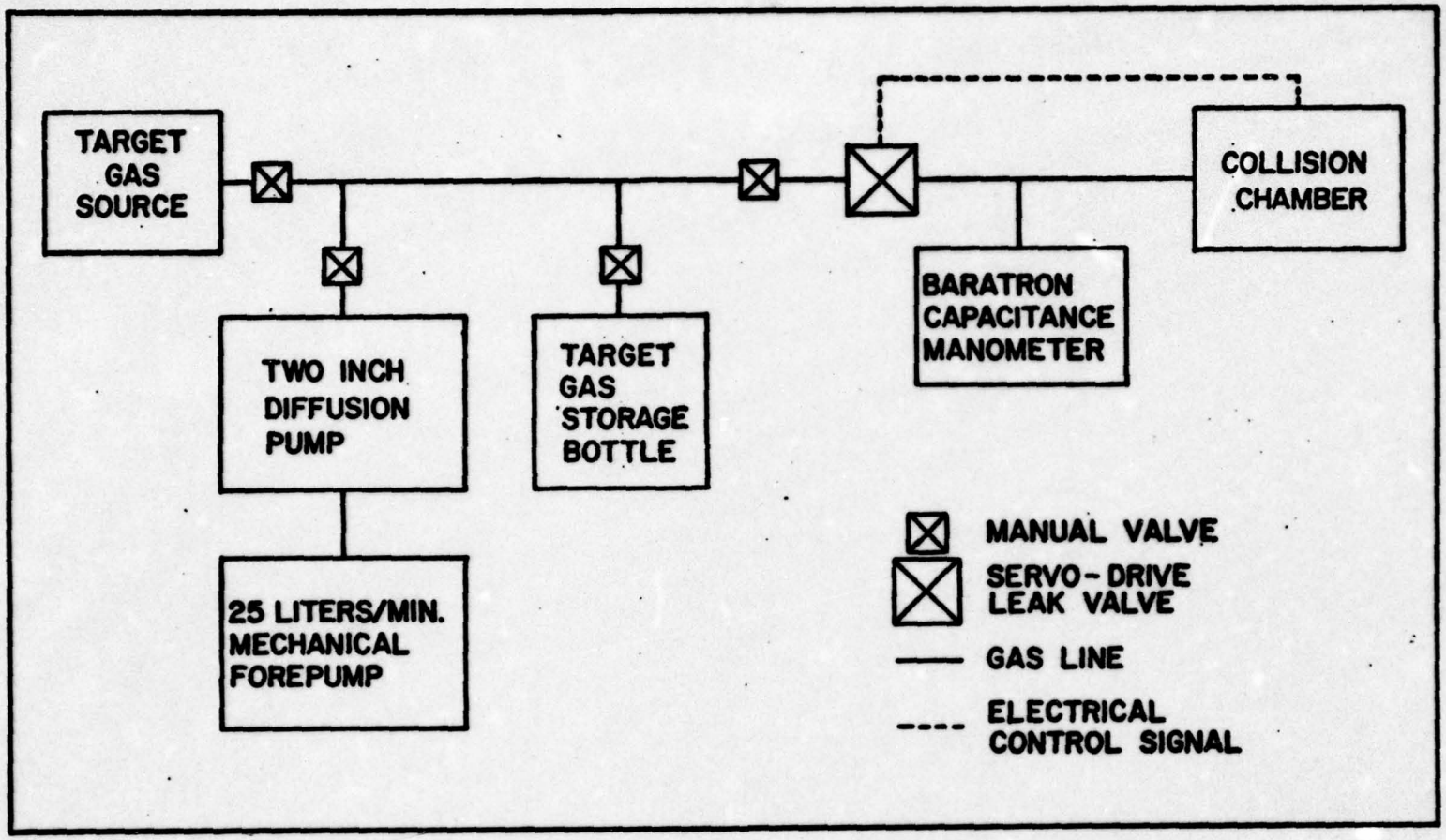

Fig. 4. Block Diagram of the Target Gas System.

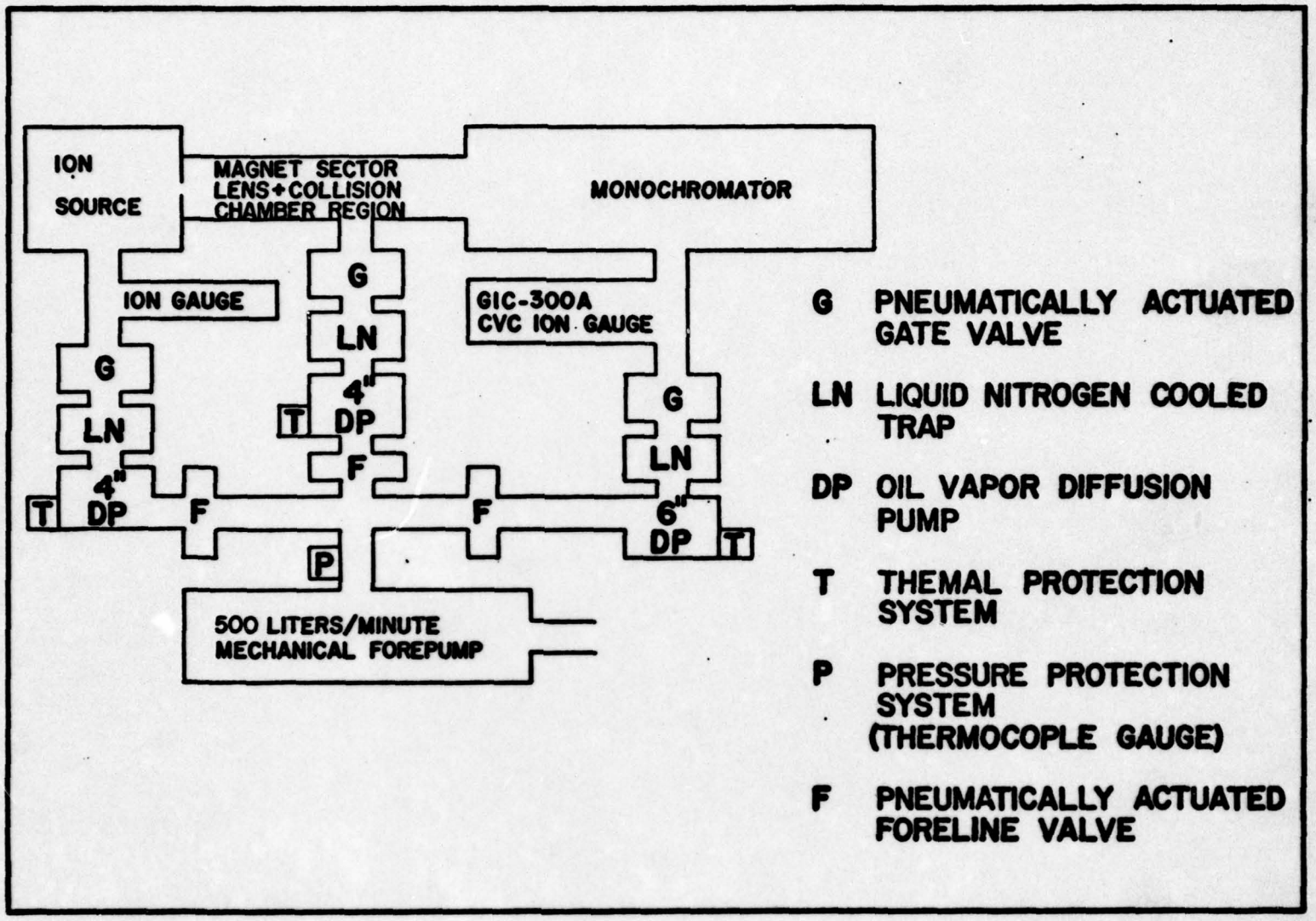

Fig. 5. Block Diagram of the Vacuum System.

Typical pressures in the monochromator with no gas in the collision chamber are in the 5×10^{-7} Torr region. With a 3 mTorr target gas pressure in the collision chamber, the monochromator pressure is about 1×10^{-6} Torr. Typical pressure readings on the ionization gauge near the ionization chamber are 4×10^{-7} Torr with no helium in the ionization chamber and 1.5×10^{-5} Torr while performing an experiment with helium in the ionization chamber.

Several protection systems are used to prevent damage to the diffusion pumps. An automatic system for filling the traps with liquid nitrogen insures that the traps are always cooled. An automatic system which will close all of the gate valves and shut off the diffusion pumps is actuated when (1) the ion gauge near the ion source detects high pressure, or (2) the thermocouple gauge near the forepump detects high pressure, or (3) there is an electrical power failure. Each diffusion pump also has a thermal protection system such that if the temperature of that pump becomes too high the pump will shut off.

Target-Gas Pressure Calibration

The pressure of the target gas in the collision chamber was controlled by differential pumping and by regulation of the inflow of gas. The gas input was measured and regulated by an MKS Baratron capacitance manometer and the pressure controller. Since the Baratron is located several inches from the chamber the pressure measured by the Baratron gauge

needed correction to obtain the true value of the pressure in the collision chamber. To determine this factor, a calibration experiment was performed.

The correction factors were obtained by comparison of the pressures measured by the Baratron gauge in two different configurations as shown in Figs. 6a and 6b. Figure 6a is that of the experiment and Fig. 6b is with the gauge at the end of a 1/8" tube projecting into the center of the collision chamber. The pressure readings, obtained for air and xenon, are plotted in Figs. 7 and 8 against the pressure at the mouth of the six-inch diffusion pump. A CVC ion gauge (GIC-300A) was used to measure these pressures where the diffusion pump enters the monochromator. As can be seen by inspection of the figures, it is evident that deviations occur at pressures above 4 mTorr. Since there is no significant difference between the calibration for air (atomic weight of 28) and xenon (atomic weight of 131), it is assumed that this calibration is also valid for chlorine, bromine and iodine.

Ion Beam Current Calibration

Following each cross section measurement, the ion beam current was calibrated to determine an upper limit on the uncertainty of measuring the current of the helium ion beam which enters the collision chamber. The purpose of this ion beam calibration was to determine the efficiency of collection of ions passing through the collision chamber at

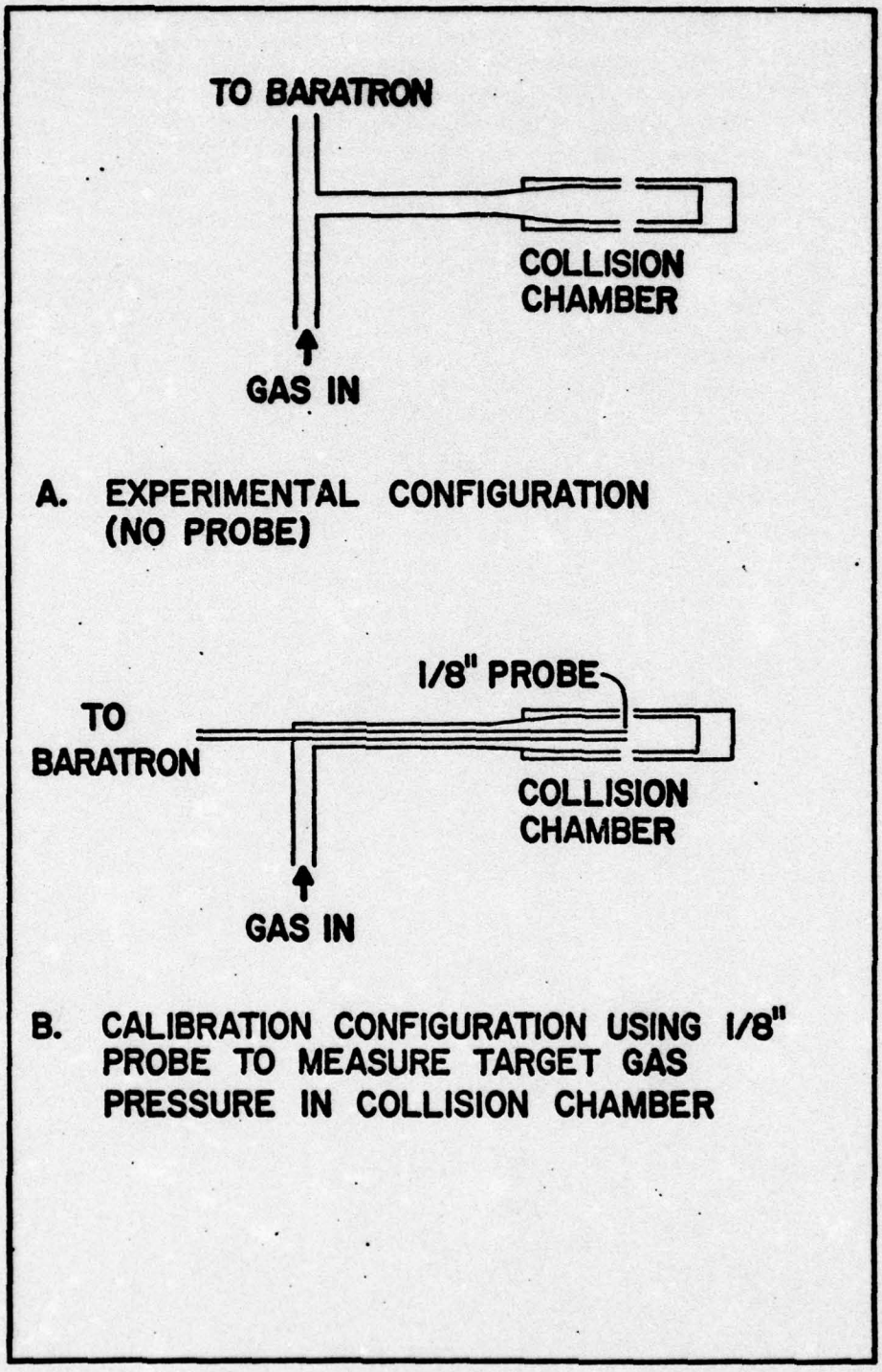

Fig. 6. Configurations Used for Target Gas Pressure Calibration.

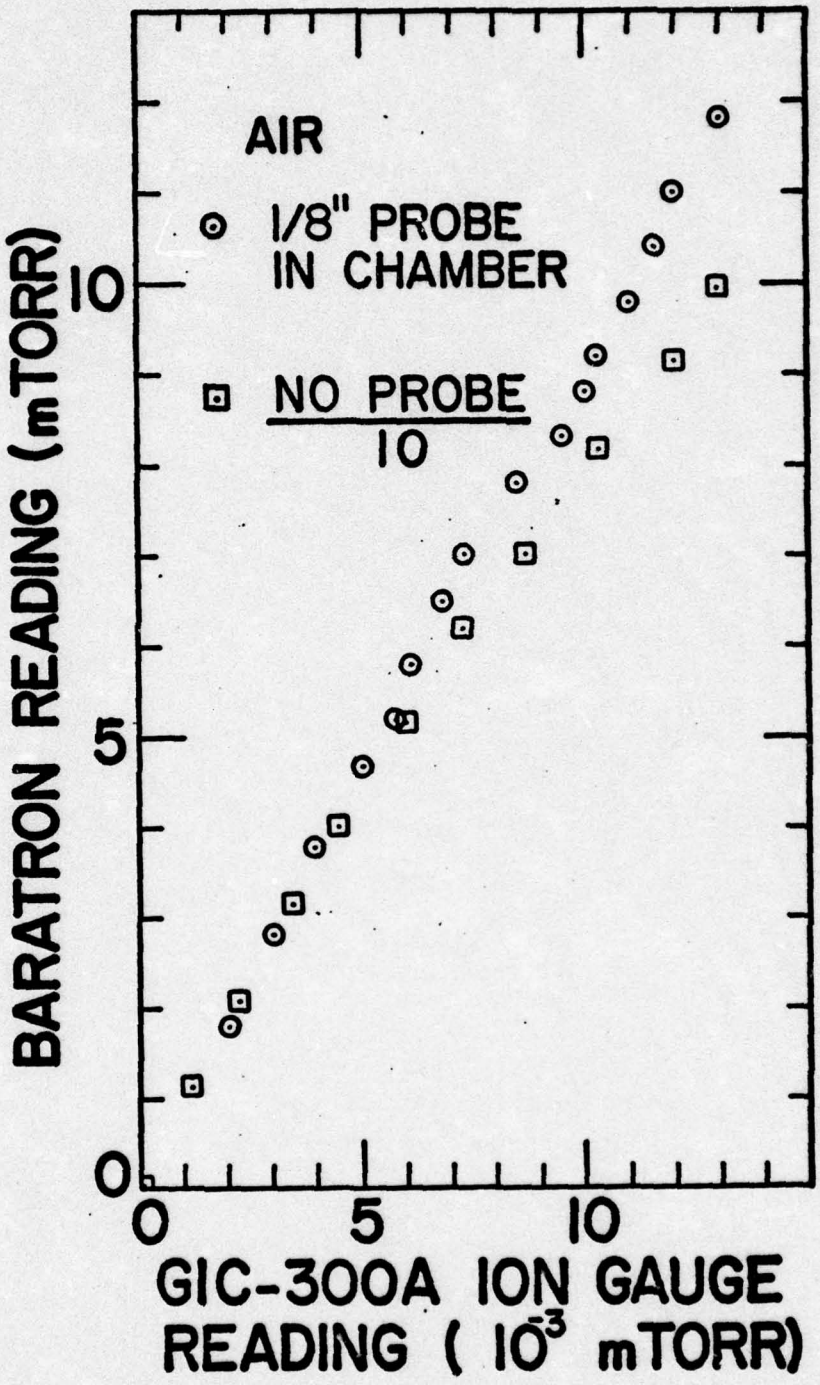

Fig. 7. Target Gas Pressure Calibration Using Air.

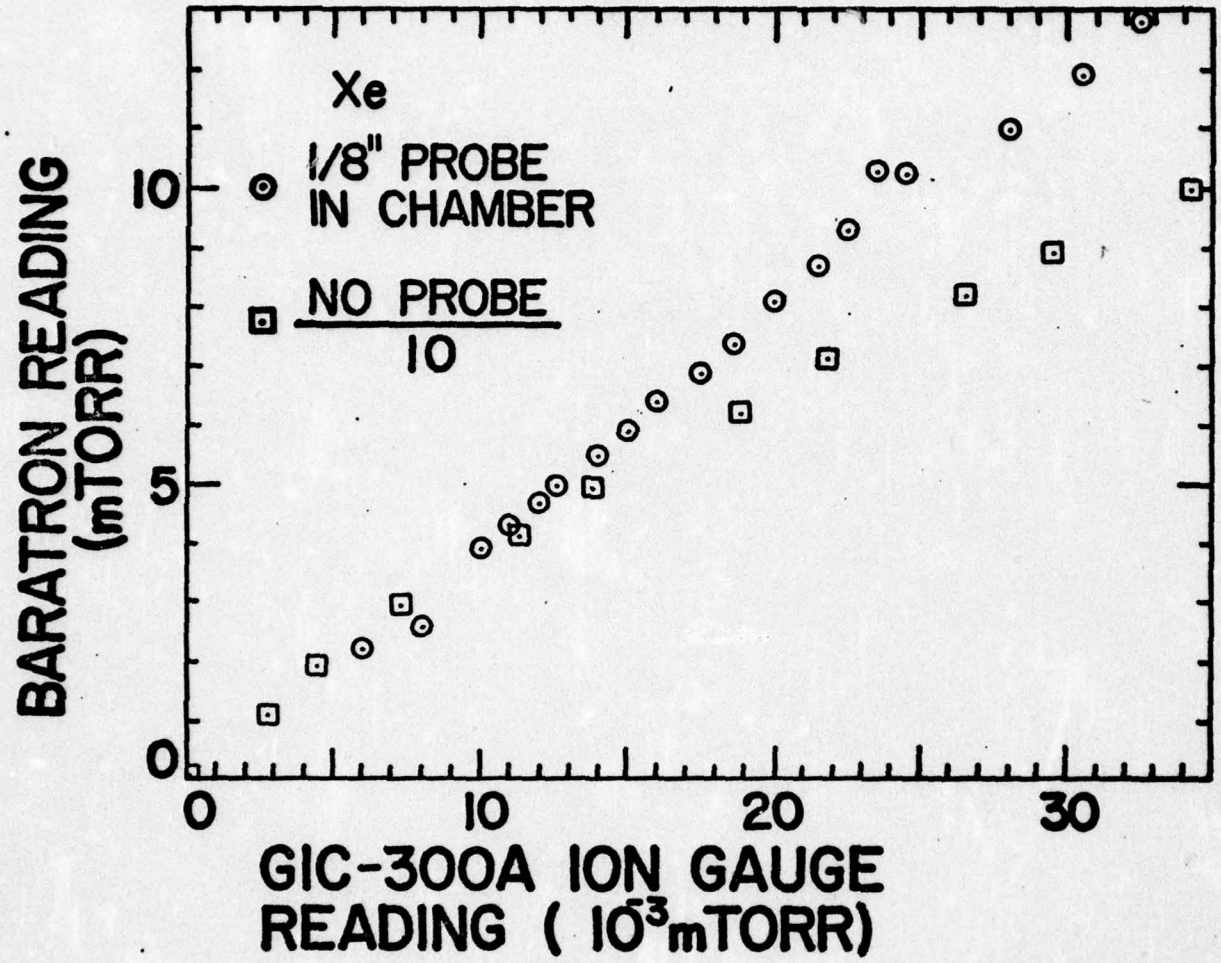

Fig. 8. Target Gas Pressure Calibration Using Xenon.

the ion collector in the monochromator [on the exit side of the collision chamber (see Fig. 9)]. This calibration was performed with no target gas in the collision chamber.

The calibration consisted of three measurements of the current. The difference between the first two, i_1-i_2, is a measure of the number of helium ions which passed through the aperture in the ion collection plate at the entrance to the electrostatic lens (see Fig. 3). The currents i_1 and i_2 were obtained with the ion beam deflected to one side of the aperture and aligned with the aperture respectively. The third current i_3 was measured at the ion collector at the exit of the collision chamber. The quantity i_1-i_2-i_3 is a measure of the number of helium ions which passed through the entrance sperture of the electrostatic lens, but did not exit the collision chamber.

A typical set of values for i_1, i_2, and i_3 are approximately 1.3 nA, 0.6 nA, and 0.7 nA respectively. This suggests that for these conditions very few ions which enter the electrostatic lens (i_1-i_2) fail to exit from the collision chamber. When i_1 was increased to 2 nanoamps the i_3 value decreased to about 70% of the i_1-i_2 value. Examination of the collision chamber after this experiment revealed an ion burn spot completely encircling the entrance slit. The total area of the ion burn spot is nearly equal to the area of the entrance slit. It appears that as the ion beam current is increased, the divergent characteristics of ion beam (space charge effects) cause more and more of the ions to ultimately

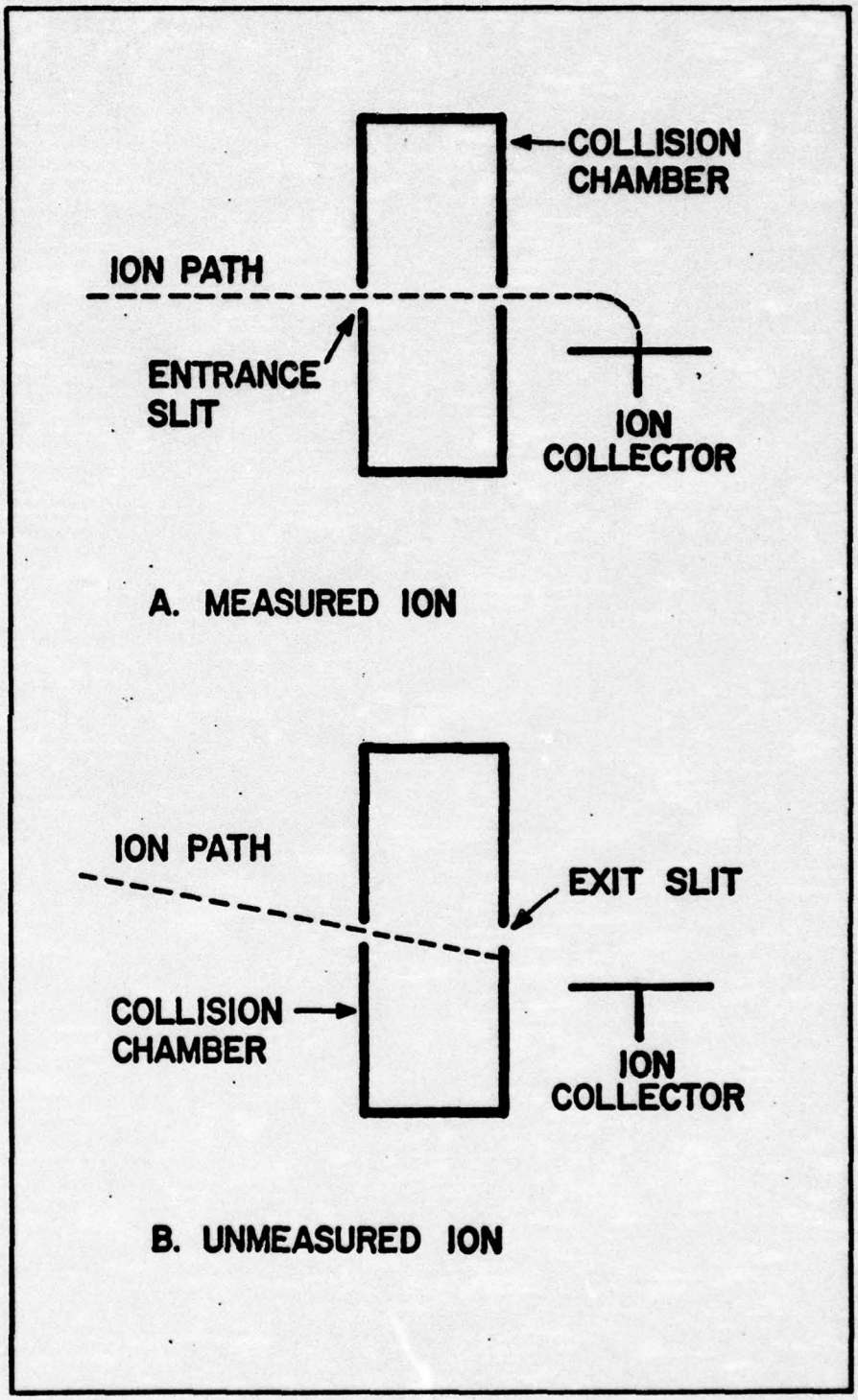

Fig. 9. Possible Ion Paths of Measured and Unmeasured Ions Available for Excitation of Atoms/Molecules in Collision Chamber.

collide with the entrance wall of the collision chamber. At ion energies of 2 to 5 eV, this divergence of the beam and the weaker focusing characteristics of the lens reduce the transmission through the collision chamber to about 50%.

This calibration shows that for i_3 values of 0.7 nA at 100 eV the ion beam current measured at the ion collector on the exit side of the collision chamber is an accurate measure of the ions which are available for excitation in the reaction region of the collision chamber. The He^+ ion currents recorded at this ion collector with no target gas in the chamber are the values used in the cross section calculations for the experiments reported here. Typical He^+ ion flux through the collision chamber during this experiment was 6×10^{10} ions/sec-cm^2 (10 nanoamps/cm^2).

It should be noted that for experiments at ion energies above 110 eV the cross section measurements are probably lower than the actual values. This is due to the fact that at energies above 110 eV the ion beam is not efficiently collected with the potentials used on the ion collector. (This potential could not be increased without a major modification to the apparatus.) Therefore, energy dependence measurements at energies above 110 eV were made by tuning the beam at 100 eV, where accurate ion collection measurements can be made. (This is the ion current value used in the cross section calculations.) Then the deceleration voltage was adjusted to the desired value for the experiment. The deceleration voltage adjustment tends to defocus the

ion beam to some degree, resulting in the calculated cross sections being smaller than the actual cross sections. Thus the error in the cross section values probably increases as the energy is increased from 100 eV to 170 eV (see Figs. 26, 27, 36 to 41 and 53 to 60). This error is estimated to be as large as 50% at 170 eV.

Instrument Calibration for 400 nm to 870 nm Region

In the 400 nm to 870 nm region the instrument function $F(\lambda)$ was determined by using a calibrated tungsten light source (Ref 33). The calibration arrangement is shown in Fig. 10. This calibration was based on the black body radiation law from a gray body (Ref 31:126) and the law of conservation of radiance in an elementary beam (Ref 31:134). The instrument function $F(\lambda)$ is defined as

$$F(\lambda) \equiv \frac{Q}{P_\lambda} \tag{7}$$

where

Q = Counts/sec recorded on the SSRI photon counter converted to power (watts)

P_λ = Spectral power incident on the grating (watts)

The calibration procedure was as follows. First the image of the tungsten filament is focused on the entrance slit of the monochromator. Then the image in the slit is treated as a source for the monochromator. Referring to Fig. 11 one can see that a differential area of the grating perpendicular to a line from the source is

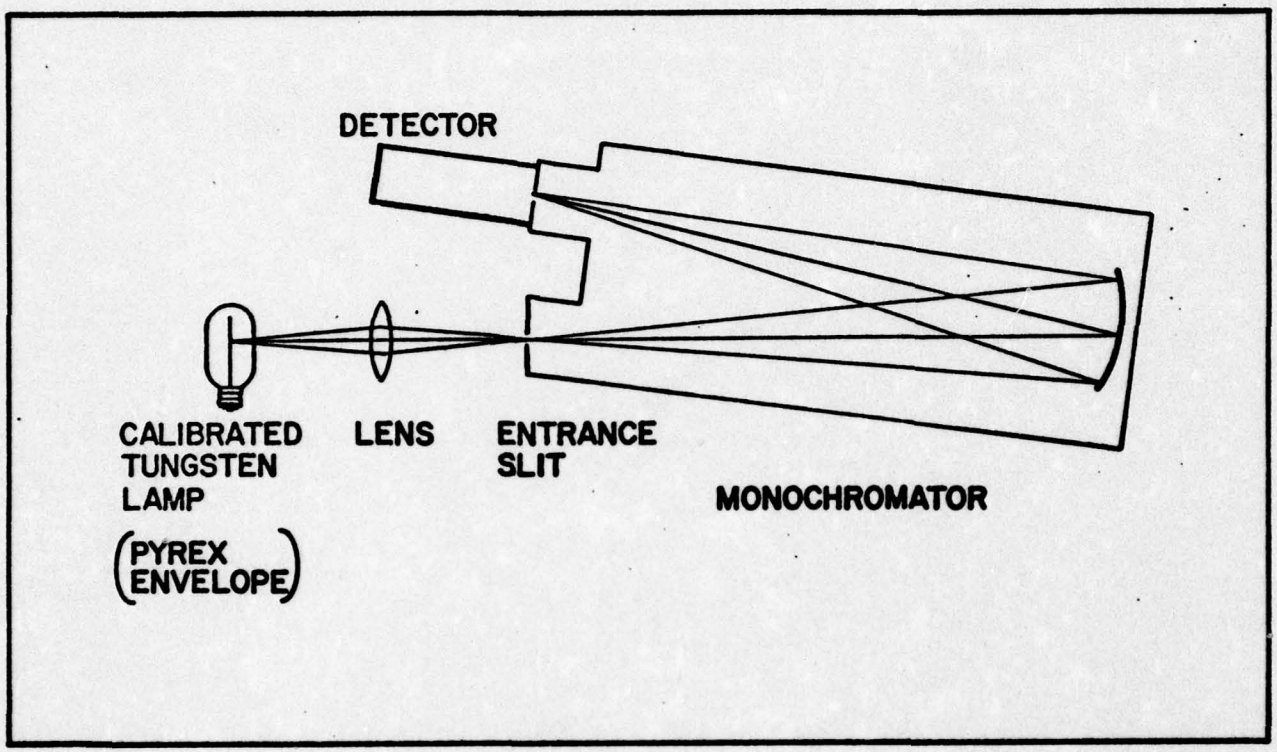

Fig. 10. The 400 nm to 870 nm Instrument Function [F(λ)] Calibration Setup.

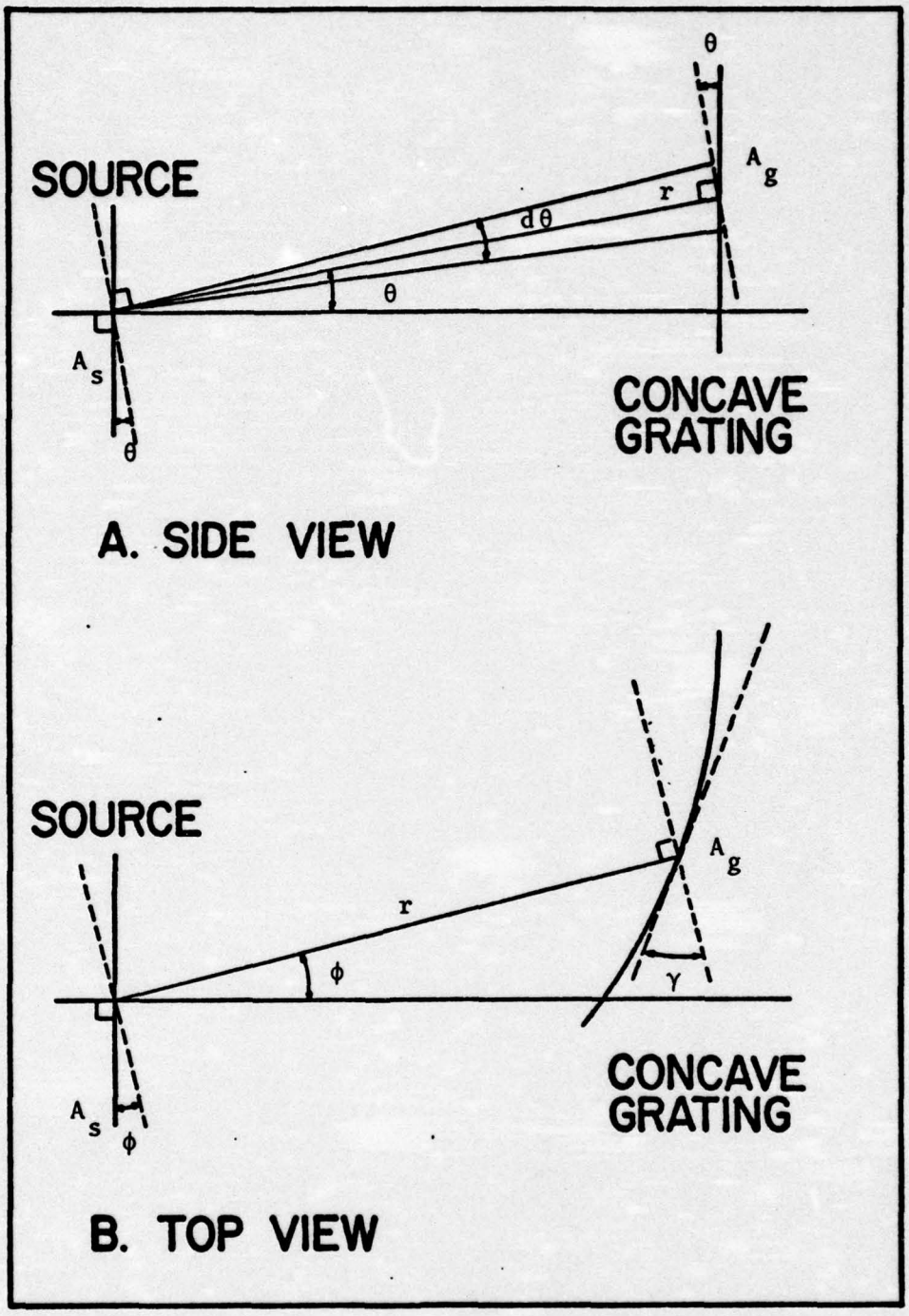

Fig. 11. Geometric Diagram of Monochromator.

$$dA_{g_\perp} = (rd\phi)(r \cos \theta d\theta) \tag{8}$$

where the symbols are explained in Table III. A similar differential area of the source perpendicular to a line from a point on the grating is

$$dA_{s_\perp} = dA_s \cos \theta \cos \phi \tag{9}$$

The differential solid angle subtended by $dA_{g_\perp}$ at the source is

$$d\Omega = \frac{dA_{g_\perp}}{r^2} = \cos \theta d\theta d\phi \tag{10}$$

The differential spectral power d^2P_λ from the source that is incident on the grating is

$$d^2P_\lambda = L_\lambda dA_{s_\perp} d\Omega \tag{11}$$

Therefore the total spectral power is

$$P_\lambda = L_\lambda A_s \iint A_g \cos^2 \theta d\theta \cos \phi d\phi = L_\lambda A_s \Phi \tag{12}$$

where

$$\Phi = \iint A_g \cos^2 \theta d\theta \cos \phi d\phi$$

Now

$$L_\lambda = T_{\lambda_{Pyrex}} T_{\lambda_{Lens}} \varepsilon_{\lambda_{Tungsten}} L_\lambda^{BB} \tag{14}$$

and assuming the source is a Lambert emitter

Table III

Symbols Used in the Derivation of the Visible Instrument Function F(λ)

h	Plancks constant
c	Velocity of light
k	Boltzmann's constant
λ	Wavelength
T	Temperature °K
R	Radiant Emittance (watts/cm^2)
P	Power (watts)
L	Radiance (watts/ster-cm^2)
$R_\lambda, P_\lambda, L_\lambda$	Spectral Radiant Emittance, Spectral Power and Spectral Radiance
$R_\lambda^{BB}, P_\lambda^{BB}, L_\lambda^{BB}$	Spectral Radiant Emittance of a Blackbody, etc.
T_λ	Spectral transmittance
ε_λ	Spectral emissivity
Q	Counts/sec of SSRI Photon Counter (Photons/sec)
A_s	Area of source (cm^2)
A_g	Area of grating (cm^2)
Ω	Solid angle (ster)
θ	Vertical angle between normal to source and a line to a point on the grating
ϕ	Horizontal angle between normal to source and a line to a point on the grating
γ	Horizontal angle of rotation of the grating from parallel to source
r	Distance from source to a point on the grating

$$L_\lambda^{BB} = \frac{R_\lambda^{BB}}{\pi} \tag{15}$$

where

$$R_\lambda^{BB} = \frac{C_1}{\lambda^5} \frac{1}{\left[e^{C_2/\lambda T} - 1\right]} d\lambda \tag{16}$$

with

$$C_1 = 2\pi c^2 h \tag{17}$$

$$C_2 = \frac{hc}{k} \tag{18}$$

The total spectral radiance incident on the grating is

$$L_\lambda = T_{\lambda_{Pyrex}} T_{\lambda_{Lens}} \varepsilon_{\lambda_{Tungsten}} \frac{C_1}{\pi\lambda^5} \frac{1}{\left[e^{C_2/\lambda T} - 1\right]} d\lambda \tag{19}$$

$$\left.\begin{matrix}\text{The energy of} \\ \text{one photon}\end{matrix}\right\} = \frac{hc}{\lambda} \tag{20}$$

Therefore the photons/sec incident on the grating as a result of the total spectral power is

$$P_\lambda(\text{photons/sec}) = \frac{T_{\lambda_{Pyrex}} T_{\lambda_{Lens}} \varepsilon_{\lambda_{Tungsten}} C_1 \lambda d\lambda A_s \Phi}{hc\pi\lambda^5 \left[e^{C_2/\lambda T} - 1\right]} \tag{21}$$

The instrument function $F(\lambda)$ is defined as

$$F(\lambda) \equiv \frac{Q}{P_\lambda} \tag{7}$$

Therefore

$$F(\lambda) = \frac{Q\lambda^4 \left[e^{hc/k\lambda T} - 1\right]}{2cT_{\lambda_{Pyrex}} T_{\lambda_{Lens}} \varepsilon_\lambda A_s \Phi d\lambda} \qquad (22)$$

The resulting instrument function from 400 nm to 870 nm is shown in Fig. 12.

VUV Instrument Calibration

The calibration of gratings in the VUV region is a difficult task. The only experts whom the author was able to locate with the capability to accomplish this type of calibration are located at the Naval Research Laboratories (NRL), and this is not readily available to people outside of NRL (Ref 22). Bausch and Lomb, the company which manufactured the grating, does not routinely calibrate gratings at less than 200 nm (Ref 54). In addition, grating reflectance changes over a period of time, and absolute calibrations would therefore change. In view of these considerations it was decided to use the measurements of an emission line for which radiative cross section data is available as a calibration standard. The use of a known reaction as a standard has the advantages of eliminating the need for periodic absolute calibration of the system, since the calibration of the grating can be checked at any time by merely observing the standard reaction. The experimental arrangement is in no way disturbed, and the grating need not be removed.

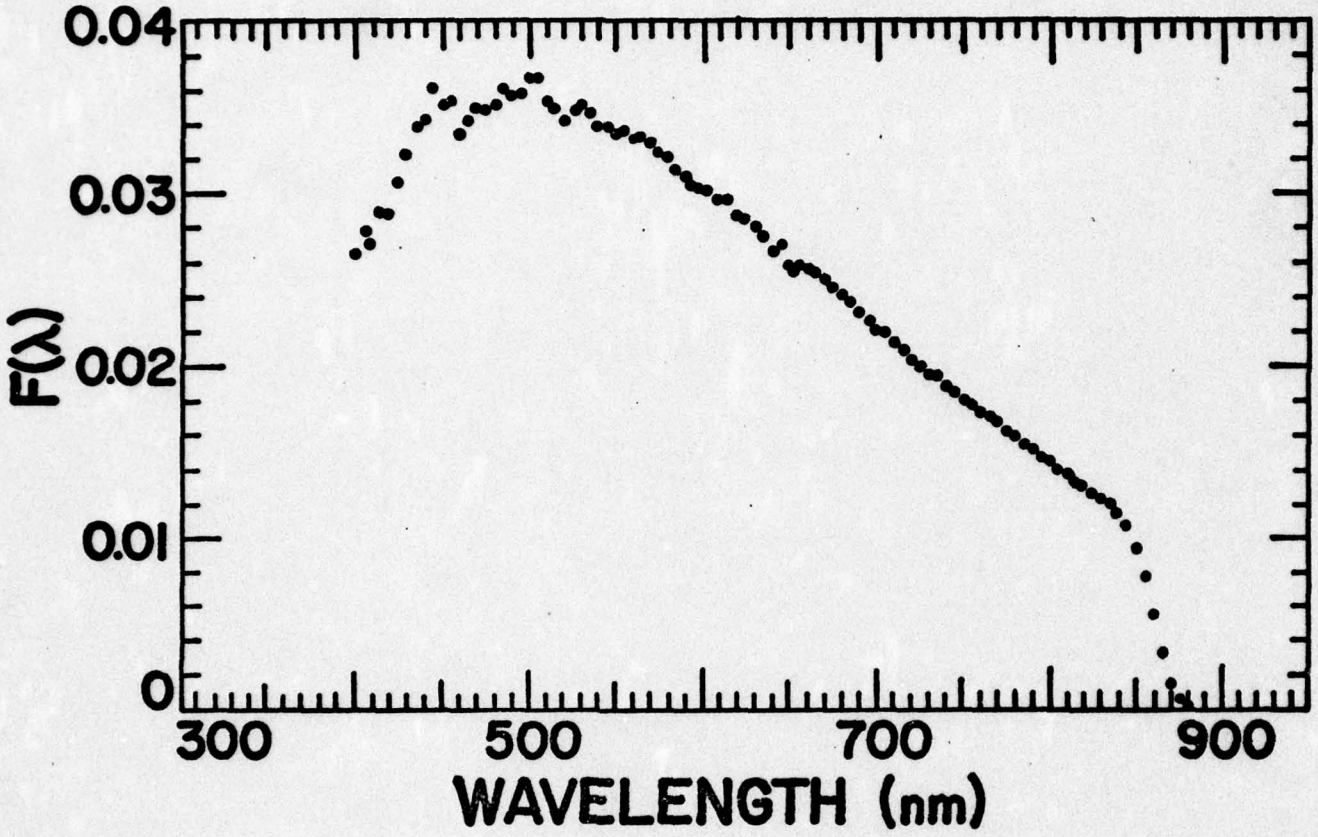

Fig. 12. Instrument Function [F(λ)] from 400 nm to 870 nm.

In the VUV region, the instrument function was calibrated by measuring the cross section for the L_α hydrogen line (121.6 nm from the reaction of 100 eV He^+ with H_2. A value of 0.60×10^{-16} cm^2 was used as a reference standard. This value was obtained in other studies using the same apparatus (Ref 21). This value for the L_α hydrogen line from the reaction of 100 eV He^+ with H_2 is in good agreement with Dunn's value of 0.52×10^{-16} cm^2 for the L_α hydrogen line from the reaction of 120 eV He^+ with H_2 (Refs 6 and 7).

A profile of the 90 nm blazed platinum grating was obtained by consideration of the following factors: (a) the measured reflectance curves from similar gratings (Ref 14), (b) the theoretical reflectance curve for blazed gratings (Ref 31:342-347), and (c) the reflectance curves for platinum (Refs 61 and 71). The reflectivity profile was assumed constant between 88.9 nm and 121.6 nm because the reflectivity of platinum increases from 88.9 nm to 121.6 nm (Ref 71:67), while the theoretical blaze reflectance decreases by approximately the same amount. The 88.9 nm line is the shortest wavelength line detected in this experiment. This assumed reflectivity profile was multiplied by the published spectral response of the Bendix Channeltron (Ref 26) to obtain the instrument function profile from 88.9 nm to 121.6 nm. This instrument function profile was then normalized to the calibrated value of the L_α hydrogen line at 121.6 nm (see Fig. 13).

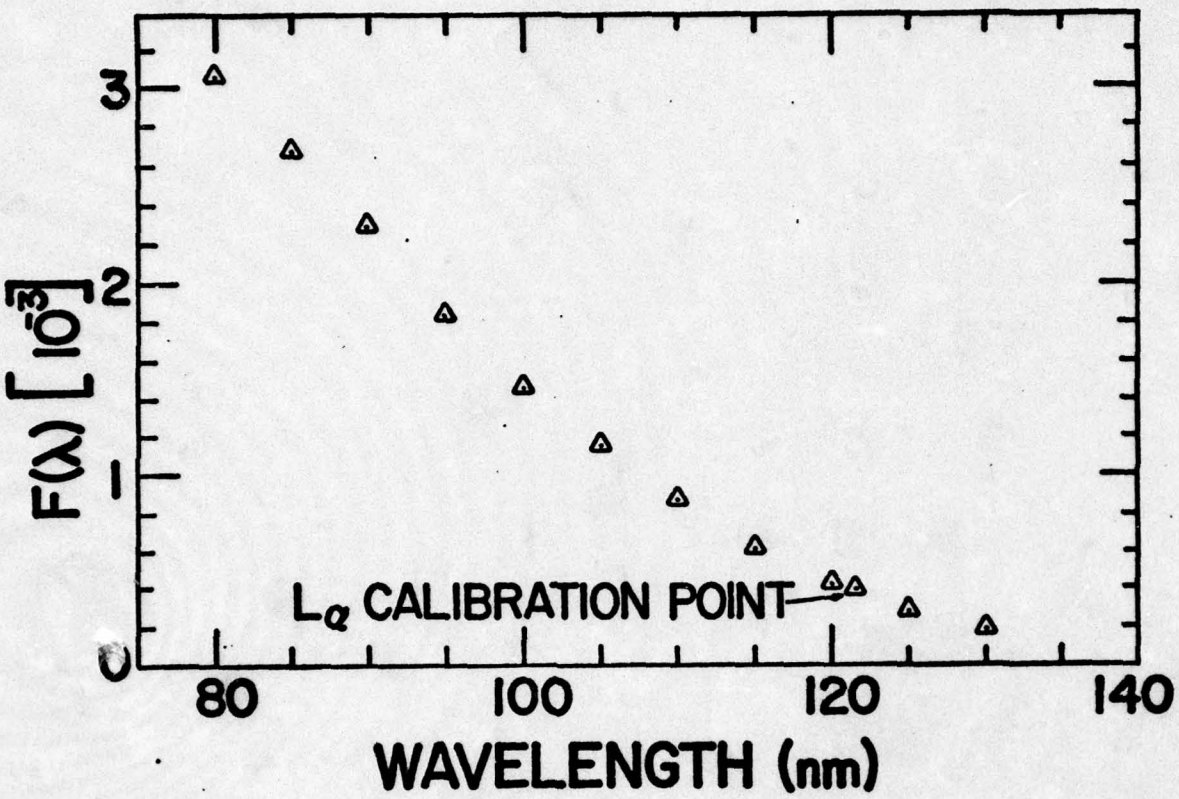

Fig. 13. VUV Instrument Function [F(λ)] from 80 nm to 125 nm.

After examining a number of blazed grating calibrated reflectance curves for the VUV (Ref 14), and comparing them to the theoretical curve, the reflectivity profile between 121.6 nm and 183.0 nm was assumed to decreased by one-half linearly. This reflectivity profile was multiplied by the factory calibrated spectral response of the EMR photomultiplier to obtain the instrument function profile for the 121.6 nm to 183.0 nm region. This instrument function profile was then normalized to the calibrated value of the L_α hydrogen line at 121.6 nm (see Figs. 14 and 15).

This total instrument function calibration results in an instrument function profile that is calibrated at the 121.6 nm point and is less accurate at the extreme ends, the maximum error being at 183.0 nm. Due to the possible variation of the actual reflectivity profile of the platinum grating from the theoretical profile, this error could be as large as a factor of four. The uncertainty of this profile is taken into account in citing the accuracy of the cross section measurements in this region.

Other detector and grating combinations were used to investigate the 190 nm to 400 nm spectral region. Since no emissions were observed in this region, the instrument functions in the 190 nm to 400 nm spectral region are not discussed in this report.

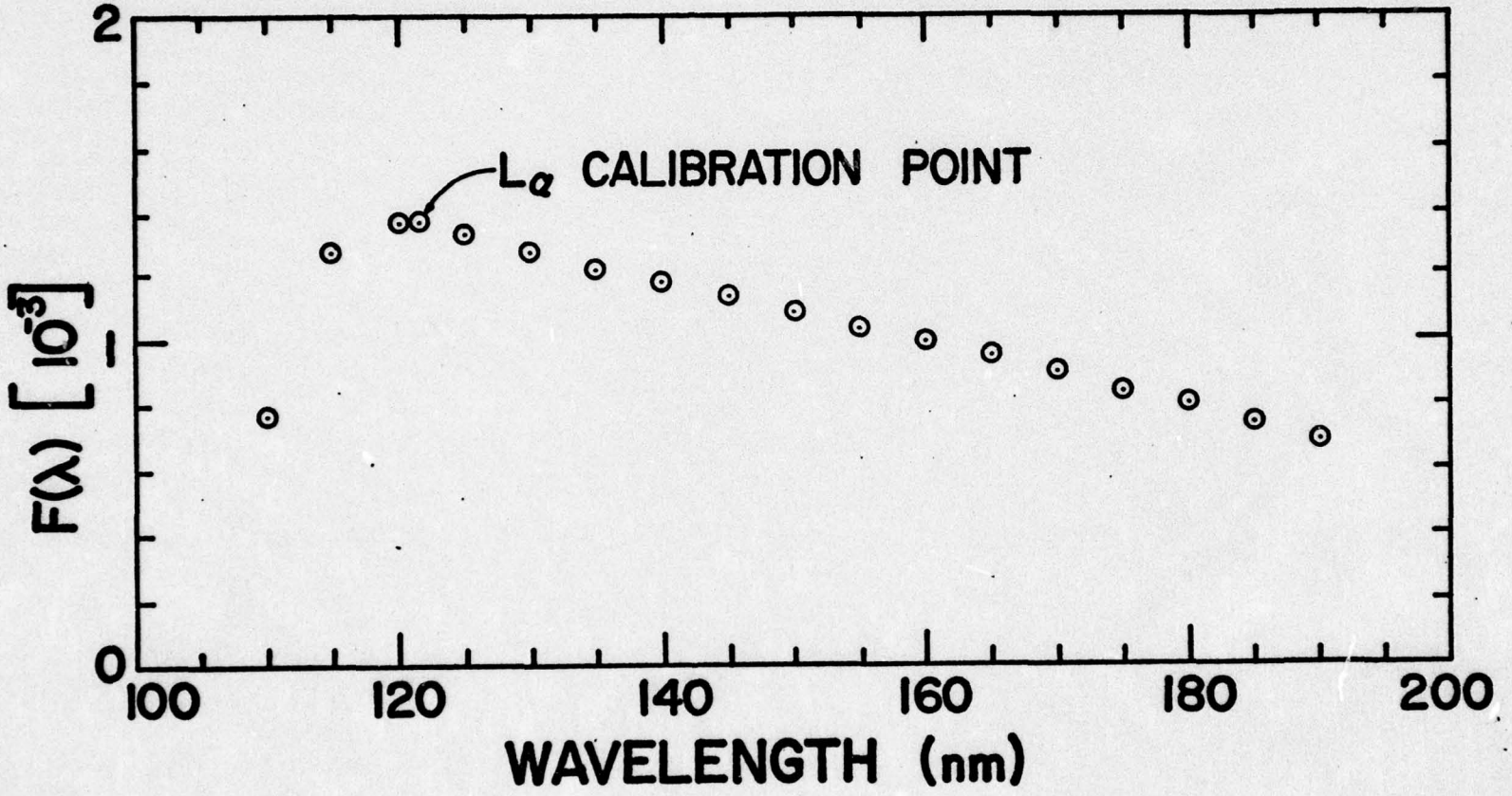

Fig. 14. VUV Instrument Function [F(λ)] from 120 nm to 185 nm Using EMR LiF Window Detector.

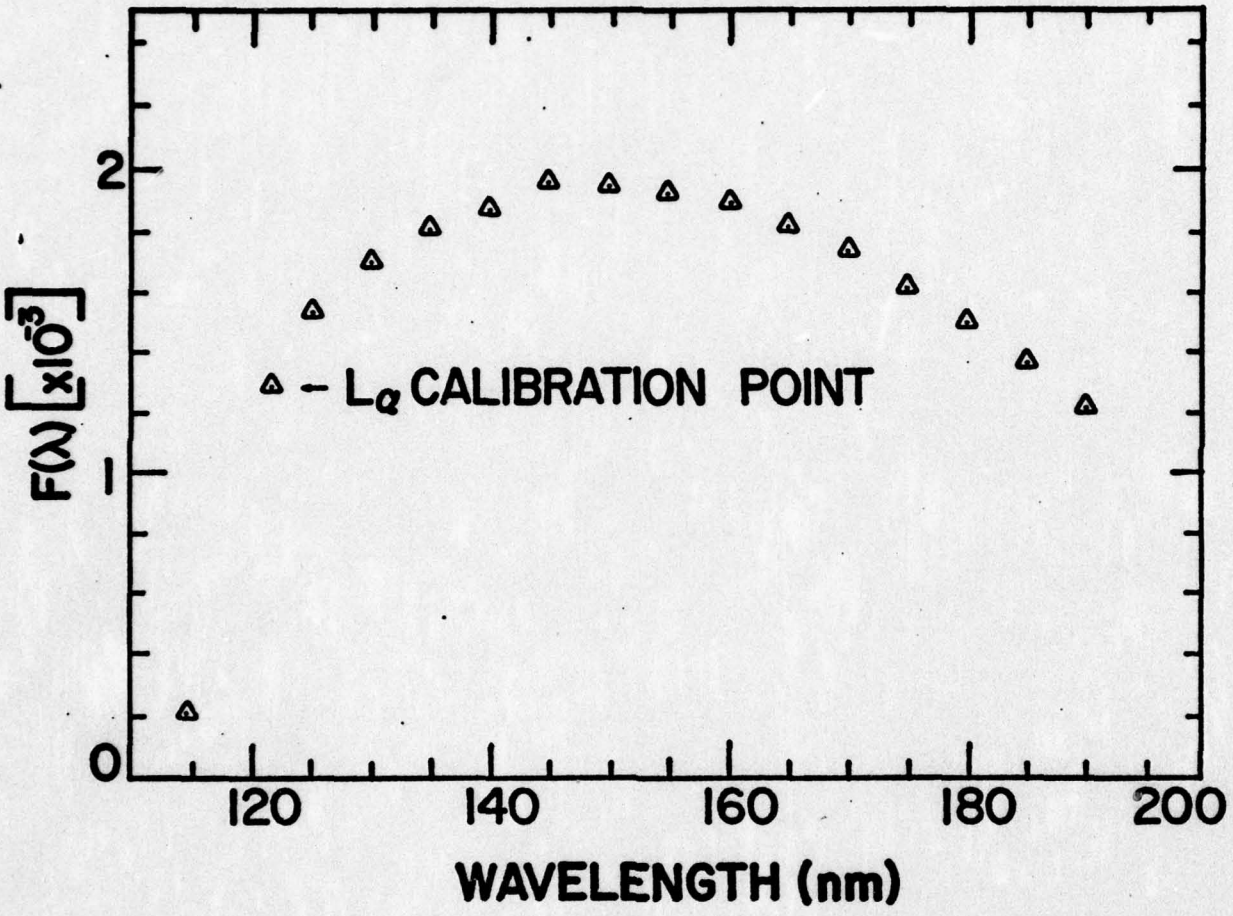

Fig. 15. VUV Instrument Function [F(λ)] from 120 nm to 185 nm Using EMR MgF_2 Window Detector.

III. Experimental Procedures

Bimolecular-Reaction Determination

The purpose of the He^+/halogen experiment is to study bimolecular ion neutral collisions. Before performing the experiment it is necessary to determine the maximum pressure at which the experiment can be performed while avoiding the occurrence of multiple collisions. This information is obtained by positioning the monochromator on an intense line from the reaction, and obtaining the response for various pressures of the target gas. Next a plot is made of the response as a function of target gas pressure. As long as the plot is linear, single collision events are occurring (Ref 49:278-282); whereas when the curve becomes nonlinear, multiple events are occurring. The resulting pressure dependence curves for the He^+/Cl_2, Br_2, I_2 reactions at 100 eV are shown in Figs. 16, 17 and 18. The Cl_2 and Br_2 curves become nonlinear at about 4 mTorr. The I_2 curve extends only to 2 mTorr because that is the vapor pressure of I_2 in the instrument at room temperature.

The linear portions of the curves in Figs. 16, 17 and 18 are also an indication that the effect of any secondary electrons generated in or near the collision region are negligible. If these secondary electrons were significant, the reaction would be a higher order process, and there would not be a linear region. If any secondary electrons are generated, they probably have low energies in the 1 eV to 12 eV region (Ref 29:276). Because of the shielding of the colli-

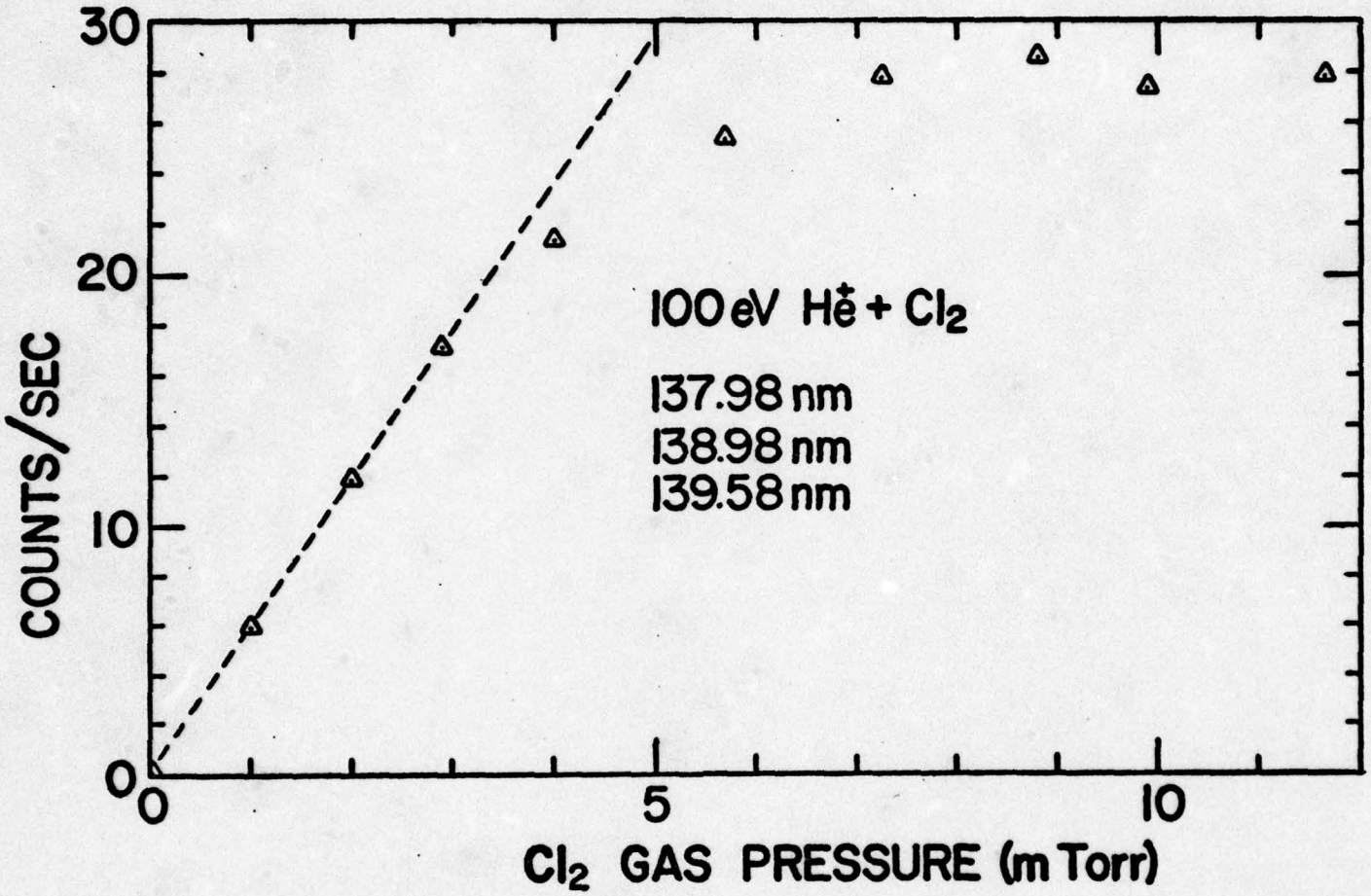

Fig. 16. Cl_2 Target Gas Pressure Dependence.

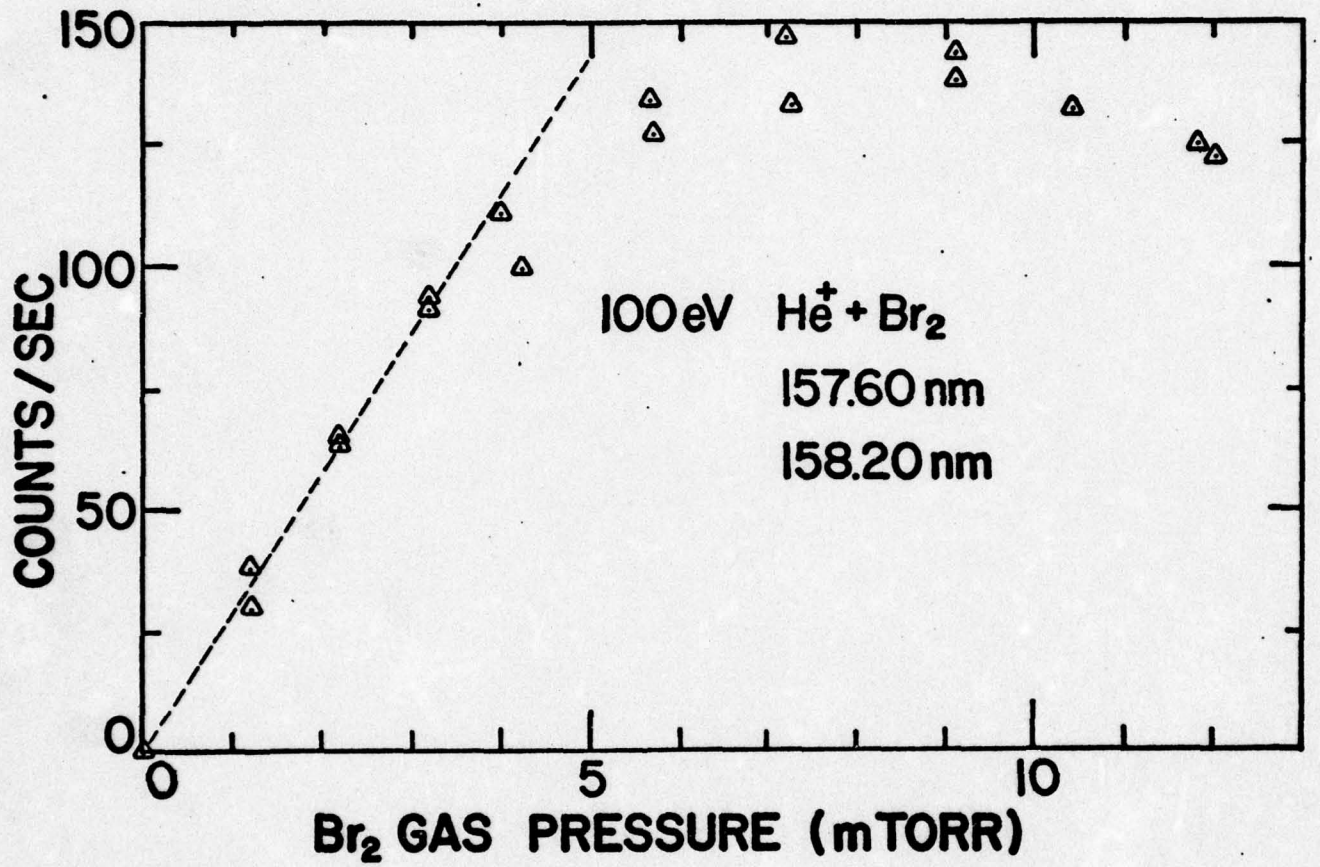

Fig. 17. Br_2 Target Gas Pressure Dependence.

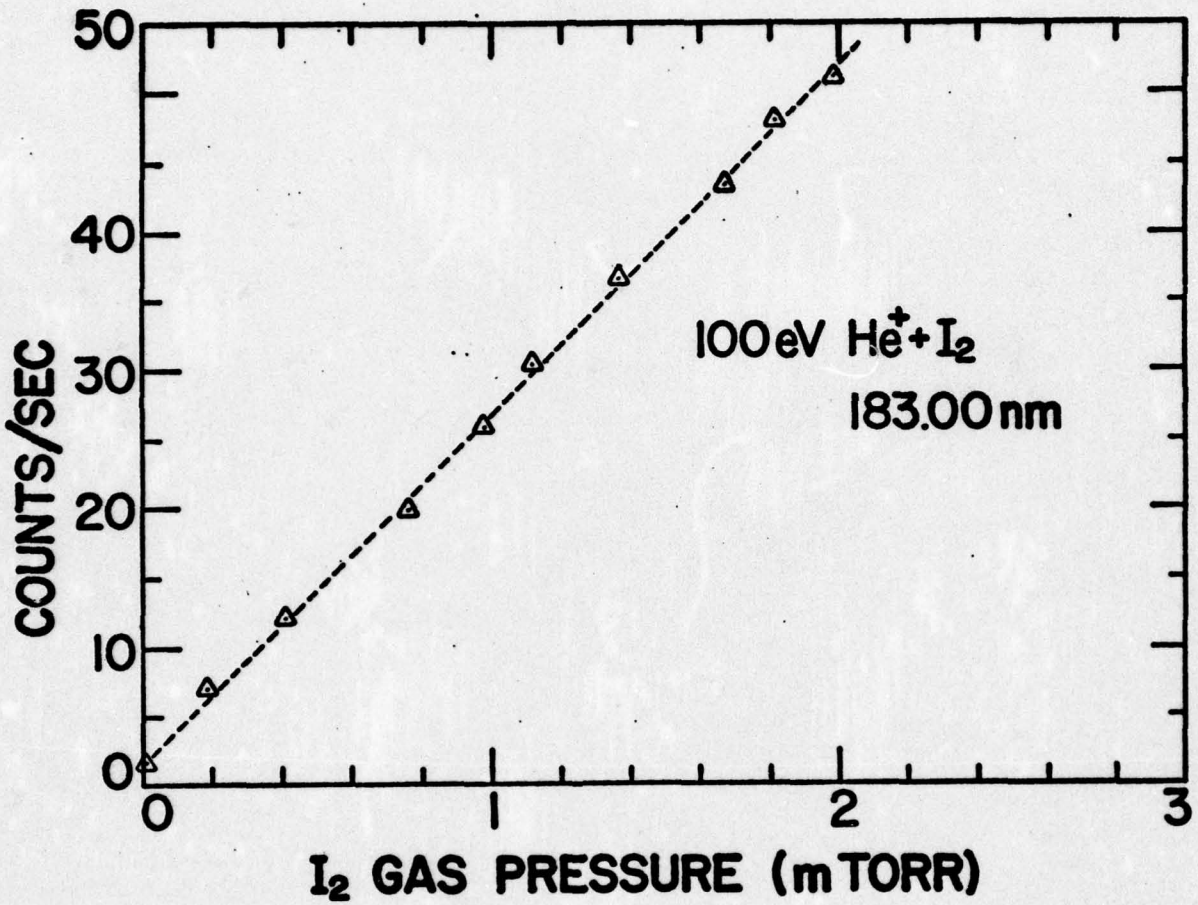

Fig. 18. I_2 Target Gas Pressure Dependence.

sion chamber, the experimental collision region is in a field-free environment. The generation of any secondary electrons would generally be outside of the collision region. If any secondary electrons are generated by the collision of He^+ ions with the edges of the entrance slit of the collision chamber, they would be quickly collected by the positively charged plate of the electrostatic lens. If they are generated at the ion collector in the monochromator on the exit side of the collision chamber (see Fig. 3), the low energy electrons would be repelled by the ion collector plate toward the opposite plate. Even if an electron collided with a halogen molecule in this region, the emission from the excited product species would occur so far from the focal point of the monochromator that it would not be focused on the exit slit of the monochromator.

Emission Wavelength Determination

The proper detector and grating for the wavelength region to be investigated (see Table II) are installed prior to an experiment. Initially, the 1 mm slit chamber was installed and the detector slit was set at 1 mm. A central image scan was performed to obtain the correction to be applied to the monochromator readings. A low resolution scan was then taken of the complete wavelength region to be studied. The low resolution half-width-at-half-maximum (HWHM) values were generally ± 1.5 nm in the VUV and 3.0 nm in the visible. Next, the 0.1 mm slit chamber was installed and the detector slit was set at 0.1 nm (some scans were

performed with larger exit slit settings). Another central image scan was performed to obtain a new monochromator reading correction. A high resolution scan was then taken of the regions of particular interest in which peaks were observed in the low resolution scan. The high resolution HWHM values were generally ± 0.3 nm from 80 nm to 120 nm, ± 0.1 nm from 120 nm to 400 nm and ± 0.5 nm from 400 nm to 860 nm.

The uncertainties $\Delta\lambda_0$ of the measured wavelengths λ_0 were determined by a combination of the accuracy of the counter reading on the monochromator, the resolution of the instrument for the given grating and slit combination used for the scan, and the shape of the peak being evaluated. Usually $\Delta\lambda_0$ was given the value of the half-width-at-half-maximum of the observed peak plus the uncertainty of the counter reading of the monochromator.

The ion beam was focused for the experiment by varying the magnetic field in the mass spectrometer until the maximum number of ions entered the electrostatic lens systems. The voltage on the electrostatic lens was then varied until the maximum number of ions were collected at the ion collector inside the monochromator (see Fig. 3). This procedure for tuning the instrument assures that the ion beam is properly focused at the collision region which is located at the focal point of the monochromator, regardless of the He^+ ion translational kinetic energy. This procedure is particulary important when measurements are taken at various ion energies as described in the next section. The ion beam is very

sensitive to even minute adjustments. The 100 eV He^+ ion beam was the most stable beam, as well as having the largest number of ions incident on the collision region which could be accurately measured. Therefore, the 100 eV He^+ ion beam was used for most spectral scans.

Cross Section Measurements at Various Translational Energies

In order to obtain data which would aid in determining if a specific emission line was produced by an endothermic or exothermic process, the cross section of a specific emission line was measured at various He^+ ion translational energies. To obtain this data the following procedure was used.

With the 1 mm collision chamber slit installed and a 1 mm detector slit setting, the monochromator was positioned on one of the most intense peaks. Then the ion translational energy was adjusted to a specific setting and many readings were manually recorded. For example, ten 20-sec readings at 100 eV were recorded. Then the ion translational energy was adjusted to 0 eV at which energy no ions are transmitted into the collision chamber and ten more 20 sec readings were taken to obtain the background. The average of the background readings was subtracted from the average of the 100 eV readings. This process was repeated for the translational energy values of 2, 5, 10, 15, 20, 30, 40, 50, 60, 70, 80, 90, 100, 110, 120, 130, 140, 150, 160, and 170 eV. Typical energy dependence plots are seen in Figs. 26, 27, 36 through 41, and 53 through 60.

It is important to measure a background reading with the ion translational energy adjusted to 0 eV. Because of differential pumping, there is a flow of target gas through the collision chamber entrance slit into the electrostatic lens region. Collisions of the ion beam with the target gas in this region (where the effective energy is higher than at the collision chamber) also produces radiation. Typical background corrections were on the order of 30% in the VUV region and 45% in the visible region. In the near infra-red region from 700 nm to 870 nm there was also a significant amount of blackbody radiation from the ion source, causing corrections on the order of 65%.

IV. Data Analysis

In this chapter the general outline of the data analysis used for all three systems will be explained. The next three chapters will discuss the results of the data analysis of that particular system. It must be remembered that the limitations of the experimental apparatus dictate that only emissions from energy states with lifetimes of 10^{-6} sec or less will be observed. Therefore metastable states of the product species will not be identified in this analysis.

When a 100 eV He^+ ion beam collides with Cl_2, Br_2, or I_2, the following possibilities exist:

Collision

Reactants $\longrightarrow$ Product Species

$$100 \text{ eV } He^+ + X_2 \rightarrow He^+ + X_2^* \quad (1)$$

$$He + (X_2^+)^* \quad (2)$$

$$He^* + X_2^+ \quad (3)$$

$$He^* + X + X^+ \quad (4)$$

$$He + X^* + X^+ \quad (5)$$

$$He + X + (X^+)^* \quad (6)$$

$$He^+ + X + X^* \quad (7)$$

where * represents an excited atom/molecule/ion

X represents Cl, Br, or I

If reactions (1) or (2) are significant, molecular emission lines should be observed. Upon examination of the experimental spectra none of the reported emissions for Cl_2, Cl_2^+, Br_2, Br_2^+, I_2, or I_2^+ were present (Refs 16, 27, and 51). Consequently, it is assumed that molecular emissions are insignificant in this experiment. Reaction (3) will be examined in the Further Analysis section of this chapter.

In the cases of Cl_2, Br_2, I_2 all of the charge transfer processes, reactions (4), (5) and (6), are exothermic by a much greater amount than the dissociation energy of the (X_2^+) molecule. The overall processes (including dissociation) for the three systems, when both He^+ and X_2 are at thermal energies, are exothermic as indicated

$$He^+ + Cl_2 \rightarrow He + Cl^+ + Cl + 9.09 \text{ eV} \qquad (8)$$

$$He^+ + Br_2 \rightarrow He + BR^+ + Br + 10.77 \text{ eV} \qquad (9)$$

$$He^+ + I_2 \rightarrow He + I^+ + I + 12.58 \text{ eV} \qquad (10)$$

Therefore there is a large amount of energy available in the charge transfer process for excitation of neutral atoms or atomic ions.

Reaction (7) is not considered significant. The observed emission lines are still present at He^+ ion energies of less than 10 eV. This is not enough energy to account for molecular dissociation and excitation of the neutral halogen atom to the excited energy levels detected in this experiment.

Line Identification

The experimental data obtained was in the form of low and high resolution spectra (see Figs. 21 through 25, 30 through 35, and 44 through 52), and measured emission cross section energy dependence curves (see Figs. 26, 27, 36 through 41, and 53 through 60). The analysis of the data began with an examination of the high resolution spectra to determine the observed peak center wavelengths (λ_0). Then using the instrument function for each λ_0, all of the observed peak intensities were normalized. By use of the measured cross section values of the more intense peaks as references, each observed wavelength was assigned a partial emission cross section value. Next the observed wavelength λ_0 values with a search interval of $\pm\Delta\lambda_0$ were matched (using a computer search program developed by Dr. Darrell Hopper (Ref 17) with allowed transitions between the energy levels of He I (Ref 42), Cl I (Ref 55), Cl II (Ref 56), Br I (Ref 68), Br II (Ref 58), I I (Refs 30 and 48), and I II (Ref 41). The selection criteria used in the search program were

1. $\Delta J = \pm 1, 0$ where $0 \not\leftrightarrow 0$
2. Change of parity
3. $\pm\Delta\lambda_0$ from observed peak center wavelength λ_0

These criteria are valid for LS, JJ or any intermediate type of coupling (Ref 36:271). The complete listings of transitions which meet these criteria are given in Tables XV, XVII, and XVII in Appendices A, B, and C.

The computer identification program can be used in various modes. In the search mode the program applies any or all of the selection criteria listed above to match the wavelengths of allowed transitions to the measured wavelengths λ_0 (see computer output in Fig. 19). For convenience in this discussion, these allowed transitions which meet the above criteria are called A type transitions. Included in this computer output is information as to the electronic configurations, the energy levels, and the J values of both the upper and lower energy states of each allowed A type transition. It also states the wavelength of each allowed A type transition and how closely it matches with the measured wavelength λ_0. The program can indicate the endothermicity of a particular A type transition for the given reaction. [Note it is not programmed to do this on the output in Fig. 19.]

The computer identification program can also be used in a mode where it will not only list the allowed A type transitions whose wavelengths match the measured wavelength λ_0, but also lists all of the allowed transitions from the populated upper energy state of the selected A type transition (see Fig. 20). For convenience these additionally listed transitions are called B type transitions. The electron configurations, energy levels, and J values are listed for all the lower energy levels of these B type transitions. In each case the wavelength for the allowed B type transition is listed.

04/15/75 12.54.42.

MATCHING OF OBSERVED TRANSITIONS ARISING FROM IMPACT OF AN EV HE+ BEAM
ON CL2 GAS: HE+(2S) + CL2(X1SI+) = HE (*) + 2CL/CL2 SEARCH OF HE I
= HE+(2S) + CL(*) + CL($) SEARCH OF CL I
= HE+(2S) + CL+(*) + CL-($) SEARCH OF CLII

HIGH RESOLUTION DATA

MATCH # 1 OBSERVED TRANSITION TO BE MATCHED -- 1088.00 ± 3.50 ANGSTROMS WITHIN 3.50 ANGSTROMS .

LOWER STATE NUMBER	CONFIGURATION	DESIGNATION	J	LEVEL(EV)	UPPER STATE NUMBER	CONFIGURATION	DESIGNATION	J	LEVEL(EV)	SMOOTH. LAMDA	DIFFERENCES (A) OBSVD	SAME OBSI
MATCHES FOR HE I .												
.....NONE FOUND.....												
MATCHES FOR CL I .												
1.	3P5 2P0	3P5 2P0	1.5	0.0000	136.	3P4(3P)3D4P	3D 4P	2.5	11.3641	11.364	1090.99	2.99
1.	3P5 2P0	3P5 2P0	1.5	0.0000	137.	3P4(3P)5S2(2)	5S2(2)	1.5	11.3666	11.367	1090.74	2.74
1.	3P5 2P0	3P5 2P0	1.5	0.0000	138.	3P4(3P)3D2F	3D 2F	2.5	11.3946	11.395	1088.06	.06
1.	3P5 2P0	3P5 2P0	1.5	0.0000	139.	3P4(3P)5S1(1)	5S1(1)	1.5	11.4235	11.424	1085.30	-2.73
1.	3P5 2P0	3P5 2P0	1.5	0.0000	140.	3P4(3P)5S1(1)	5S1(1)	.5	11.4243	11.425	1085.17	-2.83
1.	3P5 2P0	3P5 2P0	1.5	0.0000	141.	3P4(3P)3D2P	3D 2P	1.5	11.4302	11.430	1084.67	-3.33
2.	3P5 2P0	3P5 2P0	.5	.1094	142.	3P4(3P)5S0(0)	5S0(0)	.5	11.4403	11.441	1090.27	2.27
7 MATCHES FOUND												
MATCHES FOR CL II .												
5.	3P4 1S	3P4 1S	0.0	3.4563	167.	3P3(4S)3D3D0	3D 3D0	1.0	14.8582	14.858	1087.37	-.63
5.	3P4 1S	3P4 1S	0.0	3.4563	167.	3P3(2D)3D3D0	3D 3D0	1.0	14.8582	14.858	1087.37	-.63
147.	3S3P53P0	3P5 3P0	2.0	11.5757	138.	3P3(4S)4F5F	4F 5F	3.0	22.9504	22.950	1089.96	1.96
150.	3P3(2D)3D3P0	3D 3P0	2.0	11.5757	138.	3P3(4S)4F5F	4F 5F	3.0	22.9504	22.950	1089.96	1.96
147.	3S3P53P0	3P5 3P0	2.0	11.5757	139.	3P3(4S)4F5F	4F 5F	2.0	22.9504	22.950	1089.96	1.96
150.	3P3(2D)3D3P0	3D 3P0	2.0	11.5757	139.	3P3(4S)4F5F	4F 5F	2.0	22.9504	22.950	1089.96	1.96
147.	3S3P53P0	3P5 3P0	2.0	11.5757	141.	3P3(4S)4F3F	4F 3F	3.0	22.9536	22.954	1089.65	1.66
150.	3P3(2D)3D3P0	3D 3P0	2.0	11.5757	140.	3P3(4S)4F3F	4F 3F	3.0	22.9536	22.954	1089.65	1.66
8 MATCHES FOUND												

Fig. 19. Computer Listing of Allowed Transitions Matching Observed Lines.

04/15/76 12.53.52.

MATCHING OF OBSERVED TRANSITIONS ARISING FROM IMPACT OF AN EV HE+ BEAM
ON CL2 GAS: HE+(2S) + CL2(X1SI+) = HE (*) + 2CL/CL2 SEARCH OF HE I
= HE+(2S) + CL(*) + CL(*) SEARCH OF CL I
= HE+(2S) + CL+(*) + CL-(*) SEARCH OF CLII

HIGH RESOLUTION DATA

MATCH # 1 OBSERVED TRANSITION TO BE MATCHED -- 7414.00 ± 5.00 ANGSTROMS WITHIN 5.00 ANGSTROMS , CASCADED

LOWER STATE NUMBER	CONFIGURATION	DESIGNATION	J	LEVEL(EV)	UPPER STATE NUMBER	CONFIGURATION	DESIGNATION	J	LEVEL(EV)	ENDOTH.	DIFFERENCES (A) L&MDA	DL&MDA	SAME UPSI
MATCHES FOR HE I .													
.....NONE FOUND.....													
MATCHES FOR CL I .													
113.	3P4(3P)4S4P	4S	4P	2.5	8.9214	13.	3P4(3P)4P2P0	4P	2P0	1.5	10.5932	10.593	7416.16	2.16
113.	3P4(3P)4S4P	4S	4P	2.5	8.9214	MAY BE POPULATED FROM UPPER LEVEL 13 WITH A TRANSITION OF 7416.16 ANGSTROMS								
114.	3P4(3P)4S4P	4S	4P	1.5	8.9471	MAY BE POPULATED FROM UPPER LEVEL 13 WITH A TRANSITION OF 7719.71 ANGSTROMS								
115.	3P4(3P)4S4P	4S	4P	.5	9.0291	MAY BE POPULATED FROM UPPER LEVEL 13 WITH A TRANSITION OF 7926.82 ANGSTROMS								
116.	3P4(3P)4S2P	4S	2P	1.5	9.2025	MAY BE POPULATED FROM UPPER LEVEL 13 WITH A TRANSITION OF 8315.37 ANGSTROMS								
117.	3P4(3P)4S2P	4S	2P	.5	9.2918	MAY BE POPULATED FROM UPPER LEVEL 13 WITH A TRANSITION OF 9454.63 ANGSTROMS								
15.	3P4(3P)4P2S0	4P	2S0	.5	10.6521	16*.	3P4(3P)5D2(1)	5D2(1)		.5	12.3246	12.325	7412.91	-1.09
1.	3P5 2P0	3P5	2P0	1.5	0.0000	MAY BE POPULATED FROM UPPER LEVEL 16A WITH A TRANSITION OF 1005.96 ANGSTROMS								
2.	3P5 2P0	3P5	2P0	.5	.1004	MAY BE POPULATED FROM UPPER LEVEL 16A WITH A TRANSITION OF 1014.97 ANGSTROMS								
4.	3P4(3P)4P4P0	4P	4P0	1.5	10.3044	MAY BE POPULATED FROM UPPER LEVEL 16A WITH A TRANSITION OF 6147.64 ANGSTROMS								
5.	3P4(3P)4P4P0	4P	4P0	.5	10.3356	MAY BE POPULATED FROM UPPER LEVEL 16A WITH A TRANSITION OF 6233.26 ANGSTROMS								
8.	3P4(3P)4P4D0	4P	4D0	1.5	10.4745	MAY BE POPULATED FROM UPPER LEVEL 16A WITH A TRANSITION OF 6701.25 ANGSTROMS								
10.	3P4(3P)4P4D0	4P	4D0	.5	10.4907	MAY BE POPULATED FROM UPPER LEVEL 16A WITH A TRANSITION OF 6793.82 ANGSTROMS								
11.	3P4(3P)4P2D0	4P	2D0	1.5	10.5369	MAY BE POPULATED FROM UPPER LEVEL 16A WITH A TRANSITION OF 6935.09 ANGSTROMS								
12.	3P4(3P)4P2D0	4P	2D0	.5	10.5686	MAY BE POPULATED FROM UPPER LEVEL 16A WITH A TRANSITION OF 7061.36 ANGSTROMS								
13.	3P4(3P)4P2D0	4P	2D0	1.5	10.5932	MAY BE POPULATED FROM UPPER LEVEL 16A WITH A TRANSITION OF 7160.51 ANGSTROMS								
14.	3P4(3P)4P4S0	4P	4S0	1.5	10.6294	MAY BE POPULATED FROM UPPER LEVEL 16A WITH A TRANSITION OF 7313.78 ANGSTROMS								
15.	3P4(3P)4P2S0	4P	2S0	.5	10.6521	MAY BE POPULATED FROM UPPER LEVEL 16A WITH A TRANSITION OF 7412.91 ANGSTROMS								
2 MATCHES FOUND														
MATCHES FOR CL II .														
.....NONE FOUND.....														

Fig. 20. Computer Listing of Allowed Transitions Matching Observed Lines Plus Other Allowed Transitions from the Same Upper Energy Levels.

Further Analysis

Up to this point, the analysis described is firmly based on instrument resolution and quantum mechanical selection rules. Further considerations require the introduction of various assumptions.

An examination of Tables XV, XVI, and XVII reveals a number of lines which could be assigned to allowed He I transitions. It is noticed that these transitions are all in the 400 nm to 870 nm region and are between the higher He I energy levels. If these transitions do originate from He I, then transitions from these upper levels to the ground state should also be observed, but in fact, none are detected. This situation prevails in all of the results from studies of reactions of He^+ with Cl_2, Br_2, and I_2, as well as for reactions of He^+ with H_2, Ar, Kr, and Xe, studied by Hughes, Jones, and Tiernan (Refs 18, 10, 20, 21 and 28). Also all lines observed which could be assigned to He I transitions can also be assigned to other processes. All of the processes leading to the He I transitions in the upper levels are highly endothermic (in the neighborhood of 15 eV), and the energy dependence curves obtained for emission lines which might originate from He I all have thresholds below 10 eV. For these several reasons, the author assumes that no significant He I transitions [reactions (3) and (4)] are actually observed in the present experiments.

If a light-emission experiment were performed in a field-free environment the ratio of the actual intensities

of the transitions from a particular energy state should be the same as the ratio of the theoretical A factors (transition probabilities) for the respective transitions from that particular energy state. The He^+/halogen experiments are conducted in such a field-free environment and it is therefore assumed that the normalized relative intensities of the observed emissions should be in good agreement with the A factors for these transitions. Unfortunately A factors are available for only a very small number of the transitions observed in our study (Refs 2 and 35). There is a great deal of difficulty in performing an experiment to accurately measure A factors. The most commonly accepted method of measuring A factors is with shock tube experiments. In these experiments errors of less than 50% are considered very good results. In order to do any furhter analysis, it is thus necessary to make several assumptions. The author feels it is justifiable to compare the ratio of relative intensities reported in the literature (obtained from discharge experiments) with the ratios of relative intensities in the He^+/halogen experiments, provided that certain precautions are made.

The change in the emission intensity of a transition caused by the presence of an electric field is dependent upon the extent to which the transition matrix is perturbed by the electric field. The extent to which this perturbation affects the intensity of the other possible transitions from the same energy level is dependent upon the total number of

transitions possible from that particular upper energy level. For neutral halogen atoms radiating from low energy states to the ground state there are usually only two transitions possible. If one transition matrix is greatly perturbed, the intensity of the other transition will also be affected. The ratio of the two lines can therefore be greatly affected. This is the case in the VUV region. In the visible and near infrared region, where there are many possible transitions between the higher level energy states, the perturbing of one particular transition matrix has less effect on the other possible transitions.

In such an approach, the next step is to use the computer search program in a form in which it will not only list the allowed type A transitions using the original resolution and quantum mechanical criteria, but will also list the other transitions (including their wavelengths) which are quantum mechanically allowed from the upper energy level of each of these type A transitions. These other transitions are called type B transitions in the present discussion. A sample page of the computer output from this type of search is given in Fig. 20. In Fig. 20 the A type transitions have wavelengths of 7416.16Å and 7412.91Å. All the other listed transitions are type B transitions. These wavelengths can now be compared with the wavelengths and intensities previously tabulated in the literature for the excited neutral atoms X I (Refs 30, 48, 55 and 68), and for the excited atomic ions X II (Refs 41, 56 and 58).

It should be noted that the optical resolution was much higher for the experiments which yielded the tabulated energy level data than the resolution in the present He^+/halogen experiments.

The following criteria were established to aid in assignment of the transitions for the measured line wavelengths (λ_0).

1. If a particular type A transition and all of its associated type B transitions were not reported in the tabulated literature data and none of the type B transitions were observed in the He^+/halogen experiment, then that particular type A transition was eliminated. For the example shown in Fig. 20, this means that if the 7412.91Å and all of its associated type B transitions (1005.96Å, etc.) were not observed in the discharge experiment in Ref 55, and if none of the type B transitions (1005.96Å, etc.) were observed in the He^+/halogen experiment; then the 7412.91Å wavelength of the $4p\ ^2S^0_{1/2} \leftarrow 5d\ 2(1)_{1/2}$ transition would be eliminated as a possible match for the λ_0 value of 7414.00Å.

2. In the 400 nm to 870 nm region the additional criterion is used: If in the discharge experiment a particular type B transition was much more intense than the type A transition with which it was associated, and in the He^+/halogen experiment that particular type B transition was less intense than the type A transition, then that particular type A transition was eliminated. For the example shown in Fig. 20, this means that if in the literature tables the

7313.78Å line of the $4p\ {}^4S^0_{3/2} \leftarrow 5d\ 2(1)_{1/2}$ transition was much more intense than the 7412.91Å line of the $4p\ {}^2S^0_{1/2} \leftarrow 5d\ 2(1)_{1/2}$ transition, and the 7313.78Å line was much less intense than the 7414.00Å line in the He^+/halogen experiment, then the 7412.91Å wavelength of the $4p\ {}^2S^0_{1/2} \leftarrow 5d\ 2(1)_{1/2}$ transition would be eliminated as a possible match for the λ_0 value of 7414.00Å.

Another criterion that was used was that if the energy dependence curve for a particular λ_0 was exothermic and only one of the type A transitions matching that λ_0 was exothermic; then that type A transition was selected as the assigned transition.

It would be well here to explain what is meant by exothermic and endothermic reaction energy dependence curves. Examination of the cross section energy dependence curve can help to determine whether the reaction causing the observed radiation is endothermic or exothermic. The characteristic shape of endothermic reaction energy dependence curves is a threshold somewhere above thermal energies and the curve increases in value with an increase of energy until it reaches a leveling off point. (Actually a true endothermic reaction energy dependence curve would have a step function profile with the threshold at the value of the energy necessary to be added to thermal reactants for the endothermic reaction to occur.) A typical example of the profile of an endothermic reaction energy dependence curve is illustrated by the 821.7 and 822.4 nm emission lines in Fig. 27. Exothermic reaction energy

dependence curves have the characteristic profile of small values at higher energies and rapidly increasing in value as thermal energies are approached. A typical example of the profile of an exothermic reaction energy dependence curve is illustrated by the 178.23 nm emission line in Fig. 54.

After applying these criteria to the total list of type A transitions for the He^+/Cl_2 and He^+/Br_2 experiments it was found that over 80% of the total emission lines could be assigned to specific transitions (Tables V and IX). These transition assignments are then used to construct a term diagram (Figs. 28 and 42). Next each energy level on the term diagram is individually examined to determine whether that state is predominantly directly excited or populated primarily by cascading from higher energy states (Tables VI and X).

A plot of the emission cross sections and of the direct excitation cross sections as a function of the energy levels of the populated energy states provides an indication of the energy partitioning in these reactions (Figs. 29 and 43).

Error Analysis

The accuracy of the 100 eV cross sections reported in this experiment vary. As noted before, the emission cross section is given by

$$\sigma = \frac{4\pi R_o T_o N_R}{P\ell N_A I \Omega g_\perp F(\lambda)} \qquad (6)$$

where the symbols are defined in Table I. The maximum temperature T_o variation is 1% so it will be considered a constant.

Relative Cross Sections. When referring to the accuracy of relative cross sections it is necessary to consider only the variables appearing in the expression, $\frac{N_R}{PIF(\lambda)}$. The accuracy of N_R depends on the signal to noise ratio. For very intense peaks it is very accurate (to within ±5%) and for very weak peaks it can be accurate to within ±50%. The accuracy of N_R also depends upon how many measurements were taken. Because more measurements were taken, the cross sections measured for the energy dependence curves are generally more accurate than the cross sections calculated from the peak heights in scans. The 100 eV He^+ ion beam cross-section measurements for the energy dependence curves have a sampling accuracy of within ±5%. Even the 5 eV He^+ ion beam cross-section measurements for the more intense peaks generally have a sampling accuracy of within ±10% to ±15%. Occasionally the statistical error increases to ±30%. Of course the cross section measurements for the weaker emissions obtained only from spectral scans, have a greater statistical error. The relative pressure P has a 5% or less error. The relative current I could have errors of 10 to 20%. The error in the relative instrument function $F(\lambda)$ in the visible region is less than 10% and as explained in Chapter II could be as high as 200% in the VUV region. The relative cross-section measurements in this experiment are consistent with

present published work using ion beam experiments for similar reactions.

Absolute Cross Sections. In absolute cross section measurements, the systematic errors no longer cancel out. Such things as the exact length of the collision region are difficult to measure. Also the beam is not uniform over the area of the collision region, although this error appears not to be large since an ion beam on the order of 1 nA is measured with the collision chamber having a 1 mm slit and an ion beam on the order of 0.1 nA is measured with the collision chamber having a 0.1 mm slit. For the stronger peaks, the accuracy is believed to be within a factor of 4 in the 400 nm to 870 nm region and a factor of 8 in the VUV. Because of the difficulties in the accurate measurements of the ion beam above 110 eV and below 20 eV the error in the measurement of absolute cross sections in these regions can be very large. The consistency of the cross section measurements is very good, even with the use of different detectors. This is illustrated in Fig. 55, where the cross section measurements for the production of the 145.7 nm iodine emission line vary up to ±40% on three separate days with two different detectors. In Fig. 56 the cross section measurements for the intense 183.0 nm iodine emission line vary generally less than ±15%. The 183.0 nm line measurements were made on two separate days using two different detectors.

V. Chlorine

Introduction

The general outline of the next three chapters follows the data analysis procedures described in Chapter IV. First the experimental data is presented in the form of the spectra obtained in the experiment and curves showing the He^+ ion translational energy dependence of some of the measured emission cross sections. Complete listings of the measured cross sections of all of the observed emission lines are given in the tables in the appendices. These tables include the measured cross sections of each emission line and a listing of all of the allowed transition assignments for each emission line which meet the measurement uncertainty $\Delta\lambda_0$ and quantum-mechanical criteria stated in Chapter IV. Other detailed information for each allowed transition is given in these tables. A summary of the tables in the appendices is then presented in the text depicting important general features of the reaction. In the case of chlorine and bromine, further analysis is conducted resulting in term diagrams and graphs which give further insight into the reactions.

All of the spectra illustrated in this chapter and all of the cross sections listed in the tables of this chapter, were obtained from the reaction of 100 eV He^+ ions with Cl_2 at room temperature. The translational energy of the He^+ ions was varied only in the measurements of the energy dependence of the cross sections depicted in Figs. 26 and 27.

Spectra

The 35 measureable chlorine emission lines observed in the 60 nm to 870 nm wavelength region are presented in Figs. 21 to 25. A high resolution spectrum of the 96 nm to 120 nm VUV region is shown in Fig. 21. Figures 22 and 23 depict examples of low and high resolution spectra of the 100 nm to 145 nm VUV region. The remaining spectra in Figs. 24 and 25 are high resolution spectra in the 720 nm to 860 nm region.

Cross Section Energy Dependence Curves

The curves in Figs. 26 and 27 depicting the energy dependence of the chlorine cross sections, were obtained from measurements made under low resolution conditions. The wavelengths assigned to each curve are the observed wavelengths at high resolution. It should be noted again that cross section measurements using this instrument are most accurate in the 100 eV region. In the 120 eV to 170 eV region not all of the ions can be collected on the ion collector so the actual cross section values are probably greater than the measured values in this energy region. In the 0 eV to 20 eV region the ion beam starts to diverge and is difficult to focus. Consequently, the size of the ion beam drops off, increasing the % error in the ion beam measurement. The curves indicate that all of the lines except the 137.93 nm, 138.98, and 139.58 nm curve are produced by endothermic processes with low thresholds in the 0 eV to 5 eV region.

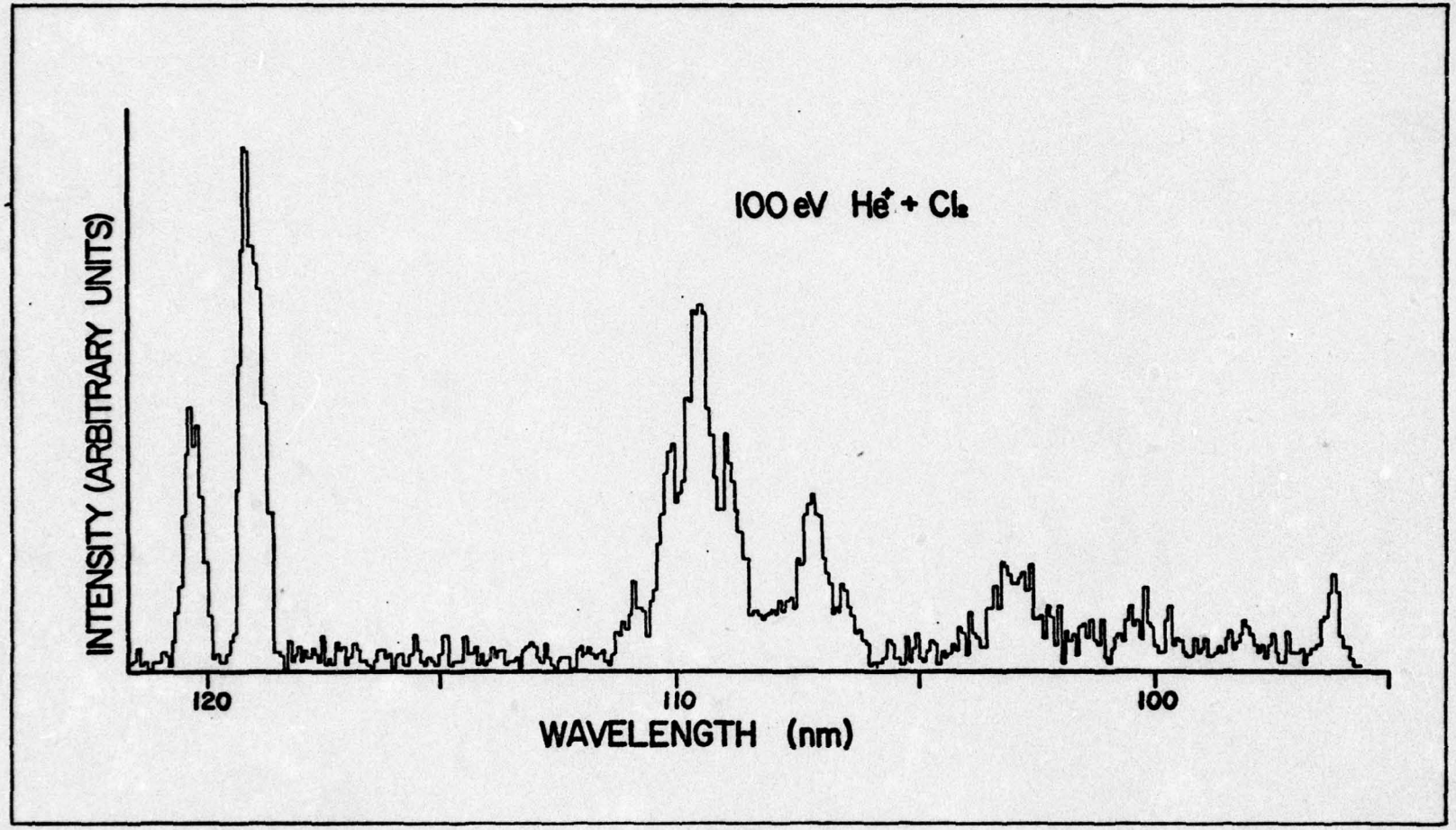

Fig. 21. High Resolution Spectra of 100 eV He^+ Cl_2 Reaction in 95 nm to 122 nm Region.

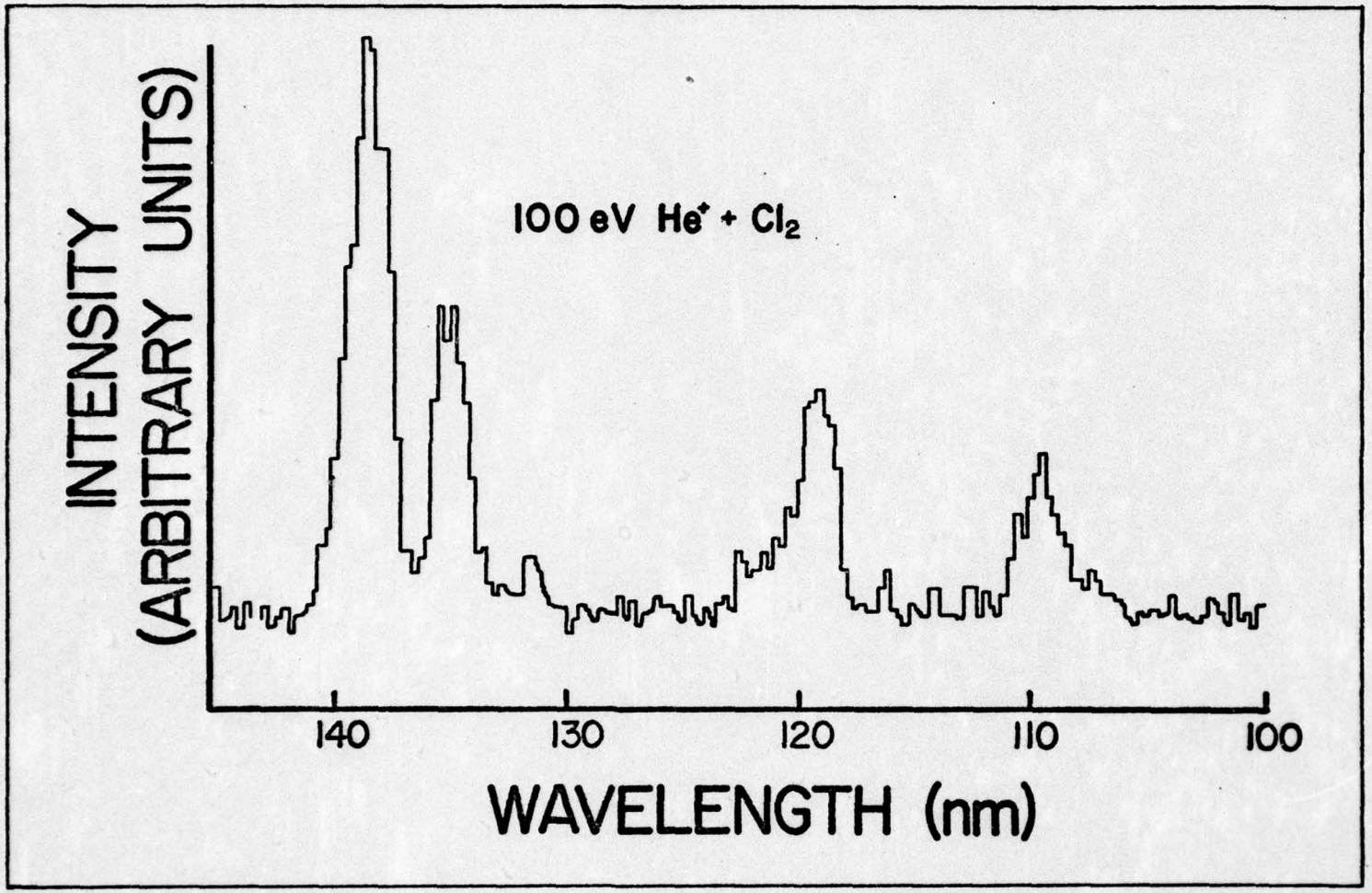

Fig. 22. Low Resolution Spectra of 100 eV He^+ + Cl_2 Reaction in 100 nm to 145 nm Region.

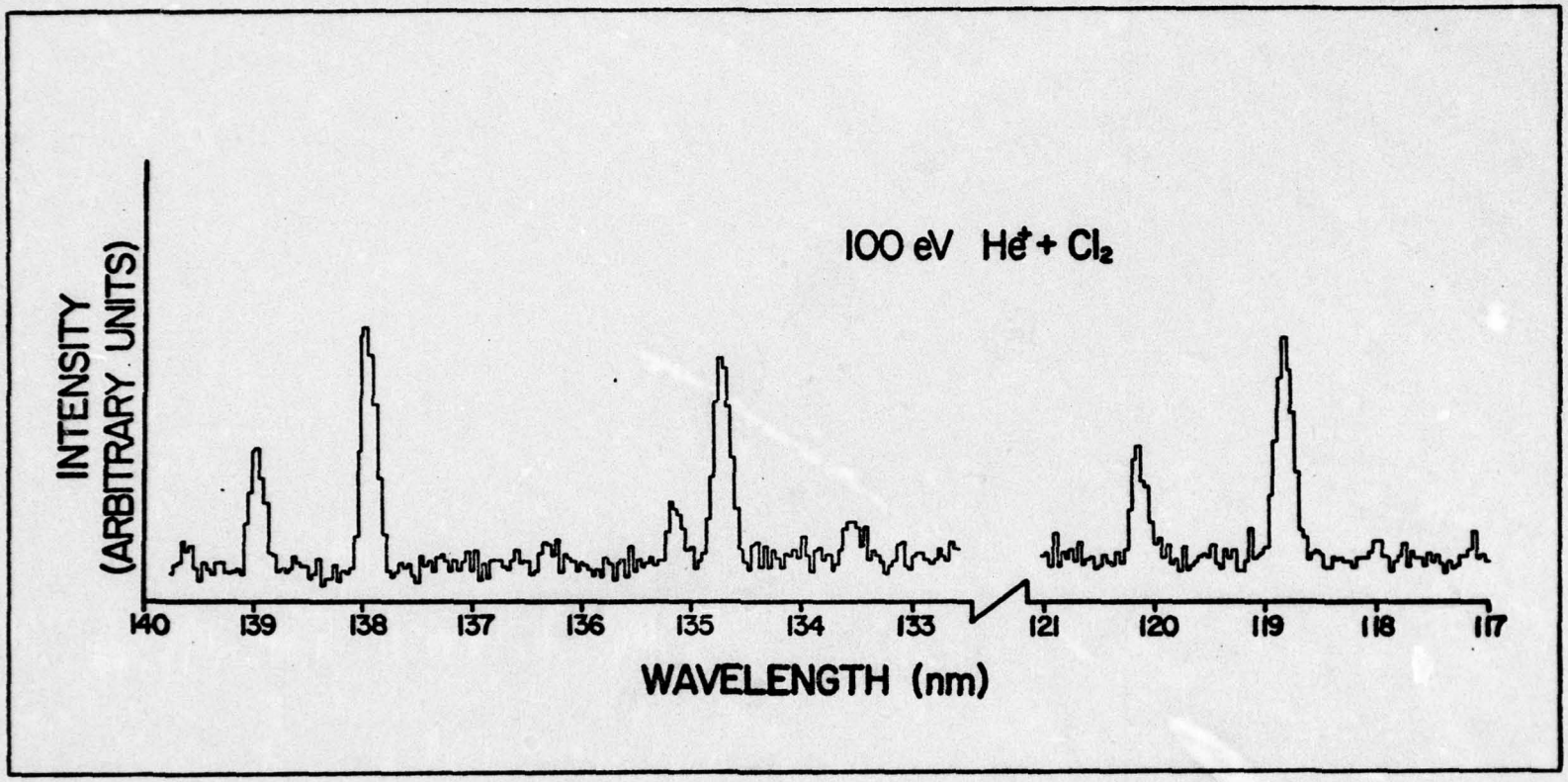

Fig. 23. High Resolution Spectra of 100 eV He^+ + Cl_2 Reaction in 117 nm to 140 nm Region.

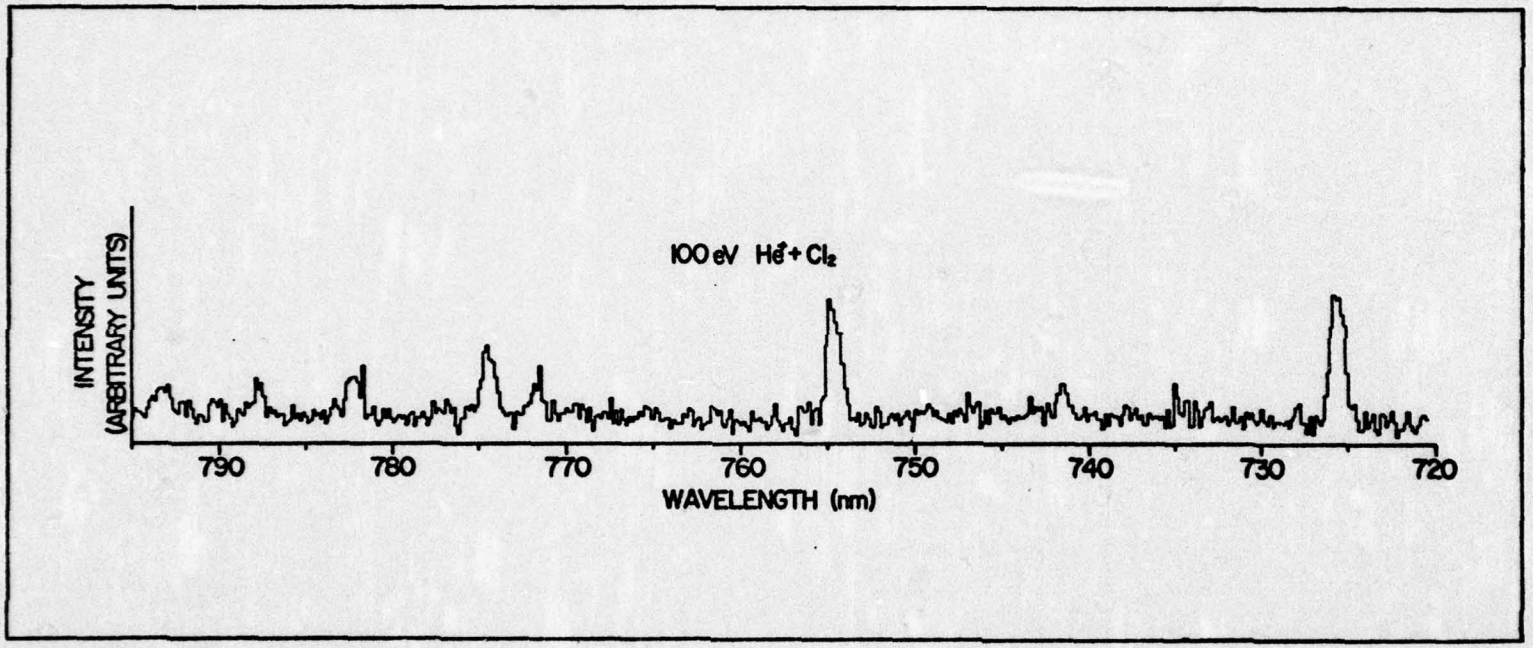

Fig. 24. High Resolution Spectra of 100 eV He^+ + Cl_2 Reaction in 720 nm to 795 nm Region.

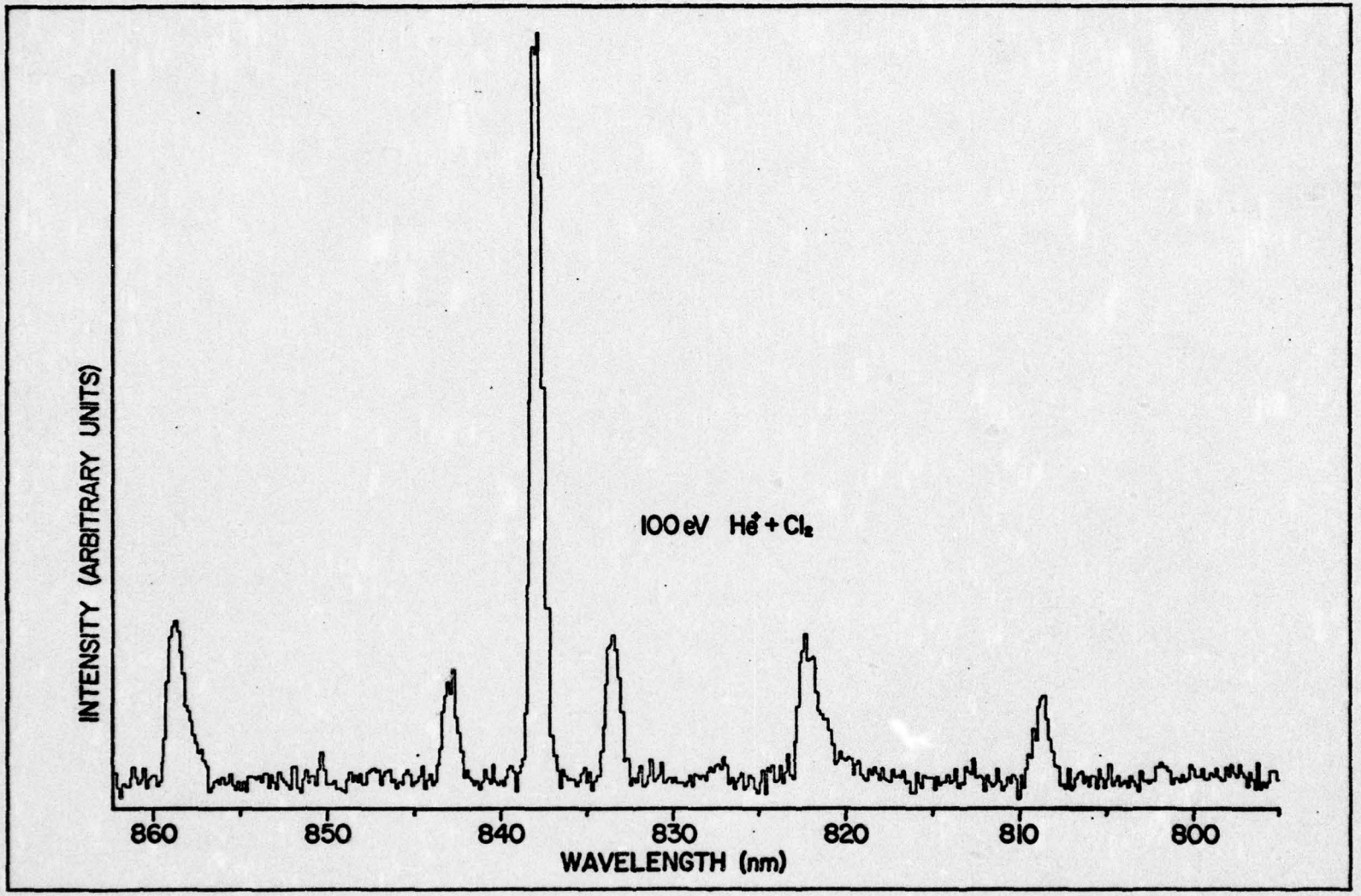

Fig. 25. High Resolution Spectra of 100 eV He^+ + Cl_2 Reaction in 795 nm to 865 nm Region.

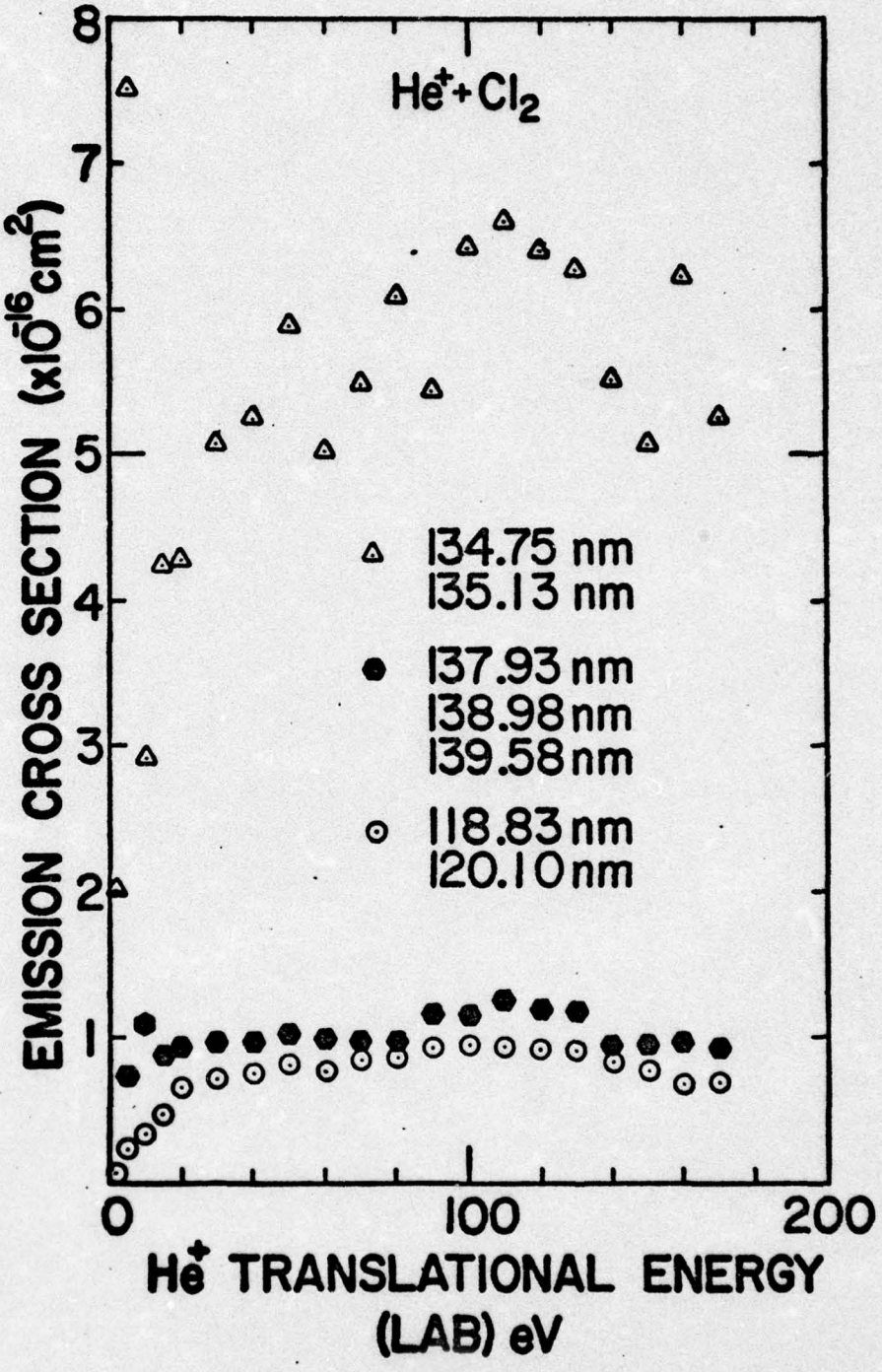

Fig. 26. The Energy Dependence of the Emission Cross Sections of Selected VUV Lines from the $He^+ + Cl_2$ Reaction.

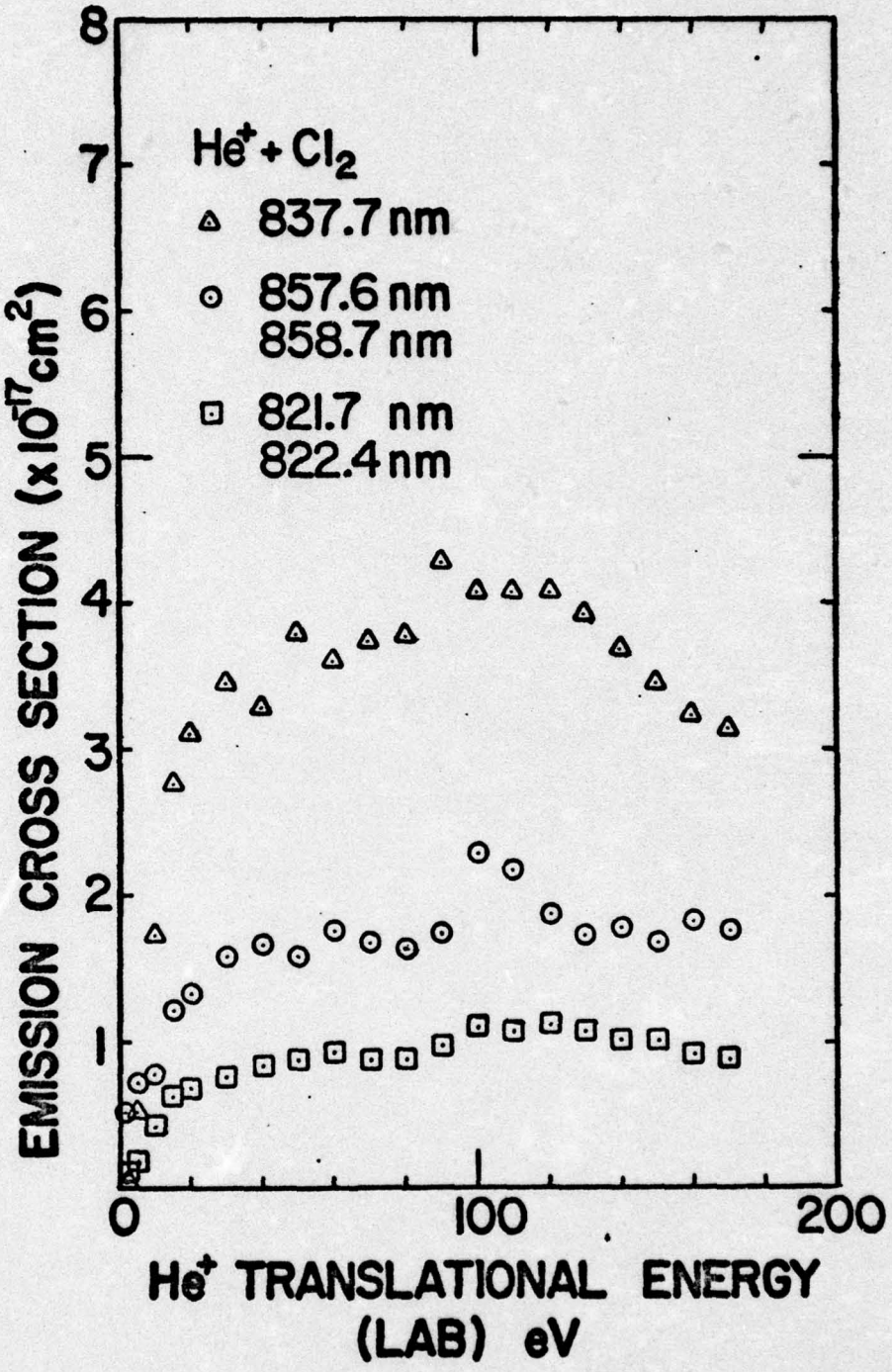

Fig. 27. The Energy Dependence of the Emission Cross Sections of Selected Lines from the $He^+ + Cl_2$ Reaction.

The uncertainties listed above, plus the limited 0 eV to 170 eV energy region, preclude extensive analysis as to structure and oscillations being present in the curves. The structure and oscillations of the cross section energy dependence curves discussed in the investigations of He^+-rare gas systems extended over the 0 eV to 10 keV energy region (Refs 5, 8, 9, 24, 38, 59, and 60). The 0 eV to 170 eV energy range is too limited to interpret separately. The data is presented here to aid in the selection of transition assignments and for completeness. As in the case of the He^+-rare gas studies, these curves could be used in conjunction with other studies in higher energy regions for a more complete analysis of the kinetic energy behavior of the reaction.

Line Identification

A listing of all of the allowed transitions which meet the measurement uncertainty $\Delta\lambda_0$ and quantum-mechanical criteria explained in Chapter IV for each observed wavelength λ_0 in the spectra, are listed in Table XV in Appendix A. The measured cross-section for each observed wavelength is also listed. The endothermicity in eV (for thermal energy reactants) is listed for each allowed transition's upper state. This endothermicity is measured above and below the 9.09 eV energy released by the thermal energy charge exchange reaction between He^+ and Cl_2. Of course there are 100 eV of translational energy of the He^+ ion available in the collision process for possible conversion to excitational energy

of the product species. One goal of the present experiment is to determine if this translational energy conversion is very efficient in the 100 eV He^+/Cl_2, Br_2, and I_2 reactions. Comparison of the energy level of the upper radiating energy states with the energy available from thermal energy charge transfer is an aid in determining whether the dominant excitation mechanism for the product species is charge exchange or conversion of translational energy. It should be noted that the 438.0 nm and 579.6 nm observed wavelengths were very weak peaks observed only on low resolution scans. They are included for completeness.

Further Analysis

Table IV is a summary of the complete listings in Table XV. It is noteworthy that the 497.0×10^{-18} cm^2 total emission cross-section is very large and that 76% of the total cross section is accounted for by the 17 observed VUV lines. Since 23 lines match both allowed Cl I and Cl II transitions, it is evident that further analysis is necessary.

Application of the relative intensity criteria described in Chapter IV on the allowed transitions listed in Table XV revealed that the reaction yields emission arising predominantly from Cl I. The resulting Cl I transition assignments are listed in Table V. They account for 85% of the total 483.7×10^{-18} cm^2 emission cross section of the lines listed in Table XV having possible Cl I transition assignments. A large number of the transitions which were eliminated by the relative intensity criteria violate the conservation of

Table IV

Summary of 100 eV $He^+ + Cl_2$ Reaction Allowed Transitions Selected by the Computer Search Program

Classification of Allowed Transitions Listed in Computer Search	Number of Lines	$\sum\sigma$ ($\times 10^{-18}$ cm^2)	$\frac{\sum\sigma}{\sum_{Total}\sigma}$	Number of VUV Lines	$\sum_{VUV}\sigma$ ($\times 10^{-18}$ cm^2)	$\frac{\sum_{VUV}\sigma}{\sum_{Total}\sigma_{VUV}}$	Number of Visible Lines	$\sum_{Visible}\sigma$ ($\times 10^{-18}$ cm^2)	$\frac{\sum_{Visible}\sigma}{\sum_{Total}\sigma_{Visible}}$
Cl I	9	63.5	0.13	6	56.7	0.15	3	6.8	0.06
Cl II	3	13.3	0.03	3	13.3	0.04	0	---	---
Cl I and Cl II	23	420.2	0.85	8	305.9	0.81	15	114.3	0.94
Total	35	497.0		17	375.9		18	121.1	
					76% of $\sum_{Total}\sigma$			24% of $\sum_{Total}\sigma$	

Table V

Cl I Transition Assignments for the 100 eV $He^+ + Cl_2$ Reaction

λ_T[a] (nm)	Transition Assignment Lower ← Upper	ΔH[b] (eV)	σ[c] ($cm^2 \times 10^{18}$)
118.875	$3p^5\ ^2P^o_{3/2} \leftarrow 4s'\ ^2D_{3/2}$	1.34	61.9
118.877	$3p^5\ ^2P^o_{3/2} \leftarrow 4s'\ ^2D_{5/2}$	1.34	
120.135	$3p^5\ ^2P^o_{1/2} \leftarrow 4s'\ ^2D_{3/2}$	1.34	33.4
133.573	$3p^5\ ^2P^o_{3/2} \leftarrow 4s\ ^2P_{1/2}$	0.19	9.2
134.724	$3p^5\ ^2P^o_{3/2} \leftarrow 4s\ ^2P_{3/2}$	0.11	45.6
135.166	$3p^5\ ^2P^o_{1/2} \leftarrow 4s\ ^2P_{1/2}$	0.19	11.9
136.345	$3p^5\ ^2P^o_{1/2} \leftarrow 4s\ ^2P_{3/2}$	0.11	13.8
137.953	$3p^5\ ^2P^o_{3/2} \leftarrow 4s\ ^4P_{3/2}$	-0.10	73.0
138.969	$3p^5\ ^2P^o_{3/2} \leftarrow 4s\ ^4P_{5/2}$	-0.17	47.9
138.996	$3p^5\ ^2P^o_{1/2} \leftarrow 4s\ ^4P_{1/2}$	-0.06	
139.653	$3p^5\ ^2P^o_{1/2} \leftarrow 4s\ ^4P_{3/2}$	-0.10	5.4
725.862	$4s\ ^4P_{5/2} \leftarrow 4p\ ^4S^o_{3/2}$	1.54	5.7
741.616	$4s\ ^4P_{5/2} \leftarrow 4p\ ^2P^o_{3/2}$	1.50	1.6
754.915	$4s\ ^4P_{3/2} \leftarrow 4p\ ^4S^o_{3/2}$	1.54	6.1
771.971	$4s\ ^4P_{3/2} \leftarrow 4p\ ^2P^o_{3/2}$	1.50	1.5
774.710	$4s\ ^4P_{1/2} \leftarrow 4p\ ^4S^o_{3/2}$	1.54	3.2
782.351	$4p\ ^4P^o_{5/2} \leftarrow 4d\ 2(3)_{7/2}$	2.78	2.0
788.038	$4s\ ^4P_{5/2} \leftarrow 4p\ ^2D^o_{5/2}$	1.40	1.5
821.430	$4s\ ^4P_{5/2} \leftarrow 4p\ ^4D^o_{5/2}$	1.34	3.3
822.400	$4s\ ^4P_{3/2} \leftarrow 4p\ ^2D^o_{5/2}$	1.40	7.7

Table V (continued)

Cl I Transition Assignments for the 100 eV $He^+ + Cl_2$ Reaction

λ_T[a] (nm)	Transition Assignment Lower ← Upper	ΔH[b] (eV)	σ[c] ($cm^2 \times 10^{18}$)
833.560	$4s\ ^4P_{3/2} \leftarrow 4p\ ^4D^o_{3/2}$	1.38	7.6
837.824	$4s\ ^4P_{5/2} \leftarrow 4p\ ^4D^o_{7/2}$	1.31	40.7
843.057	$4s\ ^4P_{1/2} \leftarrow 4p\ ^4D^o_{1/2}$	1.41	5.6
857.760	$4s\ ^4P_{1/2} \leftarrow 4p\ ^4D^o_{3/2}$	1.38	8.9
858.834	$4s\ ^4P_{3/2} \leftarrow 4p\ ^4D^o_{5/2}$	1.34	14.0
			411.5

[a] Calculated vacuum wavelength using the energy level tables (Ref. 55).

[b] Enthalpy change required to populate the upper energy state for the thermal reaction $He^+ + Cl_2 \rightarrow He + Cl^+ + Cl^*$.

[c] Emission cross section for 100 $He^+ + Cl_2$ reaction.

spin $\Delta S = 0$ and the conservation of angular momentum $\Delta L = \pm 1, 0$ selection rules of LS coupling (Ref 36:271). For example, the computer search program has listed the Cl II $4s\ ^3S^0_1 \leftarrow 8f\ ^5F_2$ transition as an allowed transition for the observed 137.925 nm emission line. This transition violates both the conservation of spin and conservation of momentum rules of LS coupling. Since chlorine is a relatively light atom, a large amount of LS coupling would be expected. This agreement is a further supportive check of the selection criteria.

A term diagram illustrating the assigned Cl I transitions in Table V is shown in Fig. 28. The total emission cross section of each energy state is shown in parentheses, next to the energy state designation. The small numbers next to each energy level are the $2J + 1$ values for that specific energy level. The energy available from the thermal charge transfer process is indicated by a dashed line. Only the $4s\ ^4P$ state is a low enough energy level to be populated exclusively by the 9.09 eV available from the thermal charge transfer process. There must be a conversion of up to 1.5 eV of the kinetic energy of the incident He^+ ion to populate the upper states depicted on the term diagram. This explains the endothermic reaction profiles of the cross section energy dependence curves. This also explains the smaller cross sections of the high level energy states. Since the lowest energy state of Cl II is about 2.5 eV endothermic, this also explains why few ionic transitions are observed.

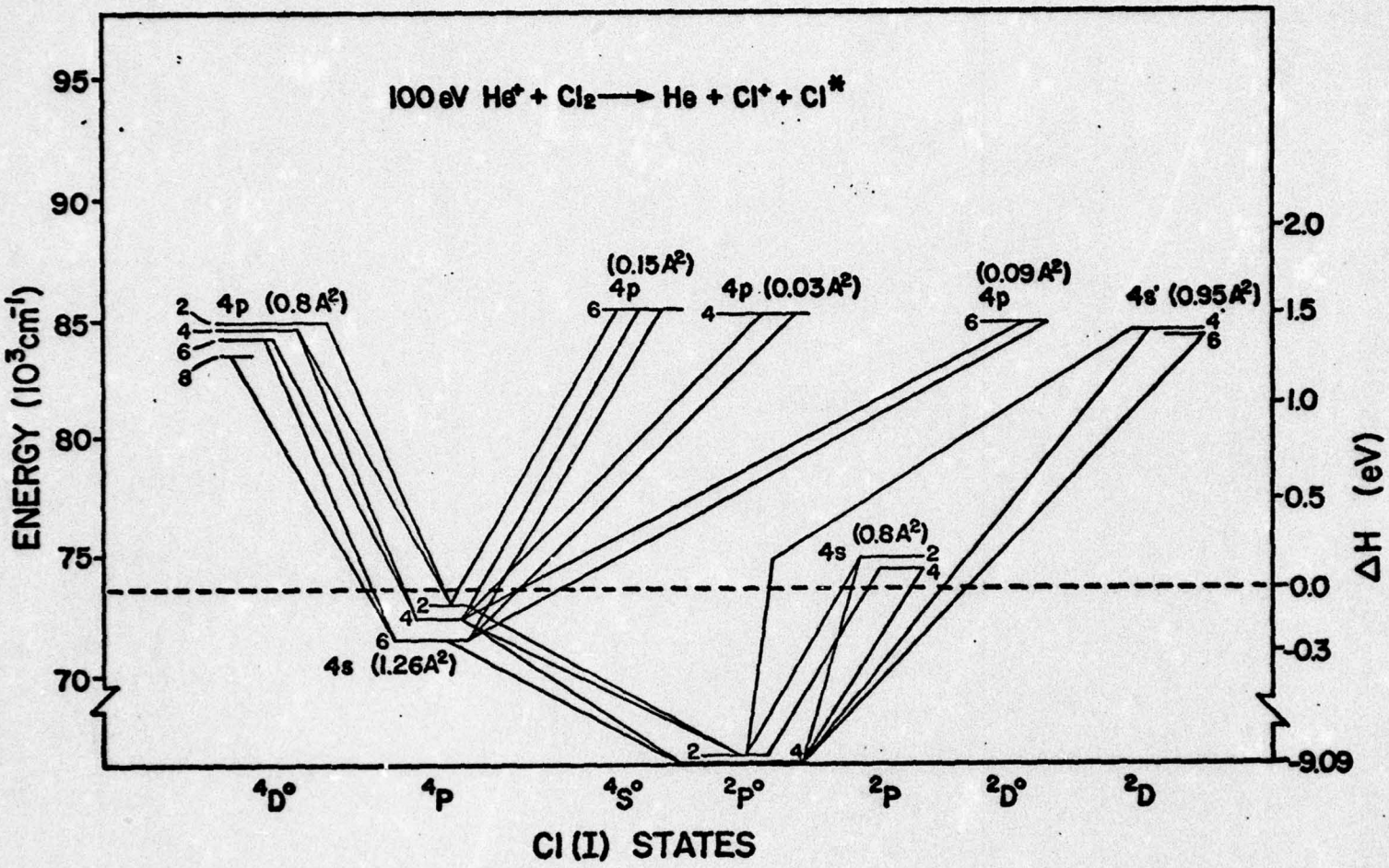

Fig. 28. Cl I Term Diagram for 100 eV He^+ + Cl_2 Reaction.

Another interesting observation in Fig. 28 is that there are three cases of violation of spin ($\Delta S = 0$) for LS coupling. The $4s\ ^4P \leftarrow 4p\ ^2P^o$ and $4s\ ^4P \leftarrow 4p\ ^2D^o$ transitions are explainable since they have small emission cross sections (0.03 A^2 and 0.09 A^2 respectively). Although the chlorine atom is relatively light, it is heavy enough not to be a perfect model for LS coupling. The $3p^5\ ^2P^o \leftarrow 4s\ ^4P$ transition is at first puzzling, because this transition has the largest emission cross section on the term diagram. The most reasonable explanation is that the $4s\ ^4P$ state is the lowest even energy state in the neutral chlorine atom, and the only radiative transition for decay is to the $3p^5\ ^2P^o$ ground state. This means that is is possible the $4p\ ^4P$ state has a longer lifetime than the upper states of the transitions cascading into the $4s\ ^4P$ state. If the ratio of these lifetimes is a factor of ten or greater, it may be possible that a properly designed chlorine laser would radiate in the VUV at 137.953 nm, 138.969 nm, 138.99 nm or 139.653 nm.

The results of examining each energy level in the Cl I term diagram to determine its direct excitation cross section are listed in Table VI. This is done by subtracting the sum of the cross sections of the transitions having this energy level as a lower energy state, from the sum of the cross sections of transitions having this energy level as an upper energy state. The results are that the total direct formation cross section is 326.7×10^{-18} cm^2, which is 79% of the

Table VI

Emission and Cascading Cross Sections for Cl I States Observed in the 100 eV $He^+ + Cl_2$ Reactions

Cl I State Designation	ΔH^2 (eV)	Cross Section ($cm^2 \times 10^{18}$) Total Emission	Cascading	Direct Formation
$3p^4$ 4s $^2P_{1/2}$	0.19	21.1	--	21.1
4s $^2P_{3/2}$	0.11	59.4	--	59.4
4s $^4P_{1/2}$	-0.06	47.9	70.5	-22.6
4s $^4P_{5/2}$	-0.17			
4s $^4P_{3/2}$	-0.10	78.4	36.9	41.5
4s' $^2D_{3/2}$	1.34	95.3	--	95.3
4s' $^2D_{5/2}$	1.34			
4p $^4S^o_{3/2}$	1.54	15.0	--	15.0
4p $^2P^o_{3/2}$	1.50	3.1	--	3.1
4p $^4P^o_{5/2}$	1.19	--*	2.0	-2.0
4p $^2D^o_{5/2}$	1.40	9.2	--	9.2
4p $^4D^o_{1/2}$	1.41	5.6	--	5.6
4p $^4D^o_{3/2}$	1.38	16.5	--	16.5
4p $^4D^o_{5/2}$	1.34	17.3	--	17.3
4p $^4D^o_{7/2}$	1.31	40.7	--	40.7
4d $^2(3)_{7/2}$	2.78	2.0	--	2.0
		411.5		326.7[b]

*Note: 4p $^4P^o_{1/2,3/2,5/2}$ states radiate outside wavelength range of detector.

[a]Enthalpy change required to populate this energy state for the thermal reaction $He^+ + Cl_2 \rightarrow He + Cl^+ + Cl^*$ (the first radiating Cl^+ state is 2.43 eV endothermic).

[b]This total does not include the negative direct formation cross sections in this column.

AD-A034 035 AIR FORCE INST OF TECH WRIGHT-PATTERSON AFB OHIO SCH--ETC F/G 20/8
EMISSION CROSS-SECTION MEASUREMENTS OF LOW ENERGY HE(+) IONS WI--ETC(U)
SEP 76 K E SIEGENTHALER

UNCLASSIFIED DS/PH/76-2 NL

2 OF 4
AD
A034035

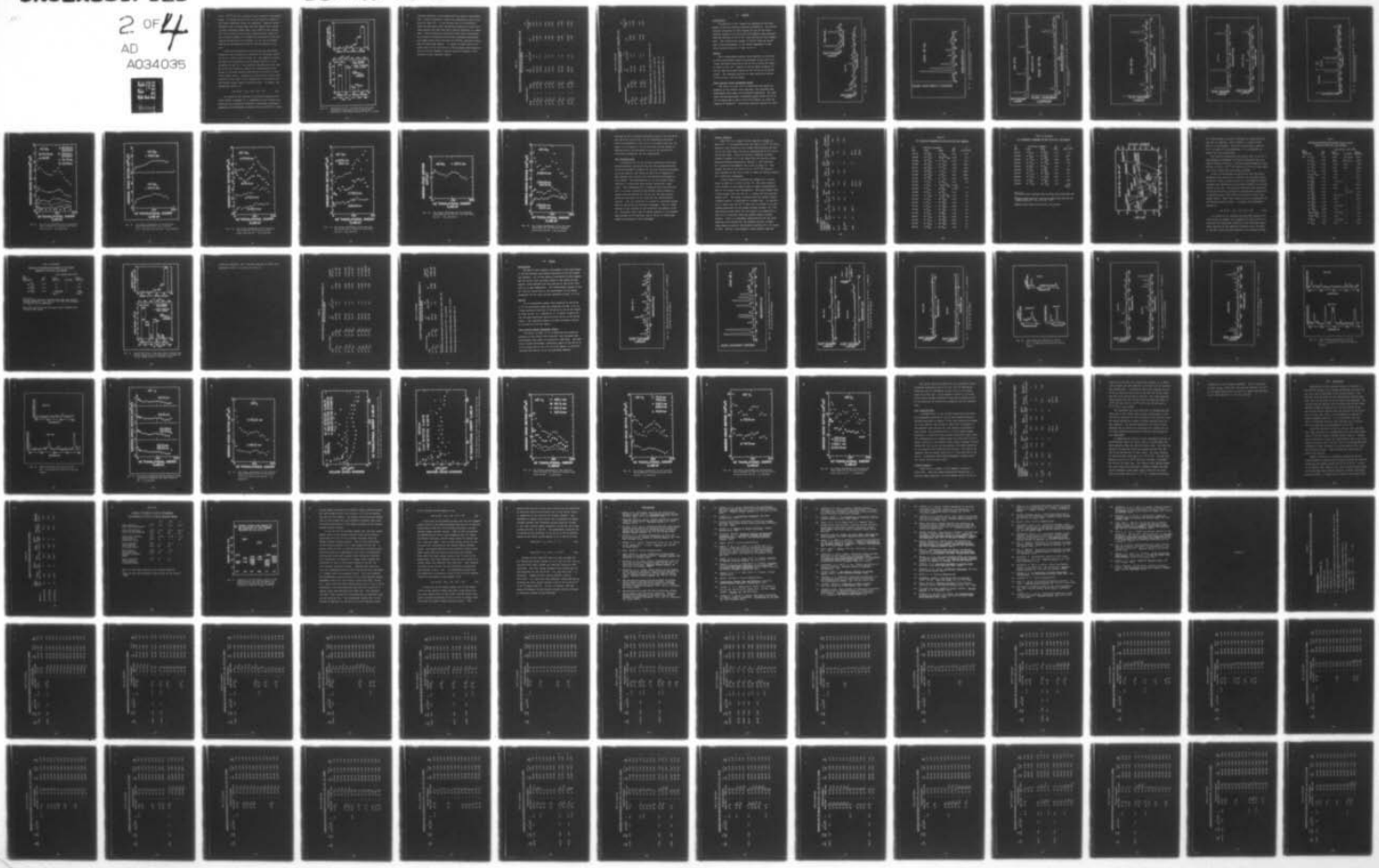


OF 4
34035

411.5 x 10^{-18} cm^2 total emission cross section of the neutral model. It should be noted that the two negative numbers in the direct formation column are neglected. Negative direct formation cross sections mean that the energy level either, (1) has a lifetime longer than 1 μsec which is the average time for an atom to stay in the collision focal region of the collision chamber, (2) decays in a radiative region outside of the 50 nm to 870 nm region, or (3) the instrument function of the apparatus used for the VUV region is too low.

A plot of the emission cross sections and the direct formation cross sections as a function of the energy levels of the Cl I atom is given in Fig. 29. The number of states available for population in each energy interval is also presented in Fig. 29. This analysis indicates that the energy of the 100 eV He^+/Cl_2 reaction is predominantly transferred to chlorine neutral atoms which are excited to their lower energy states. Formation of these states requires the addition of less than 2 eV of energy than is available from the thermal energy charge transfer process. It appears the predominant process is

$$100 \text{ eV } He^+ + Cl_2 \rightarrow He + Cl^* + Cl^+ \qquad (11)$$

As a check on the validity of using the intensity criteria stated in Chapter IV, a comparison of the relative intensities for transitions observed in discharge experiments reported in the tabulated literature data (see Ref 55), cross

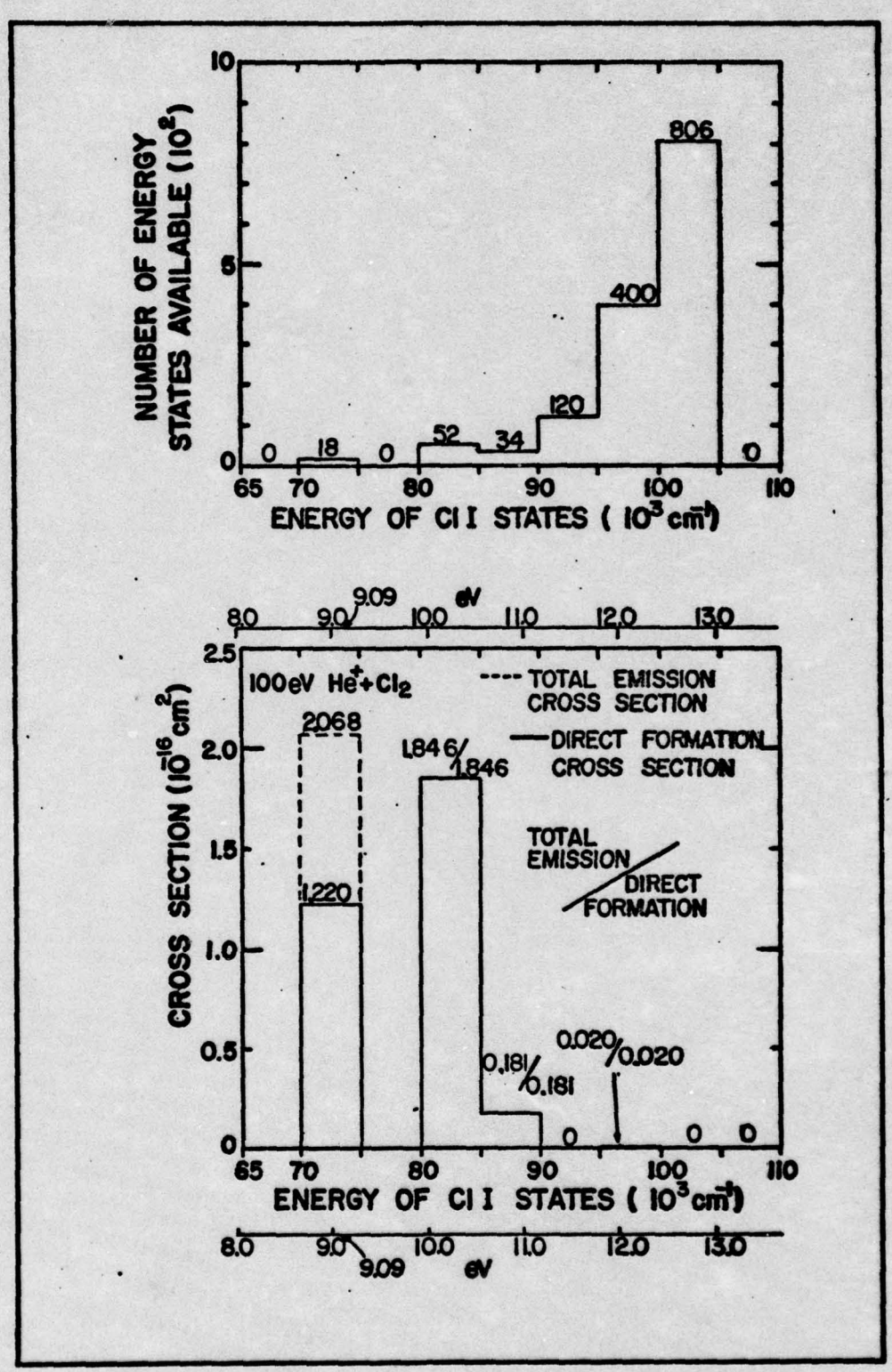

Fig. 29. Comparison of Cl I Emission Cross Sections and Direct Formation Cross Sections as a Function of the Energy Levels of the Cl I Atom.

sections measured in the present He^+/Cl_2 reaction experiment, and A factors measured in shock tube experiments (Ref 2) are given in Table VII. It can be seen that for transitions from the same upper state the He^+/Cl_2 experiment yields data which agrees very well with the A factors obtained in a shock tube. Both of these are relatively field free environments. The relative intensities derived from discharge experiments also agree fairly well with both the He^+/Cl_2 reaction results and the shock tube results. It should be noted that all of these lines are in the 700 nm to 900 nm region which supports the use of the intensity criteria stated in Chapter IV for analysis in this spectral region.

Table VII

Relative Transition Probabilities for Selected Cl I Transitions in the 700 nm to 870 nm Region

Transition State			λ_T[a] (nm)	σ[b] ($cm^2 \times 10^{18}$)	RI[c]	A[d] (10^8 sec^{-1}) ±30%
Lower		Upper				
$4s\ ^4P_{1/2}$	←	$4p\ ^4S^o_{3/2}$	774.710	3.2	10,000	0.063
$4s\ ^4P_{3/2}$	←	$4p\ ^4S^o_{3/2}$	754.915	6.1	11,000	0.120
$4s\ ^4P_{5/2}$	←	$4p\ ^4S^o_{3/2}$	725.862	5.7	7,500	0.152
$4s\ ^4P_{1/2}$	←	$4p\ ^2P^o_{3/2}$	792.66	<1.0	3,000	0.021
$4s\ ^4P_{3/2}$	←	$4p\ ^2P^o_{3/2}$	771.971	1.5	7,000	0.030
$4s\ ^4P_{5/2}$	←	$4p\ ^2P^o_{3/2}$	741.616	1.6	5,000	0.047
$4s\ ^4P_{3/2}$	←	$4p\ ^2D^o_{5/2}$	822.400	7.7	20,000	0.056
$4s\ ^4P_{5/2}$	←	$4p\ ^2D^o_{5/2}$	788.038	1.5	3,000	0.0179
$4s\ ^4P_{1/2}$	←	$4p\ ^4D^o_{1/2}$	843.057	5.6	15,000	0.190
$4s\ ^4P_{3/2}$	←	$4p\ ^4D^o_{1/2}$	819.67	<1.0	2,500	0.042

Table VII (continued)

Relative Transition Probabilities for Selected Cl I Transitions in the 700 nm to 870 nm Region

Transition State			λ_T[a] (nm)	σ[b] ($cm^2 \times 10^{18}$)	RI[c]	A[d] (10^8 sec^{-1}) ±30%
Lower		Upper				
$4s\ ^4P_{1/2}$	←	$4p\ ^4D^o_{3/2}$	857.760	8.9	20,000	0.114
$4s\ ^4P_{3/2}$	←	$4p\ ^4D^o_{3/2}$	833.560	7.6	18,000	0.089
$4s\ ^4P_{3/2}$	←	$4p\ ^4D^o_{5/2}$	858.834	14.0	75,000	0.99
$4s\ ^4P_{5/2}$	←	$4p\ ^4D^o_{5/2}$	821.430	3.3	18,000	0.055

[a] Calculated vacuum wavelength using the energy level tables (Ref. 55).

[b] Emission cross section for 100 eV $He^+ + Cl_2$ reaction.

[c] Relative intensity in discharge experiments (Ref. 55).

[d] A-factors measured in shock tube experiment (Ref. 2).

VI. Bromine

Introduction

The material in this chapter is presented in the same manner as for the chlorine reaction in Chapter V. All of the spectra illustrated in this chapter and all of the cross sections listed in the tables of this chapter, were obtained from the reaction of 100 eV He^+ ions with Br_2 at room temperature. The translational energy of the He^+ ions was varied only in the measurements of the energy dependence of the cross sections depicted in Figs. 36 to 41.

Spectra

The 57 measureable bromine lines observed in the 60 nm to 870 nm wavelength region are presented in Figs. 30 to 35. A high resolution spectrum of the 85 nm to 159 nm VUV region is shown in Fig. 30. Figures 31 and 32 depict examples of low and high resolution spectra of the 110 nm to 170 nm VUV region. The remaining spectra are high resolution spectra in the 440 nm to 870 nm region.

Cross Section Energy Dependence Curves

The curves in Figs. 36 to 41 depicting the energy dependence of the bromine cross sections, were obtained from measurements made under low resolution conditions. The same cross section measurement limitations apply in the 120 eV to 170 eV region and in the 0 eV to 20 eV region, as cited for chlorine in Chapter V. The curves indicate evidence of lines

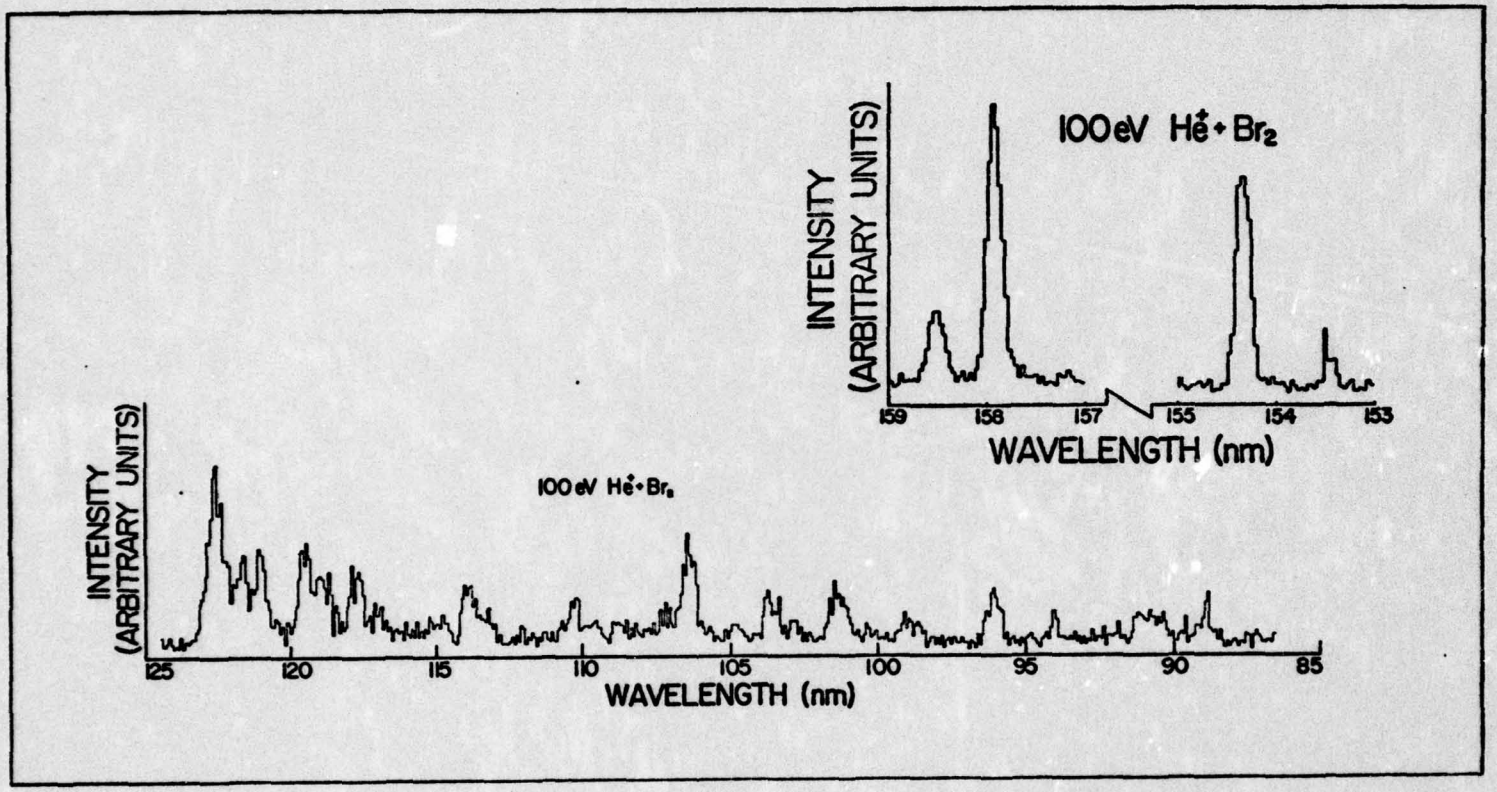

Fig. 30. High Resolution Spectra of 100 eV He^+ + Br_2 Reaction in 85 nm to 159 nm Region.

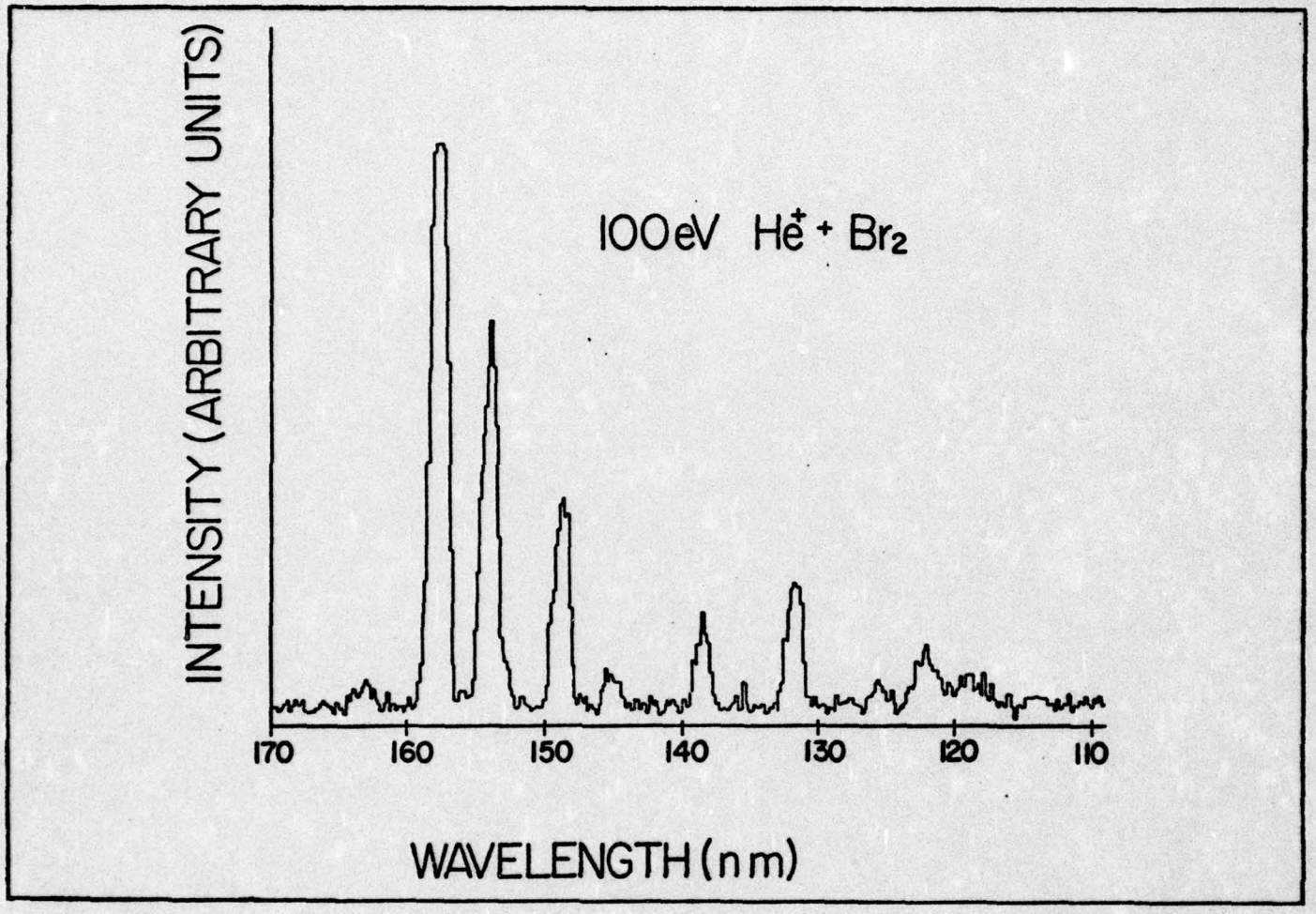

Fig. 31. Low Resolution Spectra of 100 eV He^+ + Br_2 Reaction in 110 nm to 170 nm Region.

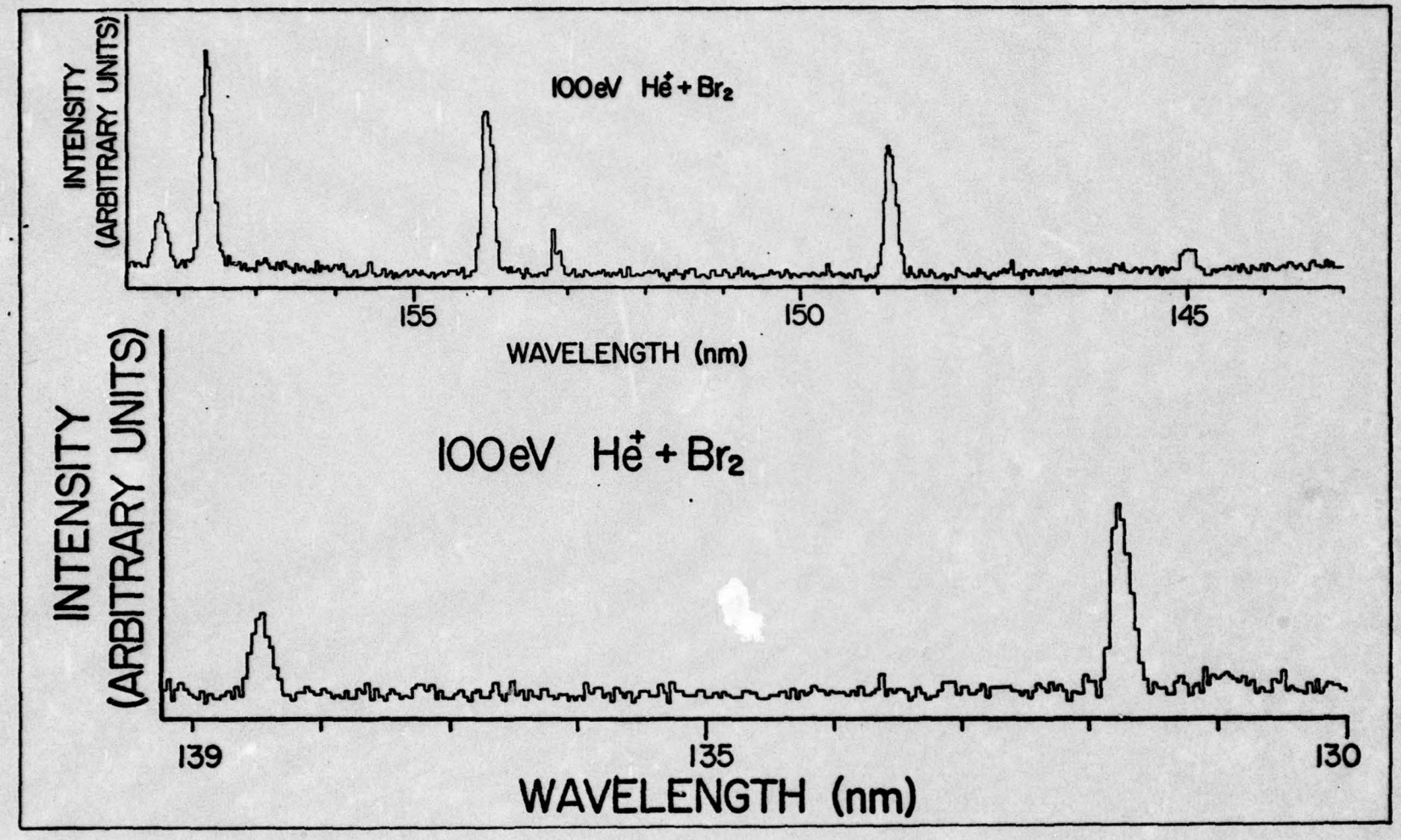

Fig. 32. High Resolution Spectra of 100 eV He^+ + Br_2 Reaction in 130 nm to 160 nm Region.

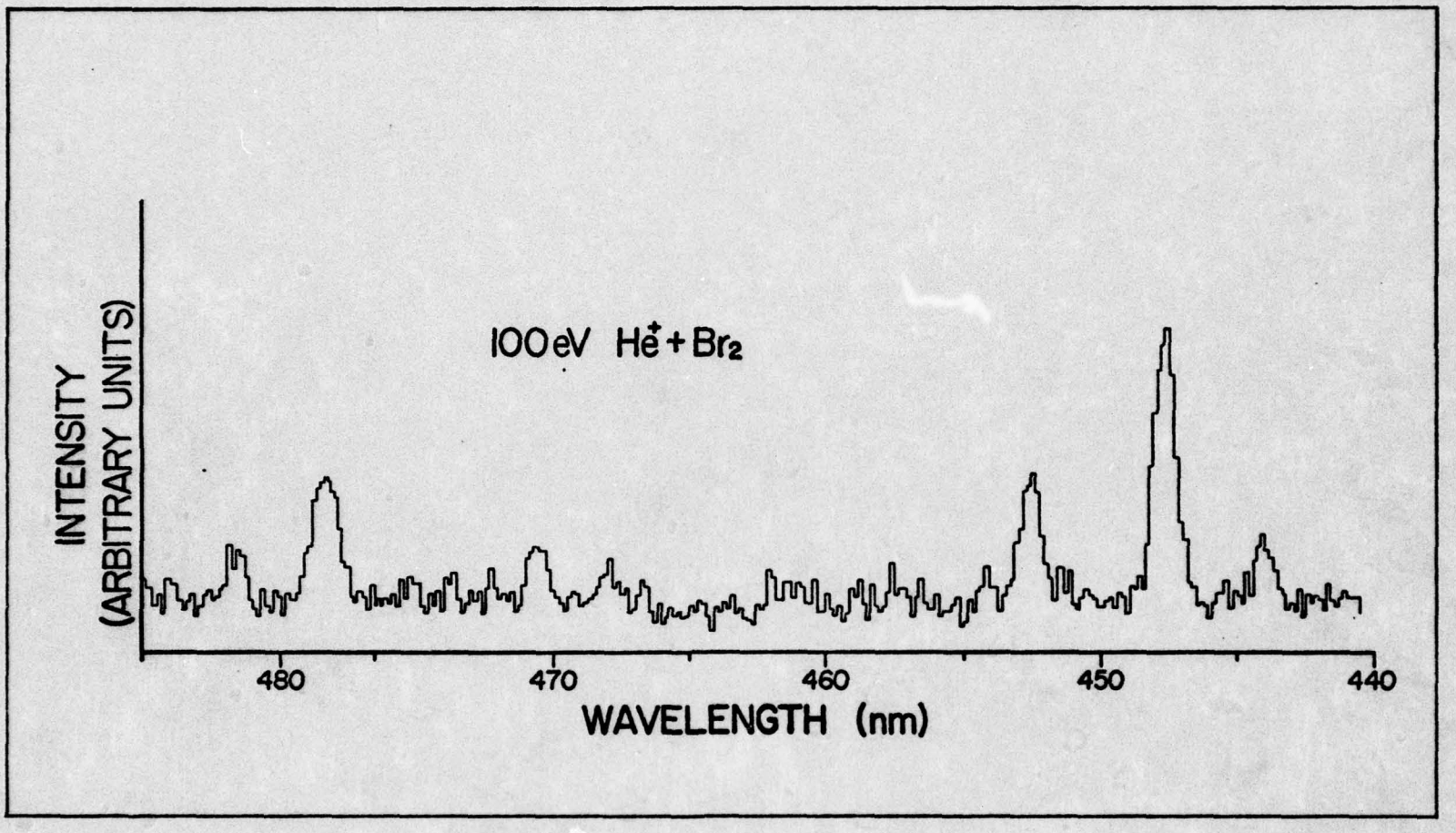

Fig. 33. High Resolution Spectra of 100 eV He^+ + Br_2 Reaction in 440 nm to 485 nm Region.

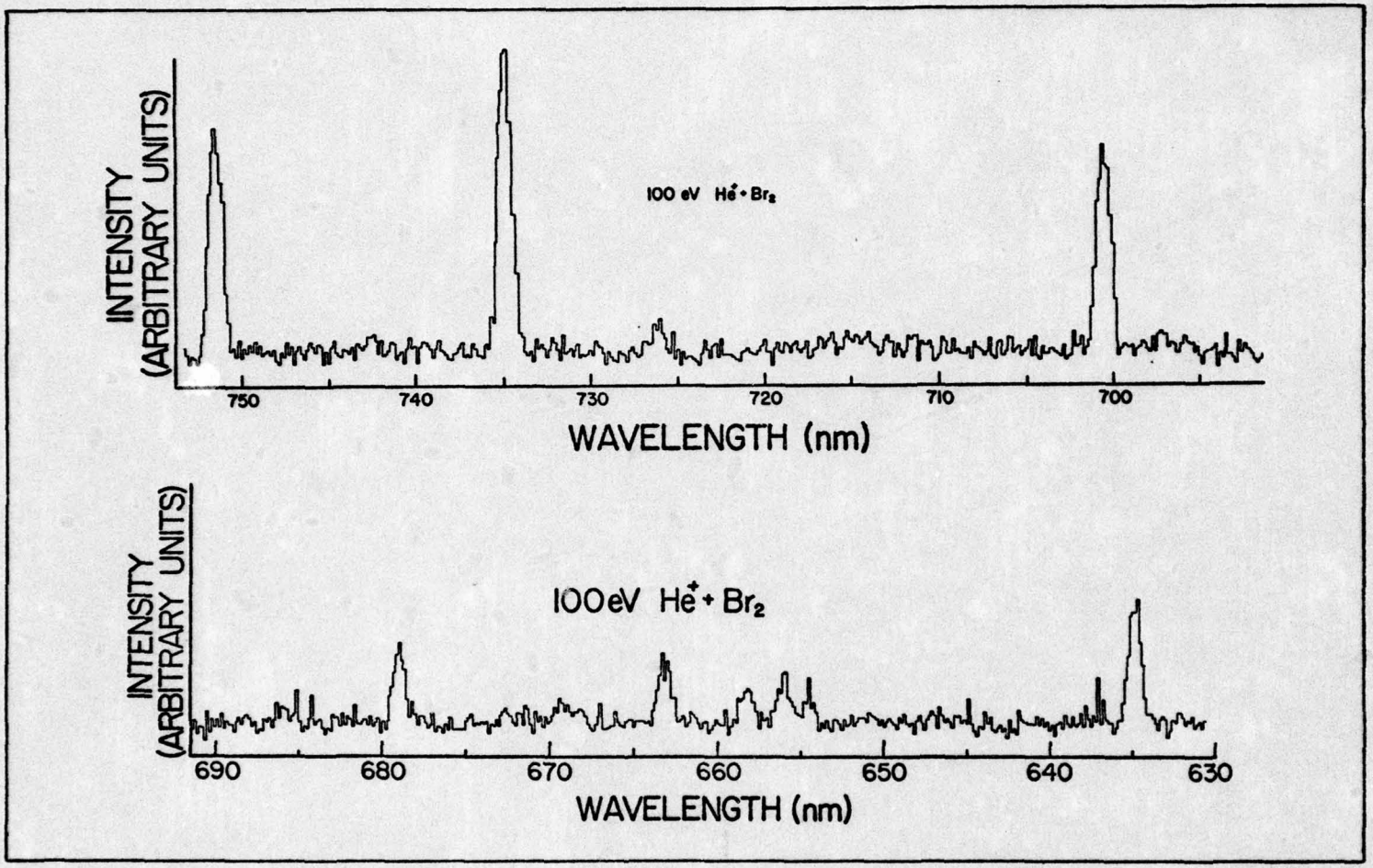

Fig. 34. High Resolution Spectra of 100 eV He^+ + Br_2 Reaction in 630 nm to 755 nm Region.

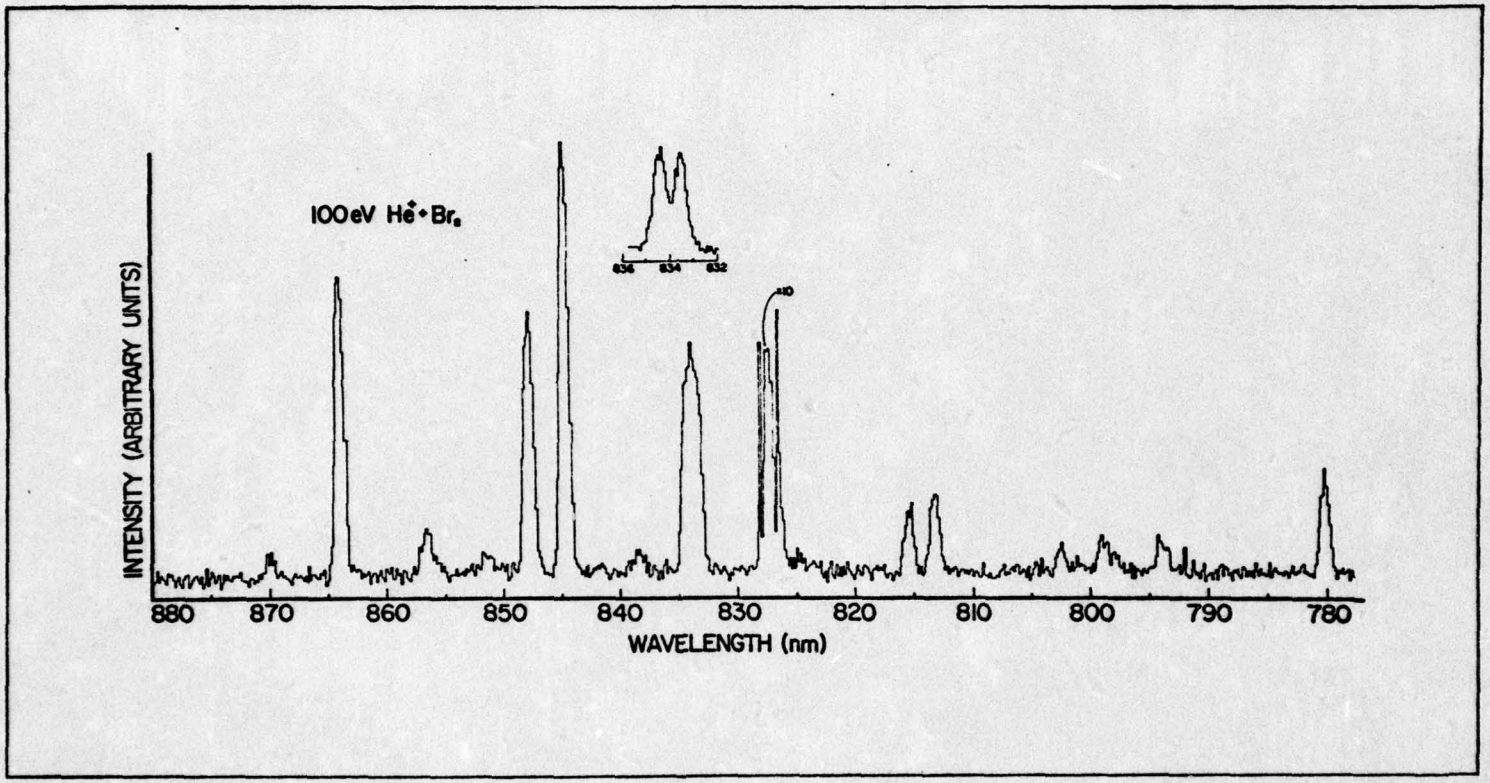

Fig. 35. High Resolution Spectra of 100 eV He^+ + Br_2 Reaction in 775 nm to 880 nm Region.

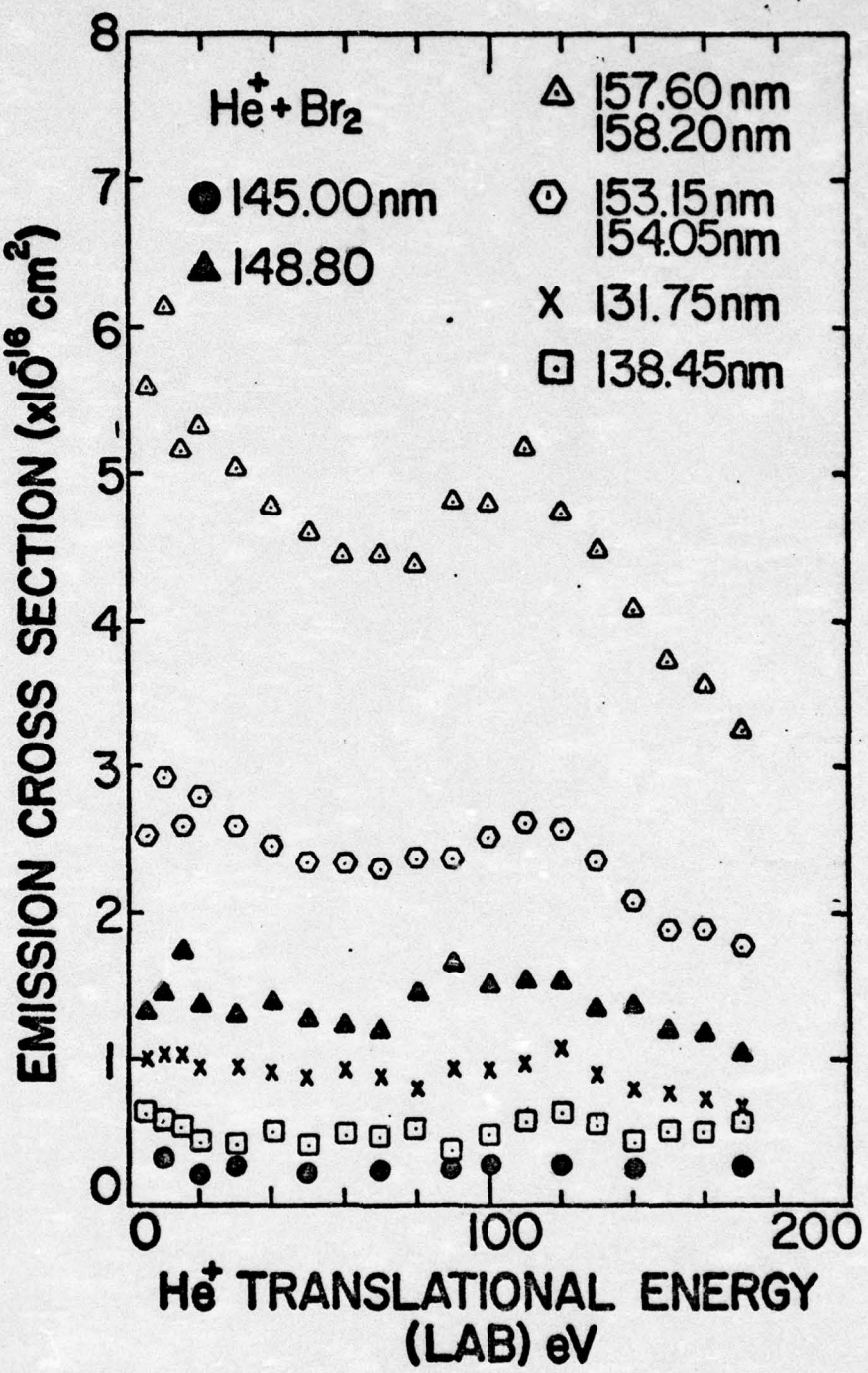

Fig. 36. The Energy Dependence of the Emission Cross Sections of Selected VUV Lines from the $He^+ + Br_2$ Reaction.

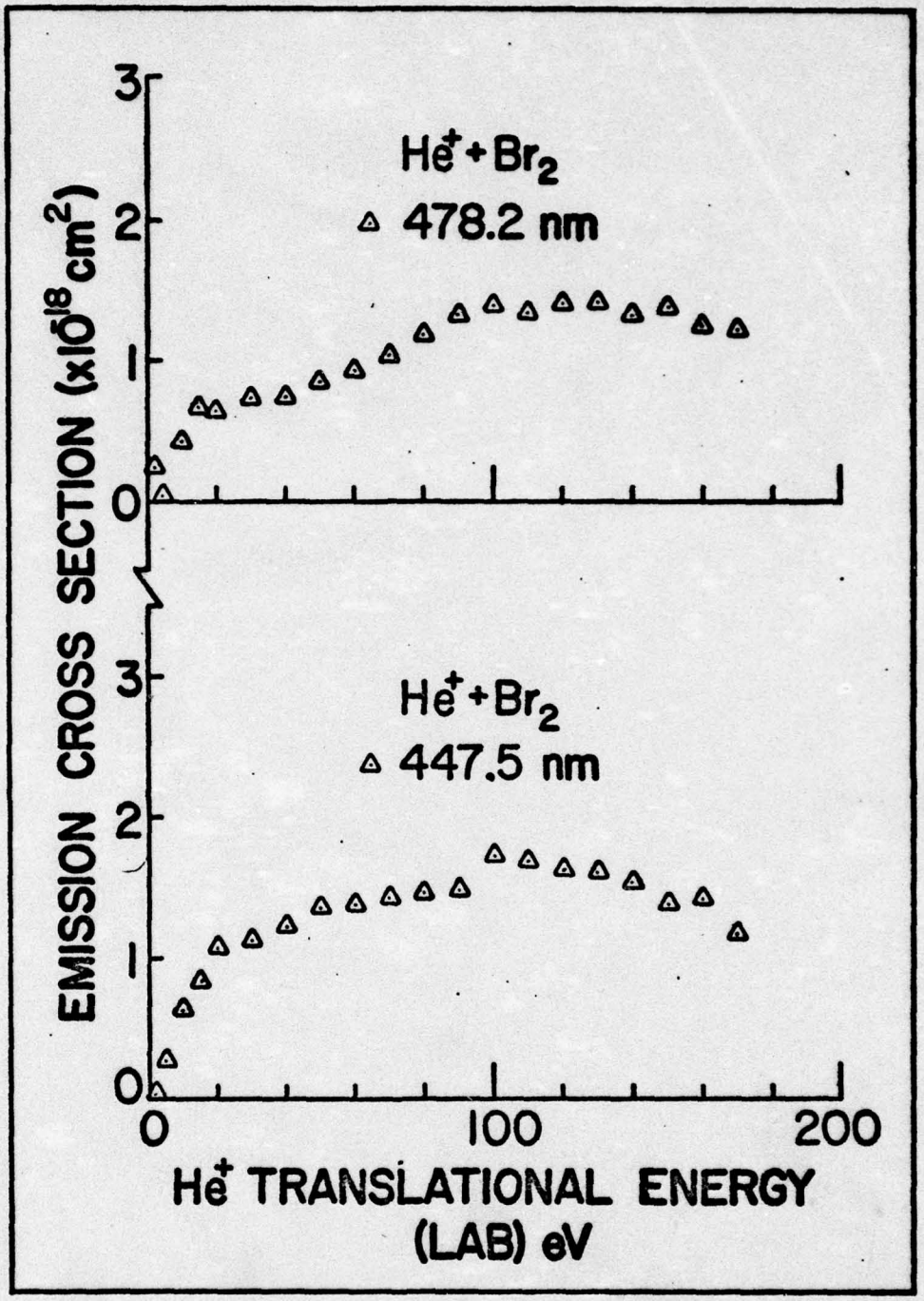

Fig. 37. The Energy Dependence of the Emission Cross Sections of the 447.5 nm and 478.2 nm Lines from the $He^+ + Br_2$ Reaction.

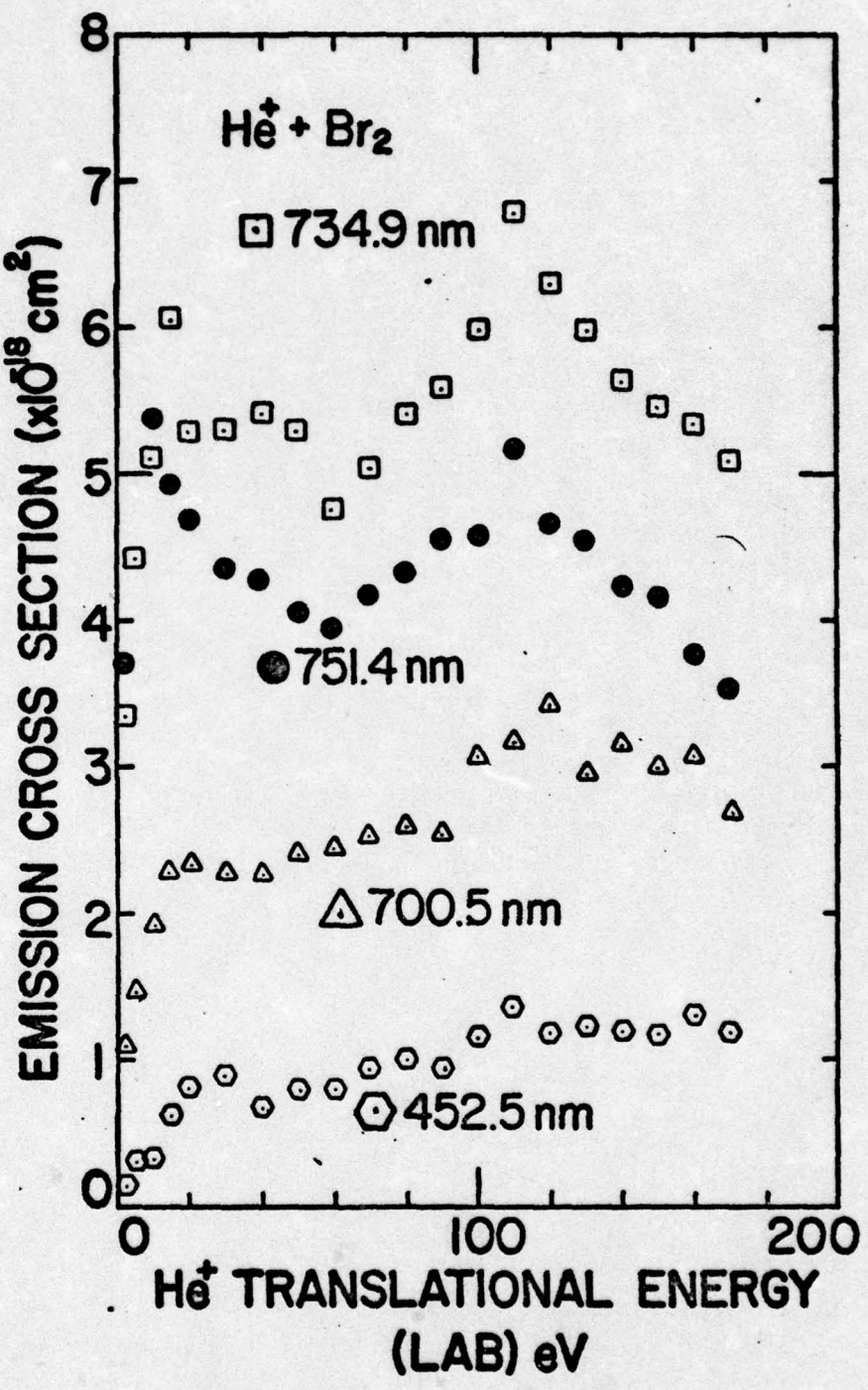

Fig. 38. The Energy Dependence of the Emission Cross Sections of Selected Visible Lines from the $He^+ + Br_2$ Reaction.

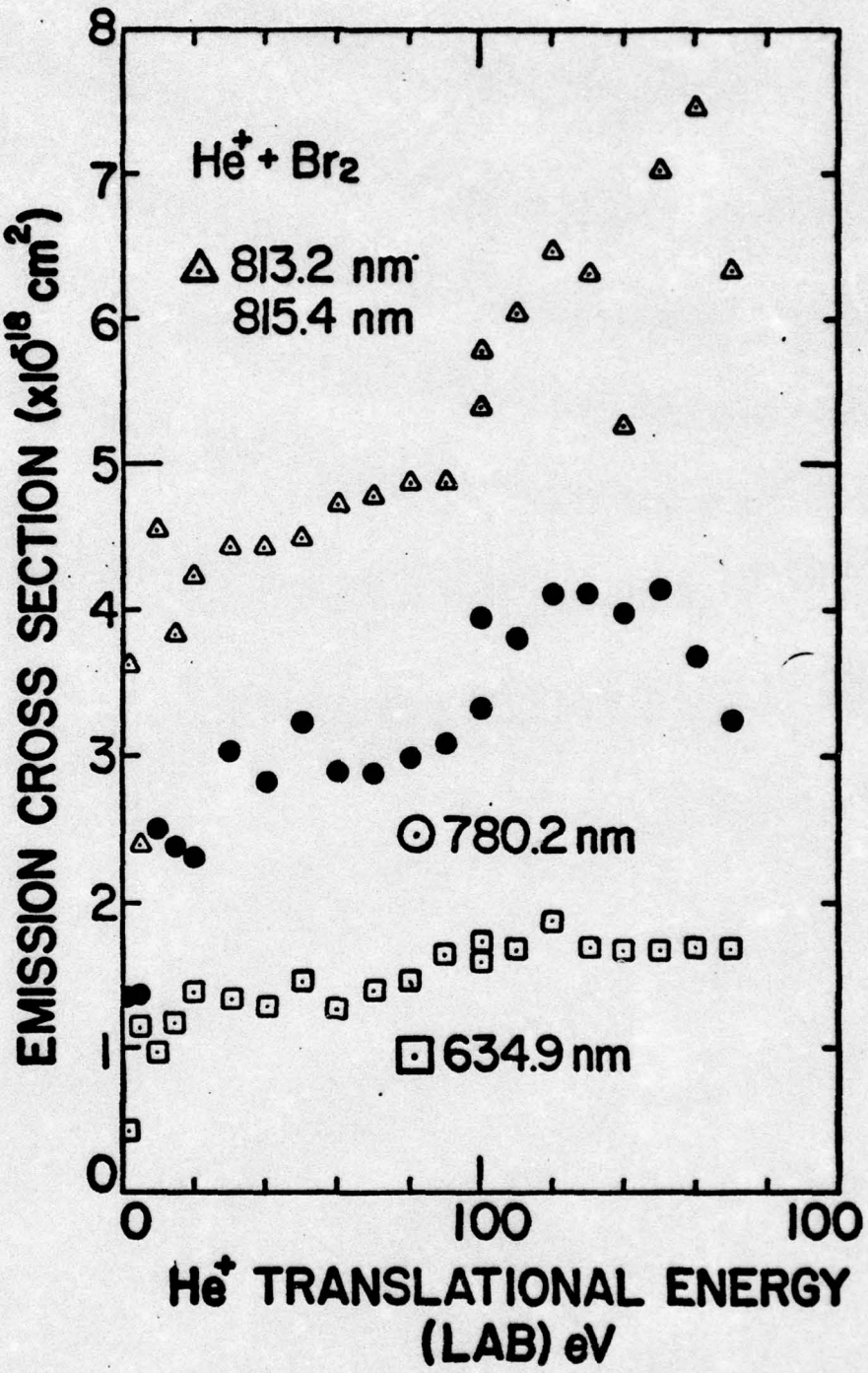

Fig. 39. The Energy Dependence of the Emission Cross Sections of Selected Lines from the $He^+ + Br_2$ Reaction.

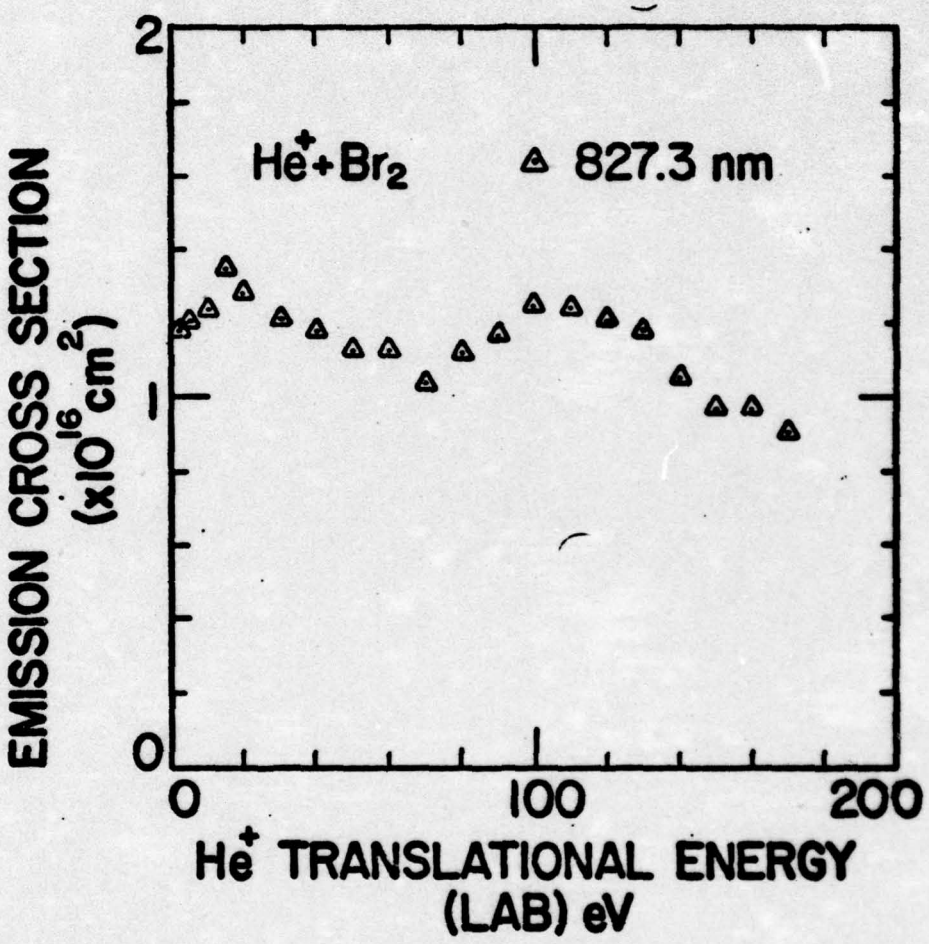

Fig. 40. The Energy Dependence of the Emission Cross Section of the 827.3 nm Line from the $He^+ + Br_2$ Reaction.

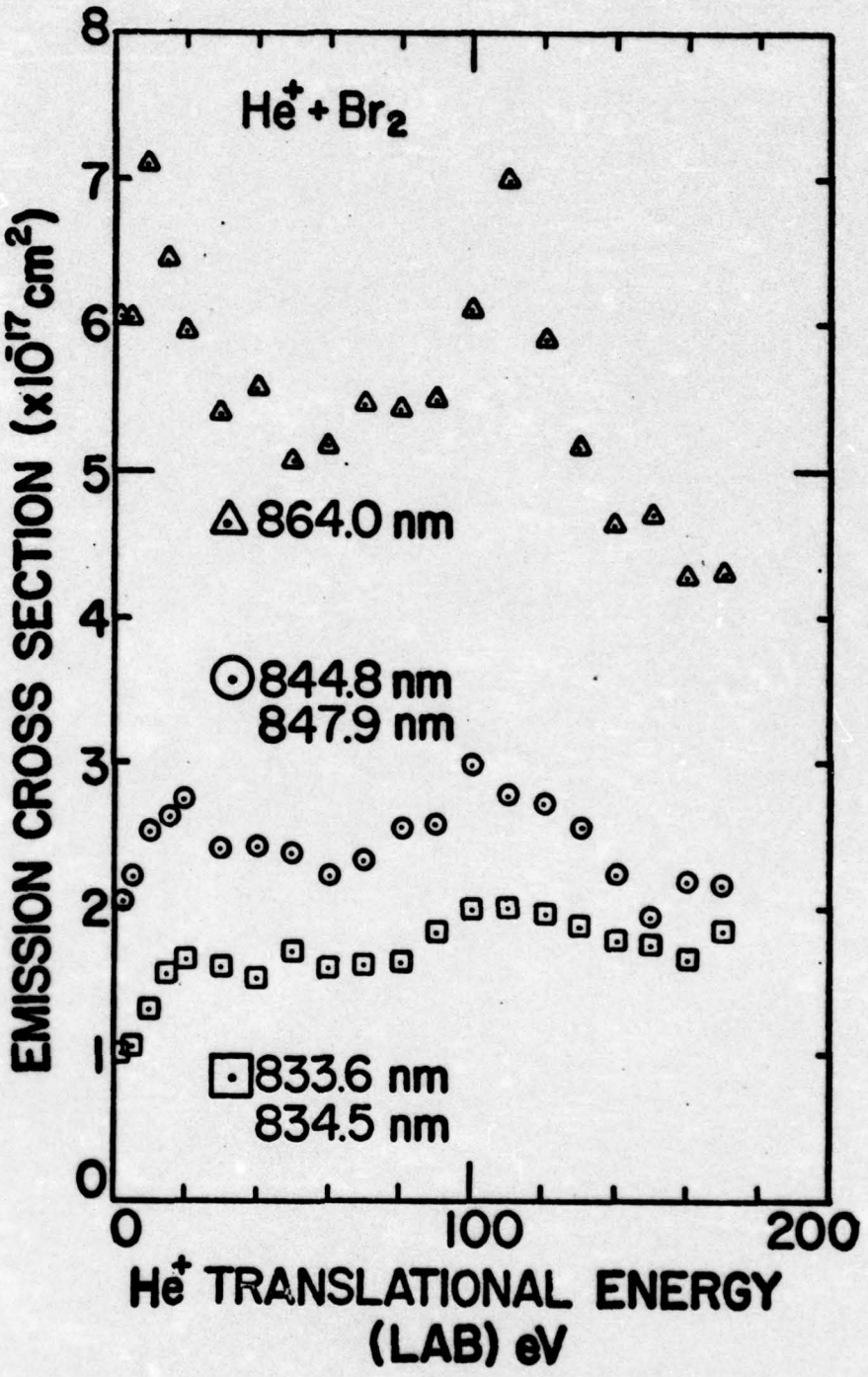

Fig. 41. The Energy Dependence of the Emission Cross Sections of Selected Infrared Lines from the $He^+ + Br_2$ Reaction.

produced by both exothermic processes (such as the 157.60 nm and 158.20 nm line in Fig. 36) and endothermic processes with low thresholds in the 0 eV to 5 eV region (see Fig. 37). Again, as in Chapter V, all of the cross section energy dependence curves are presented to aid in the selection of transition assignments and for completeness.

Line Identification

A listing of all of the allowed transitions which meet the measurements uncertainty $\Delta\lambda_0$ and the quantum-mechanical criteria described in Chapter IV for each observed wavelength λ_0 in the spectra, are listed in Table XVI in Appendix B. The measured cross section for each observed wavelength is also listed. The endothermicity in eV for thermal energy reactants is listed for each allowed transition's upper state. This endothermicity is measured above and below the 10.77 eV energy released by the thermal energy charge exchange reaction between He^+ and Br_2 for the same purpose discussed previously in the chlorine line identification section. A Br III transition is listed as a possible assignment for the 96.075 nm observed wavelength. This is listed because it was selected as the transition assignment in Ref 45. The author feels that if charge transfer is the predominant process in the reaction, one of the Br II transitions should be assigned to this wavelength.

Further Analysis

Table VIII is a summary of the complete listings in Table XVI. It is noteworthy that the 1493.3 x 10^{-18} cm^2 total emission cross section is even larger than chlorine and that 77% of the total cross section is accounted for by the 26 observed VUV lines. Using the relative intensity criteria stated in Chapter IV, it was found that the reaction yields emission arising predominantly from Br I. The resulting Br I transition assignments are listed in Table IX. They account for 86% of the total 1476.0 x 10^{-18} cm^2 emission cross section of the lines listed in Table XVI having possible Br I transition assignments.

A term diagram illustrating the assigned Br I transitions in Table IX is shown in Fig. 42. The total emission cross section of each energy state is shown in parentheses, next to the energy state designation. The small numbers next to each energy level are the 2J + 1 values for that specific energy level. The energy available from the thermal charge transfer process is indicated by a dashed line. In contrast to Cl I where only the 4s ^4P state was low enough to be populated exclusively by the charge transfer process, Br I has many energy states which are low enough to be populated by the 10.77 eV available from the thermal charge transfer process. This is a reasonable explanation of why the total emission cross section for the bromine reaction is about three times as large as the chlorine reaction (14.7 A^2 versus 5.0 A^2). The Br I term diagram is more complex than the

Table VIII

Summary of 100 eV $He^+ + Br_2$ Reaction Allowed Transitions Selected by the Computer Search Program

Classification of Allowed Transitions Listed in Computer Search	Number of Lines	$\sum\sigma$ ($\times 10^{-18}$ cm^2)	$\frac{\sum\sigma}{\sum_{Total}\sigma}$	Number of VUV Lines	$\sum_{VUV}\sigma$ ($\times 10^{-18}$ cm^2)	$\frac{\sum_{VUV}\sigma}{\sum_{Total}\sigma_{VUV}}$	Number of Visible Lines	$\sum_{visible}\sigma$ ($\times 10^{-18}$ cm^2)	$\frac{\sum_{visible}\sigma}{\sum_{Total}\sigma_{Visible}}$
Br I	29	869.8	0.58	12	593.7	0.50	17	276.1	0.91
Br II	10	15.1	0.01	9	14.5	0.01	1	0.6	0.002
Br I and Br II	18	608.4	0.41	5	580.7	0.49	13	27.7	0.09
Total	57	1493.3		26	1188.9 80% of $\sum_{Total}\sigma$		31	304.4 20% of $\sum_{Total}\sigma$	

Table IX

Br I Transition Assignments for the 100 eV $He^+ + Br_2$ Reaction

λ_T[a] (nm)	Transition Assignment Lower		Upper	ΔH[b] (eV)	σ[c] ($cm^2 \times 10^{18}$)
121.601	$4p^5\ ^2P^o_{3/2}$	←	$6s\ ^4P_{5/2}$	-0.57	15.8
138.459	$4p^5\ ^2P^o_{1/2}$	←	$(^1D_2)5s\ ^2D_{3/2}$	-1.36	47.1
144.990	$4p^5\ ^2P^o_{3/2}$	←	$5s''\ ^2P_{1/2}$	-2.22	28.2
148.846	$4p^5\ ^2P^o_{3/2}$	←	$5s'\ ^2P_{3/2}$	-2.44	151.2
153.175	$4p^5\ ^2P^o_{1/2}$	←	$5s''\ ^2P_{1/2}$	-2.22	41.8
154.066	$4p^5\ ^2P^o_{3/2}$	←	$5s\ ^4P_{3/2}$	-2.72	209.1
157.638	$4p^5\ ^2P^o_{3/2}$	←	$5s\ ^4P_{5/2}$	-2.91	384.2
158.231	$4p^5\ ^2P^o_{1/2}$	←	$5s'\ ^4P_{1/2}$	-2.48	96.0
444.298	$5s\ ^4P_{5/2}$	←	$6p\ ^4D^o_{3/2}$	-0.11	0.4
447.385	$5s\ ^4P_{3/2}$	←	$(^1D_2)5p\ ^2P^o_{3/2}$	0.05	1.8
447.898	$5s\ ^4P_{5/2}$	←	$6p\ ^4D^o_{7/2}$	-0.14	
452.686	$5s\ ^4P_{5/2}$	←	$6p\ ^4P^o_{5/2}$	-0.17	1.2
470.473	$5s'\ ^2P_{3/2}$	←	$(^1D_2)5p\ ^2D^o_{3/2}$	0.20	0.6
635.248	$5s\ ^4P_{5/2}$	←	$5p'\ ^4S^o_{3/2}$	-0.95	1.7
663.343	$5s\ ^4P_{5/2}$	←	$5p'\ ^2D^o_{5/2}$	-1.04	1.0
700.715	$5s\ ^4P_{3/2}$	←	$5p'\ ^4S^o_{3/2}$	-0.95	3.1
735.056	$5s\ ^4P_{3/2}$	←	$5p'\ ^2D^o_{5/2}$	-1.04	6.0
751.505	$5s\ ^4P_{5/2}$	←	$5p\ ^4D^o_{3/2}$	-1.26	4.5
780.517	$5s'\ ^4P_{1/2}$	←	$5p''\ ^2P^o_{3/2}$	-0.89	3.9
799.213	$5s'\ ^2P_{3/2}$	←	$5p''\ ^2P^o_{3/2}$	-0.89	1.5
813.374	$5s'\ ^4P_{1/2}$	←	$5p'\ ^4S^o_{3/2}$	-0.95	3.7
815.597	$5p\ ^4P^o_{5/2}$	←	$5d\ ^4D_{5/2}$	0.01	1.5

Table IX (continued)

Br I Transition Assignments for the 100 eV $He^+ + Br_2$ Reaction

λ_T[a] (nm)	Transition Assignment Lower		Upper	ΔH[b] (eV)	σ[c] ($cm^2 \times 10^{18}$)
815.621	$5s\ ^4P_{5/2}$	←	$5p\ ^4D^o_{5/2}$	-1.39	1.5
827.469	$5s\ ^4P_{5/2}$	←	$5p\ ^4D^o_{7/2}$	-1.41	123.9
833.698	$5s'\ ^2P_{3/2}$	←	$5p'\ ^4S^o_{3/2}$	-0.95	10.4
834.596	$5s'\ ^4P_{1/2}$	←	$5p'\ ^4D^o_{1/2}$	-0.99	10.6
838.634	$5p\ ^4P^o_{3/2}$	←	$5d\ ^4D_{5/2}$	0.01	1.3
844.888	$5s\ ^4P_{3/2}$	←	$5p\ ^4D^o_{3/2}$	-1.26	24.0
847.976	$5s'\ ^4P_{1/2}$	←	$5p'\ ^2D^o_{3/2}$	-1.02	15.7
856.008	$5s'\ ^2P_{3/2}$	←	$5p'\ ^4D^o_{1/2}$	-0.99	5.1
864.104	$5s\ ^4P_{5/2}$	←	$5p\ ^4P^o_{3/2}$	-1.47	63.0
870.090	$5s'\ ^2P_{3/2}$	←	$5p'\ ^2D^o_{3/2}$	-1.02	9.6
					1269.4

[a] Calculated vacuum wavelength using the energy level tables (Ref. 68).

[b] Enthalpy change required to populate the upper energy state for the thermal reaction $He^+ + Br_2 \rightarrow He + Br^+ + Br^*$.

[c] Emission cross section for 100 eV $He^+ + Br_2$ reaction.

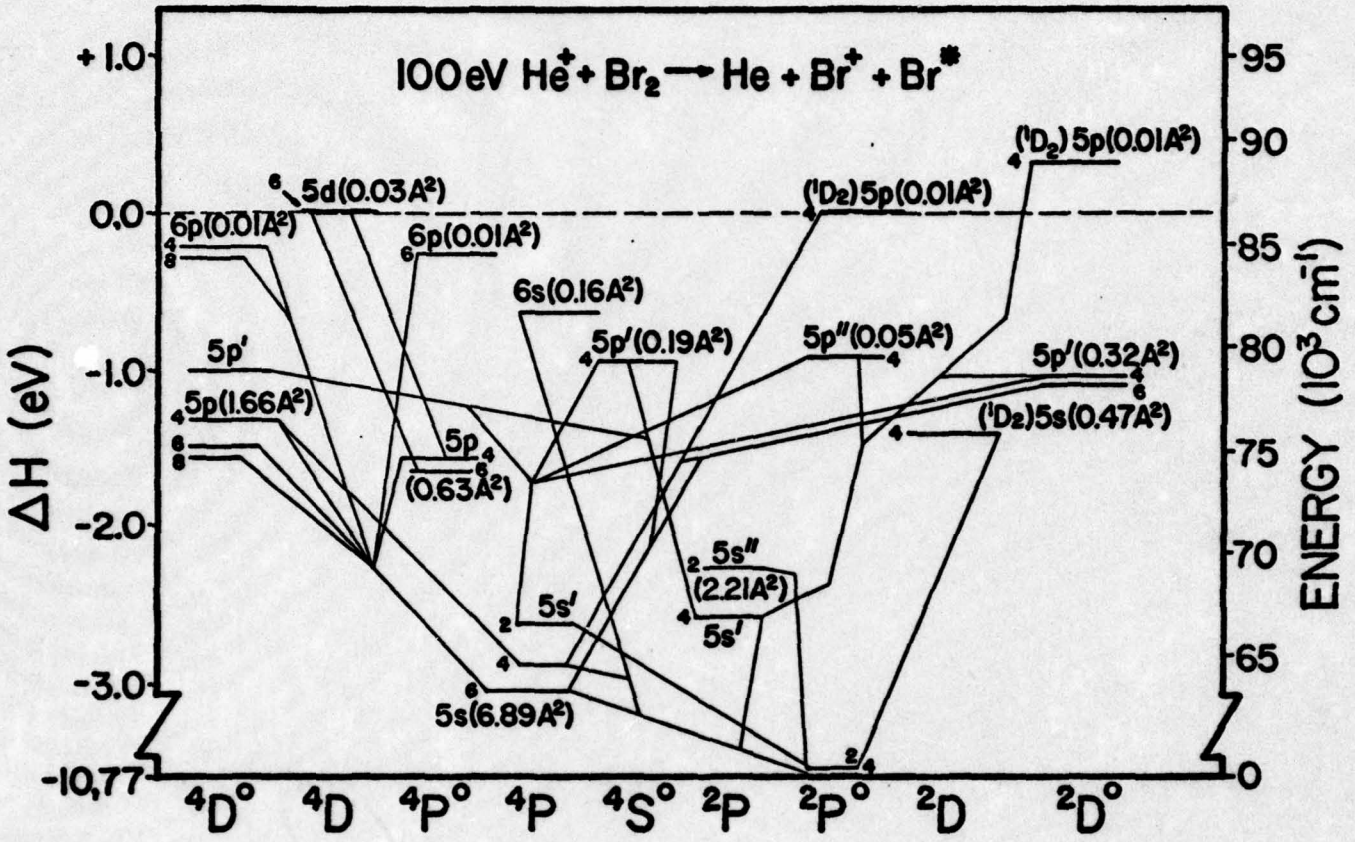

Fig. 42. Br I Term Diagram for 100 eV He^+ + Br_2 Reaction.

Cl I term diagram, with more violations of conservation of spin for LS coupling. Since bromine is a heavier atom, this is to be expected. Since the lowest energy state of Br II is about 0.75 eV endothermic, it is reasonable to expect few ionic transitions.

The results of examining each energy level in the Br I term diagram to determine its direct excitation cross section is listed in Table X. The total direct formation cross section is 973.8 x 10^{-18} cm^2, which is 77% of the total emission cross section for the He^+/Br_2 reaction.

A plot of the emission cross sections and the direct formation cross sections as a function of the energy levels of the Br I atom is given in Fig. 43. The number of states available for population in each energy interval is also presented in Fig. 43. This analysis indicates that the energy of the 100 eV He^+/Br_2 reaction is predominantly transferred to bromine neutral atoms which are excited to their lower energy states. These lower energy states are exothermic for the charge transfer process. It appears the predominant process is

$$100 \text{ eV } He^+ + Br_2 \rightarrow He + Br^* + Br^+ \qquad (12)$$

As a check on the validity of using the intensity criteria stated in Chapter IV a comparison of the relative intensities for transitions observed in the discharge experiments reported in the tabulated literature date (see Refs 67 and 68), cross sections measured in the present He^+/Br_2

Table X

Emission and Cascading Cross Sections for Br I States Observed in 100 eV $He^+ + Br_2$ Reaction

Br I State Designation		ΔH^a (eV)	Cross Section ($cm^2 \times 10^{18}$) Total Emission	Cascading	Direct Formation
$4p^4$	$5s\ ^4P_{3/2}$	-2.72	209.1	34.0 (0.9)	175.1
	$5s\ ^4P_{5/2}$	-2.91	384.2	198.2 (4.1)	186.0
	$5s'\ ^4P_{1/2}$	-2.48	96.0	34.0	62.0
	$5s'\ ^2P_{3/2}$	-2.44	151.2	24.6	126.6
	$5s''\ ^2P_{1/2}$	-2.22	70.0	--	70.0
	$(^1D_2)5s\ ^2D_{3/2}$	-1.36	47.1	--	47.1
	$5p\ ^4D^o_{3/2}$	-1.26	28.5	--	28.5
	$5p\ ^4D^o_{5/2}$	-1.39	1.5 (1.5)	--	1.5
	$5p\ ^4D^o_{7/2}$	-1.41	123.9	--	123.9
	$5p\ ^4P^o_{3/2}$	-1.47	63.0	1.3	61.7
	$5p\ ^4P^o_{5/2}$	-1.51	--	1.5 (1.5)	-1.5
	$5p'\ ^4S^o_{3/2}$	-0.95	18.9 (1.7)	--	18.9
	$5p'\ ^2D^o_{3/2}$	-1.02	25.3	--	25.3
	$5p'\ ^2D^o_{5/2}$	-1.04	7.0	--	7.0
	$5p'\ ^4D^o_{1/2}$	-0.99	12.2 (1.5)	--	12.2
	$5p''\ ^2P^o_{3/2}$	-0.89	5.4	--	5.4
	$(^1D_2)5p\ ^2P^o_{3/2}$	0.05	0.9 (0.9)	--	0.9
	$(^1D_2)5p\ ^2D^o_{3/2}$	0.20	0.6	--	0.6
	$5d\ ^4D_{5/2}$	0.01	2.8 (1.5)	--	2.8
	$6s\ ^4P_{5/2}$	-0.57	15.8	--	15.8

Table X (continued)

Emission and Cascading Cross Sections for Br I States Observed in 100 eV $He^+ + Br_2$ Reaction

Br I State Designation	ΔH^a (eV)	Cross Section ($cm^2 \times 10^{18}$) Total Emission	Cascading	Direct Formation
$6p\ ^4P^o_{5/2}$	-0.17	1.2	--	1.2
$6p\ ^4D^o_{3/2}$	-0.11	0.4	--	0.4
$6p\ ^4D^o_{7/2}$	-0.14	0.9 (0.9)	--	0.9
		1265.9		973.8[b]

[a] Enthalpy change required to populate this energy state for the thermal reaction $He^+ + Br_2 \rightarrow He + Br^+ + Br^*$ (the first radiating Cl^+ state is 0.81 eV endothermic).

[b] This total does not include the negative direct formation cross section in this column.

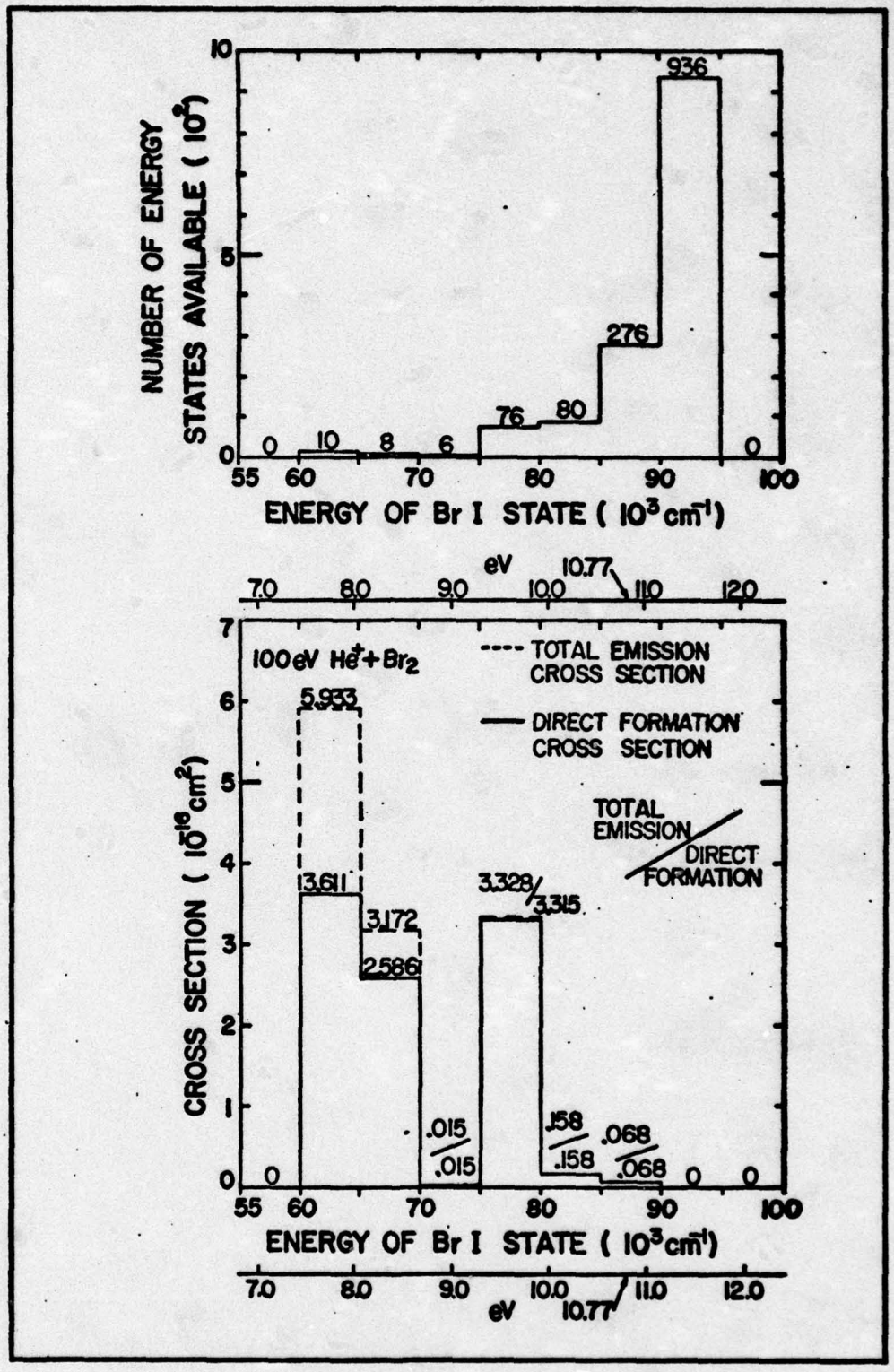

Fig. 43. Comparison of Br I Emission Cross Sections and Direct Formation Cross Sections as a Function of the Energy Levels of the Br I Atom.

reactions experiment, and A factors measured in shock tube experiments (Ref 2) are given in Table XI.

Table XI

Relative Transition Probabilities for Selected Br I Transitions in 700 nm to 870 nm Region

Transition State		λ_T[a]	σ[b]		A-factor[d]
Lower	Upper	(nm)	($cm^2 \times 10^{18}$)	RI[c]	(10^8 sec^{-1})
$5s\ ^4P_{3/2}$	$5p\ ^4D^o_{3/2}$	844.888	24.0	40,000	0.117 ±35%
$5s\ ^4P_{5/2}$	$5p\ ^4D^o_{3/2}$	751.505	4.5	40,000	0.116 ±35%
$5s'\ ^2P_{3/2}$	$5p'\ ^4S^o_{3/2}$	833.698	10.4	20,000	0.146 ±50%
$5s'\ ^4P_{1/2}$	$5p'\ ^4S^o_{3/2}$	813.374	3.7	30,000	0.0379 ±35%
$5s\ ^4P_{3/2}$	$5p'\ ^4S^o_{3/2}$	700.715	3.1	10,000	0.123 ±50%
$5s\ ^4P_{5/2}$	$5p'\ ^2D^o_{5/2}$	663.343	1.0	50,000	0.139 ±50%
$5s\ ^4P_{3/2}$	$5p'\ ^2D^o_{5/2}$	735.056	6.0	10,000	0.119 ±35%
$5s'\ ^2P_{3/2}$	$5p'\ ^4D^o_{1/2}$	856.008	5.1	1,000	not reported
$5s'\ ^4P_{1/2}$	$5p'\ ^4D^o_{1/2}$	834.596	10.6	10,000	0.219 ±35%

Table XI (continued)

Relative Transition Probabilities for Selected Br I Transitions in 700 nm to 870 nm Region

Transition State		λ_T[a]	σ[b]		A-factor[d]
Lower	Upper	(nm)	($cm^2 \times 10^{18}$)	RI[c]	(10^8 sec^{-1})
$5s'\ ^2P_{3/2}$	$5p''\ ^2P^o_{3/2}$	799.213	1.5	30,000	0.0296 ±50%
$5s'\ ^4P_{1/2}$	$5p''\ ^2P^o_{3/2}$	780.517	3.9	30,000	0.0533 ±35%

[a] Calculated vacuum wavelength using the energy level tables (Ref. 68).

[b] Emission cross section for 100 eV $He^+ + Br_2$ reaction.

[c] Relative intensity in discharge experiments (Refs. 67 and 68).

[d] A-factors measured in shock tube experiment (Ref. 2).

VII. Iodine

Introduction

The data in this chapter is presented in the same manner as for the chlorine and bromine reactions in the two preceding chapters. All of the spectra illustrated in this chapter and all of the cross sections listed in the tables of this chapter, were obtained from the reaction of 100 eV He^+ ions with I_2 at room temperature. The translational energy of the He^+ ions was varied only in the measurement of the energy dependence of the cross sections depicted in Figs. 53 to 60.

Spectra

The 81 measureable iodine lines observed in the 60 nm to 870 nm wavelength region are presented in Figs. 44 to 52. A high resolution spectrum of the 98 nm to 124 nm VUV region is shown in Fig. 44. Figures 45 to 47 depict examples of low and high resolution spectra of the 110 nm to 190 nm VUV region. The remaining figures are high resolution spectra in the 400 nm to 870 nm region.

Cross Section Energy Dependence Curves

The curves in Figs. 53 to 60 depicting the energy dependence of the iodine cross sections, were obtained from measurements made under low resolution conditions. The same cross section measurement limitations apply in the 120 eV to 170 eV region and in the 0 eV to 20 eV region, as cited for chlorine and bromine in the two preceding chapters.

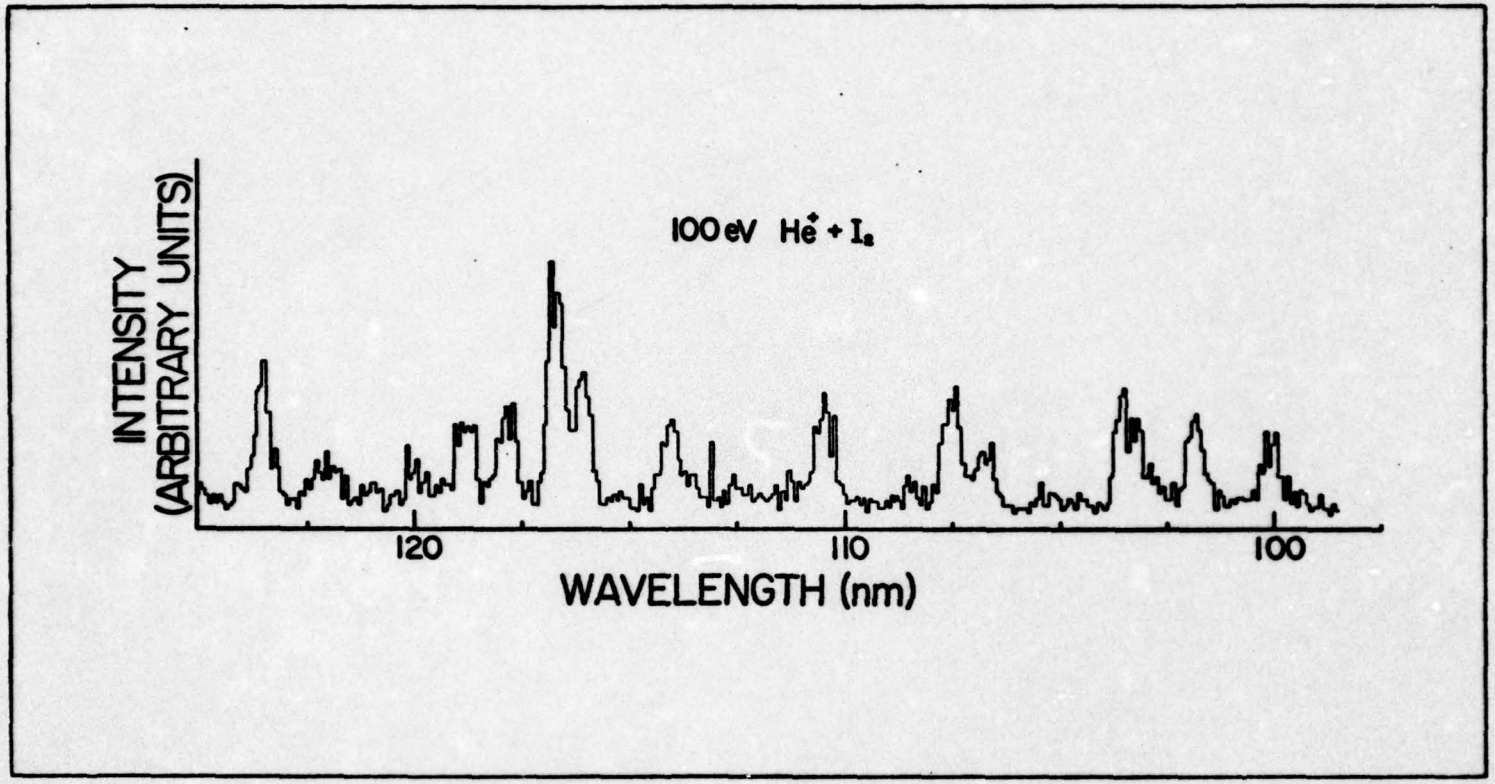

Fig. 44. High Resolution Spectra of 100 eV He^+ + I_2 Reaction in 98 nm to 124 nm Region.

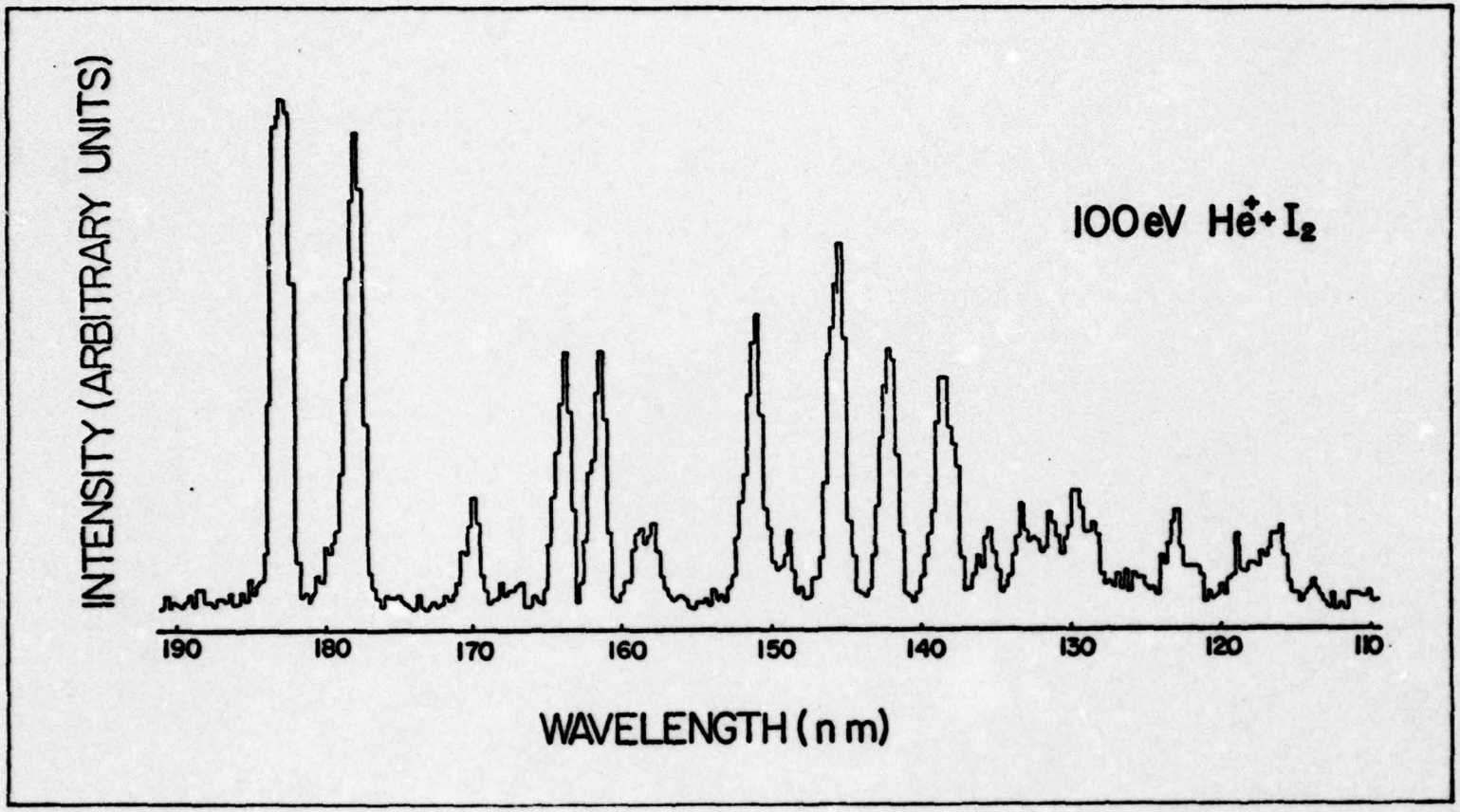

Fig. 45. Low Resolution Spectra of 100 eV $He^+ + I_2$ Reaction in 110 nm to 190 nm Region.

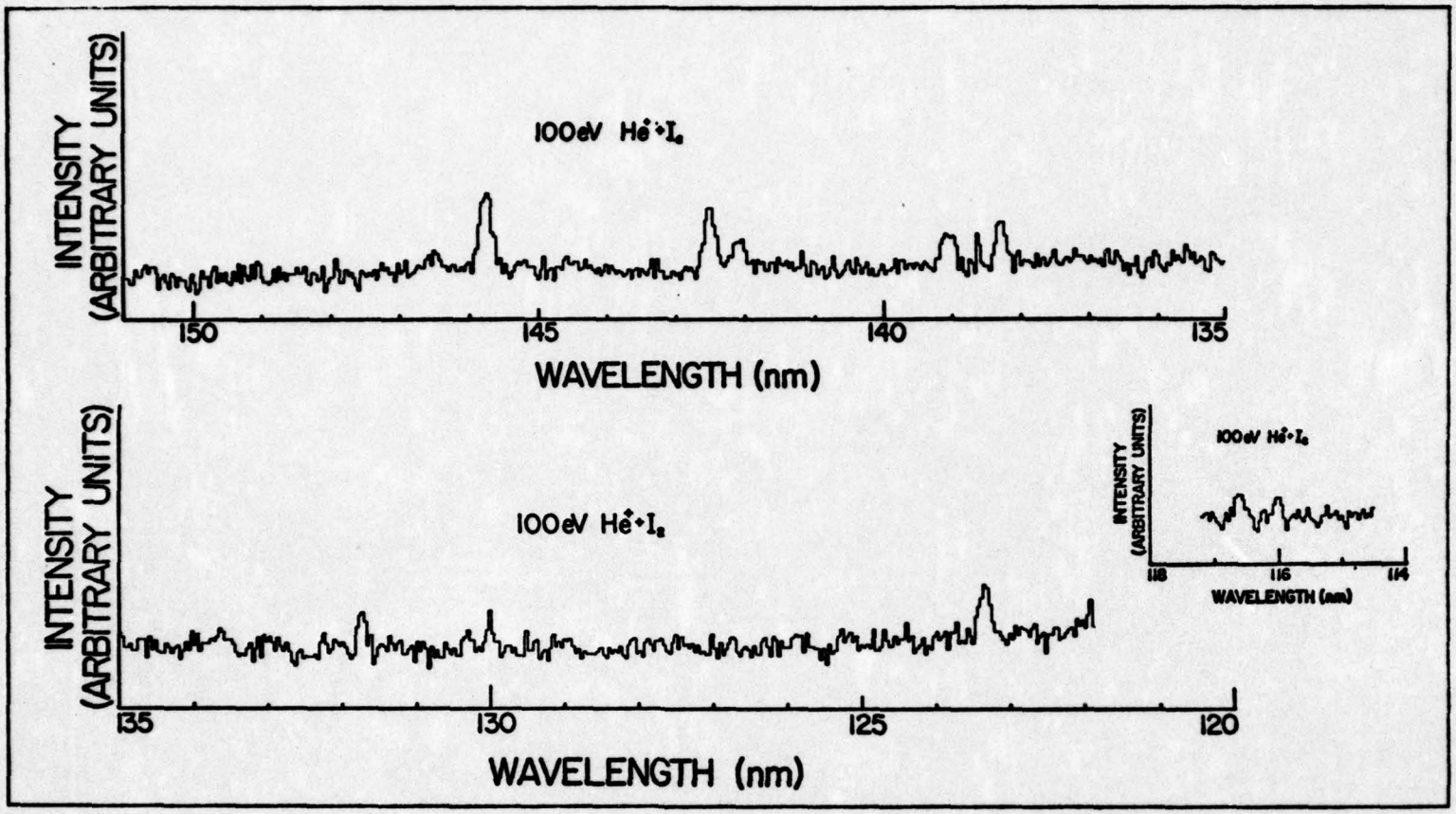

Fig. 46. High Resolution Spectra of 100 eV He^+ + I_2 Reaction in 114 nm to 150 nm Region.

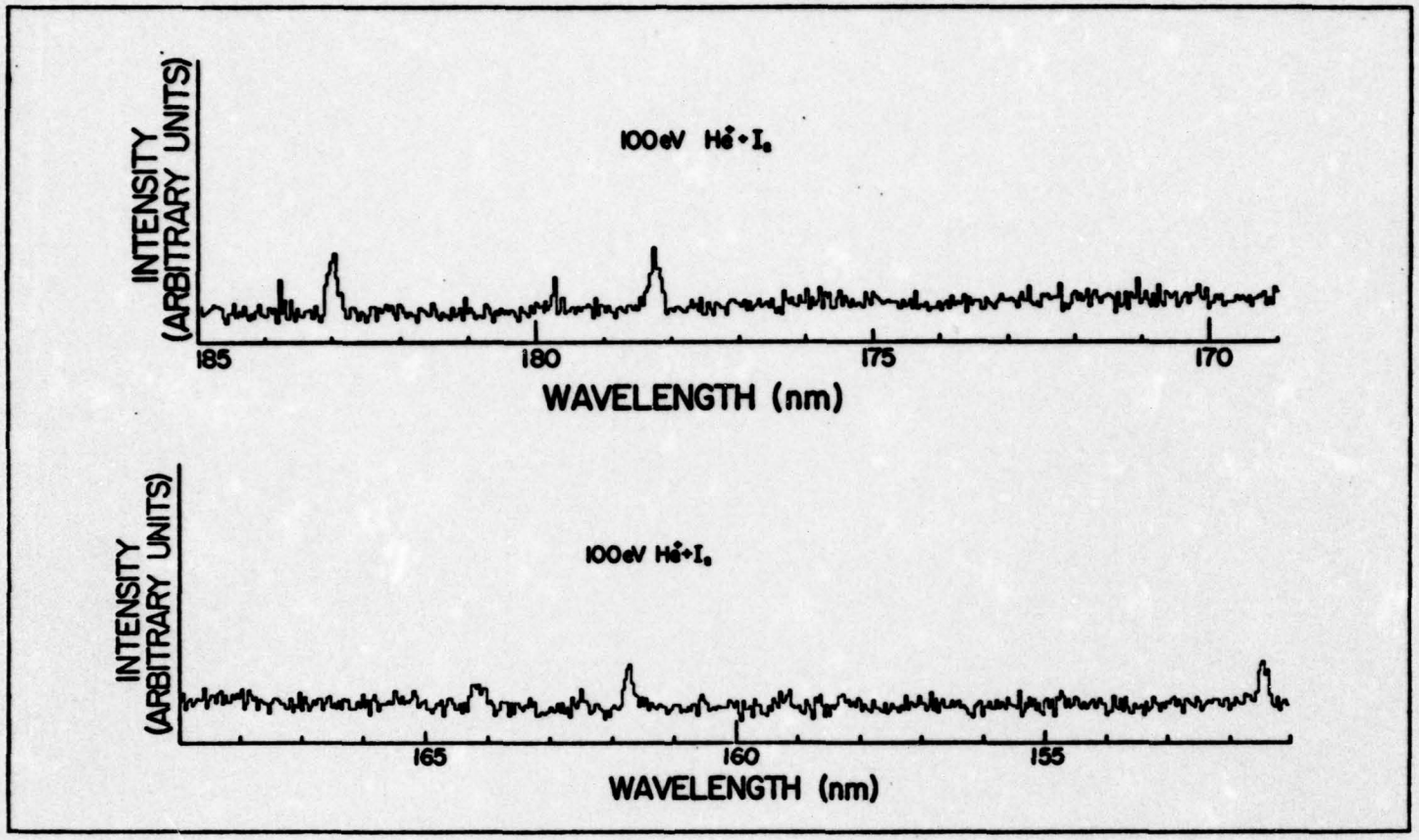

Fig. 47. High Resolution Spectra of 100 eV He^+ + I_2 Reaction in 150 nm to 185 nm Region.

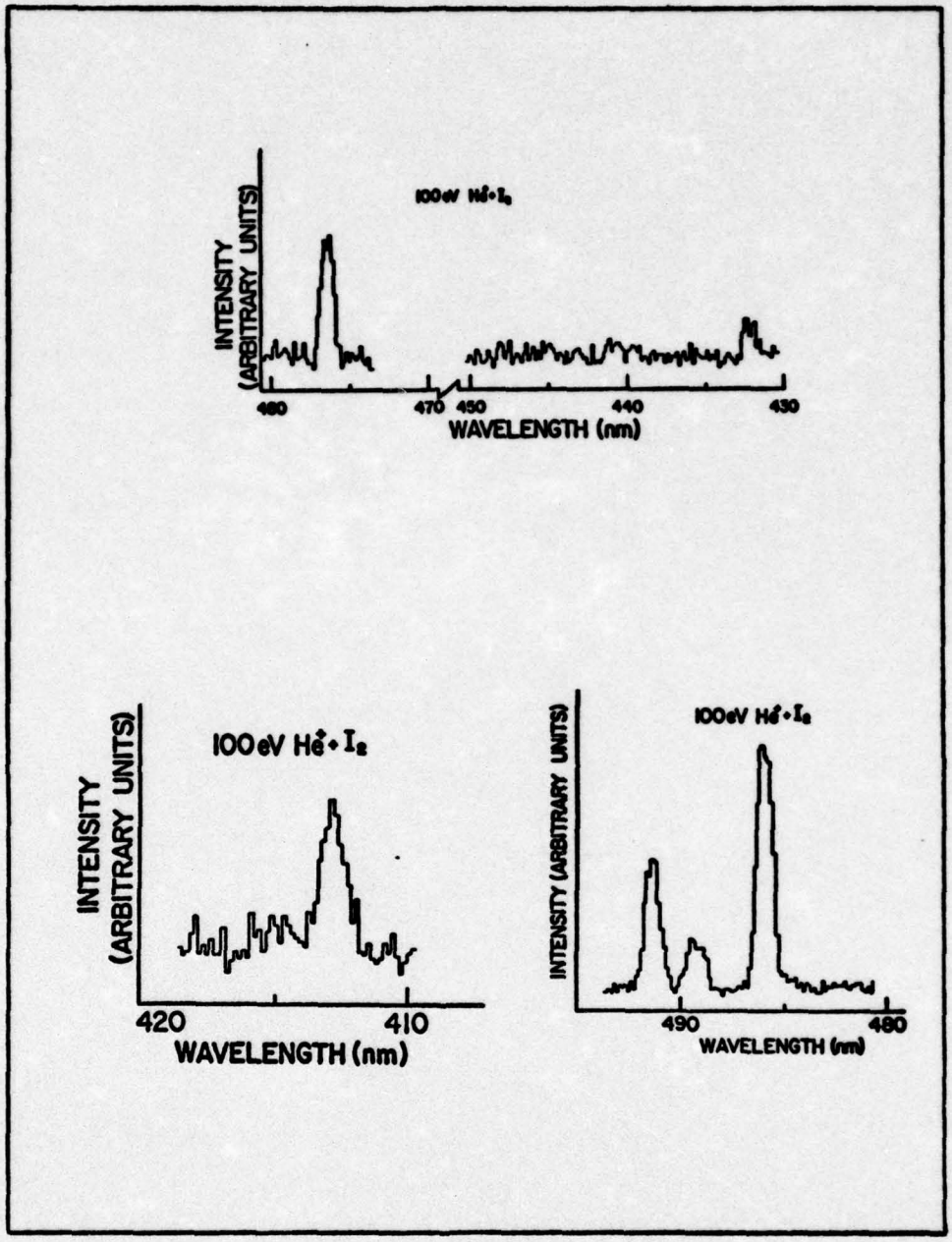

Fig. 48. High Resolution Spectra of 100 eV $He^+ + I_2$ Reaction in 410 nm to 495 nm Region.

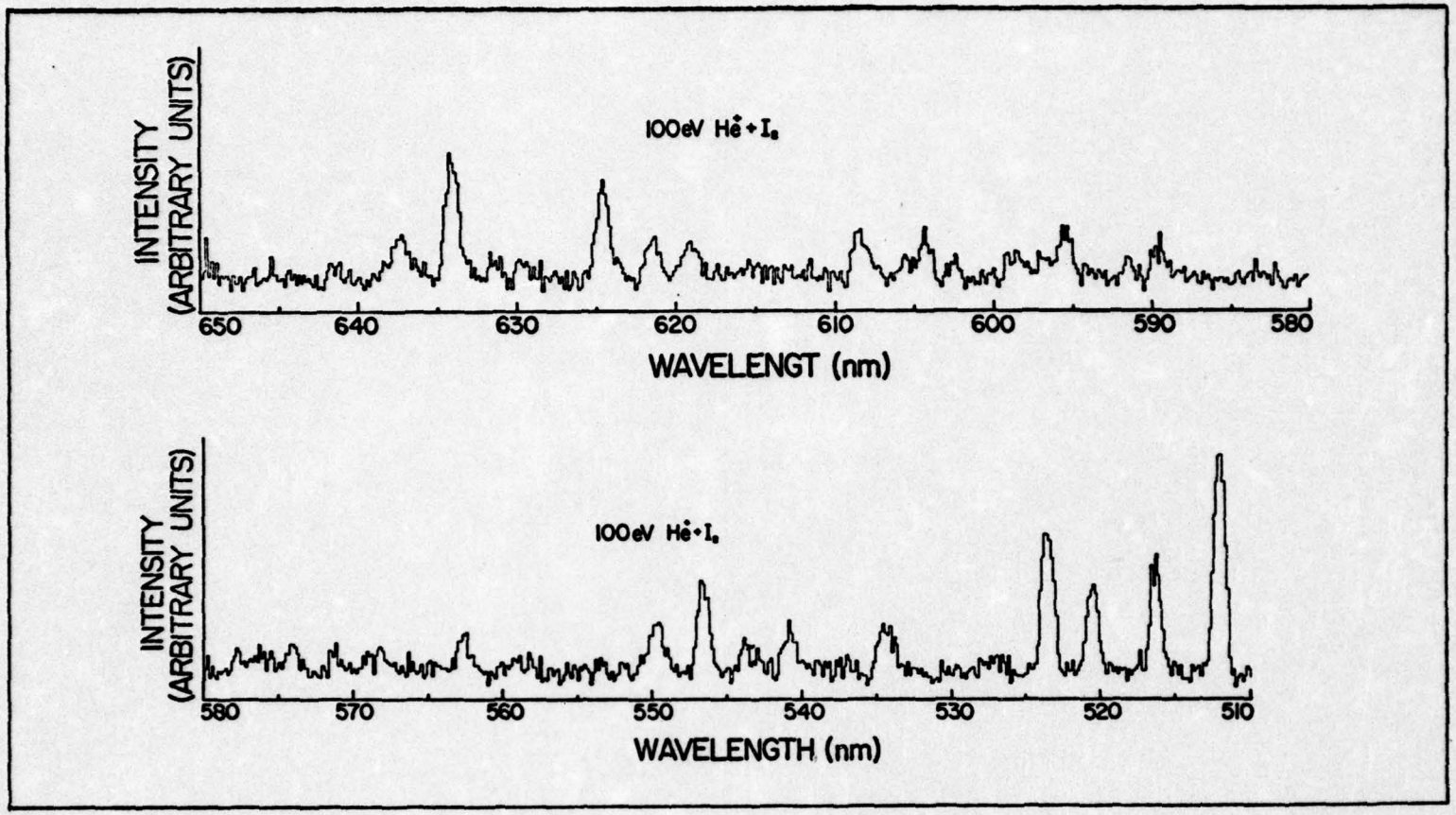

Fig. 49. High Resolution Spectra of 100 eV He^+ + I_2 Reaction in 510 nm to 650 nm Region.

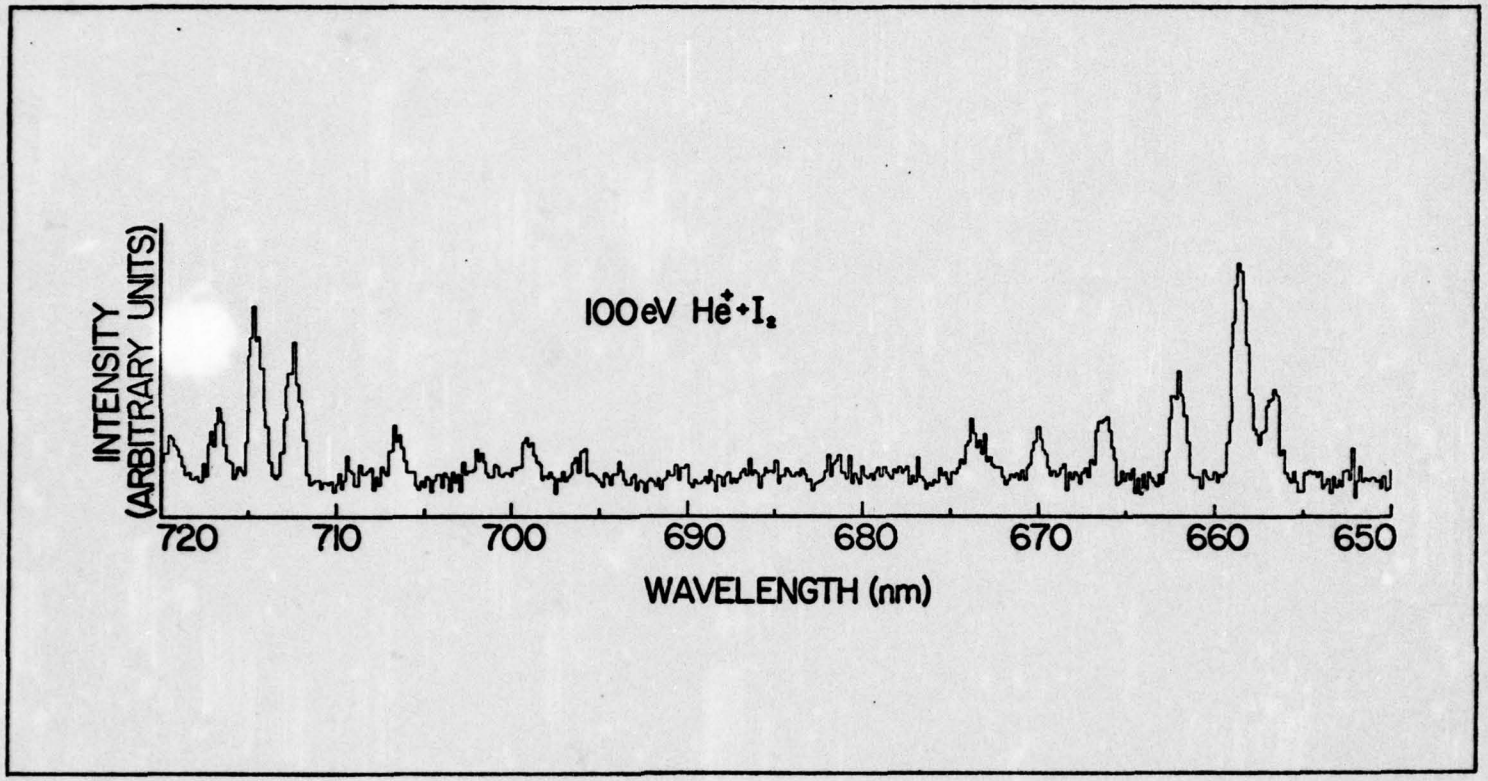

Fig. 50. High Resolution Spectra of 100 eV He^+ + I_2 Reaction in 650 nm to 720 nm Region.

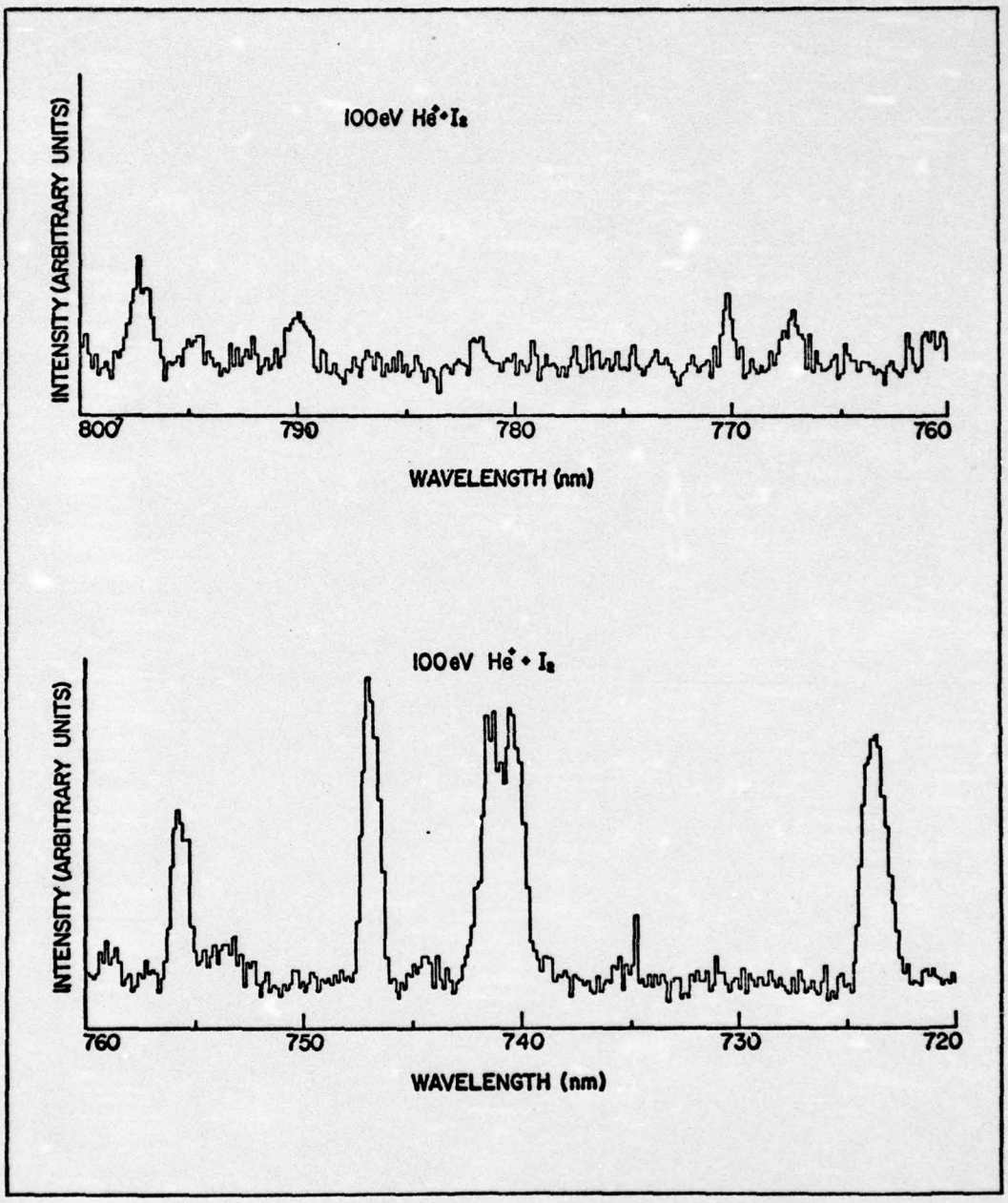

Fig. 51. High Resolution Spectra of 100 eV $He^+ + I_2$ Reaction in 720 nm to 800 nm Region.

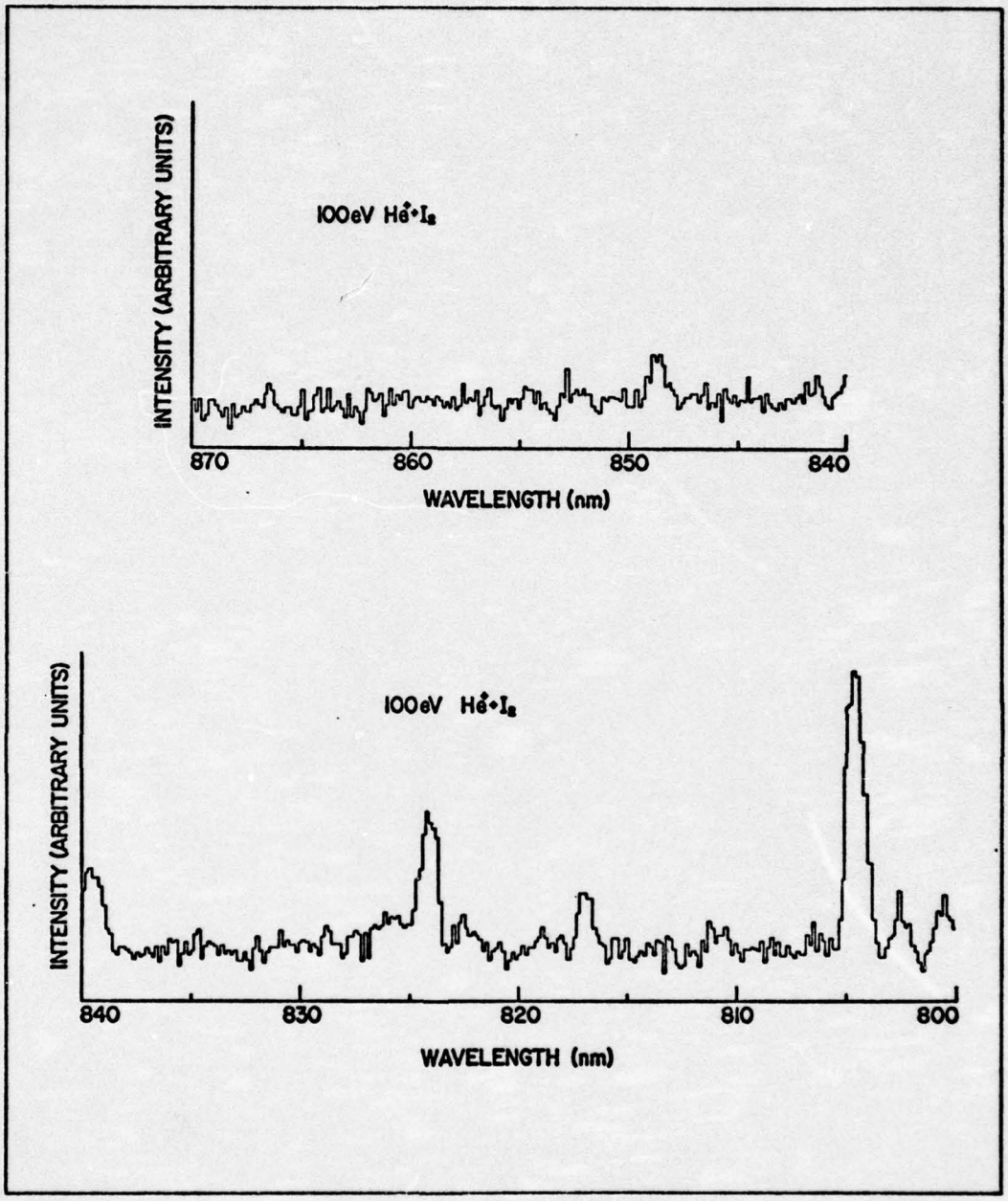

Fig. 52. High Resolution Spectra of 100 eV $He^+ + I_2$ Reaction in 800 nm to 870 nm Region.

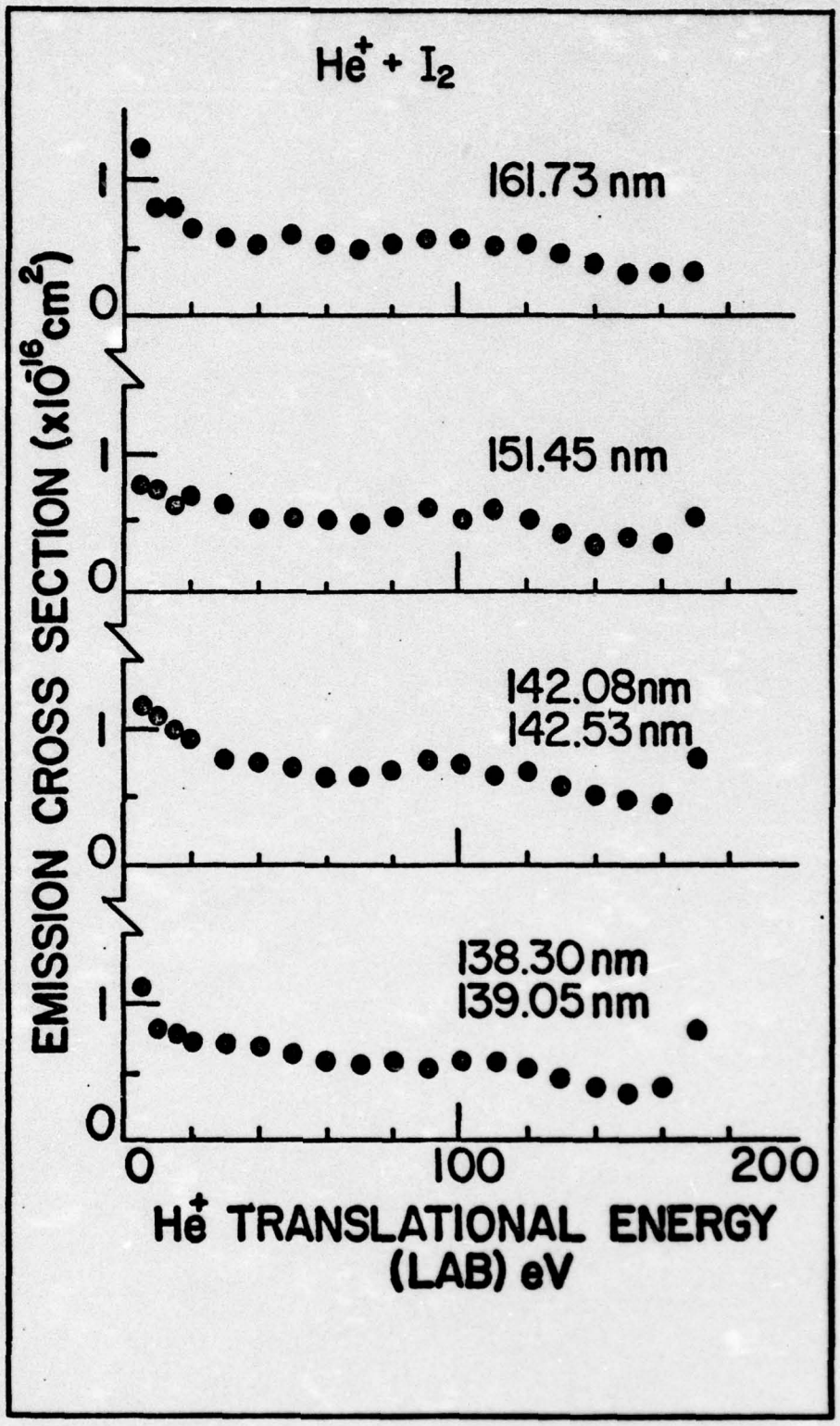

Fig. 53. The Energy Dependence of the Emission Cross Sections of Selected VUV Lines from the $He^+ + I_2$ Reaction.

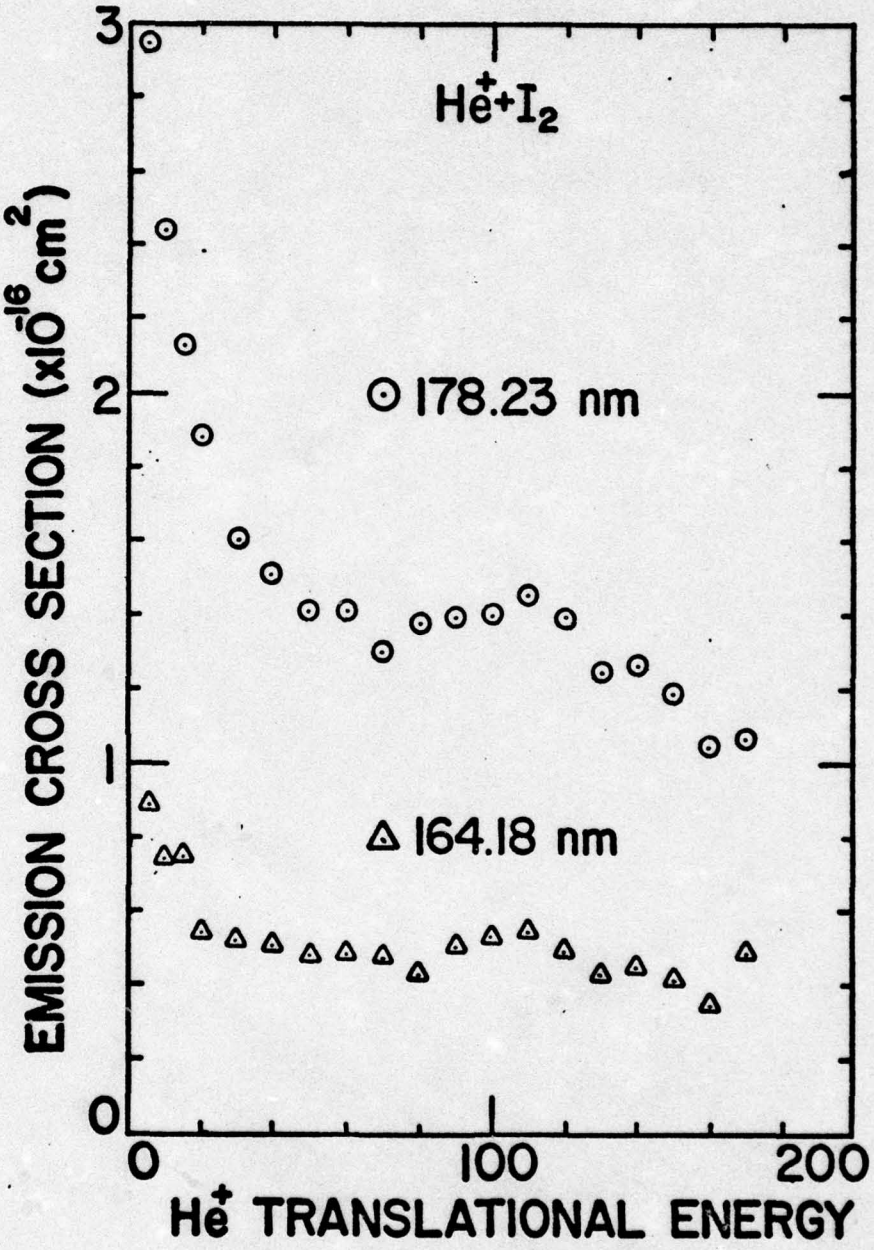

Fig. 54. The Energy Dependence of the Emission Cross Sections of the 164.18 nm and 178.23 nm Lines from the $He^+ + I_2$ Reaction.

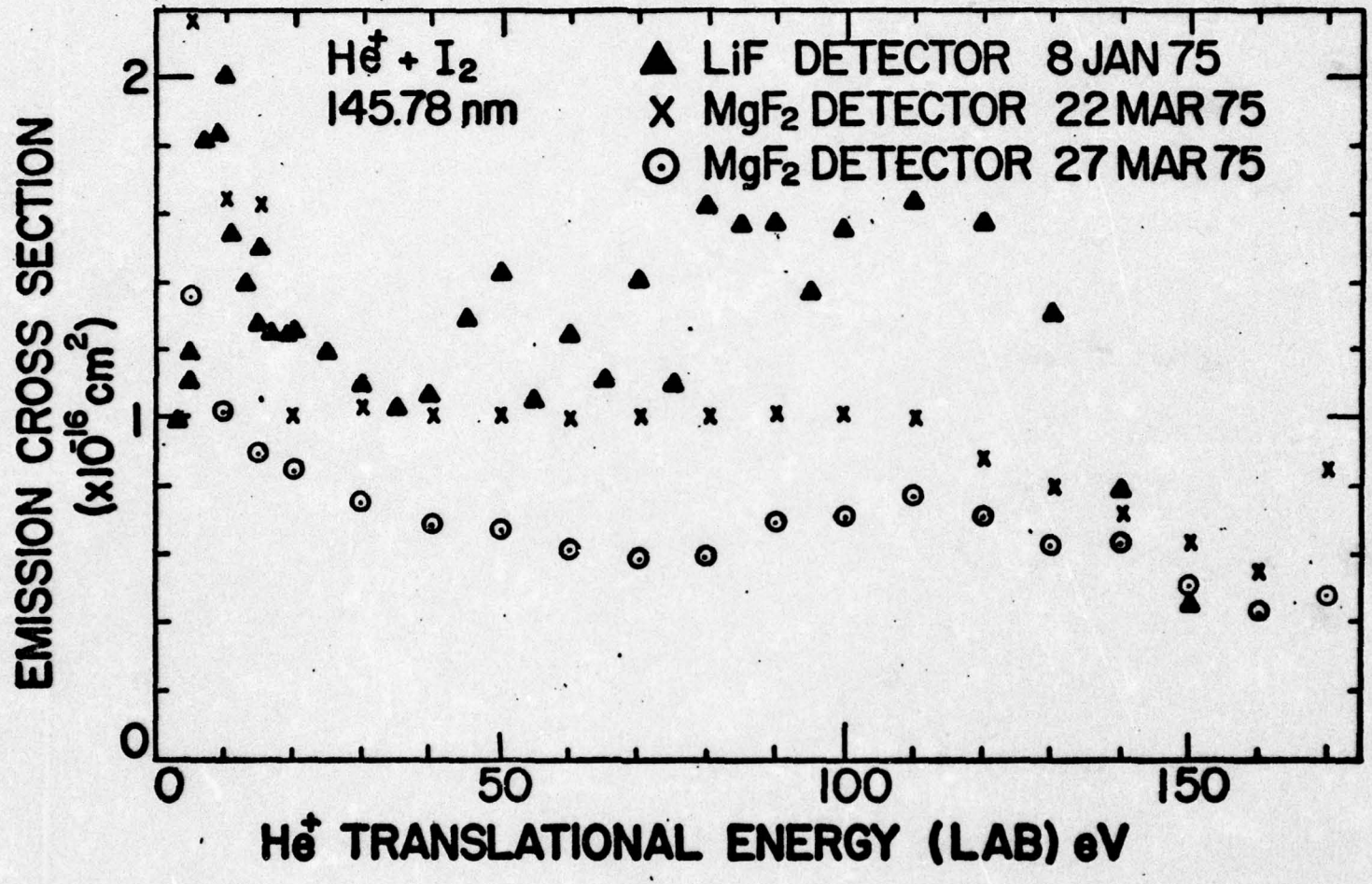

Fig. 55. The Energy Dependence of the Emission Cross Section of the 145.78 nm Line from the $He^+ + I_2$ Reaction Using Various Detectors.

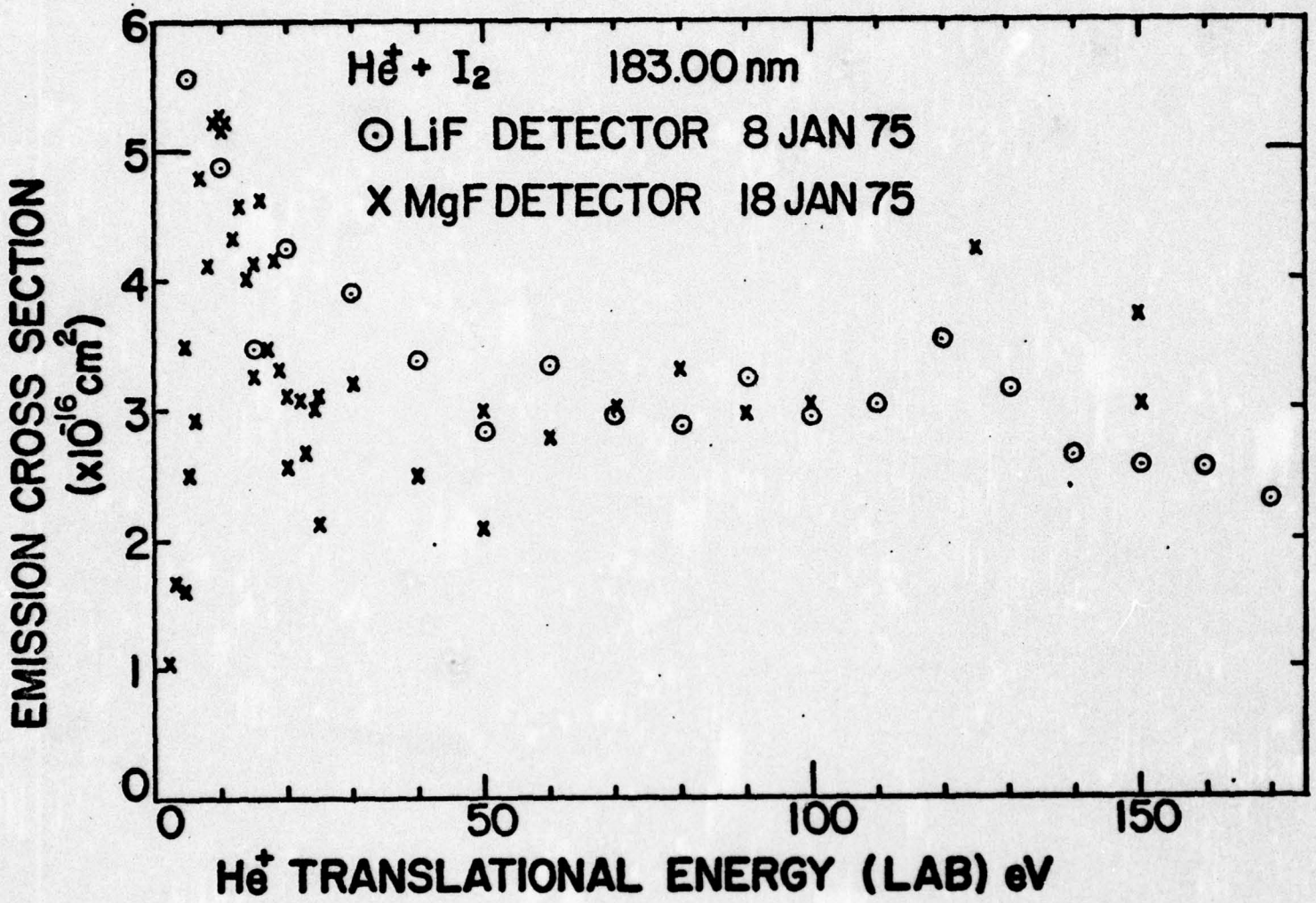

Fig. 56. The Energy Dependence of the Emission Cross Section of the 183.00 nm Line from the $He^+ + I_2$ Reaction Using Various Detectors.

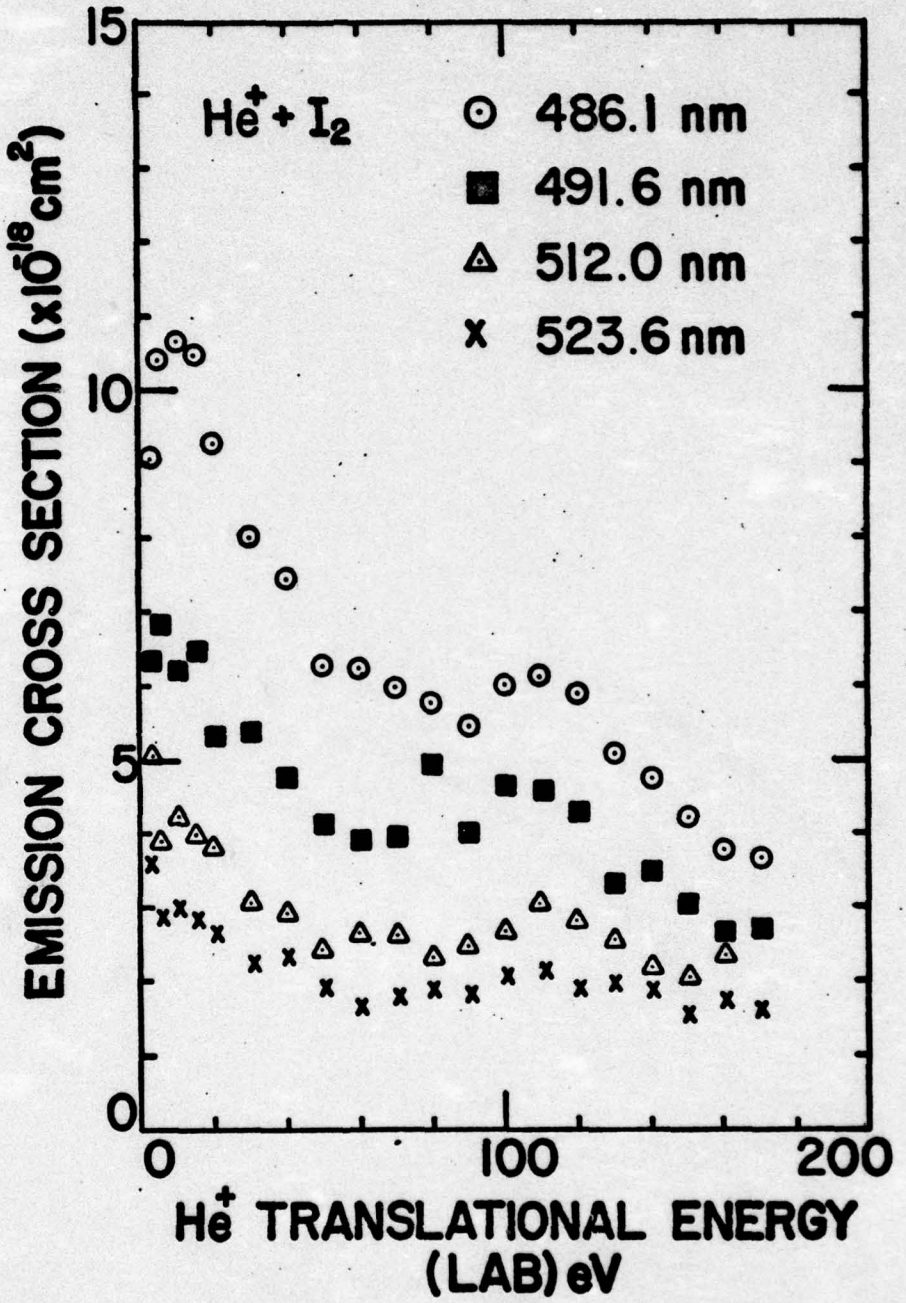

Fig. 57. The Energy Dependence of the Emission Cross Sections of Selected Visible Lines from the $He^+ + I_2$ Reaction.

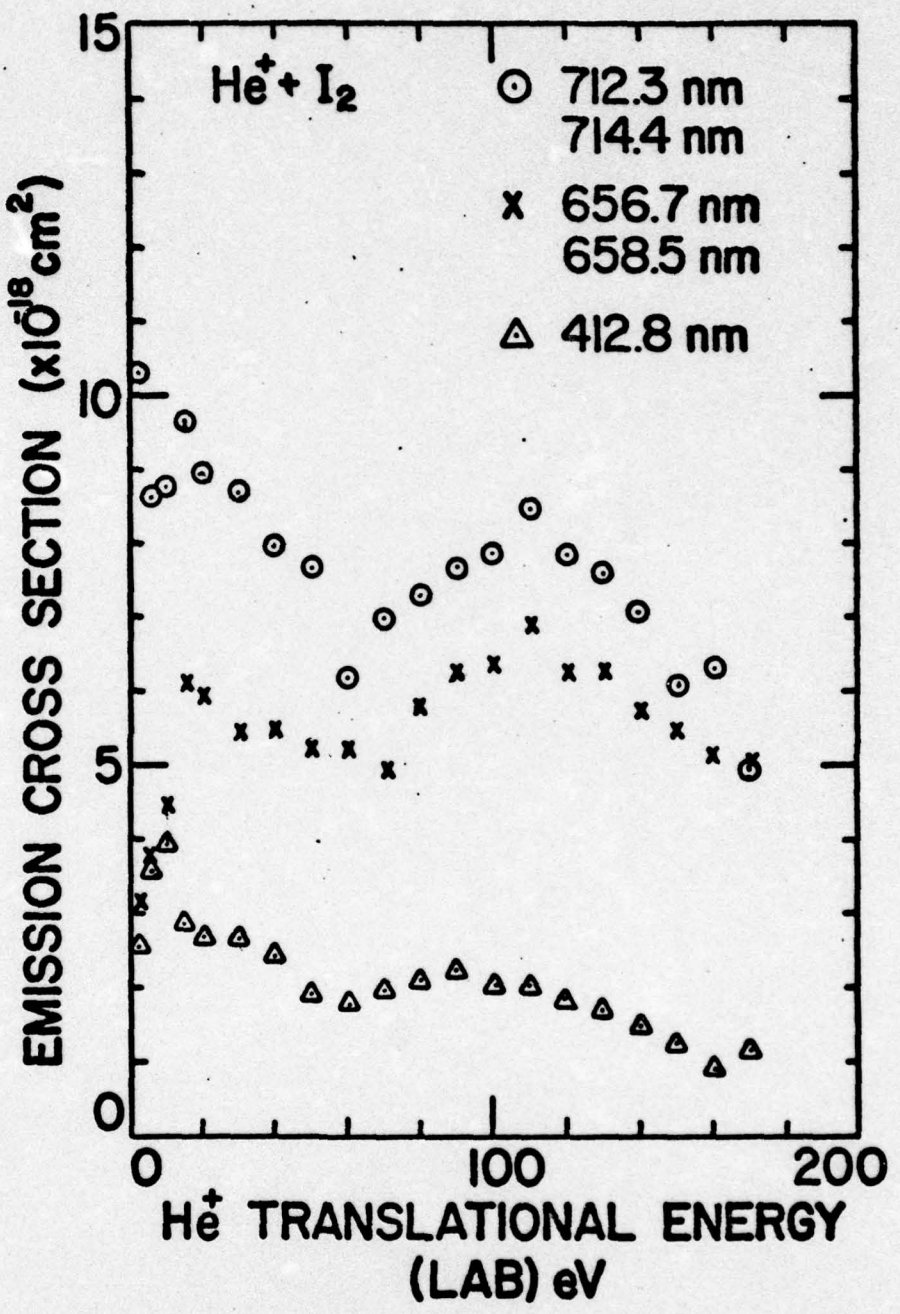

Fig. 58. The Energy Dependence of the Emission Cross Sections of Selected Lines from the $He^+ + I_2$ Reaction.

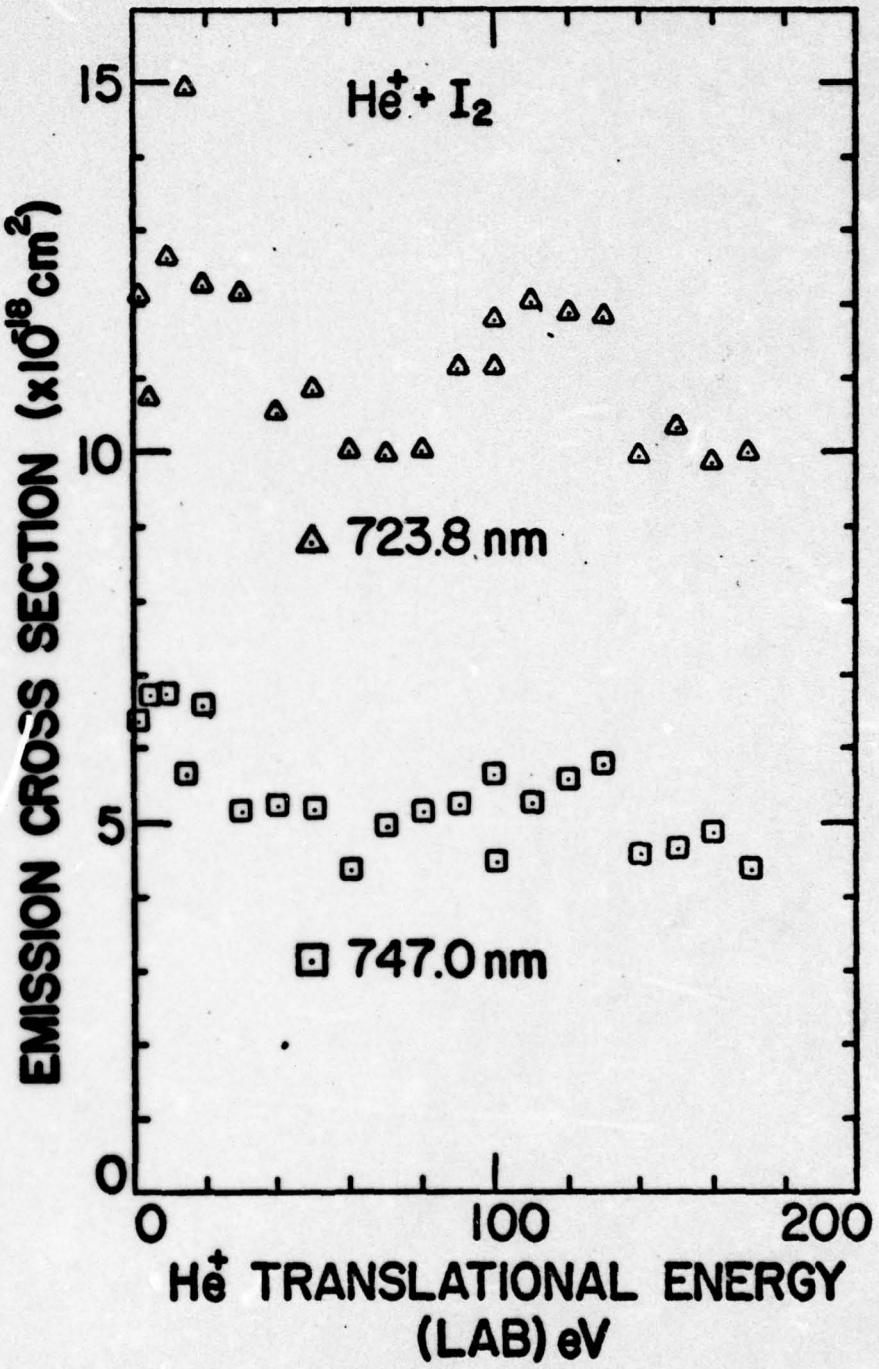

Fig. 59. The Energy Dependence of the Emission Cross Sections of the 723.8 nm and 747.0 nm Lines from the $He^+ + I_2$ Reaction.

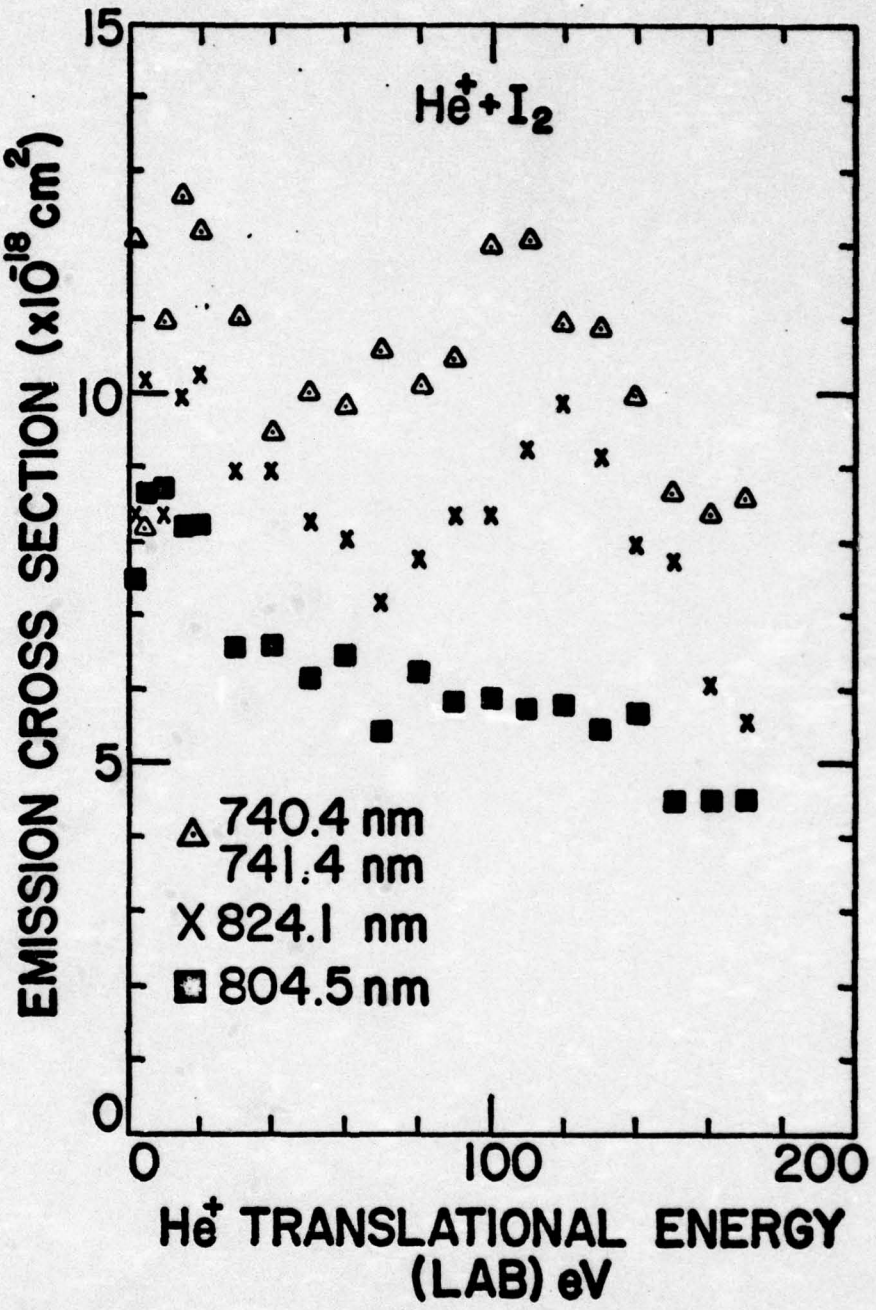

Fig: 60. The Energy Dependence of the Emission Cross Sections of Selected Infrared Lines from the $He^+ + I_2$ Reaction.

The curves indicate evidence of lines produced by both exothermic processes (such as in Fig. 54) and endothermic processes with low thresholds in the 0 eV to 5 eV region (such as in Fig. 56). As in Chapters V and VI, all of the cross section energy dependence curves are presented to aid in the selection of transition assignments and for completeness.

Line Identification

A listing of all of the allowed transitions which meet the measurement uncertainty $\Delta\lambda_0$ and the quantum-mechanical criteria described in Chapter IV for each observed wavelength λ_0 in the spectra, are listed in Table XVII in Appendix C. The measured cross section for each observed wavelength is also listed. The endothermicity in eV for thermal energy reactants is listed for each allowed transition's upper state. This endothermicity is measured above and below the 12.58 eV energy released by the thermal energy charge exchange reaction between He^+ and I_2 for the same purpose discussed previously in the chlorine line identification section. The search was compared with the energy levels for I I from both Ref 30 and Ref 48. Transitions which match Minnhagen's energy levels are listed in Table XVII as MI I.

Further Analysis

Table XII is a summary of the complete listings in Table XVII. Since the energy differences between the I I neutral iodine atom and I II ionic energy levels are not as

Table XII

Summary of 100 eV $He^+ + I_2$ Reaction Allowed Transitions Selected by the Computer Search Program

Classification of Allowed Transitions Listed in Computer Search	Number of Lines	$\sum\sigma$ ($\times 10^{-18}$ cm^2)	$\frac{\sum\sigma}{\sum_{Total}\sigma}$	Number of VUV Lines	$\sum_{VUV}\sigma$ ($\times 10^{-18}$ cm^2)	$\frac{\sum_{VUV}\sigma}{\sum_{Total}\sigma_{VUV}}$	Number of Visible Lines	$\sum_{Visible}\sigma$ ($\times 10^{-18}$ cm^2)	$\frac{\sum_{Visible}\sigma}{\sum_{Total}\sigma_{Visible}}$
I I	8	472.0	0.30	8	472.0	0.33	0	---	---
I II	14	202.6	0.13	11	200.1	0.14	3	2.5	0.02
I I and I II	59	917.8	0.58	8	765.2	0.53	51	152.6	0.98
Total	81	1592.4		27	1437.3		54	155.1	
					90% of $\sum_{Total}\sigma$			10% of $\sum_{Total}\sigma$	

large as in the cases of chlorine and bromine, it is difficult to apply the same analysis as was done for the chlorine and bromine data. It should be noted that although only 27 of the 81 observed lines were in the VUV, 90% of the total emission cross section was in the VUV. The total emission cross section for the 100 nm to 860 nm region was 1592.4 x 10^{-18} cm^2 with 1437.3 x 10^{-18} cm^2 in the VUV and 155.1 x 10^{-18} cm^2 in the visible.

The experiment has been successful in determining that iodine has a very large cross section, particularly in the VUV and has measured the cross sections of 81 emission lines. The energy dependence of many of these emission lines has been measured. Any further modeling in the form of term diagrams and the effects of cascading will require the use of a more sophisticated analysis than has been applied in this experiment.

In comparing the results of this experiment with the reported helium iodine ion laser lines it is found that only three emission lines are possible laser lines. The 540.8 nm and 562.6 nm emission lines are possible matches for the 540.736 nm and 562.569 nm laser lines. The cross sections of these emission lines were 1.0 x 10^{-18} cm^2. The 658.5 nm emission line (6.4 x 10^{-18} cm^2 cross section) is possibly the 658.521 nm laser line. The reason so few helium iodine ion laser lines were observed is probably because the metastable lifetimes of the upper energy levels of the laser lines are longer than the 1 x 10^{-6} sec lifetime observation

limitation of the ion-beam experiment. This is supported by Shay, et al. report that the measured lifetimes of most of the upper energy states of the I II laser lines measured were on the order of 3×10^{-4} sec (Ref 63).

VIII. Conclusion

Observations of the internal energy distribution of the product species of low energy He^+/halogen reactions for Cl_2, Br_2, and I_2 were made in the present studies. The emission cross sections for 173 individually resolved emission lines in the 60 nm to 870 nm region were measured. The variation of the emission cross sections with the He^+ translational energy was measured for the more intense lines. The excited product species from the reaction of 100 eV He^+ ions with Cl_2, Br_2, and I_2 are predominantly produced by charge exchange processes. It was discovered that the 100 eV He^+/halogen reaction total emission cross sections are very large and are predominantly in the VUV.

Additional analysis in the Cl_2 and Br_2 cases indicate that these emissions are predominantly from the lower energy levels of excited neutral halogen product species. Cascading is believed to account for approximately 20% of the total measured emission cross section, with the remaining 80% being produced by direct formation of excited energy states from the collision process. These findings are summarized in Tables XIII and XIV.

Figure 61 presents a reasonable explanation for the large increase in emission cross section between the chlorine system and the bromine system (5.0 A^2 to 14.9 A^2). In Fig. 61 the energy level range of all of the excited energy states of neutral and singly ionized chlorine, bromine, and iodine atoms are shown. A dashed line is drawn at the energy level

Table XIII

Summary of 100 eV He^+/Halogen Emission Cross Sections

Reaction	Total Number of Lines	$\sum_{Total}\sigma$ ($\times 10^{-18} cm^2$)	Number of VUV Lines	$\sum_{VUV}\sigma$ ($\times 10^{-18} cm^2$)	$\frac{\sum_{VUV}\sigma}{\sum_{Total}\sigma}$	Number of Visible Lines	$\sum_{Visible}\sigma$ ($\times 10^{-18} cm^2$)	$\frac{\sum_{Visible}\sigma}{\sum_{Total}\sigma}$
100 eV He^+/Cl_2	35	497.0	17	375.9	0.76	18	121.1	0.24
100 eV He^+/Br_2	57	1493.3	26	1188.9	0.80	31	304.4	0.20
100 eV He^+/I_2	81	1592.4	27	1437.3	0.90	54	155.1	0.10

Table XIV

Summary of Results of 100 eV He^+/Halogen Investigation in 60 nm to 870 nm Spectral Region

		Cl	Br	I
Total Emission Cross Section Observed	(A^2)	5.0	14.9	15.9
Total VUV Emission Cross Section Observed	(A^2)	3.8	11.9	14.4
	(%)[a]	76	80	90
Total Cross Section Identified as Definitely Ionic	(A^2)	0.13	0.15	2.0
	(%)[a]	3	1	13
Total Emission Cross Section of Neutral Model	(A^2)	4.1	12.7	-
	(%)[a]	83	85	-
Total Direct Formation Cross Section in Neutral Model	(A^2)	3.3	9.7	-
	(%)[b]	79	77	-
Total Cascading Cross Section in Neutral Model	(%)[b]	21	23	-

[a]The % of the total emission cross section observed.

[b]The % of the total emission cross section of the neutral model.

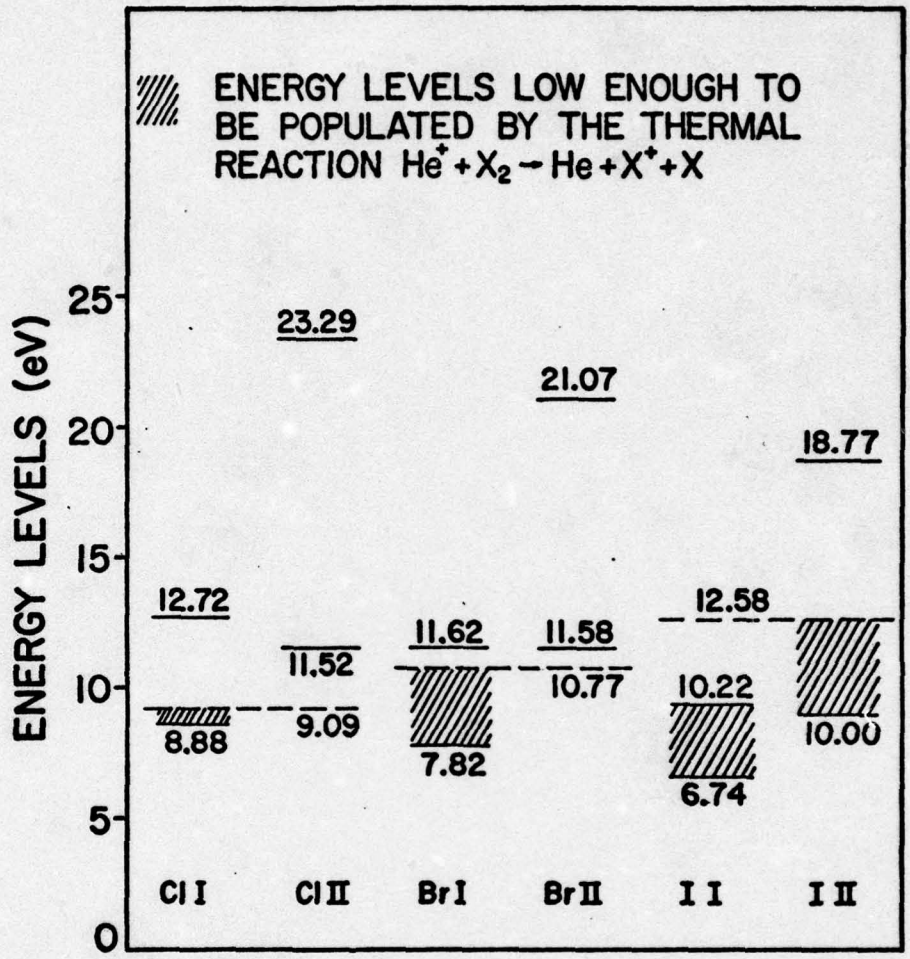

Fig. 61. Comparison of the Energy Levels of the Halogen Atoms and Ions Available for Population Exclusively by the Energy Released in Thermal Charge Transfer.

of the energy released in the thermal charge transfer process for each system (9.09 eV for chlorine, 10.77 eV for bromine, and 12.58 eV for iodine). The energy levels below the dashed line in each system are cross hatched to indicate they could be excited exclusively by the energy available in the thermal charge transfer process.

In the case of the chlorine system, only the very lowest energy states of the neutral chlorine atom can be excited exclusively by the 9.09 eV of energy available from the thermal charge transfer process. This is also illustrated in the chlorine neutral (Cl I) term diagram in Fig. 28. A direct result of this, is that the emissions observed in the chlorine system are predominantly the result of transitions from excited lower-level energy states of neutral chlorine. To be populated, the higher Cl I energy levels require the conversion of some of the kinetic energy of the He^+ ion into internal excitation energy. Therefore the cross sections for producing emissions from transitions from the higher Cl I energy levels are generally small. This also explains the endothermic process profiles of the cross sections energy dependence curves for the chlorine system (see Figs. 26 and 27). Since even the lowest energy levels of Cl II are 2.43 eV endothermic, only weak emissions from the very lowest Cl II energy states were observed (see Table XV). This explains the small cross sections for the production of emissions from excited chlorine ions. The predominant process for the production of emissions in the 60 nm to 870 nm spectral region

by the chlorine system appears to be

$$100 \text{ eV } He^+ + Cl_2 \rightarrow He + Cl^* + Cl^+ \qquad (11)$$

In the case of the bromine system, only the very highest energy states of the neutral bromine atom can not be excited exclusively by the 10.77 eV of energy available from the thermal charge transfer process. This is also illustrated in bromine neutral (Br I) term diagram in Fig. 42, where transitions from many excited energy states of bromine neutral atoms are shown. Since so many energy states are now available for excitation by the thermal charge transfer energy, the bromine emission cross section is nearly three times larger than the chlorine emission cross section. Since even the lowest energy levels of Br II are 0.71 eV endothermic, only weak emissions from the very lowest Br II energy states were observed (see Table XVI). This explains the small cross sections for the production of emissions from excited bromine ions. The predominant process for the production of emissions in the 60 nm to 870 nm spectral region by the bromine system appears to be

$$100 \text{ eV } He^+ + Br_2 \rightarrow He + Br^* + Br^+ \qquad (12)$$

In the case of the iodine system, all of the energy states of the neutral iodine atom and a large portion of the lower energy states of the singly ionized iodine atom, can be excited exclusively by the 12.58 eV of energy available from the thermal charge transfer process. This

explains the increase in the cross section for the production of emissions from excited iodine ions in the iodine system in comparison to the chlorine and bromine systems. This abundance of energy states which can be populated by charge transfer explains the exothermic process profiles of many of the cross section energy dependence curves for the iodine system (see Figs. 53 and 54). The predominant processes for the production of emissions in the 60 nm to 870 nm spectral region by the iodine system appears to be a result of both

$$100 \text{ eV } He^+ + I_2 \rightarrow He + I^* + I^+ \qquad (13)$$

and

$$100 \text{ eV } He^+ + I_2 \rightarrow He + I + (I^+)^* \qquad (14)$$

Because of the large VUV emission cross sections for the bromine and iodine systems (11.9 A^2 and 14.4 A^2), one can speculate that these systems are efficient sources of VUV radiation. The total charge transfer cross section has not been measured for the 100 eV $He^+ + Br_2$ and 100 eV $He^+ + I_2$ reactions. Comparison with similar systems, such as 100 eV He^+ + Ar, which have been measured, would lead one to estimate the total charge transfer value to be in the 20 A^2 to 50 A^2 region (Ref 37). If this is correct, then low energy He^+/Bromine and He^+/Iodine systems could be utilized as efficient sources of VUV radiation.

Bibliography

1. Bates, D. R. "Collisions Involving the Crossing of Potential Energy Curves". Proceedings of Royal Society (London), A257: 22-31 (27 September 1960).

2. Bengtson, Roger D., et al. "Atomic Transition Probabilities of the Halogens". Physical Review A, 3: 16-24 (January 1971).

3. Collins, C. B., et al. "Stimulated Emission from Charge-Transfer Reactions in the Afterglow of an e-Beam Discharge into High-Pressure Helium-Nitrogen Mixtures". Applied Physics Letters, 24: 477-478 (15 May 1974).

4. Collins, G. J. "Excitation Mechanisms in He-Cd and He-Zn Ion Lasers". Journal of Applied Physics, 44: 4633-4652 (October 1973).

5. DeHeer, F. J., et al. "Excitation of Ne, Ar, Kr, and Xe by He^+ Impact (0.3 - 10 keV)." Physics, 41: 588-619 (27 March 1969).

6. Dunn, Gordon H. Private Communication.

7. Dunn, Gordon H., et al. "Production of Lyman Alpha Radiation in Ion-atom Collisions". Physical Review, 128: 2200-2206 (1 December 1962).

8. Dworetsky, S. H. and R. Novick. "Experimental Tests of the Post-Collision-Interaction Model for the He^+ - He Excitation Functions". Physical Review Letters, 23: 1484-1488 (29 December 1969(.

9. Dworetsky, S. H., et al. "Gross Failure of the Conventional Adiabatic Criterion; Structure and Coherence in the Low-Energy Excitation of Helium Atoms by Helium Atoms". Physical Review Letters, 18: 939-941 (29 May 1967).

10. EMR Photoelectric Model 541F-08-18-03900 LiF Window Serial Number 15245 Multiplier Phototube. Spectral response was calibrated on 24 February 1971 by EMR Division of Weston Instruments, Inc., Box 44, Princeton, New Jersey 08540.

11. EMR Photoelectric Model 541F-09-18-03900 MgF_2 Window Serial Number 17891 Multiplier Phototube. Spectral response was calibrated on 29 January 1975 by EMR Division of Weston Instruments, Inc., Box 44, Princeton, New Jersey 08540.

12. Fannery, M. R., et al. "Theoretical and Experimental Zero-Field Reduced Mobilities for Molecular Ion-Molecule Systems". Chemical Physics Letters, 27: 221-223 (15 July 1974).

13. Franklin, J. L. Ion-Molecule Reactions. New York: Plenum Press, 1972.

14. Grating Calibrations performed by Analytical Systems Division, 820 Linden Avenue, Bausch and Lomb, Rochester, New York, 14625.

15. Hasted, J. B. Physics of Atomic Collisions. London: Butterworths, 1964.

16. Hertzberg, Gerhard. Molecular Spectra and Molecular Structure, Vol. I, Spectra of Diatomic Molecules, (Second Edition). New York: Van Nostrand Reinhold Company, 1950.

17. Hopper, Darrel. Private Communication.

18. Hughes, B. M., E. G. Jones, C. D. Miller and T. O. Tiernan. "Light Emission from Low-Energy Ion-Neutral Collisions". American Society for Mass Spectrometry Twenty-First Annual Conference on Mass Spectrometry and Allied Topics, San Francisco, California, 20-25 May 1973.

19. Hughes, B. M., E. G. Jones and T. O. Tiernan. Bulletin of American Physical Society, 19: 156 (1974).

20. Hughes, B. M., E. G. Jones and T. O. Tiernan. Abstracts of VIII International Conference on the Physics of Electronic and Atomic Collisions. Vol. I: 223. Institute of Physics, Beograd, Yugoslavia (1973).

21. Hughes, B. M., E. G. Jones and T. O. Tiernan. Private Communication.

22. Hunter, William R. Private Communication.

23. Interactions Between Ions and Molecules, edited by Pierre Ausloos. New York: Plenum Press, 1974.

24. Jaecks, D., F. J. DeHeer and A. Salop. "Excitation of Ne, Ar, Kr, and Xe by He^+ Impact (0.3 - 35 keV; 3000Å - 6000Å)". Physica, 36: 606-619 (1967).

25. Jensen, R. C. and G. R. Fowles. "New Laser Transitions in Iodine - Inert Gas Mixtures". Proceedings of the IEEE, 52: 1350 (November 1964).

26. Johnson, M. C. and J. Svenson. "Absolute Quantum Efficiency of a Channeltron Photomultiplier". A Technical Paper from the Bendix Corporation, Research Laboratories Division, Southfield, Michigan.

27. Johnson, Raynor C. An Introduction to Molecular Spectra. London: Methuen and Co., Ltd., 1949.

28. Jones, E. G., B. M. Hughes and T. O. Tiernan. "Low Energy He^+/H_2 Interactions". American Society for Mass Spectrometry Twenty-Third Annual Conference on Mass Spectrometry and Allied Topics, Houston, Texas, 25-30 May 1975.

29. Kaminsky, Manfred. Atomic and Ionic Impact Phenomena on Metal Surfaces. New York: Academic Press, Inc., 1965.

30. Kiess, C. C. and C. H. Corliss. "Description and Analysis of the First Spectrum of Iodine". Journal of Research of the National Bureau of Standards A. Physics and Chemistry, 63A: 1-18 (July-August 1959).

31. Klein, Miles V. Optics. New York: John Wiley and Sons, Inc., 1970.

32. Kobayashi, N. and Y. Kaneko. "Molecular Charge Transfer Reactions in the Thermal and Suprathermal Range". Abstracts of VIII International Conference on the Physics of Electronic and Atomic Collisions. Vol. I: 81-82. Institute of Physics, Beograd, Yugoslavia (1973).

33. Kostkouski, H. J. and R. D. Lee. "Theory and Methods of Optical Pyrometry". National Bureau of Standards Monograph 41. 1962.

34. Laidler, Keith J. The Chemical Kinetics of Excited States. Oxford: Oxford University Press, 1955.

35. Lawrence, G. M. "Resonance Transition Probabilities in Intermediate Coupling for Some Neutral Non-Metals". The Astrophysical Journal, 148: 261-268 (April 1967).

36. Leighton, Robert B. Principles of Modern Physics. New York: McGraw-Hill Book Compan, Inc., 1959.

37. Lindholm, Einar. "Mass Spectra and Appearance Potentials Studied by Use of Charge Exchange in a Tandem Mass Spectrometer". Ion-Molecule Interactions, edited by J. L. Franklin. New York: Plenum Press, 1972.

38. Lipeles, M. R. et al. "Energy Dependence of the 4610- and 4765A Lines of Ar^+ Excited in Low-Energy He^+ + Ar Collisions". Physical Review Letters, 24: 799-801 (13 April 1970).

39. Lipeles, M., R. Novick, and N. Tolk. "Optical Excitation with Very Low Energy Ions". Physical Review Letters, 15: 815-818 (22 November 1965).

40. Maier, William B. "Charge Transfer and Ionization in Collisions between Atomic Ions and Rare-Gas Atoms for Primary-Ion Energy below 100 eV". Physical Review A, 5: 1256-1267 (March 1972).

41. Martin, William C. and Charles H. Corliss. "The Spectrum of Singly Ionized Atomic Iodine (I II)". Journal of Research of the National Bureau of Standards A. Physics and Chemistry, 64A: 443-479 (November-December 1960).

42. Martin, William C. "Energy Levels and Spectrum of Neutral Helium (^{4}He I)". Journal of Research of the National Bureau of Standards A. Physics and Chemistry, 64: 19-28 (January-February 1960).

43. Marx, R. "Luminescence from Low Energy Ion Molecule Interaction". Interactions Between Ions and Molecules, edited by Pierre Ausloos. New York: Plenum Press, 1974.

44. Massey, H. S. W. "Collisions Between Atoms and Molecules at Ordinary Temperatures". The Physical Society (London) Reports on Progress in Physics, 12: 248-269 (1949).

45. McDaniel, E. W. Collision Phenomena in Ionized Gases. New York: John Wiley and Sons, Inc., 1964.

46. McDaniel, E. W., et al. Ion-Molecule Reactions. New York: Wiley-Interscience, 1970.

47. Miller, C. D. Private Communication.

48. Minnhagen, Lennart. "The Energy Levels of Neutral Atomic Iodine". Arkiv for Fysik, 21: 415-478 (1962).

49. Moore, Walter J. Physical Chemistry (Third Edition). Englewood Cliffs, New Jersey: Prentice-Hall, Inc., 1962.

50. "Nitrogen Ion Laser Pumped by Charge Transfer". Optical Spectra, 8: 29 (September 1974).

51. Pearse, R. W. B. and A. G. Gaydon. The Identification of Molecular Spectra (Third Edition). New York: John Wiley and Sons, Inc., 1963.

52. Piper, J. A. "Increased Efficiency and New CW Transitions in the Helium-Iodine Laser System". Journal of Physics, D: Applied Physics, 7: 323-328 (21 January 1974).

53. Pretzer, Donavon, et al. "Lyman Alpha Production in Proton-Rare Gas Collisions". Physical Review Letters, 10: 340-342 (15 April 1963).

54. Quartz, Jerry. Private Communication.

55. Radziemski, Leon J., Jr., and Victor Kaufman. "Wavelengths, Energy Levels, and Analysis of Neutral Chlorine (Cl I)". The Journal of the Optical Society of America, 59: 424-443 (April 1969).

56. Radziemski, Leon J., Jr., and Victor Kaufman. "Wavelengths, Energy Levels, and Analysis of the Second Spectrum of Chlorine (Cl II)". The Journal of the Optical Society of America, 64: 366-389 (March 1974).

57. Rao, Y. Bhupala. "Structure of the Spectrum of Doubly Ionized Bromine". Indian Journal of Physics, 35: 386-400 (August 1961).

58. Rao, Y. Bhupala. "Structure of the Spectrum of Singly Ionized Bromine". Indian Journal of Physics, 32: 497-515 (November 1958).

59. Rosenthal, H. "Nonadiabatic Effects in Slow Atomic Collisions I. $He^+ + He$". Physical Review A, 4: 1030-1042 (September 1971).

60. Rosenthal, H. and H. M. Foley. "Phase-Interference Effects in Inelastic $He^+ + He$ Collisions". Physical Review Letters, 23: 1480-1483 (29 December 1969).

61. Samson, J. A. R. Techniques of Vacuum Ultraviolet Spectroscopy. New York: John Wiley and Sons, Inc., 1967.

62. Schuebel, W. K. Private Communication.

63. Shay, T., et al. "Excitation Mechanism of the $He^+ - I^+$ Laser". Applied Physics Letters, 26: 531-534 (1 May 1975).

64. SSR Model 1110 Photon Counter System. SSR Instruments Co., 1001 Colorado Avenue, Santa Monica, California 90404.

65. Stebbins, R. F., et al. "Lyman-Alpha Production in $He^+ - H$ (1s) Collisions". Physical Review, 138: A1312-A1316 (31 May 1965).

66. Stedeford, J. B. H. and J. B. Hasted. "Further Investigations of Charge Exchange and Electron Detachment", Proceedings of the Royal Society of London, 227: 466-486 (8 February 1955).

67. Striganov, A. R. and N. S. Sventitskii. Tables of Spectral Lines of Neutral and Ionized Atoms. New York: Plenum, 1968.

68. Tech, Jack L. "Analysis of the Spectrum of Neutral Atomic Bromine (Br I)". Journal of Research of the National Bureau of Standards A. Physics and Chemistry 67A: 505-531 (November-December 1963).

69. Tolk, N. H., et al. "Phase Interference Effects in Low Energy $Na^+ - Ne^o$ and $Ne^o - Ne^o$ Collisions". in Abstracts of Papers of the VIIth International Conference on the Physics of Electronic and Atomic Collisions, edited by L. M. Branscomb, et al. Amsterdam: North-Holland Publishing Co., 1971.

70. Tolk, N. H. et al. "Quantum-Mechanical Phase Interference and Optical Polarization in Low-Energy Na^+ - Ne Inelastic Collisions". Physical Review A, 13 969-984 (March 1976).

71. Zaidel, A. N. and E. Ya. Shreider. Vacuum Ultraviolet Spectroscopy. Translated by Z. Lerman. Ann Arbor: Ann Arbor-Humphrey Science Publishers, 1970.

72. Zaidel, A. N., et al. Tables of Spectral Lines. New York: Plenum, 1970..

73. Zener, Clarence. "Non-Adiabatic Crossing of Energy Levels". The Proceedings of the Royal Society (London), A137: 696-702 (September 1932).

Appendix A

Table XV

Luminescence from the Reaction 100 eV $He^+ + Cl_2 \rightarrow He + Cl^+ + Cl + Energy$

Explanation of Symbols

λ_o = Observed vacuum wavelength (nm)

$\Delta\lambda_o$ = Search interval (nm)

σ = Emission cross section ($cm^2 \times 10^{18}$)

X = Emitting atom or ion

λ_T = Calculated vacuum wavelength in nm using the energy level tables (Refs. 42, 55 and 56).

ΔH = Enthalpy change in eV required to populate the upper energy state for the thermal reaction $He^+ + Cl_2 \rightarrow He + Cl^+ + Cl^*$.

\# = Transition selected by criteria stated in Chapter IV.

Inner electron configuration designation (Refs. 55 and 56).

Cl I Unprimed = (^3P) ' = (^1D)

Cl II Unprimed = (^4S) ' = (^2D) '' = (^2P)

Table XV (continued)

Luminescence from the Reaction 100 eV $He^+ + Cl_2 \rightarrow He + Cl^+ + Cl + Energy$

λ_o (nm)	$\Delta\lambda_o$ (nm)	σ ($cm^2 \times 10^{18}$)	X	Transition Assignment Lower State	←	Upper State	λ_T (nm)	$\lambda_T - \lambda_o$ (nm)	ΔH (eV)
96.15	0.30	2.2	Cl II	$3p^4\ ^1D_2$	←	$3d'\ ^1P^o_1$	96.150	0.000	5.25
					←	$3p^5\ ^1P^o_1$	96.150	0.000	5.25
102.80	0.60	8.1	Cl I	$3p^5\ ^2P^o_{3/2}$	←	$4d\ 2(0)_{1/2}$	103.167	0.367	2.93
					←	$4d\ 2(3)_{5/2}$	103.151	0.351	2.93
					←	$4d\ 2(1)_{3/2}$	103.088	0.288	2.94
					←	$4d\ 1(1)_{1/2}$	102.934	0.134	2.95
					←	$6s\ 2(2)_{5/2}$	102.841	0.041	2.97
					←	$4d\ 1(1)_{3/2}$	102.817	0.017	2.97
					←	$4d\ 1(3)_{5/2}$	102.734	-0.066	2.98
					←	$4d\ 1(2)_{3/2}$	102.718	-0.082	2.98
					←	$6s\ 2(2)_{3/2}$	102.584	-0.216	3.00
					←	$4d\ 1(2)_{5/2}$	102.528	-0.272	3.00
					←	$4d\ 0(2)_{5/2}$	102.241	-0.559	3.04
					←	$4d\ 0(2)_{3/2}$	102.205	-0.595	3.04

Table XV (continued)

Luminescence from the Reaction 100 eV $He^+ + Cl_2 \rightarrow He + Cl^+ + Cl + Energy$

λ_o (nm)	$\Delta\lambda_o$ (nm)	σ ($cm^2 \times 10^{18}$)	X	Transition Assignment Lower State	←	Upper State	λ_T (nm)	$\lambda_T - \lambda_o$ (nm)	ΔH (eV)
			Cl I	$3p^5\ ^2P^o_{1/2}$	←	$4d\ 0(2)_{3/2}$	103.135	0.335	3.04
					←	$6s\ 1(1)_{3/2}$	102.920	0.120	3.07
					←	$6s\ 1(1)_{1/2}$	102.862	0.062	3.07
					←	$6s\ 0(0)_{1/2}$	102.555	-0.245	3.11
106.40	0.30	3.4	Cl II	$3p^4\ ^3P_2$	←	$3p^5\ ^3P^o_1$	106.383	-0.017	2.56
					←	$3d'\ ^3P^o_1$	106.383	-0.017	2.56
107.10	0.50	7.7	Cl II	$3p^4\ ^3P_2$	←	$3p^5\ ^3P^o_2$	107.104	0.004	2.49
					←	$3d'\ ^3P^o_2$	107.104	0.004	2.49
				$3p^4\ ^3P_1$	←	$3p^5\ ^3P^o_1$	107.177	0.077	2.56
					←	$3d'\ ^3P^o_1$	107.177	0.077	2.56
					←	$3p^5\ ^3P^o_0$	106.794	-0.306	2.61
					←	$3d'\ ^3P^o_0$	106.794	-0.306	2.61
				$3p^4\ ^3P_0$	←	$3p^5\ ^3P^o_1$	107.523	0.423	2.56
					←	$3d'\ ^3P^o_1$	107.523	0.423	2.56

Table XV (continued)

Luminescence from the Reaction 100 eV $He^+ + Cl_2 \rightarrow He + Cl^+ + Cl$ + Energy

λ_o (nm)	$\Delta\lambda_o$ (nm)	σ ($cm^2 \times 10^{18}$)	X	Transition Assignment Lower State	←	Upper State	λ_T (nm)	$\lambda_T - \lambda_o$ (nm)	ΔH (eV)
108.80	0.35	13.0	Cl I	$3p^5\ ^2P^o_{3/2}$	←	$3d\ ^4P_{5/2}$	109.098	0.298	2.27
					←	$5s\ 2(2)_{3/2}$	109.074	0.274	2.28
					←	$3d\ ^2F_{5/2}$	108.806	0.006	2.30
					←	$5s\ 1(1)_{3/2}$	108.530	-0.270	2.33
					←	$5s\ 1(1)_{1/2}$	108.517	-0.283	2.33
					←	$3d\ ^2P_{3/2}$	108.467	-0.333	2.34
				$3p^5\ ^2P^o_{1/2}$	←	$5s\ 0(0)_{1/2}$	109.027	0.227	2.39
			Cl II	$3p^4\ ^1S_0$	←	$3d\ ^3D^o_1$	108.737	-0.063	5.77
					←	$3d'\ ^3D^o_1$	108.737	-0.063	5.77
				$3p^5\ ^3P^o_2$	←	$8f\ ^5F_3$	108.996	0.196	13.86
					←	$8f\ ^5F_2$	108.996	0.196	13.86
					←	$8f\ ^3F_3$	108.966	0.166	13.86
				$3d'\ ^3P^o_2$	←	$8f\ ^5F_3$	108.996	0.196	13.86
					←	$8f\ ^5F_2$	108.996	0.196	13.86
					←	$8f\ ^3F_3$	108.966	0.166	13.86

Table XV (continued)

Luminescence from the Reaction 100 eV $He^+ + Cl_2 \rightarrow He + Cl^+ + Cl + Energy$

λ_o (nm)	$\Delta\lambda_o$ (nm)	σ ($cm^2 \times 10^{18}$)	Transition Assignment X	Lower State	←	Upper State	λ_T (nm)	$\lambda_T - \lambda_o$ (nm)	ΔH (eV)
109.45	0.40	21.9	Cl I	$3p^5\ ^2P^o_{3/2}$	←	$3d\ ^4P_{1/2}$	109.807	0.357	2.20
					←	$3d\ ^2D_{5/2}$	109.737	0.287	2.21
					←	$3d\ ^2D_{3/2}$	109.681	0.231	2.21
					←	$5s\ 2(2)_{5/2}$	109.477	0.027	2.23
					←	$3d\ ^4P_{3/2}$	109.244	-0.206	2.26
					←	$3d\ ^2P_{1/2}$	109.213	-0.237	2.26
					←	$3d\ ^4P_{5/2}$	109.098	-0.352	2.27
					←	$5s\ 2(2)_{3/2}$	109.074	-0.376	2.28
				$3p^5\ ^2P^o_{1/2}$	←	$5s\ 1(1)_{3/2}$	109.580	0.130	2.33
					←	$5s\ 1(1)_{1/2}$	109.566	0.116	2.33
					←	$3d\ ^2P_{3/2}$	109.515	0.065	2.34
			Cl II	$3p^5\ ^3P^o_1$	←	$8f\ ^5F_2$	109.753	0.303	13.86
				$3d'\ ^3P^o_1$	←	$8f\ ^5F_2$	109.753	0.303	13.86

Table XV (continued

Luminescence from the Reaction 100 eV $He^+ + Cl_2 \rightarrow He + Cl^+ + Cl + Energy$

λ_o (nm)	$\Delta\lambda_o$ (nm)	σ ($cm^2 \times 10^{18}$)	X	Transition Assignment Lower State	←	Upper State	λ_T (nm)	$\lambda_T - \lambda_o$ (nm)	ΔH (eV)	
110.10	0.30	13.7	Cl I	$3p^5\ ^2P^o_{3/2}$	←	$3d\ ^4F_{5/2}$	110.194	0.094	2.16	
					←	$3d\ ^4F_{3/2}$	109.952	-0.148	2.19	
					←	$3d\ ^4P_{1/2}$	109.807	-0.293	2.20	
				$3p^5\ ^2P^o_{1/2}$	←	$3d\ ^4P_{3/2}$	110.307	0.207	2.26	
					←	$3d\ ^2P_{1/2}$	110.276	0.176	2.26	
					←	$5s\ 2(2)_{3/2}$	110.134	0.034	2.28	
110.75	0.30	3.8	Cl I	$3p^5\ ^2P^o_{1/2}$	←	$3d\ ^4F_{3/2}$	111.029	0.279	2.19	
					←	$3d\ ^4P_{1/2}$	110.881	0.131	2.20	
					←	$3d\ ^2D_{3/2}$	110.753	0.003	2.21	
118.825	0.100	61.9	Cl I	$3p^5\ ^2P^o_{3/2}$	←	$4s'\ ^2D_{5/2}$	118.877	0.052	1.34	#
					←	$4s'\ ^2D_{3/2}$	118.875	0.050	1.34	#
			Cl II	$3p^5\ ^3P^o_2$	←	$5p'\ ^3D_2$	118.890	0.065	12.91	
					←	$5p'\ ^3D_3$	118.791	-0.034	12.92	

Table XV (continued)

Luminescence from the Reaction 100 eV $He^+ + Cl_2 \rightarrow He + Cl^+ + Cl + Energy$

λ_o (nm)	$\Delta\lambda_o$ (nm)	σ ($cm^2 \times 10^{18}$)	Transition Assignment X	Lower State	←	Upper State	λ_T (nm)	$\lambda_T - \lambda_o$ (nm)	ΔH (eV)
			Cl II	$3p^5\ ^3P^o_2$	←	$5p'\ ^1P_1$	118.759	-0.066	12.93
					←	$5p'\ ^3F_3$	118.791	-0.034	12.92
					←	$5p'\ ^3D_1$	118.759	-0.066	12.93
				$3d'\ ^3P^o_2$	←	$5p'\ ^3D_2$	118.890	0.065	12.91
					←	$5p'\ ^3D_3$	118.791	-0.034	12.92
					←	$5p'\ ^1P_1$	118.759	-0.066	12.93
					←	$5p'\ ^3F_3$	118.791	-0.034	12.92
					←	$5p'\ ^3D_1$	118.759	-0.066	12.93
				$3p^5\ ^3P^o_1$	←	$5p'\ ^3P_2$	118.832	0.007	13.00
					←	$5p'\ ^3P_1$	118.797	-0.028	13.00
					←	$5p'\ ^3P_0$	118.782	-0.043	13.00
				$3d'\ ^3P^o_1$	←	$5p'\ ^3P_2$	118.832	0.007	13.00
					←	$5p'\ ^3P_1$	118.797	-0.028	13.00
					←	$5p'\ ^3P_0$	118.782	-0.043	13.00

Table XV (continued)

Luminescence from the Reaction 100 eV $He^+ + Cl_2 \rightarrow He + Cl^+ + Cl + Energy$

λ_o (nm)	$\Delta\lambda_o$ (nm)	σ ($cm^2 \times 10^{18}$)	X	Transition Assignment Lower State	←	Upper State	λ_T (nm)	$\lambda_T - \lambda_o$ (nm)	ΔH (eV)	
			Cl II	$3p^5\ ^3P^o_0$	←	$7p\ ^5P_1$	118.806	-0.019	13.04	
				$3d'\ ^3P^o_0$	←	$7p\ ^5P_1$	118.806	-0.019	13.04	
120.125	0.100	33.4	Cl I	$3p^5\ ^2P^o_{1/2}$	←	$4s'\ ^2D_{3/2}$	120.135	0.010	1.34	#
			Cl II	$3p^5\ ^3P^o_0$	←	$5p'\ ^1P_1$	120.137	0.012	12.93	
					←	$5p'\ ^3D_1$	120.137	0.012	12.93	
				$3d'\ ^3P^o_0$	←	$5p'\ ^1P_1$	120.137	0.012	12.93	
					←	$5p'\ ^3D_1$	120.137	0.012	12.93	
133.550	0.100	9.2	Cl I	$3p^5\ ^2P^o_{3/2}$	←	$4s\ ^2P_{1/2}$	133.573	0.023	0.19	#
			Cl II	$3d\ ^5D^o_4$	←	$8f\ ^3F_3$	133.614	0.064	13.86	
					←	$8f\ ^3F_4$	133.614	0.064	13.86	
				$3d\ ^5D^o_3$	←	$8f\ ^3F_3$	133.615	0.065	13.86	
					←	$8f\ ^3F_4$	133.615	0.065	13.86	
				$3d\ ^5D^o_2$	←	$8f\ ^3F_3$	133.621	0.071	13.86	

Table XV (continued)

Luminescence from the Reaction 100 eV $He^+ + Cl_2 \rightarrow He + Cl^+ + Cl + Energy$

λ_o (nm)	$\Delta\lambda_o$ (nm)	σ ($cm^2 \times 10^{18}$)	Transition Assignment X	Lower State	←	Upper State	λ_T (nm)	$\lambda_T - \lambda_o$ (nm)	ΔH (eV)	
134.700	0.100	45.6	Cl I	$3p^5\ ^2P^o_{3/2}$	←	$4s\ ^2P_{3/2}$	134.724	0.024	0.11	#
			Cl II	$4s\ ^5S^o_2$	←	$4f'\ ^3G_3$	134.741	0.041	13.49	
135.125	0.100	11.9	Cl I	$3p^5\ ^2P^o_{1/2}$	←	$4s\ ^2P_{1/2}$	135.166	0.041	0.19	#
136.300	0.100	13.8	Cl I	$3p^5\ ^2P^o_{1/2}$	←	$4s\ ^2P_{3/2}$	136.345	0.045	0.11	#
137.925	0.100	73.0	Cl I	$3p^5\ ^2P^o_{3/2}$	←	$4s\ ^4P_{3/2}$	137.953	0.028	-0.10	#
			Cl II	$4s\ ^3S^o_1$	←	$8f\ ^5F_2$	137.922	-0.003	13.86	
138.975	0.100	47.9	Cl I	$3p^5\ ^2P^o_{3/2}$	←	$4s\ ^4P_{5/2}$	138.969	-0.006	-0.17	#
				$3p^5\ ^2P^o_{1/2}$	←	$4s\ ^4P_{1/2}$	138.996	0.021	-0.06	#
			Cl II	$4s\ ^5S^o_2$	←	$5p'\ ^1D_2$	138.901	-0.074	13.21	
				$3d\ ^5D^o_4$	←	$4f'\ ^3G_5$	139.026	0.051	13.50	
					←	$4f'\ ^3F_4$	139.013	0.038	13.50	
					←	$4f'\ ^3F_3$	138.973	-0.002	13.51	

Table XV (continued)

Luminescence from the Reaction 100 eV $He^+ + Cl_2 \rightarrow He + Cl^+ + Cl + Energy$

λ_o (nm)	$\Delta\lambda_o$ (nm)	σ ($cm^2 \times 10^{18}$)	X	Transition Assignment Lower State	←	Upper State	λ_T (nm)	$\lambda_T - \lambda_o$ (nm)	ΔH (eV)
			Cl II	$3d\ ^5D^o_4$	←	$4f'\ ^1H_5$	138.965	-0.010	13.51
					←	$4f'\ ^3G_4$	139.013	0.038	13.50
					←	$4f'\ ^3G_3$	138.973	-0.002	13.51
					←	$4f'\ ^3H_5$	138.965	-0.010	13.51
					←	$8p\ ^5P_3$	138.933	-0.042	13.51
				$3d\ ^5D^o_3$	←	$4f'\ ^3F_4$	139.014	0.039	13.50
					←	$4f'\ ^3F_3$	138.975	0.000	13.51
					←	$4f'\ ^3G_4$	139.014	0.039	13.50
					←	$4f'\ ^3G_3$	138.975	0.000	13.51
					←	$8p\ ^5P_2$	138.942	-0.033	13.51
					←	$4f'\ ^3F_2$	138.936	-0.039	13.51
					←	$8p\ ^5P_3$	138.935	-0.040	13.51
					←	$4f'\ ^3D_2$	138.936	-0.039	13.51

Table XV (continued)

Luminescence from the Reaction 100 eV $He^+ + Cl_2 \rightarrow He + Cl^+ + Cl + Energy$

λ_o (nm)	$\Delta\lambda_o$ (nm)	σ ($cm^2 \times 10^{18}$)	Transition Assignment X	Lower State	←	Upper State	λ_T (nm)	$\lambda_T - \lambda_o$ (nm)	ΔH (eV)
			Cl II	$3d\ ^5D^o_2$	←	$4f'\ ^3F_3$	138.980	0.005	13.51
					←	$4f'\ ^3G_3$	138.980	0.005	13.51
					←	$8p\ ^5P_1$	138.952	-0.023	13.51
					←	$8p\ ^5P_2$	138.948	-0.027	13.51
					←	$4f'\ ^3F_2$	138.942	-0.033	13.51
					←	$8p\ ^5P_3$	138.940	-0.035	13.51
					←	$4f'\ ^1P_1$	138.927	-0.048	13.51
					←	$4f'\ ^3D_2$	138.942	-0.033	13.51
					←	$4f'\ ^3P_1$	138.927	-0.048	13.51
				$3d\ ^5D^o_1$	←	$8p\ ^5P_1$	138.957	-0.018	13.51
					←	$8p\ ^5P_2$	138.953	-0.022	13.51
					←	$4f'\ ^3F_2$	138.946	-0.029	13.51
					←	$4f'\ ^1P_1$	138.932	-0.043	13.51
					←	$4f'\ ^3D_2$	138.946	-0.029	13.51

Table XV (continued)

Luminescence from the Reaction 100 eV $He^+ + Cl_2 \rightarrow He + Cl^+ + Cl + Energy$

λ_o (nm)	$\Delta\lambda_o$ (nm)	σ ($cm^2 \times 10^{18}$)	X	Transition Assignment Lower State	←	Upper State	λ_T (nm)	$\lambda_T - \lambda_o$ (nm)	ΔH (eV)	
			Cl II	$3d\ ^5D^o_1$	←	$4f'\ ^3P_1$	138.932	-0.043	13.51	
				$3d\ ^4D^o_0$	←	$8p\ ^5P_1$	138.959	-0.016	13.51	
					←	$4f'\ ^1P_1$	138.935	-0.040	13.51	
					←	$4f'\ ^3P_1$	138.935	-0.040	13.51	
139.575	0.100	5.4	Cl I	$3p^5\ ^2P^o_{1/2}$	←	$4s\ ^4P_{3/2}$	139.653	0.078	-0.10	#
438.0	2.0	2.4	He I	$2p\ ^1P^o_1$	←	$5d\ ^3D_2$	438.938	0.938	14.95	
					←	$5d\ ^3D_1$	438.938	0.938	14.95	
					←	$5d\ ^1D_2$	438.916	0.916	14.95	
			Cl I	$4s\ ^4P_{5/2}$	←	$5p\ ^4D^o_{7/2}$	439.098	1.098	2.65	
					←	$5p\ ^2D^o_{5/2}$	437.277	-0.723	2.67	
				$4s\ ^4P_{3/2}$	←	$5p\ ^4D^o_{3/2}$	438.113	0.113	2.73	
					←	$5p\ ^4D^o_{5/2}$	436.449	-1.551	2.74	

Table XV (continued)

Luminescence from the Reaction 100 eV $He^+ + Cl_2 \rightarrow He + Cl^+ + Cl + Energy$

λ_o (nm)	$\Delta\lambda_o$ (nm)	σ ($cm^2 \times 10^{18}$)	X	Transition Assignment Lower State	←	Upper State	λ_T (nm)	$\lambda_T - \lambda_o$ (nm)	ΔH (eV)
			Cl I	$4s\ ^4P_{1/2}$	←	$5p\ ^4D^o_{1/2}$	439.164	1.164	2.76
					←	$5p\ ^4S^o_{3/2}$	438.879	0.879	2.76
					←	$5p\ ^2D^o_{3/2}$	437.073	-0.927	2.78
				$4s\ ^2P_{1/2}$	←	$4f\ 2(2)^o_{3/2}$	437.867	-0.133	3.02
					←	$4f\ 2(1)^o_{1/2}$	437.190	-0.810	3.03
					←	$4f\ 2(1)^o_{3/2}$	437.184	-0.816	3.03
			Cl II	$4p\ ^3P_1$	←	$4d\ ^5D^o_0$	437.408	-0.592	10.08
					←	$4d\ ^5D^o_1$	437.388	-0.612	10.08
					←	$4d\ ^5D^o_2$	437.353	-0.647	10.08
				$4p\ ^3P_2$	←	$4d\ ^5D^o_1$	437.628	-0.372	10.08
					←	$4d\ ^5D^o_2$	437.593	-0.407	10.08
					←	$4d\ ^5D^o_3$	437.543	-0.457	10.08
				$4p\ ^3P_0$	←	$4d\ ^5D^o_1$	437.643	-0.357	10.08
				$4p'\ ^3D_1$	←	$6s\ ^3S^o_1$	436.373	-1.627	11.89

Table XV (continued)

Luminescence from the Reaction 100 eV $He^+ + Cl_2 \rightarrow He + Cl^+ + Cl + Energy$

λ_o (nm)	$\Delta\lambda_o$ (nm)	σ ($cm^2 \times 10^{18}$)	X	Transition Assignment Lower State	←	Upper State	λ_T (nm)	$\lambda_T - \lambda_o$ (nm)	ΔH (eV)
			Cl II	$4p'\ ^3D_2$	←	$6s\ ^3S^o_1$	436.445	-1.555	11.89
				$4p'\ ^3F_2$	←	$5d\ ^5D^o_1$	439.665	1.665	11.96
					←	$5d\ ^5D^o_2$	439.660	1.660	11.96
					←	$5d\ ^5D^o_3$	439.650	1.650	11.96
				$4p'\ ^1F_3$	←	$5s'\ ^3D^o_2$	436.115	-1.885	12.05
				$4p'\ ^3P_2$	←	$4d'\ ^3F^o_2$	439.085	1.085	12.31
					←	$4d'\ ^3F^o_3$	437.592	-0.408	12.32
				$5p\ ^5P_1$	←	$5s'\ ^3P^o_0$	436.907	-1.093	13.52
					←	$5s'\ ^3P^o_1$	436.249	-1.751	13.52
				$5p\ ^5P_2$	←	$5s'\ ^3P^o_1$	436.533	-1.467	13.52
				$4p''\ ^1P_1$	←	$5s'\ ^3P^o_0$	439.291	1.291	13.52
					←	$5s'\ ^3P^o_1$	438.625	0.625	13.52
					←	$5s'\ ^3P^o_2$	437.162	-0.838	13.53

Table XV (continued)

Luminescence from the Reaction 100 eV $He^+ + Cl_2 \rightarrow He + Cl^+ + Cl + Energy$

λ_o (nm)	$\Delta\lambda_o$ (nm)	σ ($cm^2 \times 10^{18}$)	X	Transition Assignment Lower State	←	Upper State	λ_T (nm)	$\lambda_T - \lambda_o$ (nm)	ΔH (eV)
			Cl II	$3d'\ ^3D^o_3$	←	$4f\ ^5F_4$	438.936	0.936	11.26
					←	$4f\ ^5F_3$	438.928	0.928	11.26
					←	$4f\ ^5F_2$	438.921	0.921	11.26
					←	$4f\ ^3F_2$	437.425	-0.575	11.27
					←	$4f\ ^3F_3$	437.423	-0.577	11.27
					←	$4f\ ^3F_4$	437.415	-0.585	11.27
				$3d\ ^3D^o_2$	←	$4f\ ^5F_3$	438.928	0.928	11.26
					←	$4f\ ^5F_2$	438.921	0.921	11.26
					←	$4f\ ^5F_1$	438.915	0.915	11.26
					←	$4f\ ^3F_2$	437.425	-0.575	11.27
					←	$4f\ ^3F_3$	437.423	-0.577	11.27
				$4f\ ^5F_4$	←	$6s'\ ^3D^o_3$	439.238	1.238	14.08
				$4f\ ^5F_3$	←	$6s'\ ^3D^o_2$	439.967	1.967	14.08
					←	$6s'\ ^3D^o_3$	439.247	1.247	14.08

Table XV (continued)

Luminescence from the Reaction 100 eV $He^+ + Cl_2 \rightarrow He + Cl^+ + Cl + Energy$

λ_o (nm)	$\Delta\lambda_o$ (nm)	σ ($cm^2 \times 10^{18}$)	X	Transition Assignment			λ_T (nm)	$\lambda_T - \lambda_o$ (nm)	ΔH (eV)
				Lower State	←	Upper State			
			Cl II	$4f\ ^5F_2$	←	$6s'\ ^3D^o_2$	439.975	1.975	14.08
					←	$6s'\ ^3D^o_3$	439.254	1.254	14.08
				$4f\ ^5F_1$	←	$6s'\ ^3D^o_2$	439.981	1.981	14.08
				$4f\ ^3F_2$	←	$6s'\ ^1D^o_2$	436.094	-1.906	14.11
				$4f\ ^3F_3$	←	$6s'\ ^1D^o_2$	436.096	-1.904	14.11
				$4d\ ^5D^o_0$	←	$5p'\ ^3D_1$	438.084	0.084	12.91
					←	$5p'\ ^1P_1$	438.084	0.084	12.91
				$4d\ ^5D^o_1$	←	$5p'\ ^3D_1$	438.104	0.104	12.91
					←	$5p'\ ^3D_2$	437.445	-0.555	12.91
					←	$5p'\ ^1P_1$	438.104	0.104	12.91
				$4d\ ^5D^o_2$	←	$5p'\ ^3D_1$	438.140	0.140	12.91
					←	$5p'\ ^3D_2$	437.481	-0.519	12.91
					←	$5p'\ ^3D_3$	436.152	-1.848	12.92
					←	$5p'\ ^1P_1$	438.140	0.140	12.91

Table XV (continued)

Luminescence from the Reaction 100 eV $He^+ + Cl_2 \rightarrow He + Cl^+ + Energy$

λ_o (nm)	$\Delta\lambda_o$ (nm)	σ ($cm^2 \times 10^{18}$)	X	Transition Assignment Lower State	←	Upper State	λ_T (nm)	$\lambda_T - \lambda_o$ (nm)	ΔH (eV)
			Cl II	$4d\ ^5D^o_2$	←	$5p'\ ^3F_3$	436.152	-1.848	12.92
				$4d\ ^5D^o_3$	←	$5p'\ ^3D_2$	437.530	-0.470	12.91
					←	$5p'\ ^3D_3$	436.202	-1.798	12.92
					←	$5p'\ ^3F_3$	436.202	-1.798	12.92
				$4d\ ^5D^o_4$	←	$5p'\ ^3D_3$	436.222	-1.778	12.92
					←	$5p'\ ^3F_3$	436.222	-1.778	12.92
				$3d'\ ^3P^o_2$	←	$5p'\ ^1D_2$	438.694	0.694	13.21
				$3p\ ^3P^o_2$	←	$5p'\ ^1D_2$	438.694	0.694	13.21
579.6	2.0	3.6	Cl I	$4p\ ^4P^o_{5/2}$	←	$5d\ 1(3)_{7/2}$	580.453	0.853	3.33
					←	$5d\ 1(1)_{3/2}$	579.640	0.040	3.33
					←	$5g\ 2(4)_{7/2}$	578.955	-0.645	3.33
					←	$5g\ 2(3)_{5/2}$	578.746	-0.854	3.33
					←	$5g\ 2(3)_{7/2}$	578.745	-0.855	3.33

Table XV (continued)

Luminescence from the Reaction 100 eV $He^+ + Cl_2 \rightarrow He + Cl^+ + Cl + Energy$

λ_o (nm)	$\Delta\lambda_o$ (nm)	σ ($cm^2 \times 10^{18}$)	X	Transition Assignment			λ_T (nm)	$\lambda_T - \lambda_o$ (nm)	ΔH (eV)
				Lower State	←	Upper State			
			Cl I	$4p\ ^4P^o_{5/2}$	←	$5g\ 2(2)_{5/2}$	578.476	-1.124	3.33
					←	$5g\ 2(2)_{3/2}$	578.476	-1.124	3.33
				$4p\ ^4D^o_{5/2}$	←	$8s\ 2(2)_{5/2}$	578.237	-1.363	3.48
				$4p\ ^4P^o_{3/2}$	←	$5d\ 1(2)_{5/2}$	580.846	1.246	3.35
				$4p\ ^4D_{3/2}$	←	$6d\ 1(1)_{3/2}$	580.044	0.444	3.52
				$4p\ ^4D^o_{7/2}$	←	$6d\ 2(4)_{9/2}$	580.152	0.552	3.45
					←	$3d'\ ^2G_{7/2}$	579.806	0.206	3.45
					←	$3d'\ ^2G_{9/2}$	579.791	0.191	3.45
					←	$5g\ 0(4)_{9/2}$	578.059	-1.541	3.46
					←	$5g\ 0(4)_{7/2}$	578.059	-1.541	3.46
				$4p\ ^2D^o_{5/2}$	←	$6d\ 1(2)_{3/2}$	581.479	1.879	3.54
					←	$6d\ 1(2)_{5/2}$	581.028	1.428	3.54
					←	$3d'\ ^2P_{3/2}$	578.132	-1.468	3.55

Table XV (continued)

Luminescence from the Reaction 100 eV $He^+ + Cl_2 \rightarrow He + Cl^+ + Cl + Energy$

λ_o (nm)	$\Delta\lambda_o$ (nm)	σ ($cm^2 \times 10^{18}$)	X	Transition Assignment Lower State	←	Upper State	λ_T (nm)	$\lambda_T - \lambda_o$ (nm)	ΔH (eV)
			Cl I	$4p\ ^4D^o_{1/2}$	←	$3d'\ ^2P_{1/2}$	579.490	-0.110	3.55
					←	$3d'\ ^2P_{3/2}$	579.490	-0.110	3.55
					←	$6d\ 0(2)_{3/2}$	577.643	-1.957	3.56
				$4p\ ^2D^o_{3/2}$	←	$3d'\ ^2D_{5/2}$	581.428	1.828	3.58
				$4p\ ^2P^o_{3/2}$	←	$8d\ 2(2)_{5/2}$	581.264	1.664	3.64
			Cl II	$4p\ ^5P_3$	←	$3d''\ ^3P^o_2$	578.572	-1.028	9.01
					←	$3d'\ ^3P^o_2$	578.572	-1.028	9.01
				$4s'\ ^1D^o_2$	←	$4p'\ ^3D_1$	579.213	-0.387	9.05
					←	$4p'\ ^3D_2$	579.086	-0.514	9.05
				$4p'\ ^1D_2$	←	$5s'\ ^3D^o_1$	579.439	-0.161	12.05
					←	$5s'\ ^3D^o_2$	578.755	-0.845	12.05
				$5p\ ^5P_1$	←	$7s\ ^5S^o_2$	581.110	1.510	12.81
				$4p''\ ^3P_1$	←	$6d\ ^5D^o_1$	579.146	-0.454	12.89
				$4p''\ ^3P_2$	←	$4d'\ ^3S^o_1$	578.697	-0.903	12.91

Table XV (continued)

Luminescence from the Reaction 100 eV $He^+ + Cl_2 \rightarrow He + Cl^+ + Cl + Energy$

λ_o (nm)	$\Delta\lambda_o$ (nm)	σ ($cm^2 \times 10^{18}$)	X	Transition Assignment Lower State	←	Upper State	λ_T (nm)	$\lambda_T - \lambda_o$ (nm)	ΔH (eV)
			Cl II	$3d''\ ^3F^o_2$	←	$5p\ ^3P_2$	578.325	-1.275	10.95
					←	$5p\ ^3P_1$	577.666	-1.934	10.95
					←	$4p''\ ^3P_2$	578.325	-1.275	10.95
					←	$4p''\ ^3P_1$	577.666	-1.934	10.95
				$3d'\ ^3F^o_2$	←	$5p\ ^3P_2$	578.325	-1.275	10.95
					←	$5p\ ^3P_1$	577.666	-1.934	10.95
					←	$4p''\ ^3P_2$	578.325	-1.275	10.95
					←	$4p''\ ^3P_1$	577.666	-1.934	10.95
				$5p\ ^3P_1$	←	$6d\ ^5D^o_1$	579.146	-0.454	12.89
				$5p\ ^3P_2$	←	$4d'\ ^3S^o_1$	578.697	-0.903	12.91
				$4f\ ^3F_3$	←	$7d\ ^5D^o_4$	577.938	-1.662	13.41
				$4f\ ^3F_4$	←	$7d\ ^5D^o_4$	577.953	-1.647	13.41
				$3d'\ ^3F_3$	←	$5p'\ ^3F_4$	580.288	0.688	12.95
				$3d'\ ^1F_3$	←	$5p'\ ^3F_4$	580.288	00.688	12.95

Table XV (continued)

Luminescence from the Reaction 100 eV $He^+ + Cl_2 \rightarrow He + Cl^+ + Cl + Energy$

λ_o (nm)	$\Delta\lambda_o$ (nm)	σ ($cm^2 \times 10^{18}$)	X	Transition Assignment Lower State	←	Upper State	λ_T (nm)	$\lambda_T - \lambda_o$ (nm)	ΔH (eV)	
725.60	0.50	5.7	Cl I	$4p\ ^4P^o_{1/2}$	←	$4d\ 1(1)_{1/2}$	725.458	-0.142	2.95	
				$4s\ ^4P_{5/2}$	←	$4p\ ^4S^o_{3/2}$	725.862	0.262	1.54	#
			Cl II	$4p''\ ^3D_3$	←	$4d'\ ^3F^o_2$	725.347	-0.253	12.31	
				$3d'\ ^1D^o_2$	←	$6p\ ^5P_1$	725.954	0.354	12.24	
					←	$6p\ ^5P_2$	725.583	-0.017	12.24	
				$3d''\ ^1D^o_2$	←	$6p\ ^5P_1$	725.954	0.354	12.24	
					←	$6p\ ^5P_2$	725.583	-0.017	12.24	
741.40	0.50	1.6	Cl I	$4s\ ^4P_{5/2}$	←	$4p\ ^2P^o_{3/2}$	741.616	0.216	1.50	#
				$4p\ ^2S^o_{1/2}$	←	$5d\ 2(1)_{1/2}$	741.291	-0.109	3.23	
754.80	0.50	6.1	Cl I	$4s\ ^4P_{3/2}$	←	$4p\ ^4S^o_{3/2}$	754.915	0.115	1.54	#
			Cl II	$5p\ ^5P_3$	←	$4d'\ ^3F^o_4$	754.582	-0.218	12.33	

Table XV (continued)

Luminescence from the Reaction 100 eV $He^+ + Cl_2 \rightarrow He + Cl^+ + Cl + Energy$

λ_o (nm)	$\Delta\lambda_o$ (nm)	σ ($cm^2 \times 10^{18}$)	X	Transition Assignment Lower State	←	Upper State	λ_T (nm)	$\lambda_T - \lambda_o$ (nm)	ΔH (eV)	
771.80	0.50	1.5	He I	$3s\ ^1S_0$	←	$15p\ ^3P^o_1$	771.969	0.169	15.44	
					←	$15p\ ^3P^o_0$	771.969	0.169	15.44	
					←	$15p\ ^1P^o_1$	771.666	-0.134	15.44	
			Cl I	$4s\ ^4P_{3/2}$	←	$4p\ ^2P^o_{3/2}$	771.971	0.171	1.50	#
			Cl II	$5f\ ^5F_3$	←	$6s'\ ^1D^o_2$	772.228	0.428	14.11	
				$5f\ ^5F_2$	←	$6s'\ ^1D^o_2$	772.247	0.447	14.11	
				$5f\ ^5F_1$	←	$6s'\ ^1D^o_2$	772.261	0.461	14.11	
				$4d'\ ^1G^o_4$	←	$9f\ ^5F_5$	771.569	-0.231	14.04	
774.50	0.50	3.2	Cl I	$4s\ ^4P_{1/2}$	←	$4p\ ^4S^o_{3/2}$	774.710	0.210	1.54	#
				$3d\ ^4D_{7/2}$	←	$5f\ 1(3)^o_{7/2}$	774.571	0.071	3.42	
					←	$5f\ 1(3)^o_{5/2}$	774.555	0.055	3.42	
782.30	0.50	2.0	He I	$3s\ ^3S_1$	←	$7p\ ^3P^o_2$	781.830	-0.470	15.21	
					←	$7p\ ^3P^o_1$	781.830	-0.470	15.21	
					←	$7p\ ^3P^o_0$	781.829	-0.471	15.21	

Table XV (continued)

Luminescence from the Reaction 100 eV $He^+ + Cl_2 \rightarrow He + Cl^+ + Cl + Energy$

λ_o (nm)	$\Delta\lambda_o$ (nm)	σ ($cm^2 \times 10^{18}$)	X	Transition Assignment Lower State	←	Upper State	λ_T (nm)	$\lambda_T - \lambda_o$ (nm)	ΔH (eV)	
			He I	$3s\ ^1S_0$	←	$13p\ ^3P^o_1$	781.867	-0.433	15.42	
					←	$13p\ ^3P^o_0$	781.867	-0.433	15.42	
			Cl I	$4p\ ^4P^o_{5/2}$	←	$4d\ 2(3)_{7/2}$	782.351	0.051	2.78	#
				$3d\ ^4D_{5/2}$	←	$5f\ 1(2)^o_{3/2}$	782.147	-0.153	3.42	
					←	$5f\ 1(2)^o_{5/2}$	782.119	-0.181	3.42	
787.70	0.50	1.5	Cl I	$4s\ ^4P_{5/2}$	←	$4p\ ^2D^o_{5/2}$	788.038	0.338	1.40	#
				$4p\ ^2D^o_{5/2}$	←	$4d\ 1(3)_{5/2}$	787.973	0.273	2.98	
				$3p^6\ ^2S_{1/2}$	←	$4f\ 1(2)^o_{3/2}$	787.772	0.072	3.11	
				$3d\ ^4D_{3/2}$	←	$7p\ 2(2)^o_{3/2}$	788.074	0.374	3.42	
					←	$5f\ 1(3)^o_{5/2}$	787.304	-0.396	3.42	
			Cl II	$4p\ ^5P_2$	←	$3d'\ ^3D^o_3$	788.173	0.473	8.43	
					←	$3d\ ^3D^o_2$	788.173	0.473	8.43	

Table XV (continued)

Luminescence from the Reaction 100 eV $He^+ + Cl_2 \rightarrow He + Cl^+ + Cl + Energy$

λ_o (nm)	$\Delta\lambda_o$ (nm)	σ ($cm^2 \times 10^{18}$)	X	Transition Assignment Lower State	←	Upper State	λ_T (nm)	$\lambda_T - \lambda_o$ (nm)	ΔH (eV)
793.40	0.60	1.5	Cl I	$4p\ ^4D^o_{7/2}$	←	$4d\ 2(4)_{9/2}$	793.608	0.208	2.87
				$4p\ ^4D^o_{5/2}$	←	$4d\ 2(4)_{7/2}$	793.719	0.319	2.90
				$4p\ ^2D^o_{5/2}$	←	$4d\ 1(1)_{3/2}$	792.914	-0.486	2.97
				$4p\ ^2P^o_{1/2}$	←	$4d\ 0(2)_{3/2}$	793.748	0.348	3.04
				$4p\ ^2P^o_{3/2}$	←	$6s\ 1(1)_{3/2}$	793.490	0.090	3.07
				$3d\ ^4D^o_{1/2}$	←	$7p\ 2(2)^o_{3/2}$	793.337	-0.063	3.42
			Cl II	$6p\ ^5P_2$	←	$4d''\ ^3F^o_3$	793.319	-0.081	13.80
					←	$4d''\ ^3F^o_2$	793.133	-0.267	13.80
				$6p\ ^5P_3$	←	$4d''\ ^3F^o_2$	793.860	0.460	13.80
				$5f\ ^3F_2$	←	$6s'\ ^3D^o_2$	793.333	-0.067	14.08
				$5f\ ^3F_3$	←	$6s'\ ^3D^o_2$	793.340	-0.060	14.08
808.70	0.40	4.2	He I	$3p\ ^3P^o_2$	←	$17d\ ^3D_3$	808.649	-0.051	15.45
					←	$17d\ ^3D_2$	808.649	-0.051	15.45

Table XV (continued)

Luminescence from the Reaction 100 eV $He^+ + Cl_2 \rightarrow He + Cl^+ + Cl + Energy$

λ_o (nm)	$\Delta\lambda_o$ (nm)	σ ($cm^2 \times 10^{18}$)	X	Transition Assignment Lower State	←	Upper State	λ_T (nm)	$\lambda_T - \lambda_o$ (nm)	ΔH (eV)
			He I	$3p\ ^3P^o_2$	←	$17d\ ^3D_1$	808.649	-0.051	15.45
					←	$17d\ ^1D_2$	808.646	-0.054	15.45
				$3p\ ^3P^o_1$	←	$17d\ ^3D_2$	808.650	-0.050	15.45
					←	$17d\ ^3D_1$	808.650	-0.050	15.45
					←	$17d\ ^1D_2$	808.648	-0.052	15.45
				$3p\ ^3P^o_0$	←	$17d\ ^3D_1$	808.668	-0.032	15.45
			Cl I	$4p\ ^2D^o_{3/2}$	←	$4d\ 1(2)_{3/2}$	808.697	-0.003	2.98
				$4p\ ^2P^o_{3/2}$	←	$4d\ 0(2)_{5/2}$	808.716	0.016	3.04
				$4p\ ^4S^o_{3/2}$	←	$6s\ 1(1)_{1/2}$	808.718	0.018	3.07
				$4s'\ ^2D_{5/2}$	←	$4p'\ ^2D^o_{5/2}$	808.890	0.190	2.87
					←	$4p'\ ^2D^o_{3/2}$	808.673	-0.027	2.87
				$4s'\ ^2D_{3/2}$	←	$4p'\ ^2D^o_{5/2}$	808.995	0.295	2.87
					←	$4p'\ ^2D^o_{3/2}$	808.778	0.078	2.87

Table XV (continued)

Luminescence from the Reaction 100 eV $He^+ + Cl_2 \rightarrow He + Cl^+ + Cl + Energy$

λ_o (nm)	$\Delta\lambda_o$ (nm)	σ ($cm^2 \times 10^{18}$)	X	Transition Assignment Lower State	←	Upper State	λ_T (nm)	$\lambda_T - \lambda_o$ (nm)	ΔH (eV)	
			Cl II	$4d'\ ^3F^o_4$	←	$8f\ ^5F_5$	808.361	-0.339	13.86	
					←	$8f\ ^5F_4$	808.361	-0.339	13.86	
					←	$8f\ ^5F_3$	808.361	-0.339	13.86	
821.20	0.40	3.3	He I	$3p\ ^3P^o_1$	←	$14s\ ^1S_o$	821.356	0.156	15.43	
			Cl I	$4s\ ^4P_{5/2}$	←	$4p\ ^4D^o_{5/2}$	821.430	0.230	1.34	#
				$4p\ ^2S^o_{1/2}$	←	$6s\ 1(1)_{1/2}$	820.856	-0.344	3.07	
			Cl II	$4s''\ ^3P^o_0$	←	$4p'\ ^3P_1$	820.856	-0.344	9.50	
822.20	0.50	7.7	He I	$3p\ ^3P^o_2$	←	$14s\ ^3S_1$	822.252	0.052	15.42	
				$3p\ ^3P^o_1$	←	$14s\ ^3S_1$	822.254	0.054	15.42	
				$3p\ ^3P^o_0$	←	$14s\ ^3S_1$	822.272	0.072	15.42	
			Cl I	$4s\ ^4P_{3/2}$	←	$4p\ ^2D^o_{5/2}$	822.400	0.200	1.40	#
				$4s\ ^4P_{1/2}$	←	$4p\ ^2D^o_{3/2}$	822.271	0.071	1.45	
				$4p\ ^2D^o_{3/2}$	←	$4d\ 1(1)_{1/2}$	822.311	0.111	2.95	

Table XV (continued)

Luminescence from the Reaction 100 eV $He^+ + Cl_2 \rightarrow He + Cl^+ + Cl + Energy$

λ_o (nm)	$\Delta\lambda_o$ (nm)	σ ($cm^2 \times 10^{18}$)	X	Transition Assignment Lower State	←	Upper State	λ_T (nm)	$\lambda_T - \lambda_o$ (nm)	ΔH (eV)	
			Cl II	$3d'' \ ^3P^o_2$	←	$4p'' \ ^3S_1$	822.096	-0.104	10.52	
				$3d' \ ^3P^o_2$	←	$4p'' \ ^3S_1$	822.096	-0.104	10.52	
				$7s \ ^5S^o_2$	←	$5p'' \ ^3D_2$	822.508	0.308	14.32	
833.40	0.50	7.6	Cl I	$4s \ ^4P_{3/2}$	←	$4p \ ^4D^o_{3/2}$	833.560	0.160	1.38	#
				$3d \ ^4D_{3/2}$	←	$5f \ 2(2)^o_{3/2}$	833.565	0.165	3.33	
					←	$5f \ 2(2)^o_{5/2}$	833.550	0.150	3.33	
			Cl II	$4s'' \ ^3P^o_1$	←	$4p' \ ^3P_2$	833.752	0.352	9.48	
				$4p' \ ^3P_2$	←	$3d \ ^3D^o_3$	833.468	0.068	10.97	
					←	$4d \ ^3D^o_3$	833.468	0.068	10.97	
				$5d \ ^3D^o_3$	←	$7f \ ^5F_4$	833.383	-0.017	13.60	
					←	$7f \ ^5F_3$	833.383	-0.017	13.60	
					←	$7f \ ^5F_2$	833.383	-0.017	13.60	
				$5d \ ^3D^o_2$	←	$7f \ ^3F_2$	833.267	-0.133	13.60	
					←	$7f \ ^3F_3$	833.265	-0.135	13.60	

Table XV (continued)

Luminescence from the Reaction 100 eV $He^+ + Cl_2 \rightarrow He + Cl^+ + Cl + Energy$

λ_o (nm)	$\Delta\lambda_o$ (nm)	σ ($cm^2 \times 10^{18}$)	X	Transition Assignment Lower State	←	Upper State	λ_T (nm)	$\lambda_T - \lambda_o$ (nm)	ΔH (eV)	
837.70	0.40	40.7	He I	$3d\ ^3D_3$	←	$20p\ ^3P^o_2$	838.001	0.301	15.46	
				$3d\ ^3D_2$	←	$20p\ ^3P^o_2$	838.001	0.301	15.46	
					←	$20p\ ^3P^o_1$	838.001	0.301	15.46	
					←	$20p\ ^1P^o_1$	837.862	0.162	15.46	
				$3d\ ^3D_1$	←	$20p\ ^3P^o_2$	838.005	0.305	15.46	
					←	$20p\ ^3P^o_1$	838.005	0.305	15.46	
					←	$20p\ ^3P^o_0$	838.005	0.305	15.46	
					←	$20p\ ^1P^o_1$	837.865	0.165	15.46	
			Cl I	$4s\ ^4P_{5/2}$	←	$4p\ ^4D^o_{7/2}$	837.824	0.124	1.31	#
				$4p\ ^2D^o_{3/2}$	←	$4d\ 2(0)_{1/2}$	837.402	-0.298	2.93	
			Cl II	$4p'\ ^3D_1$	←	$3d'\ ^1D^o_2$	837.639	-0.061	10.53	
					←	$3d''\ ^1D^o_2$	837.639	-0.061	10.53	
				$4p'\ ^3D_2$	←	$3d'\ ^1D^o_2$	837.906	0.206	10.53	
					←	$3d''\ ^1D^o_2$	837.906	0.206	10.53	

Table XV (continued)

Luminescence from the Reaction 100 eV $He^+ + Cl_2 \rightarrow He + Cl^+ + Cl + Energy$

λ_o (nm)	$\Delta\lambda_o$ (nm)	σ ($cm^2 \times 10^{18}$)	X	Transition Assignment Lower State	←	Upper State	λ_T (nm)	$\lambda_T - \lambda_o$ (nm)	ΔH (eV)	
842.90	0.40	5.6	He I	$3d\ ^3D_3$	←	$18p\ ^3P^o_2$	842.594	-0.306	15.45	
				$3d\ ^3D_2$	←	$18p\ ^3P^o_2$	842.595	-0.305	15.45	
					←	$18p\ ^3P^o_1$	842.595	-0.305	15.45	
				$3d\ ^3D_1$	←	$18p\ ^3P^o_2$	842.598	-0.302	15.45	
					←	$18p\ ^3P^o_1$	842.598	-0.302	15.45	
					←	$18p\ ^3P^o_0$	842.598	-0.302	15.45	
				$3d\ ^1D_2$	←	$18p\ ^3P^o_2$	842.837	-0.063	15.45	
					←	$18p\ ^3P^o_1$	842.837	-0.063	15.45	
					←	$18p\ ^1P^o_1$	842.636	-0.264	15.45	
			Cl I	$4s\ ^4P_{1/2}$	←	$4p\ ^4D^o_{1/2}$	843.057	0.157	1.41	#
				$3d\ ^2D_{3/2}$	←	$7f\ 1(2)^o_{3/2}$	843.072	0.172	3.68	
					←	$7f\ 1(2)^o_{5/2}$	843.063	0.163	3.68	

AD-A034 035 AIR FORCE INST OF TECH WRIGHT-PATTERSON AFB OHIO SCH--ETC F/G 20/8
EMISSION CROSS-SECTION MEASUREMENTS OF LOW ENERGY HE(+) IONS WI--ETC(U)
SEP 76 K E SIEGENTHALER

UNCLASSIFIED DS/PH/76-2 NL

3 OF 4
AD
A034035

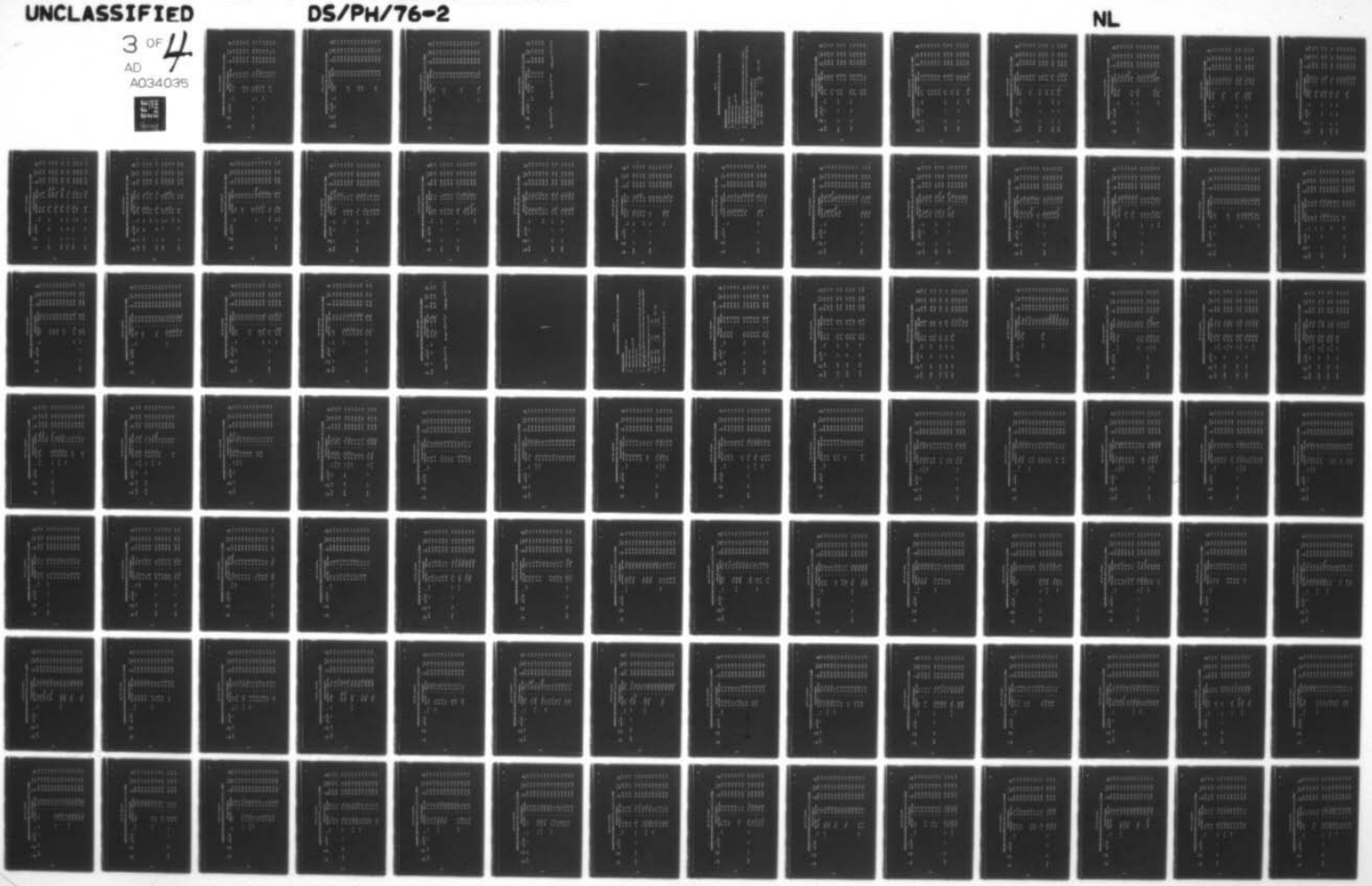

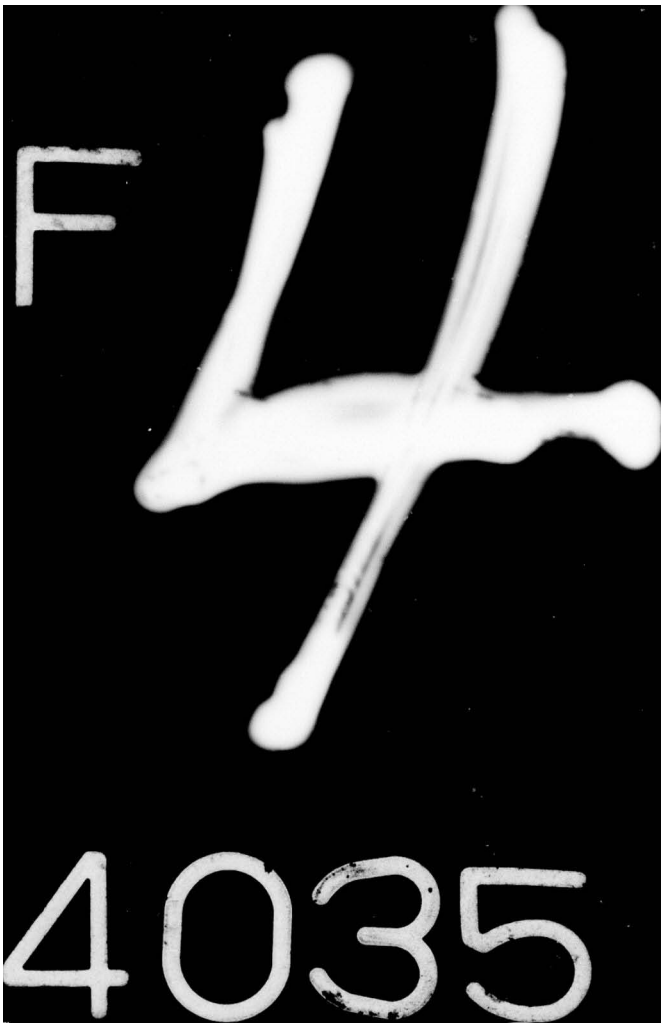
F
4
4035

Table XV (continued)

Luminescence from the Reaction 100 eV $He^+ + Cl_2 \rightarrow He + Cl^+ + Cl + Energy$

λ_o (nm)	$\Delta\lambda_o$ (nm)	σ ($cm^2 \times 10^{18}$)	X	Transition Assignment Lower State	←	Upper State	λ_T (nm)	$\lambda_T - \lambda_o$ (nm)	ΔH (eV)	
			Cl II	$4d'\ ^3G^o_4$	←	$8f\ ^5F_5$	842.630	-0.270	13.86	
					←	$8f\ ^5F_4$	842.630	-0.270	13.86	
					←	$8f\ ^5F_3$	842.630	-0.270	13.86	
				$4d'\ ^3G^o_5$	←	$8f\ ^3F_4$	843.192	0.292	13.86	
				$7s\ ^3S^o_1$	←	$5p''\ ^3D_2$	843.111	0.211	14.32	
857.60	0.50	8.9	He I	$3p\ ^1P^o_1$	←	$16s\ ^3S_1$	857.898	0.298	15.44	
			Cl I	$4p\ ^4D^o_{5/2}$	←	$4d\ 2(2)_{5/2}$	858.038	0.438	2.79	
				$4s\ ^4P_{1/2}$	←	$4p\ ^4D^o_{3/2}$	857.760	0.160	1.38	#
			Cl II	$5s'\ ^3D^o_1$	←	$4f'\ ^3D_2$	857.359	-0.241	13.50	
					←	$4f'\ ^1D_2$	857 359	-0.241	13.50	
				$5s'\ ^3D^o_3$	←	$4f'\ ^3F_4$	857.974	0.374	13.50	
					←	$4f'\ ^3G_4$	857.974	0.374	13.50	

Table XV (continued)

Luminescence from the Reaction 100 eV $He^+ + Cl_2 \rightarrow He + Cl^+ + Cl + Energy$

λ_o (nm)	$\Delta\lambda_o$ (nm)	σ ($cm^2 \times 10^{18}$)	X	Transition Assignment Lower State	←	Upper State	λ_T (nm)	$\lambda_T - \lambda_o$ (nm)	ΔH (eV)
858.70	0.50	14.0	He I	$3p\ ^3P^o_2$	←	$10d\ ^3D_3$	858.500	-0.200	15.36
					←	$10d\ ^3D_2$	858.500	-0.200	15.36
					←	$10d\ ^3D_1$	858.500	-0.200	15.36
					←	$10d\ ^1D_2$	858.486	-0.214	15.36
				$3p\ ^3P^o_1$	←	$10d\ ^3D_2$	858.501	-0.199	15.36
					←	$10d\ ^3D_1$	858.501	-0.199	15.36
					←	$10d\ ^1D_2$	858.487	-0.213	15.36
				$3p\ ^3P^o_0$	←	$10d\ ^3D_1$	858.521	-0.179	15.36
				$3d\ ^3D_3$	←	$14p\ ^3P^o_2$	858.811	0.111	15.43
					←	$14f\ ^3F^o_4$	858.422	-0.278	15.43
					←	$14f\ ^3F^o_3$	858.422	-0.278	15.43
					←	$14f\ ^3F^o_2$	858.422	-0.278	15.43
				$3d\ ^3D_2$	←	$14p\ ^3P^o_2$	858.811	0.111	15.43
					←	$14p\ ^3P^o_1$	858.811	0.111	15.43

Table XV (continued)

Luminescence from the Reaction 100 eV $He^+ + Cl_2 \rightarrow He + Cl^+ + Cl + Energy$

λ_o (nm)	$\Delta\lambda_o$ (nm)	σ ($cm^2 \times 10^{18}$)	Transition Assignment X	Lower State	←	Upper State	λ_T (nm)	$\lambda_T - \lambda_o$ (nm)	ΔH (eV)	
			He I	3d $^3D_2$	←	14f $^3F^o_3$	858.423	-0.277	15.43	
					←	14f $^3F^o_2$	858.423	-0.277	15.43	
					←	14p $^1P^o_1$	858.347	-0.353	15.43	
				3d $^3D_1$	←	14p $^3P^o_2$	858.814	0.114	15.43	
					←	14p $^3P^o_1$	858.814	0.114	15.43	
					←	14p $^3P^o_0$	858.814	0.114	15.43	
					←	14f $^3F^o_2$	858.426	-0.274	15.43	
					←	14p $^1P^o_1$	858.351	-0.349	15.43	
				3d $^1D_2$	←	14p $^3P^o_2$	859.063	0.363	15.43	
					←	14p $^3P^o_1$	859.063	0.363	15.43	
					←	14f $^3F^o_3$	858.675	-0.025	15.43	
					←	14f $^3F^o_2$	858.675	-0.025	15.43	
					←	14p $^1P^o_1$	858.599	-0.101	15.43	
			Cl I	4s $^4P_{3/2}$	←	4p $^4D^o_{5/2}$	858.834	0.134	1.34	#

Table XV (continued)

Luminescence from the Reaction 100 eV $He^+ + Cl_2 \rightarrow He + Cl^+ + Cl + Energy$

λ_o (nm)	$\Delta\lambda_o$ (nm)	σ ($cm^2 \times 10^{18}$)	Transition Assignment X	Lower State	←	Upper State	λ_T (nm)	$\lambda_T - \lambda_o$ (nm)	ΔH (eV)
			Cl II	$5s'\ ^3D_2^o$	←	$4f'\ ^3D_2$	858.860	0.160	13.50
					←	$4f'\ ^3D_3$	858.515	-0.185	13.50
					←	$4f'\ ^1D_2$	858.860	0.160	13.50
					←	$4f'\ ^3F_3$	858.515	-0.185	13.50

$\sigma_{TOTAL} = 497.0 \times 10^{-18}\ cm^2$ $\sigma_{VUV\ TOTAL} = 375.9 \times 10^{-18}\ cm^2$ $\sigma_{VISIBLE\ TOTAL} = 121.1 \times 10^{-18}\ cm^2$

Appendix B

Table XVI

Luminescence from the Reaction 100 eV $He^+ + Br_2 \rightarrow He + Br^+ + Br + Energy$

Explanation of Symbols

λ_o = Observed vacuum wavelength (nm)

$\Delta\lambda_o$ = Search interval (nm)

σ = Emission cross section ($cm^2 \times 10^{18}$)

X = Emitting atom or ion

λ_T = Calculated vacuum wavelength in nm using the energy level tables (Refs. 42, 58 and 68).

ΔH = Enthalpy change in eV required to populate the upper energy state for the thermal reaction $He^+ + Br_2 \rightarrow He + Br^+ + Br^*$.

\# = Transition selected by criteria stated in Chapter IV.

Inner electron configuration designation (Refs. 58 and 68).

Br I	Unprimed = $(^3P_2)$	' = $(^3P_1)$	'' = $(^3P_0)$	$(^1D_2) = (^1D_2)$	
Br II	Unprimed = (^4S)	' = (^2D)	'' = (^2P)		

Table XVI (continued)

Luminescence from the Reaction 100 eV $He^+ + Br_2 \rightarrow He + Br^+ + Br + Energy$

λ_o (nm)	$\Delta\lambda_o$ (nm)	σ ($cm^2 \times 10^{18}$)	X	Transition Assignment Lower State	←	Upper State	λ_T (nm)	$\lambda_T - \lambda_o$ (nm)	ΔH (eV)
88.925	0.3	1.5	Br II	$4p^4\ ^3P_2$	←	$4d\ ^3D_1^o$	88.971	0.046	3.16
					←	$4d\ ^3D_3^o$	88.920	-0.005	3.17
				$4p^4\ ^1S_0$	←	$5d\ ^5D_1^o$	89.010	0.085	6.61
903.75	0.3	1.0	Br II	$4p^4\ ^3P_2$	←	$5s'\ ^3D_3^o$	90.598	0.223	2.91
				$4p^4\ ^1D_2$	←	$5s''\ ^3P_2^o$	90.475	0.100	4.43
					←	$4d'\ ^1F_3^o$	90.397	0.022	4.45
90.775	0.3	0.9	Br II	$4p^4\ ^3P_2$	←	$5s'\ ^3D_3^o$	90.598	-0.177	2.91
				$4p^4\ ^3P_1$	←	$4p^5\ ^1P_1^o$	90.741	-0.034	3.28
					←	$5s'\ ^1D_2^o$	91.074	0.299	3.23
				$4p^4\ ^1D_2$	←	$5s''\ ^3P_2^o$	90.475	-0.300	4.43
				$4p^4\ ^1S_0$	←	$6s\ A_1^o$	90.702	-0.073	6.36

Table XVI (continued)

Luminescence from the Reaction 100 eV $He^+ + Br_2 \rightarrow He + Br^+ + Br + Energy$

λ_o (nm)	$\Delta\lambda_o$ (nm)	σ ($cm^2 \times 10^{18}$)	X	Transition Assignment Lower State	←	Upper State	λ_T (nm)	$\lambda_T - \lambda_o$ (nm)	ΔH (eV)
91.175	0.3	1.3	Br II	$4p^4\ ^3P_2$	←	$5s'\ ^3D^o_1$	91.384	0.209	2.80
					←	$5s'\ ^3D^o_2$	91.172	-0.003	2.83
				$4p^4\ ^3P_1$	←	$5s'\ ^1D^o_2$	91.074	-0.101	3.23
				$4p^4\ ^3P_0$	←	$4p^5\ ^1P^o_1$	91.322	0.147	3.28
				$4p^4\ ^1D_2$	←	$5s''\ ^3P^o_1$	91.362	0.187	4.30
				$4p^4\ ^1S_0$	←	$6s\ ^3S^o_1$	91.131	-0.044	6.29
94.050	0.3	1.2	Br II	$4p^4\ ^3P_1$	←	$5s'\ ^3D^o_1$	94.083	0.033	2.80
					←	$5s'\ ^3D^o_2$	93.858	-0.192	2.83
				$4p^4\ ^1D_2$	←	$4d'\ ^3F^o_3$	93.975	-0.075	3.92
96.075	0.3	1.9	Br II	$4p^4\ ^3P_2$	←	$4d\ ^5D^o_1$	96.014	-0.061	2.14
					←	$4d\ ^5D^o_2$	96.074	-0.001	2.13
					←	$4d\ ^5D^o_3$	96.113	0.038	2.13
			Br III	$4p^3\ ^4S^o_{3/2}$	←	$4p^4\ ^4P_{3/2}$	96.04	-0.035	2.14

Table XVI (continued)

Luminescence from the Reaction 100 eV $He^+ + Br_2 \rightarrow He + Br^+ + Br + Energy$

λ_o (nm)	$\Delta\lambda_o$ (nm)	σ ($cm^2 \times 10^{18}$)	X	Transition Assignment Lower State	←	Upper State	λ_T (nm)	$\lambda_T - \lambda_o$ (nm)	ΔH (eV)
98.975	0.3	1.4	Br II	$4p^4\ ^3P_1$	←	$4d\ ^5D^o_0$	98.944	-0.031	2.15
					←	$4d\ ^5D^o_1$	98.997	0.022	2.14
					←	$4d\ ^5D^o_2$	99.062	0.087	2.13
				$4p^4\ ^1D_2$	←	$4p^5\ ^1P^o_1$	98.771	-0.204	3.28
					←	$5s'\ ^1D^o_2$	99.166	0.191	3.23
101.325	0.4	2.3	Br II	$4p^4\ ^3P_2$	←	$5s\ ^3S^o_1$	101.547	0.222	1.44
					←	$4p^5\ ^3P^o_1$	101.207	-0.118	1.48
				$4p^4\ ^1S_0$	←	$4d'\ ^3D^o_1$	101.100	-0.225	4.95
103.725	0.4	3.0	Br II	$4p^4\ ^3P_2$	←	$4p^5\ ^3P^o_2$	103.692	-0.033	1.19
106.425	0.3	6.7	Br I	$4p^5\ ^2P^o_{3/2}$	←	$8s'\ ^2P_{3/2}$	106.489	0.064	0.87
					←	$8s'\ ^4P_{1/2}$	106.402	-0.023	0.88
					←	$6d''\ ^2D_{5/2}$	106.282	-0.143	0.90

Table XVI (continued)

Luminescence from the Reaction 100 eV $He^+ + Br_2 \rightarrow He + Br^+ + Br + Energy$

λ_o (nm)	$\Delta\lambda_o$ (nm)	σ ($cm^2 \times 10^{18}$)	X	Transition Assignment Lower State	←	Upper State	λ_T (nm)	$\lambda_T - \lambda_o$ (nm)	ΔH (eV)
			Br I	$4p^5\ ^2P^o_{3/2}$	←	$6d''\ ^2D_{3/2}$	106.290	-0.135	0.89
					←	$10d\ ^4D_{5/2}$	106.592	0.167	0.86
					←	$10d\ ^4D_{3/2}$	106.585	0.160	0.86
					←	$(^1D_2)4d\ ^2S_{1/2}$	106.722	0.297	0.85
			Br II	$4p^4\ ^3P_2$	←	$5s\ ^5S^o_2$	106.465	0.040	0.88
110.225	0.3	3.7	Br I	$4p^5\ ^2P^o_{3/2}$	←	$8s\ ^4P_{5/2}$	110.146	-0.079	0.49
					←	$8s\ ^4P_{3/2}$	110.135	-0.090	0.49
					←	$5d'\ ^2F_{5/2}$	110.417	0.192	0.46
					←	$5d'\ ^4P_{5/2}$	110.393	0.168	0.46
					←	$5d'\ ^4P_{3/2}$	110.451	0.226	0.45
				$4p^5\ ^2P^o_{1/2}$	←	$(^1D_2)6s\ ^2D_{3/2}$	110.150	-0.075	0.94
			Br II	$4p^4\ ^3P_1$	←	$5s\ ^5S^o_2$	110.146	-0.079	0.88

Table XVI (continued)

Luminescence from the Reaction 100 eV $He^+ + Br_2 \rightarrow He + Br^+ + Br + Energy$

λ_o (nm)	$\Delta\lambda_o$ (nm)	σ ($cm^2 \times 10^{18}$)	X	Transition Assignment Lower State	←	Upper State	λ_T (nm)	$\lambda_T - \lambda_o$ (nm)	ΔH (eV)
113.925	0.4	6.4	Br I	$4p^5\ ^2P^o_{3/2}$	←	$5d\ ^4F_{5/2}$	113.954	0.029	0.11
					←	$5d\ ^4F_{3/2}$	113.934	0.009	0.11
					←	$5d\ ^4P_{1/2}$	113.955	0.030	0.11
				$4p^5\ ^2P^o_{1/2}$	←	$7s'\ ^2P_{3/2}$	114.157	0.232	0.55
					←	$7s'\ ^4P_{1/2}$	114.074	0.149	0.56
					←	$7d\ ^4D_{1/2}$	113.629	-0.296	0.60
117.725	0.3	12.8	Br I	$4p^5\ ^2P^o_{3/2}$	←	$4p^6\ ^2S_{1/2}$	117.889	0.164	-0.25
					←	$4d''\ ^2D_{5/2}$	117.723	-0.002	-0.24
118.925	0.3	10.1	Br I	$4p^5\ ^2P^o_{3/2}$	←	$4d'\ ^4P_{3/2}$	118.938	0.013	-0.35
				$4p^5\ ^2P^o_{1/2}$	←	$5d\ ^4F_{3/2}$	118.928	0.003	0.11
					←	$5d\ ^4P_{1/2}$	118.950	0.025	0.11

Table XVI (continued)

Luminescence from the Reaction 100 eV $He^+ + Br_2 \rightarrow He + Br^+ + Br + Energy$

λ_o (nm)	$\Delta\lambda_o$ (nm)	σ ($cm^2 \times 10^{18}$)	X	Transition Assignment Lower State	←	Upper State	λ_T (nm)	$\lambda_T - \lambda_o$ (nm)	ΔH (eV)	
119.475	0.3	14.2	Br I	$4p^5\ ^2P^o_{3/2}$	←	$4d'\ ^2F_{5/2}$	119.441	-0.034	-0.39	
					←	$4d'\ ^2P_{3/2}$	119.648	0.173	-0.41	
				$4p^5\ ^2P^o_{1/2}$	←	$5d\ ^4D_{1/2}$	119.637	0.162	0.05	
120.975	0.3	18.8	Br I	$4p^5\ ^2P^o_{3/2}$	←	$6s\ ^4P_{3/2}$	120.975	0.000	-0.52	
				$4p^5\ ^2P^o_{1/2}$	←	$6s''\ ^2P_{1/2}$	121.074	0.099	-0.07	
121.525	0.3	15.8	Br I	$4p^5\ ^2P^o_{3/2}$	←	$6s\ ^4P_{5/2}$	121.601	0.076	-0.57	#
122.375	0.5	34.9	Br I	$4p^5\ ^2P^o_{3/2}$	←	$4d\ ^4F_{5/2}$	122.441	0.066	-0.64	
					←	$4d\ ^4F_{3/2}$	122.187	-0.188	-0.62	
					←	$4d\ ^4P_{1/2}$	122.805	0.430	-0.67	
				$4p^5\ ^2P^o_{1/2}$	←	$6s'\ ^2P_{3/2}$	122.324	-0.051	-0.18	
					←	$6s'\ ^2P_{1/2}$	122.113	-0.262	-0.16	
					←	$4d''\ ^2D_{3/2}$	122.690	0.315	-0.21	

Table XVI (continued)

Luminescence from the Reaction 100 eV $He^+ + Br_2 \rightarrow He + Br^+ + Br + Energy$

λ_o (nm)	$\Delta\lambda_o$ (nm)	σ ($cm^2 \times 10^{18}$)	X	Transition Assignment Lower State	←	Upper State	λ_T (nm)	$\lambda_T - \lambda_o$ (nm)	ΔH (eV)	
			Br II	$4p^4\ ^1D_2$	←	$5s\ ^5S^o_2$	122.205	-0.170	0.88	
				$4p^4\ ^1S_0$	←	$5s'\ ^3D^o_1$	122.621	0.246	2.80	
131.75	0.1	93.4	Br I	$4p^5\ ^2P^o_{3/2}$	←	$(^1D_2)5s\ ^2D_{5/2}$	131.769	0.019	-1.36	
					←	$(^1D_2)5s\ ^2D_{3/2}$	131.738	-0.012	-1.36	
				$4p^5\ ^2P^o_{1/2}$	←	$4s\ ^4D_{3/2}$	131.673	-0.077	-0.90	
138.45	0.1	47.1	Br I	$4p^5\ ^2P^o_{1/2}$	←	$(^1D_2)5s\ ^2D_{3/2}$	138.459	0.009	-1.36	#
145.00	0.1	28.2	Br I	$4p^5\ ^2P^o_{3/2}$	←	$5s''\ ^2P_{1/2}$	144.990	-0.010	-2.22	#
148.80	0.1	151.2	Br I	$4p^5\ ^2P^o_{3/2}$	←	$5s'\ ^2P_{3/2}$	148.846	0.046	-2.44	#
			Br II	$5s\ ^5S^o_2$	←	$4f'\ ^3D_2$	148.717	-0.083	9.21	
					←	$4f'\ A_2$	148.798	-0.002	9.21	
153.15	0.1	41.8	Br I	$4p^5\ ^2P^o_{1/2}$	←	$5s''\ ^2P_{1/2}$	153.175	0.025	-2.22	#

Table XVI (continued)

Luminescence from the Reaction 100 eV $He^+ + Br_2 \rightarrow He + Br^+ + Br + Energy$

λ_o (nm)	$\Delta\lambda_o$ (nm)	σ ($cm^2 \times 10^{18}$)	X	Transition Assignment Lower State	←	Upper State	λ_T (nm)	$\lambda_T - \lambda_o$ (nm)	ΔH (eV)	
154.05	0.1	209.1	Br I	$4p^5\ ^2P^o_{3/2}$	←	$5s\ ^4P_{3/2}$	154.066	0.016	-2.72	#
157.60	0.12	384.2	Br I	$4p^5\ ^2P^o_{3/2}$	←	$5s\ ^4P_{5/2}$	157.638	0.038	-2.91	#
				$4p^5\ ^2P^o_{1/2}$	←	$5s'\ ^2P_{3/2}$	157.484	-0.116	-2.44	
			Br II	$5s\ ^3S^o_1$	←	$4f'\ ^1D_2$	157.679	0.079	9.30	
158.20	0.1	96.0	Br I	$4p^5\ ^2P^o_{1/2}$	←	$5s'\ ^4P_{1/2}$	158.231	0.031	-2.48	#
444.05	0.5	0.4	He I	$2p\ ^1P^o_1$	←	$5s\ ^1S_0$	443.880	-0.170	13.24	
			Br I	$5s\ ^4P_{5/2}$	←	$6p\ ^4D^o_{3/2}$	444.298	0.248	-0.11	#
				$5s''\ ^2P_{1/2}$	←	$4f'\ (2)^o_{3/2}$	444.206	0.156	0.57	
			Br II	$5p\ ^3P_2$	←	$5d\ ^5D^o_3$	443.914	-0.136	6.62	
447.55	0.5	1.8	He I	$2p\ ^3P^o_2$	←	$4d\ ^3D_3$	447.273	-0.277	12.97	
					←	$4d\ ^3D_2$	447.273	-0.277	12.97	

Table XVI (continued)

Luminescence from the Reaction 100 eV $He^+ + Br_2 \rightarrow He + Br^+ + Br + Energy$

λ_o (nm)	$\Delta\lambda_o$ (nm)	σ ($cm^2 \times 10^{18}$)	X	Transition Assignment: Lower State	←	Upper State	λ_T (nm)	$\lambda_T - \lambda_o$ (nm)	ΔH (eV)	
			He I	$2p\ ^3P^o_2$	←	$4d\ ^3D_1$	447.272	-0.278	12.97	
					←	$4d\ ^1D_2$	447.233	-0.317	12.97	
				$2p\ ^3P^o_1$	←	$4d\ ^3D_2$	447.274	-0.276	12.97	
					←	$4d\ ^3D_1$	447.274	-0.276	12.97	
					←	$4d\ ^1D_2$	447.235	-0.315	12.97	
				$2p\ ^3P^o_0$	←	$4d\ ^3D_1$	447.294	-0.256	12.97	
			Br I	$5s\ ^4P_{3/2}$	←	$(^1D_2)5p\ ^2P^o_{3/2}$	447.385	-0.165	0.05	#
				$5s\ ^4P_{5/2}$	←	$6p\ ^4D^o_{7/2}$	447.898	0.348	-0.14	#
				$5s'\ ^2P_{3/2}$	←	$7p\ ^4P^o_{5/2}$	447.122	-0.428	0.33	
					←	$7p\ ^4P^o_{3/2}$	447.290	-0.260	0.33	
			Br II	$5p\ ^3P_2$	←	$5d\ ^3D^o_2$	447.309	-0.241	6.60	
452.55	0.5	1.2	Br I	$5s\ ^4P_{5/2}$	←	$6p\ ^4P^o_{5/2}$	452.686	0.136	-0.17	#
			Br II	$5d\ ^5D^o_1$	←	$4f'\ ^3F_2$	452.669	0.119	9.35	

Table XVI (continued)

Luminescence from the Reaction 100 eV $He^+ + Br_2 \rightarrow He + Br^+ + Br + Energy$

λ_o (nm)	$\Delta\lambda_o$ (nm)	σ ($cm^2 \times 10^{18}$)	X	Transition Assignment Lower State	←	Upper State	λ_T (nm)	$\lambda_T - \lambda_o$ (nm)	ΔH (eV)	
470.55	0.5	0.6	Br I	$5s'\ ^2P_{3/2}$	←	$(^1D_2)5p\ ^2D^o_{3/2}$	470.473	-0.077	0.20	#
					←	$4f\ (1)^o_{3/2}$	470.768	0.218	0.19	
					←	$4f\ (1)^o_{1/2}$	470.781	0.231	0.19	
			Br II	$5s\ ^5S^o_2$	←	$5p\ ^5P_3$	470.617	0.067	3.51	
				$5d\ ^5D^o_3$	←	$4f'\ ^1G_4$	470.989	0.439	9.26	
				$5d\ ^5D^o_4$	←	$4f'\ ^1G_4$	470.936	0.386	9.26	
478.20	0.6	1.4	Br I	$5s\ ^4P_{3/2}$	←	$6p\ ^4D^o_{5/2}$	478.164	-0.036	-0.13	
					←	$6p\ ^4P^o_{1/2}$	478.652	0.452	-0.13	
				$5s''\ ^2P_{1/2}$	←	$6p''\ ^2P^o_{1/2}$	477.654	-0.546	0.38	
			Br II	$5s\ ^5S^o_2$	←	$5p\ ^5P_2$	478,684	0.484	3.47	
				$5p'\ ^3F_2$	←	$6s'\ ^3D^o_2$	478.643	0.443	8.01	
				$5s'\ ^3D^o_2$	←	$5p'\ ^3F_2$	477.842	-0.358	5.42	
				$5s'\ ^3D^o_3$	←	$5p'\ ^3F_3$	477.772	-0.428	5.51	

Table XVI (continued)

Luminescence from the Reaction 100 eV $He^+ + Br_2 \rightarrow He + Br^+ + Br + Energy$

λ_o (nm)	$\Delta\lambda_o$ (nm)	σ ($cm^2 \times 10^{18}$)	X	Transition Assignment Lower State	←	Upper State	λ_T (nm)	$\lambda_T - \lambda_o$ (nm)	ΔH (eV)	
			Br II	$5p''\ ^3P_1$	←	$6s''\ A_2^o$	478.799	0.599	9.87	
				$5d\ ^5D_1^o$	←	$4f'\ A_2$	478.238	0.038	9.21	
481.55	0.5	0.6	Br II	$5s\ ^5S_2^o$	←	$5p\ ^5P_1$	481.805	0.255	3.45	
				$5p'\ ^3F_2$	←	$6s'\ ^3D_1^o$	481.976	0.426	8.00	
				$5p'\ ^1D_2$	←	$5d'\ ^3D_1^o$	481.649	0.099	8.74	
				$5d\ ^3D_2^o$	←	$4f'\ ^3G_3$	481.672	0.122	9.18	
634.95	0.6	1.7	Br I	$5p\ ^4P_{5/2}^o$	←	$5d'\ ^2F_{7/2}$	634.706	-0.244	0.44	
					←	$6d\ ^4F_{3/2}$	635.158	0.208	0.44	
				$5s\ ^4P_{5/2}$	←	$5p'\ ^4S_{3/2}^o$	635.248	0.298	-0.95	#
				$5p'\ ^2S_{1/2}^o$	←	$10d'\ ^4D_{3/2}$	635.103	0.153	0.86	
				$(^1D_2)5s\ ^2D_{3/2}$	←	$8p\ ^4D_{3/2}^o$	634.556	-0.394	0.59	
			Br II	$5s'\ ^1D_2^o$	←	$5p'\ ^3D_1$	635.453	0.503	5.18	

Table XVI (continued)

Luminescence from the Reaction 100 eV $He^+ + Br_2 \rightarrow He + Br^+ + Br + Energy$

λ_o (nm)	$\Delta\lambda_o$ (nm)	σ ($cm^2 \times 10^{18}$)	X	Transition Assignment	λ_T (nm)	$\lambda_T - \lambda_o$ (nm)	ΔH (eV)
				Lower State ← Upper State			
654.50	0.5	0.4	Br I	$5p\ ^4D^o_{7/2} \leftarrow 8s\ ^4P_{5/2}$	654.990	0.490	0.49
				$5p\ ^4P^o_{5/2} \leftarrow 6d\ ^4D_{5/2}$	654.637	0.137	0.38
				$5p\ ^4P^o_{3/2} \leftarrow 5d'\ ^2P_{1/2}$	654.313	-0.187	0.42
				$5p'\ ^2D^o_{5/2} \leftarrow 10d\ ^4D_{7/2}$	654.144	-0.356	0.86
			Br II	$5p''\ ^3D_1 \leftarrow 5d'\ ^3D^o_1$	654.690	0.190	8.74
				$5p''\ ^3P_1 \leftarrow 5d'\ ^1D^o_2$	654.189	-0.311	9.18
655.90	0.6	0.7	Br I	$5s\ ^4P_{5/2} \leftarrow 5p'\ ^2D^o_{3/2}$	656.159	0.259	-1.02
				$5p'\ ^2S^o_{1/2} \leftarrow 9d\ ^4D_{3/2}$	655.338	-0.562	0.80
658.80	0.6	0.5	Br I	$5p\ ^4P^o_{5/2} \leftarrow 6d\ ^4D_{7/2}$	658.398	-0.402	0.37
				$5p\ ^4D^o_{3/2} \leftarrow 7d\ ^4F_{3/2}$	658.597	-0.203	0.63
				$5p\ ^4P^o_{1/2} \leftarrow 5d''\ ^2D_{3/2}$	658.443	-0.357	0.51
				$5p'\ ^2D^o_{5/2} \leftarrow 4d\ ^2F_{7/2}$	659.143	0.343	0.85

Table XVI (continued)

Luminescence from the Reaction 100 eV $He^+ + Br_2 \rightarrow He + Br^+ + Br + Energy$

λ_o (nm)	$\Delta\lambda_o$ (nm)	σ ($cm^2 \times 10^{18}$)	X	Transition Assignment Lower State	←	Upper State	λ_T (nm)	$\lambda_T - \lambda_o$ (nm)	ΔH (eV)	
			Br II	$4d'\ ^3D^o_2$	←	$5p''\ ^3D_2$	659.352	0.552	9.94	
663.15	0.5	1.0	Br I	$5p\ ^4D^o_{3/2}$	←	$7d\ ^4P_{1/2}$	663.092	-0.058	0.61	
				$5s\ ^4P_{5/2}$	←	$5p'\ ^2D^o_{5/2}$	663.343	0.193	-1.04	#
				$4d\ ^4D_{3/2}$	←	$5f''\ (3)^o_{5/2}$	663.581	0.431	0.97	
			Br II	$5p''\ ^1D_2$	←	$5d'\ C^o_2$	663.143	-0.007	9.12	
678.95	0.5	1.4	He I	$3s\ ^3S_1$	←	$18p\ ^3P^o_2$	678.755	-0.195	13.77	
					←	$18p\ ^3P^o_1$	678.755	-0.195	13.77	
					←	$18p\ ^3P^o_0$	678.755	-0.195	13.77	
					←	$18p\ ^1P^o_1$	678.625	-0.325	13.77	
			Br I	$5p\ ^4D^o_{7/2}$	←	$6d\ ^4F_{9/2}$	679.191	0.241	0.42	
				$5p\ ^4D^o_{5/2}$	←	$5d'\ ^2F_{7/2}$	678.859	-0.091	0.44	
					←	$6d\ ^4F_{3/2}$	679.376	0.426	0.44	

Table XVI (continued)

Luminescence from the Reaction 100 eV $He^+ + Br_2 \rightarrow He + Br^+ + Br + Energy$

λ_o (nm)	$\Delta\lambda_o$ (nm)	σ ($cm^2 \times 10^{-18}$)	X	Transition Assignment Lower State	←	Upper State	λ_T (nm)	$\lambda_T - \lambda_o$ (nm)	ΔH (eV)	
			Br I	$5p\ ^4P^o_{3/2}$	←	$6d\ ^4D_{1/2}$	679.335	0.385	0.35	
				$5p\ ^4P^o_{1/2}$	←	$5d'\ ^4P_{3/2}$	679.185	0.235	0.45	
				$5p'\ ^2D^o_{5/2}$	←	$6d'\ ^2F_{7/2}$	678.760	-0.190	0.79	
				$5p'\ ^2D^o_{3/2}$	←	$9d\ ^4D_{5/2}$	678.921	-0.029	0.81	
				$5p'\ ^4S^o_{3/2}$	←	$8s'\ ^2P_{3/2}$	678.965	0.015	0.87	
				$4d\ ^4D_{5/2}$	←	$5f'\ (4)^o_{7/2}$	678.711	-0.239	0.88	
					←	$5f'\ (2)^o_{5/2}$	679.004	0.054	0.88	
					←	$5f'\ (2)^o_{3/2}$	679.029	0.089	0.88	
700.55	0.5	3.1	Br I	$5s\ ^4P_{3/2}$	←	$5p'\ ^4S^o_{3/2}$	700.715	0.165	-0.95	#
				$5p'\ ^4S^o_{3/2}$	←	$6d'\ ^4P_{3/2}$	700.553	0.003	0.82	
					←	$9d\ ^4P_{1/2}$	700.616	0.066	0.82	

Table XVI (continued)

Luminescence from the Reaction 100 eV $He^+ + Br_2 \rightarrow He + Br^+ + Br + Energy$

λ_o (nm)	$\Delta\lambda_o$ (nm)	σ ($cm^2 \times 10^{18}$)	X	Transition Assignment Lower State	←	Upper State	λ_T (nm)	$\lambda_T - \lambda_o$ (nm)	ΔH (eV)	
726.00	0.5	0.6	Br I	$5s\ ^4P_{3/2}$	←	$5p'\ ^2D^o_{3/2}$	726.245	0.245	-1.02	
				$5p''\ ^2P^o_{3/2}$	←	$6d'\ ^4P_{5/2}$	725.801	-0.199	0.82	
				$5p''\ ^2P^o_{1/2}$	←	$(^1D_2)4d\ ^2P_{1/2}$	725.567	-0.433	0.84	
				$(^1D_2)5s\ ^2D_{5/2}$	←	$7p\ ^4D^o_{5/2}$	725.756	-0.244	0.35	
				$4d\ ^4D_{5/2}$	←	$7f\ (4)^o_{7/2}$	726.440	0.440	0.76	
					←	$7f\ (3)^o_{7/2}$	726.347	0.347	0.76	
					←	$7f\ (3)^o_{5/2}$	726.347	0.347	0.76	
					←	$7f\ (2)^o_{5/2}$	725.982	-0.018	0.77	
					←	$7f\ (2)^o_{3/2}$	726.001	0.001	0.76	
					←	$7f\ (1)^o_{3/2}$	725.598	-0.402	0.77	
734.90	0.4	6.0	Br I	$5p\ ^4P^o_{5/2}$	←	$7s\ ^4P_{3/2}$	735.123	0.223	0.17	
				$5p\ ^4D^o_{3/2}$	←	$6d\ ^4F_{5/2}$	734.654	-0.246	0.43	
				$5s\ ^4P_{3/2}$	←	$5p'\ ^2D^o_{5/2}$	735.056	0.156	-1.04	#

Table XVI (continued)

Luminescence from the Reaction 100 eV $He^+ + Br_2 \rightarrow He + Br^+ + Br + Energy$

λ_o (nm)	$\Delta\lambda_o$ (nm)	σ ($cm^2 \times 10^{18}$)	X	Transition Assignment Lower State	←	Upper State	λ_T (nm)	$\lambda_T - \lambda_o$ (nm)	ΔH (eV)	
751.45	0.5	4.5	Br I	$5s\ ^4P_{5/2}$	←	$5p\ ^4D^o_{3/2}$	751.505	0.055	-1.26	#
				$5p''\ ^2P^o_{3/2}$	←	$10s\ ^4P_{5/2}$	751.884	0.434	0.76	
				$4d\ ^4D_{1/2}$	←	$10p\ ^4D^o_{3/2}$	751.151	-0.299	0.80	
780.25	0.5	3.9	Br I	$5s'\ ^4P_{1/2}$	←	$5p''\ ^2P^o_{3/2}$	780.517	0.267	-0.89	#
				$5p''\ ^2P^o_{3/2}$	←	$(^1D_2)4d\ ^2D_{3/2}$	779.969	-0.281	0.70	
				$4d\ ^4D_{1/2}$	←	$7p'\ ^4S^o_{3/2}$	780.460	0.210	0.74	
793.95	0.6	1.4	Br I	$(^1D_2)5s\ ^2D_{5/2}$	←	$(^1D_2)5p\ ^2D^o_{5/2}$	794.086	0.136	0.20	
				$4d\ ^4D_{3/2}$	←	$4f''\ (3)^o_{5/2}$	793.781	-0.169	0.66	
					←	$6f\ (2)^o_{5/2}$	794.197	0.247	0.66	
					←	$6f\ (2)^o_{3/2}$	794.224	0.274	0.66	
					←	$6f\ (1)^o_{3/2}$	793.499	-0.451	0.67	
					←	$6f\ (1)^o_{1/2}$	793.524	-0.426	0.67	

Table XVI (continued)

Luminescence from the Reaction 100 eV $He^+ + Br_2 \rightarrow He + Br^+ + Br + Energy$

λ_o (nm)	$\Delta\lambda_o$ (nm)	σ ($cm^2 \times 10^{18}$)	X	Transition Assignment Lower State	←	Upper State	λ_T (nm)	$\lambda_T - \lambda_o$ (nm)	ΔH (eV)	
799.05	0.6	1.5	Br I	$5p'\ ^4S^o_{3/2}$	←	$7d\ ^4D_{1/2}$	799.194	0.144	0.60	
				$5s'\ ^2P_{3/2}$	←	$5p''\ ^2P^o_{3/2}$	799.213	0.163	-0.89	#
				$4d\ ^4D_{7/2}$	←	$8p\ ^4D^o_{5/2}$	799.194	0.144	0.58	
				$(^1D_2)5s\ ^2D_{3/2}$	←	$4f\ (1)^o_{3/2}$	798.917	-0.133	0.19	
					←	$4f\ (1)^o_{1/2}$	798.955	-0.095	0.19	
			Br II	$5p\ ^5P_3$	←	$4d'\ ^3D^o_2$	799.265	0.215	5.06	
802.55	0.6	1.3	Br I	$5p\ ^4P^o_{5/2}$	←	$5d\ ^4D_{3/2}$	802.611	0.061	0.03	
				$5p\ ^4P^o_{1/2}$	←	$7s\ ^4P_{3/2}$	802.472	-0.078	0.17	
				$5p'\ ^2S^o_{1/2}$	←	$5d'\ ^4P_{3/2}$	802.470	-0.080	0.45	
				$5p''\ ^2P^o_{3/2}$	←	$9s\ ^4P_{5/2}$	802.210	-0.340	0.66	
				$(^1D_2)5s\ ^2D_{5/2}$	←	$4f\ (3)^o_{7/2}$	802.519	-0.031	0.18	
					←	$4f\ (3)^o_{5/2}$	802.539	-0.011	0.18	

Table XVI (continued)

Luminescence from the Reaction 100 eV $He^+ + Br_2 \rightarrow He + Br^+ + Br + Energy$

λ_o (nm)	$\Delta\lambda_o$ (nm)	σ ($cm^2 \times 10^{18}$)	X	Transition Assignment Lower State	←	Upper State	λ_T (nm)	$\lambda_T - \lambda_o$ (nm)	ΔH (eV)	
			Br I	$(^1D_2)5s\ ^2D_{3/2}$	←	$4f\ (2)^o_{5/2}$	802.389	-0.161	0.19	
					←	$4f\ (2)^o_{3/2}$	802.862	0.312	0.19	
				$4d\ ^4D_{7/2}$	←	$4f'\ (4)^o_{9/2}$	803.101	0.551	0.57	
					←	$4f'\ (4)^o_{7/2}$	803.043	0.493	0.57	
				$6s\ ^4P_{5/2}$	←	$5f''\ (3)^o_{7/2}$	802.307	-0.243	0.97	
					←	$5f''\ (3)^o_{5/2}$	802.295	-0.255	0.97	
813.15	0.5	3.7	He I	$3p\ ^3P^o_2$	←	$16s\ ^3S_1$	812.928	-0.222	13.76	
				$3p\ ^3P^o_1$	←	$16s\ ^3S_1$	812.929	-0.221	13.76	
				$3p\ ^3P^o_0$	←	$16s\ ^3S_1$	812.947	-0.203	13.76	
			Br I	$5s'\ ^4P_{1/2}$	←	$5p'\ ^4S^o_{3/2}$	813.374	0.224	-0.95	#
				$4d\ ^4D_{5/2}$	←	$8p\ ^4D^o_{5/2}$	813.259	0.109	0.58	
			Br II	$5p''\ ^3D_2$	←	$5d'\ ^1P^o_1$	813.412	0.262	8.47	

Table XVI (continued)

Luminescence from the Reaction 100 eV $He^+ + Br_2 \rightarrow He + Br^+ + Br + Energy$

λ_o (nm)	$\Delta\lambda_o$ (nm)	σ ($cm^2 \times 10^{18}$)	X	Transition Assignment Lower State	←	Upper State	λ_T (nm)	$\lambda_T - \lambda_o$ (nm)	ΔH (eV)	
815.35	0.5	3.1	He I	$3p\ ^3P^o_2$	←	$15d\ ^3D_3$	815.777	0.427	13.76	
					←	$15d\ ^3D_2$	815.777	0.427	13.76	
					←	$15d\ ^3D_1$	815.777	0.427	13.76	
					←	$15d\ ^1D_2$	815.773	0.423	13.76	
				$3p\ ^3P^o_1$	←	$15d\ ^3D_2$	815.778	0.428	13.76	
					←	$15d\ ^3D_1$	815.778	0.428	13.76	
					←	$15d\ ^1D_2$	815.775	0.425	13.76	
				$3p\ ^3P^o_0$	←	$15d\ ^3D_1$	815.796	0.446	13.76	
			Br I	$5s\ ^4P_{5/2}$	←	$5p\ ^4D^o_{5/2}$	815.621	0.271	-1.39	#
				$5p\ ^4P^o_{5/2}$	←	$5d\ ^4D_{5/2}$	815.597	0.247	0.01	#
				$5p\ ^4P^o_{3/2}$	←	$5d\ ^4D_{1/2}$	815.488	0.138	0.05	
				$5p''\ ^2P^o_{3/2}$	←	$7d\ ^4F_{5/2}$	815.617	0.267	0.63	
				$4d\ ^4D_{5/2}$	←	$8p\ ^4P^o_{3/2}$	815.108	-0.242	0.58	
			Br II	$5p''\ ^1D_2$	←	$5d'\ ^3D^o_2$	815.474	0.124	8.77	

Table XVI (continued)

Luminescence from the Reaction 100 eV $He^+ + Br_2 \rightarrow He + Br^+ + Br + Energy$

λ_o (nm)	$\Delta\lambda_o$ (nm)	σ ($cm^2 \times 10^{18}$)	X	Transition Assignment			λ_T (nm)	$\lambda_T - \lambda_o$ (nm)	ΔH (eV)	
				Lower State	←	Upper State				
827.30	0.4	123.9	He I	$3p\ ^3P^o_1$	←	$13s\ ^1S_0$	827.629	0.329	13.73	
				$3p\ ^3P^o_0$	←	$13s\ ^1S_0$	827.648	0.348	13.73	
			Br I	$5s\ ^4P_{5/2}$	←	$5p\ ^4D^o_{7/2}$	827.469	0.169	-1.41	#
833.55	0.4	10.4	Br I	$5s'\ ^2P_{3/2}$	←	$5p'\ ^4S^o_{3/2}$	833.698	0.148	-0.95	#
				$5p'\ ^4S^o_{3/2}$	←	$5d''\ ^2D_{5/2}$	833.552	0.002	0.53	
				$5p''\ ^2P^o_{3/2}$	←	$7d\ ^4D_{1/2}$	833.677	0.127	0.60	
			Br II	$5p''\ ^1D_2$	←	$5d'\ ^3D^o_1$	833.354	-0.196	8.74	
				$5p''\ ^3P_0$	←	$5d'\ ^1P^o_1$	833.340	-0.210	8.47	
				$5p''\ ^1P_1$	←	$5d'\ ^3S^o_1$	833.715	0.165	8.63	
834.45	0.4	10.6	He I	$3p\ ^3P^o_2$	←	$12d\ ^3D_3$	834.463	0.013	13.72	
					←	$12d\ ^3D_2$	834.463	0.013	13.72	
					←	$12d\ ^3D_1$	834.463	0.013	13.72	
					←	$12d\ ^1D_2$	834.454	0.004	13.72	

Table XVI (continued)

Luminescence from the Reaction 100 eV $He^+ + Br_2 \rightarrow He + Br^+ + Br + Energy$

λ_o (nm)	$\Delta\lambda_o$ (nm)	σ ($cm^2 \times 10^{18}$)	X	Transition Assignment Lower State	←	Upper State	λ_T (nm)	$\lambda_T - \lambda_o$ (nm)	ΔH (eV)	
			He I	$3p\ ^3P^o_1$	←	$12d\ ^3D_2$	834.464	0.014	13.72	
					←	$12d\ ^3D_1$	834.464	0.014	13.72	
					←	$12d\ ^1D_2$	834.455	0.005	13.72	
				$3p\ ^3P^o_0$	←	$12d\ ^3D_1$	834.483	0.033	13.72	
				$3d\ ^3D_3$	←	$22d\ ^3P^o_2$	834.638	0.188	13.79	
				$3d\ ^3D_2$	←	$22d\ ^3P^o_2$	834.638	0.188	13.79	
					←	$22d\ ^3P^o_1$	834.638	0.188	13.79	
				$3d\ ^3D_1$	←	$22d\ ^3P^o_2$	834.641	0.191	13.79	
					←	$22d\ ^3P^o_1$	834.641	0.191	13.79	
					←	$22d\ ^3P^o_0$	834.641	0.191	13.79	
			Br I	$5s'\ ^4P_{1/2}$	←	$5p'\ ^4D^o_{1/2}$	834.596	0.146	-0.99	#
838.45	0.6	1.3	He I	$3d\ ^3D_3$	←	$20p\ ^3P^o_2$	838.001	-0.449	13.78	
				$3d\ ^3D_2$	←	$20p\ ^3P^o_2$	838.001	-0.449	13.78	

Table XVI (continued)

Luminescence from the Reaction 100 eV $He^+ + Br_2 \rightarrow He + Br^+ + Br + Energy$

λ_o (nm)	$\Delta\lambda_o$ (nm)	σ ($cm^2 \times 10^{18}$)	X	Transition Assignment Lower State	←	Upper State	λ_T (nm)	$\lambda_T - \lambda_o$ (nm)	ΔH (eV)	
			He I	$3d\ ^3D_2$	←	$20p\ ^3P^o_1$	838.001	-0.449	13.78	
					←	$20p\ ^1P^o_1$	837.862	-0.588	13.78	
				$3d\ ^3D_1$	←	$20p\ ^3P^o_2$	838.005	-0.445	13.78	
					←	$20p\ ^3P^o_1$	838.005	-0.445	13.78	
					←	$20p\ ^3P^o_0$	838.005	-0.445	13.78	
					←	$20p\ ^1P^o_1$	837.865	-0.585	13.78	
				$3d\ ^1D_2$	←	$20p\ ^3P^o_2$	838.242	-0.208	13.78	
					←	$20p\ ^3P^o_1$	838.242	-0.208	13.78	
					←	$20p\ ^1P^o_1$	838.102	-0.348	13.78	
			Br I	$5p\ ^4D^o_{7/2}$	←	$5d\ ^4F_{7/2}$	839.030	-0.580	0.07	
				$5p\ ^4P^o_{3/2}$	←	$5d\ ^4D_{5/2}$	838.634	0.184	0.01	#
				$5p'\ ^4D^o_{1/2}$	←	$8s\ ^4P_{3/2}$	838.094	-0.356	0.49	
				$5p''\ ^2P^o_{1/2}$	←	$7d\ ^4D_{3/2}$	838.074	-0.376	0.61	
				$4d\ ^4D_{3/2}$	←	$8p\ ^4D^o_{5/2}$	838.473	0.023	0.58	

Table XVI (continued)

Luminescence from the Reaction 100 eV $He^+ + Br_2 \rightarrow He + Br^+ + Br + Energy$

λ_o (nm)	$\Delta\lambda_o$ (nm)	σ ($cm^2 \times 10^{18}$)	X	Transition Assignment Lower State	←	Upper State	λ_T (nm)	$\lambda_T - \lambda_o$ (nm)	ΔH (eV)	
844.80	0.4	24.0	He I	3p $^3P^o_2$	←	11d $^3D_3$	844.679	-0.121	13.70	
					←	11d $^3D_2$	844.679	-0.121	13.70	
					←	11d $^3D_1$	844.679	-0.121	13.70	
					←	11d $^1D_2$	844.668	-0.132	13.70	
				3p $^3P^o_1$	←	11d $^3D_2$	844.681	-0.119	13.70	
					←	11d $^3D_1$	844.681	-0.119	13.70	
					←	11d $^1D_2$	844.670	-0.130	13.70	
				3p $^3P^o_0$	←	11d $^3D_1$	844.700	-0.100	13.70	
			Br I	5s $^4P_{3/2}$	←	5p $^4D^o_{3/2}$	844.888	0.088	-1.26	#
847.90	0.4	15.7	He I	3p $^1P^o_1$	←	19d $^3D_2$	847.653	-0.247	13.78	
					←	19d $^3D_1$	847.653	-0.247	13.78	
			Br I	5s' $^4P_{1/2}$	←	5p' $^2D^o_{3/2}$	847.976	0.076	-1.02	#
				5p' $^2S^o_{1/2}$	←	6d $^4D_{3/2}$	848.055	0.155	0.37	

Table XVI (continued)

Luminescence from the Reaction 100 eV $He^+ + Br_2 \rightarrow He + Br^+ + Br + Energy$

λ_o (nm)	$\Delta\lambda_o$ (nm)	σ ($cm^2 \times 10^{18}$)	X	Transition Assignment Lower State	←	Upper State	λ_T (nm)	$\lambda_T - \lambda_o$ (nm)	ΔH (eV)	
856.55	0.6	5.1	He I	$3p\ ^1P^o_1$	←	$16d\ ^3D_2$	856.712	0.162	13.76	
					←	$16d\ ^3D_1$	856.712	0.162	13.76	
					←	$16d\ ^1D_2$	856.712	0.162	13.76	
			Br I	$5p\ ^4D^o_{7/2}$	←	$5d\ ^4F_{9/2}$	856.864	0.314	0.04	
				$5p'\ ^2D^o_{3/2}$	←	$6d\ ^4F_{5/2}$	856.290	-0.260	0.43	
				$5s'\ ^2P_{3/2}$	←	$5p'\ ^4D^o_{1/2}$	856.008	-0.542	-0.99	#
				$5p'\ ^4D^o_{1/2}$	←	$5d'\ ^4P_{3/2}$	856.766	0.216	0.46	
				$4d\ ^4F_{7/2}$	←	$7p'\ ^2D^o_{5/2}$	856.552	0.002	0.73	
				$4d\ ^4F_{5/2}$	←	$10p\ ^4D^o_{3/2}$	857.116	0.566	0.80	
864.05	0.4	63.0	Br I	$5s\ ^4P_{5/2}$	←	$5p\ ^4P^o_{3/2}$	864.104	0.054	-1.47	#
				$4d\ ^4D_{1/2}$	←	$8p\ ^4P^o_{1/2}$	864.121	0.071	0.59	

Table XVI (continued)

Luminescence from the Reaction 100 eV $He^+ + Br_2 \rightarrow He + Br^+ + Br + Energy$

λ_o (nm)	$\Delta\lambda_o$ (nm)	σ ($cm^2 \times 10^{18}$)	X	Transition Assignment Lower State ← Upper State	λ_T (nm)	$\lambda_T - \lambda_o$ (nm)	ΔH (eV)	
869.90	0.5	9.6	Br I	$5s'\ ^2P_{3/2} \leftarrow 5p'\ ^2D^o_{3/2}$	870.090	0.190	-1.02	#
				$4d\ ^4F_{3/2} \leftarrow 10p\ ^4D^o_{3/2}$	869.770	-0.130	0.80	

$\sigma_{TOTAL} = 1493.3 \times 10^{-18}\ cm^2$ $\sigma_{VUV\ TOTAL} = 1188.9 \times 10^{-18}\ cm^2$ $\sigma_{VISIBLE\ TOTAL} = 304.4 \times 10^{-18}\ cm^2$

Appendix C

Table XVII

Luminescence from the Reaction 100 eV $He^+ + I_2 \rightarrow He + I^+ + I + Energy$

Explanation of Symbols

λ_o = Observed vacuum wavelength (nm)

$\Delta\lambda_o$ = Search interval (nm)

σ = Emission cross section ($cm^2 \times 10^{18}$)

X = Emitting atom or ion

λ_T = Calculated vacuum wavelength in nm using the energy level tables (Refs. 30, 41, 42 and 48).

ΔH = Enthalpy change in eV required to populate the upper energy state for the thermal reaction $He^+ + I_2 \rightarrow He + I^+ + I^*$.

Inner electron configuration designation (Refs. 30, 41, 42 and 48).

I (I)	Unprimed = (^3P)	' = (^1D)	" = (^1S)		
M I (I)	Unprimed = ($^3P_2$)	' = ($^3P_1$)	" = ($^3P_0$)	($^1D_2$) = ($^1D_2$)	
I (II)	Unprimed = ($^4S^o$)	' = ($^2D^o$)	" = ($^2P^o$)		

NOTE: MI I indicates use of Minnhagen's energy level tables (Ref. 48).

Table XVII (continued)

Luminescence from the Reaction 100 eV $He^+ + I_2 \rightarrow He + I^+ + I + Energy$

λ_o (nm)	$\Delta\lambda_o$ (nm)	σ ($cm^2 \times 10^{18}$)	X	Transition Assignment Lower State	←	Upper State	λ_T (nm)	$\lambda_T - \lambda_o$ (nm)	ΔH (eV)
100.075	0.300	5.3	I (II)	$5p^4\ ^3P_2$	←	$5d'\ ^3F_3^o$	100.057	-0.018	-0.19
				$5p^4\ ^3P_0$	←	$6s''\ ^3P_1^o$	100.346	0.271	0.57
				$5p^4\ ^1D_2$	←	$5d'\ ^1F_3^o$	100.335	0.260	1.48
					←	$5d''\ ^1D_2^o$	100.361	0.286	1.48
					←	$5d''\ ^3D_3^o$	100.071	-0.004	1.51
101.875	0.300	8.1	I (II)	$5p^4\ ^3P_2$	←	$5d'\ ^3D_3^o$	101.858	-0.017	-0.41
				$5p^4\ ^3P_1$	←	$6s''\ ^3P_0^o$	101.922	0.047	0.46
				$5p^4\ ^3P_0$	←	$5d'\ ^3D_1^o$	101.939	0.064	0.38
				$5p^4\ ^1D_2$	←	$6s''\ ^1P_1^o$	101.797	-0.078	1.30
				$5p^4\ ^1S_0$	←	$5d''\ ^1P_1^o$	101.637	-0.238	3.28
103.425	0.400	7.0	I (II)	$5p^4\ ^3P_2$	←	$6s'\ ^3D_3^o$	103.466	0.041	-0.60
				$5p^4\ ^1D_2$	←	$6s''\ ^3P_2^o$	103.379	-0.046	1.11

Table XVII (continued)

Luminescence from the Reaction 100 eV $He^+ + I_2 \rightarrow He + I^+ + I + Energy$

λ_o (nm)	$\Delta\lambda_o$ (nm)	σ ($cm^2 \times 10^{18}$)	X	Transition Assignment Lower State	←	Upper State	λ_T (nm)	$\lambda_T - \lambda_o$ (nm)	ΔH (eV)
106.775	0.300	6.2	I (II)	$5p^4\ ^3P_2$	←	$6s'\ ^3D_2^o$	106.733	-0.042	-0.96
				$5p^4\ ^1D_2$	←	$5d'\ ^3F_2^o$	106.627	-0.148	0.75
					←	$5d'\ ^3G_3^o$	106.498	-0.277	0.76
107.575	0.300	13.7	I (II)	$5p^4\ ^3P_2$	←	$5d\ ^3D_3^o$	107.520	-0.055	-1.05
				$5p^4\ ^1S_0$	←	$6d\ ^5D_1^o$	107.826	0.251	2.58
110.475	0.300	15.4	I (II)	$5p^4\ ^3P_2$	←	$5d\ ^3D_2^o$	110.499	0.024	-1.36
				$5p^4\ ^3P_1$	←	$6s'\ ^1D_2^o$	110.358	-0.117	-0.47
				$5p^4\ ^1S_0$	←	$7s\ ^3S_1^o$	110.635	0.160	2.28
114.025	0.300	15.8	I (II)	$5p^4\ ^3P_2$	←	$5d\ ^5D_1^o$	113.981	-0.044	-1.70
				$5p^4\ ^3P_1$	←	$6s'\ ^3D_1^o$	113.975	-0.050	-0.82

Table XVII (continued)

Luminescence from the Reaction 100 eV $He^+ + I_2 \rightarrow He + I^+ + I$ + Energy

λ_o (nm)	$\Delta\lambda_o$ (nm)	σ ($cm^2 \times 10^{18}$)	X	Transition Assignment Lower State	←	Upper State	λ_T (nm)	$\lambda_T - \lambda_o$ (nm)	ΔH (eV)
116.000	0.100	29.0	I (II)	$5p^4\ ^3P_2$	←	$5d\ ^5D^o_2$	116.057	0.057	-1.90
				$5p^4\ ^1D_2$	←	$5d'\ ^3F^o_3$	115.988	-0.012	-0.19
116.600	0.100	53.5	I (II)	$5p^4\ ^3P_2$	←	$5d\ ^5D^o_3$	116.648	0.048	-1.95
				$5p^4\ ^3P_0$	←	$5d\ ^3D^o_1$	116.707	0.107	-1.16
117.850	0.100	24.3	I (II)	$5p^4\ ^3P_2$	←	$6s\ ^3S^o_1$	117.865	0.015	-2.06
118.700	0.100	21.8	I (II)	$5p^4\ ^3P_2$	←	$5p^5\ ^3P^o_1$	118.734	0.034	-2.14
122.075	0.500	38.6	I (I)	$5p^5\ ^2P^o_{3/2}$	←	$11s\ ^4P_{5/2}$	121.841	-0.234	-2.40
					←	$8d\ ^4P_{5/2}$	122.405	0.330	-2.45
					←	nd $31.1_{3/2}$	122.408	0.333	-2.45
					←	nd $30_{1/2}$	122.450	0.375	-2.45
					←	nd $31_{3/2}$	122.486	0.411	-2.46

Table XVII (continued)

Luminescence from the Reaction 100 eV $He^+ + I_2 \rightarrow He + I^+ + I + Energy$

λ_o (nm)	$\Delta\lambda_o$ (nm)	σ ($cm^2 \times 10^{18}$)	Transition Assignment X	Lower State	←	Upper State	λ_T (nm)	$\lambda_T - \lambda_o$ (nm)	ΔH (eV)
			I (I)	$5p^5\ ^2P^o_{3/2}$	←	$nd\ 32_{3/2}$	122.343	0.268	-2.45
					←	$nd\ 32.1_{1/2}$	122.332	0.257	-2.44
					←	$nd\ 32.2_{1/2}$	121.909	-0.166	-2.41
					←	$nd\ 33_{1/2}$	121.812	-0.263	-2.40
					←	$nd\ 34_{1/2}$	121.714	-0.361	-2.39
					←	$nd\ 35_{1/2}$	121.602	-0.473	-2.38
			M I(I)	$5p^5\ ^2P^o_{3/2}$	←	$11s[2]_{5/2}$	121.841	-0.234	-2.40
					←	$11s[2]_{3/2}$	121.812	-0.263	-2.40
					←	$(^1D_2)5d[3]_{5/2}$	121.737	-0.338	-2.40
					←	$(^1D_2)5d[2]_{5/2}$	121.890	-0.185	-2.41
					←	$(^1D_2)5d[2]_{3/2}$	121.602	-0.473	-2.38
					←	$6d'[1]_{3/2}$	121.714	-0.361	-2.39
					←	$6d'[1]_{1/2}$	121.909	-0.166	-2.41
					←	$9d[3]_{5/2}$	122.405	0.330	-2.45

Table XVII (continued)

Luminescence from the Reaction 100 eV $He^+ + I_2 \rightarrow He + I^+ + I + Energy$

λ_o (nm)	$\Delta\lambda_o$ (nm)	σ ($cm^2 \times 10^{18}$)	X	Transition Assignment Lower State	←	Upper State	λ_T (nm)	$\lambda_T - \lambda_o$ (nm)	ΔH (eV)
			M I (I)	$5p^5\ ^2P^o_{3/2}$	←	$9d[2]_{5/2}$	122.486	0.411	-2.46
					←	$9d[2]_{3/2}$	122.408	0.333	-2.45
					←	$9d[1]_{3/2}$	122.343	0.268	-2.45
					←	$9d[1]_{1/2}$	122.332	0.257	-2.45
					←	nd $B_{1/2}$	122.450	0.375	-2.46
					←	nd $B_{3/2}$	122.450	0.375	-2.46
			I (II)	$5p^4\ ^3P_2$	←	$5p^5\ ^3P^o_2$	122.088	0.013	-2.43
				$5p^4\ ^1D_2$	←	$5p^5\ ^1P^o_1$	121.612	-0.463	-0.68
123.350	0.100	50.4	I (I)	$5p^5\ ^2P^o_{3/2}$	←	nd $28.2_{3/2}$	123.346	-0.004	-2.53
			M I (I)	$5p^5\ ^2P^o_{3/2}$	←	$(^1D_2)5d[1]_{3/2}$	123.346	-0.004	-2.53
			I (II)	$5p^4\ ^3P_2$	←	$6s\ ^5S^o_2$	123.407	0.057	-2.53
				$5p^4\ ^1D_2$	←	$6s'\ ^3D^o_1$	123.307	-0.043	-0.82

Table XVII (continued)

Luminescence from the Reaction 100 eV $He^+ + I_2 \rightarrow He + I^+ + I + Energy$

λ_o (nm)	$\Delta\lambda_o$ (nm)	σ ($cm^2 \times 10^{18}$)	X	Transition Assignment Lower State	←	Upper State	λ_T (nm)	$\lambda_T - \lambda_o$ (nm)	ΔH (eV)
130.00	0.100	43.7	I (I)	$5p^5\ ^2P^o_{3/2}$	←	$nd\ 21_{5/2}$	130.033	0.033	-3.05
			M I (I)	$5p^5\ ^2P^o_{3/2}$	←	$6d[2]_{5/2}$	130.034	0.034	-3.05
130.300	0.100	40.1	I (I)	$5p^5\ ^2P^o_{3/2}$	←	$nd\ 20_{1/2}$	130.298	-0.002	-3.06
			M I (I)	$5p^5\ ^2P^o_{3/2}$	←	$6d[2]_{3/2}$	130.298	-0.002	-3.06
			I (II)	$5p^4\ ^1D_2$	←	$5d\ ^3D^o_2$	130.257	-0.043	-1.36
131.750	0.100	61.8	I (I)	$5p^5\ ^2P^o_{3/2}$	←	$nd\ 17_{5/2}$	131.754	0.004	-3.17
			M I (I)	$5p^5\ ^2P^o_{3/2}$	←	$5d'[2]_{5/2}$	131.754	0.004	-3.17
138.300	0.100	39.2	I (I)	$5p^5\ ^2P^o_{3/2}$	←	$7s\ ^2P_{3/2}$	138.322	0.022	-3.62
				$5p^5\ ^2P^o_{1/2}$	←	$9s\ ^2P_{3/2}$	138.228	-0.072	-2.67
			M I (I)	$5p^5\ ^2P^o_{3/2}$	←	$7s[2]_{3/2}$	138.323	0.023	-3.62
				$5p^5\ ^2P^o_{1/2}$	←	$9s[2]_{3/2}$	138.228	-0.072	-2.67

Table XVII (continued)

Luminescence from the Reaction 100 eV $He^+ + I_2 \rightarrow He + I^+ + I + Energy$

λ_o (nm)	$\Delta\lambda_o$ (nm)	σ ($cm^2 \times 10^{18}$)	X	Transition Assignment Lower State	←	Upper State	λ_T (nm)	$\lambda_T - \lambda_o$ (nm)	ΔH (eV)
139.050	0.150	30.7	I (I)	$5p^5\ ^2P^o_{3/2}$	←	$7s\ ^4P_{5/2}$	139.075	0.025	-3.67
			M I (I)	$5p^5\ ^2P^o_{3/2}$	←	$7s[2]_{5/2}$	139.075	0.025	-3.67
142.075	0.150	36.9	I (I)	$5p^5\ ^2P^o_{3/2}$	←	$nd\ 5.1_{3/2}$	142.136	0.061	-3.86
			M I (I)	$5p^5\ ^2P^o_{3/2}$	←	$5d[2]_{3/2}$	142.137	0.062	-3.86
142.525	0.100	73.9	I (I)	$5p^5\ ^2P^o_{3/2}$	←	$nd\ 5_{5/2}$	142.549	0.024	-3.88
			M I (I)	$5p^5\ ^2P^o_{3/2}$	←	$5d[2]_{5/2}$	142.549	0.024	-3.88
145.775	0.100	119.4	I (I)	$5p^5\ ^2P^o_{3/2}$	←	$nd\ 2_{3/2}$	145.879	0.104	-4.08
					←	$nd\ 3_{5/2}$	145.798	0.023	-4.08
					←	$nd\ 4_{3/2}$	145.747	-0.028	-4.07
					←	$nd\ 4.1_{3/2}$	145.739	-0.036	-4.07

Table XVII (continued)

Luminescence from the Reaction 100 eV $He^+ + I_2 \rightarrow He + I^+ + I + Energy$

λ_o (nm)	$\Delta\lambda_o$ (nm)	σ ($cm^2 \times 10^{18}$)	X	Transition Assignment Lower State	←	Upper State	λ_T (nm)	$\lambda_T - \lambda_o$ (nm)	ΔH (eV)
			M I (I)	$5p^5\ ^2P^o_{3/2}$	←	$(^1D_2)6s[2]_{5/2}$	145.798	0.023	-4.08
					←	$(^1D_2)6s[2]_{3/2}$	145.879	0.104	-4.08
					←	$5d[0]_{1/2}$	145.739	-0.036	-4.07
151.450	0.100	73.4	I (I)	$5p^5\ ^2P^o_{3/2}$	←	$(^1D_2)6s\ ^2D_{5/2}$	151.468	0.018	-4.39
				$5p^5\ ^2P^o_{1/2}$	←	$nd\ 8_{3/2}$	151.432	-0.018	-3.45
			M I (I)	$5p^5\ ^2P^o_{3/2}$	←	$5d[3]_{5/2}$	151.468	0.018	-4.39
				$5p^5\ ^2P^o_{1/2}$	←	$5d''[2]_{3/2}$	151.432	-0.018	-3.45
			I (II)	$5p^5\ ^3P^o_2$	←	$5f'\ 3_2$	151.436	-0.014	5.76
					←	$5f'\ 3_3$	151.436	-0.014	5.76
				$5p^5\ ^3P^o_1$	←	$5f'\ 10_2$	151.521	0.071	6.04
					←	$5f'\ 12_1$	151.384	-0.066	6.05
					←	$5f'\ 12_2$	151.384	-0.066	6.05
				$6s\ ^5S^o_2$	←	$8f\ ^3F_3$	151.466	0.016	5.65

Table XVII (continued)

Luminescence from the Reaction 100 eV $He^+ + I_2 \rightarrow He + I^+ + I + Energy$

λ_o (nm)	$\Delta\lambda_o$ (nm)	σ ($cm^2 \times 10^{18}$)	X	Transition Assignment Lower State	←	Upper State	λ_T (nm)	$\lambda_T - \lambda_o$ (nm)	ΔH (eV)
161.725	0.100	66.4	I (I)	$5p^5\ ^2P^o_{3/2}$	←	$6s\ ^4P_{3/2}$	161.760	0.035	-4.92
			M I (I)	$5p^5\ ^2P^o_{3/2}$	←	$6s'[1]_{3/2}$	161.761	0.036	-4.92
164.175	0.150	70.3	I (I)	$5p^5\ ^2P^o_{3/2}$	←	$6s\ ^4P_{1/2}$	164.214	0.039	-5.03
				$5p^5\ ^2P^o_{1/2}$	←	$nd\ ^2_{3/2}$	164.078	-0.097	-4.08
			M I (I)	$5p^5\ ^2P^o_{3/2}$	←	$6s''[0]_{1/2}$	164.214	0.039	-5.03
				$5p^5\ ^2P^o_{1/2}$	←	$(^1D_2)6s[2]_{3/2}$	164.078	-0.097	-4.08
			I (II)	$5d\ ^5D^o_4$	←	$5f'\ ^2_3$	164.105	-0.070	5.64
					←	$8f\ ^5F_5$	164.242	0.067	5.64
					←	$8f\ ^5F_4$	164.199	0.024	5.64
					←	$8f\ ^5F_3$	164.209	0.034	5.64
				$5d\ ^5D^o_2$	←	$8f\ ^3F_3$	164.232	0.057	5.65

Table XVII (continued)

Luminescence from the Reaction 100 eV $He^+ + I_2 \rightarrow He + I^+ + I + Energy$

λ_o (nm)	$\Delta\lambda_o$ (nm)	σ ($cm^2 \times 10^{18}$)	X	Transition Assignment Lower State	←	Upper State	λ_T (nm)	$\lambda_T - \lambda_o$ (nm)	ΔH (eV)
170.10	0.30	29.0	I (I)	$5p^5\ ^2P^o_{1/2}$	←	$(^1D)6s\ ^2D_{3/2}$	170.207	0.107	-4.35
			M I (I)	$5p^5\ ^2P^o_{1/2}$	←	$5d[1]_{3/2}$	170.207	0.107	-4.35
			I (II)	$6s\ ^5S^o_2$	←	$7p'\ ^3F_2$	169.841	-0.259	4.77
				$5d\ ^5D^o_3$	←	$7f\ ^5F_4$	169.802	-0.298	5.35
				$5d\ ^5D^o_2$	←	$7f\ ^3F_2$	170.267	0.167	5.38
				$5d\ ^5D^o_4$	←	$7f\ ^3F_3$	170.144	0.044	5.37
					←	$7f\ ^3F_4$	169.829	-0.271	5.39
				$5d\ ^5D^o_1$	←	$5f'\ 1_2$	170.281	0.181	5.58
				$5d\ ^3D^o_2$	←	$5f'\ 7_2$	170.339	0.239	5.92
					←	$5f'\ 7_3$	170.339	0.239	5.92
					←	$5f'\ 8_1$	169.869	-0.231	5.94
					←	$5f'\ 8_2$	169.869	-0.231	5.94

Table XVII (continued)

Luminescence from the Reaction 100 eV $He^+ + I_2 \rightarrow He + I^+ + I + Energy$

λ_o (nm)	$\Delta\lambda_o$ (nm)	σ ($cm^2 \times 10^{18}$)	Transition Assignment X	Lower State	←	Upper State	λ_T (nm)	$\lambda_T - \lambda_o$ (nm)	ΔH (eV)
178.225	0.100	161.0	I (I)	$5p^5\ ^2P^o_{3/2}$	←	$6s\ ^2P_{3/2}$	178.276	0.051	-5.63
			M I (I)	$5p^5\ ^2P^o_{3/2}$	←	$6s[2]_{3/2}$	178.276	0.051	-5.63
			I (II)	$5p^5\ ^3P^o_1$	←	$7p'\ ^3P_0$	178.235	0.010	4.82
183.000	0.100	302.4	I (I)	$5p^5\ ^2P^o_{3/2}$	←	$6s\ ^4P_{5/2}$	183.038	0.038	-5.81
			M I (I)	$5p^5\ ^2P^o_{3/2}$	←	$6s[2]_{5/2}$	183.038	0.038	-5.81
			I (II)	$5p^5\ ^3P^o_2$	←	$4f'\ ^3F_2$	183.086	0.086	4.35
				$5d\ ^5D^o_0$	←	$4f'\ ^3D_1$	182.974	-0.026	4.78
				$5d\ ^5D^o_3$	←	$4f'\ ^1F_3$	182.952	-0.048	4.83
				$5d\ ^5D^o_3$	←	$7p'\ ^3F_3$	182.963	-0.037	4.82
412.80	0.50	2.0	I (I)	$6s\ ^4P_{5/2}$	←	$8p\ ^2D^o_{5/2}$	412.858	0.058	-2.80
			M I (I)	$6s[2]_{5/2}$	←	$8p[3]^o_{7/2}$	413.037	0.237	-2.80
					←	$8p[3]^o_{5/2}$	412.860	0.060	-2.80

Table XVII (continued)

Luminescence from the Reaction 100 eV $He^+ + I_2 \rightarrow He + I^+ + I + Energy$

λ_o (nm)	$\Delta\lambda_o$ (nm)	σ ($cm^2 \times 10^{18}$)	X	Transition Assignment Lower State	←	Upper State	λ_T (nm)	$\lambda_T - \lambda_o$ (nm)	ΔH (eV)
			I (II)	$6p\ ^5P_2$	←	$5d''\ ^1F_3^o$	412.322	-0.478	2.74
				$6p'\ ^3D_1$	←	$6d'\ 4_0^o$	412.725	-0.075	4.06
				$6p'\ ^3F_3$	←	$5g\ ^5G_2^o$	412.992	0.192	4.36
					←	$5g\ ^5G_3^o$	412.972	0.172	4.36
				$6p'\ ^3P_2$	←	$9s\ ^5S_2^o$	412.380	-0.420	4.77
				$4f\ ^3F_3$	←	$6d''\ 40_3^o$	412.300	-0.500	5.95
				$7p\ ^3P_2$	←	$13d\ ^3D_3^o$	413.158	0.358	6.09
				$7p\ ^3P_1$	←	$6d''\ 47_1^o$	412.365	-0.435	6.08
					←	$6d''\ 47_2^o$	412.365	-0.435	6.08
				$5d'\ ^1S_0^o$	←	$5f\ ^5F_1$	413.178	0.378	4.19
				$5d'\ ^1F_3^o$	←	$4f'\ ^3P_2$	412.405	-0.395	4.48
				$6s''\ ^1P_1^o$	←	$7p'\ ^3D_1$	412.411	-0.389	4.31
				$6d\ ^5D_1^o$	←	$5f'\ 1_2$	412.935	0.135	5.58

Table XVII (continued)

Luminescence from the Reaction 100 eV $He^+ + I_2 \rightarrow He + I^+ + I + Energy$

λ_o (nm)	$\Delta\lambda_o$ (nm)	σ ($cm^2 \times 10^{18}$)	X	Transition Assignment Lower State	←	Upper State	λ_T (nm)	$\lambda_T - \lambda_o$ (nm)	ΔH (eV)
432.20	0.60	0.8	I (I)	$6s\ ^2P_{3/2}$	←	$8p\ ^4P^o_{3/2}$	432.303	0.103	-2.76
					←	$8p\ ^4P^o_{1/2}$	432.709	0.509	-2.76
			M I (I)	$6s[2]_{3/2}$	←	$8p[1]^o_{3/2}$	432.305	0.105	-2.76
			I (II)	$6p'\ ^3F_2$	←	$7d\ ^5D^o_3$	432.085	-0.115	4.09
				$6p'\ ^3F_3$	←	$7d\ ^3D^o_3$	431.669	-0.531	4.23
				$5p^5\ ^1P^o_1$	←	$6p'\ ^1D_2$	432.396	0.196	2.18
				$6p''\ ^3P_1$	←	$6d''\ 36^o_2$	432.052	-0.148	5.81
				$6p''\ ^3D_2$	←	$12s\ ^3S^o_1$	432.305	0.105	5.81
				$4f\ ^5F_4$	←	$6d''\ 33^o_3$	432.146	-0.054	5.75
				$4f\ ^5F_3$	←	$6d''\ 33^o_3$	432.672	0.472	5.75
				$4f\ ^5F_1$	←	$6d''\ 34^o_2$	432.044	-0.156	5.77
				$7p\ ^5P_1$	←	$6d''\ 35^o_2$	432.367	0.167	5.78
				$4f\ ^3F_2$	←	$6d''\ 37^o_2$	432.304	0.104	5.85
				$7p\ ^3P_0$	←	$6d''\ 45^o_1$	431.703	-0.497	6.06

Table XVII (continued)

Luminescence from the Reaction 100 eV $He^+ + I_2 \rightarrow He + I^+ + I + Energy$

λ_o (nm)	$\Delta\lambda_o$ (nm)	σ ($cm^2 \times 10^{18}$)	X	Transition Assignment Lower State	←	Upper State	λ_T (nm)	$\lambda_T - \lambda_o$ (nm)	ΔH (eV)
			I (II)	$5d'\ ^1F^o_3$	←	$4f'\ ^3F_2$	432.265	0.065	4.35
				$5d''\ ^1D^o_2$	←	$4f'\ ^3F_2$	431.799	-0.401	4.35
				$5d''\ ^3D^o_3$	←	$4f'\ ^3H_4$	432.041	-0.159	4.38
				$5d'\ ^3P^o_2$	←	$4f'\ ^3P_2$	431.810	-0.390	4.48
				$5d''\ ^3P^o_2$	←	$6f\ ^5F_3$	432.050	-0.150	4.91
					←	$6f\ ^5F_2$	431.804	-0.396	4.91
				$6d\ ^5D^o_3$	←	$7f\ ^3F_2$	432.565	0.365	5.38
					←	$7f\ ^3F_4$	432.137	-0.063	5.39
476.40	0.50	2.2	I (I)	$6s\ ^4P_{5/2}$	←	$7p\ ^4P^o_{3/2}$	476.464	0.064	-3.20
			M I (I)	$6s[2]_{5/2}$	←	$7p[1]^o_{3/2}$	476.464	0.064	-3.20
			I (II)	$6s''\ ^3P^o_2$	←	$6p''\ ^1D_2$	476.514	0.114	3.72
				$4f\ ^5F_1$	←	$6d''\ 20^o_1$	476.282	-0.118	5.50
					←	$6d''\ 20^o_2$	476.282	-0.118	5.50

Table XVII (continued)

Luminescence from the Reaction 100 eV $He^+ + I_2 \rightarrow He + I^+ + I + Energy$

λ_o (nm)	$\Delta\lambda_o$ (nm)	σ ($cm^2 \times 10^{18}$)	Transition Assignment X	Lower State	←	Upper State	λ_T (nm)	$\lambda_T - \lambda_o$ (nm)	ΔH (eV)
			I (II)	$7p\ ^5P_3$	←	$6d''\ 24^o_2$	476.245	-0.155	5.58
				$5d'\ ^3D^o_1$	←	$4f\ ^3F_2$	476.681	0.281	2.98
				$7p\ ^3P_2$	←	$8g\ ^5G^o_3$	476.199	-0.201	5.70
					←	$8g\ ^5G^o_2$	476.100	-0.300	5.70
					←	$8g\ ^3G^o_3$	476.069	-0.331	5.70
				$7p\ ^3P_1$	←	$6d''\ 30^o_2$	476.041	-0.359	5.68
486.10	0.50	6.0	I (I)	$6s\ ^4P_{5/2}$	←	$7p\ ^2D^o_{5/2}$	486.431	0.331	-3.26
					←	$7p\ ^4D^o_{7/2}$	486.366	0.266	-3.26
			M I (I)	$6s[2]_{5/2}$	←	$7p[3]^o_{5/2}$	486.431	0.331	-3.26
					←	$7p[3]^o_{7/2}$	486.367	0.267	-3.26
			I (II)	$6p\ ^5P_2$	←	$7s\ ^3S^o_1$	486.343	0.243	2.28
				$6p'\ ^3D_2$	←	$5d''\ ^3P^o_1$	486.489	0.389	3.88
				$6p'\ ^1P_1$	←	$7d\ ^5D^o_2$	486.459	0.359	4.08

Table XVII (continued)

Luminescence from the Reaction 100 eV $He^+ + I_2 \rightarrow He + I^+ + I$ + Energy

λ_o (nm)	$\Delta\lambda_o$ (nm)	σ ($cm^2 \times 10^{18}$)	X	Transition Assignment Lower State	←	Upper State	λ_T (nm)	$\lambda_T - \lambda_o$ (nm)	ΔH (eV)
			I (II)	6p' $^1D_2$	←	6d' 14^o_3	486.587	0.487	4.73
				6p'' $^3P_2$	←	6d'' 44^o_2	486.586	0.486	6.06
					←	6d'' 44^o_3	486.586	0.486	6.06
				6p'' $^3D_3$	←	6d'' 42^o_2	486.105	0.005	6.02
				6p'' $^3P_2$	←	6d'' 45^o_1	486.069	-0.031	6.06
					←	6d'' 45^o_2	486.069	-0.031	6.06
				4f $^5F_3$	←	7g $^5G^o_4$	486.114	0.014	5.43
					←	7g $^5G^o_3$	486.052	-0.048	5.43
					←	7g $^5G^o_2$	485.895	-0.205	5.43
					←	7g $^3G^o_4$	486.068	-0.032	5.43
					←	7g $^3G^o_3$	485.867	-0.233	5.43
				5d'' $^3D^o_2$	←	7p' $^3F_2$	485.666	-0.434	4.77

Table XVII (continued)

Luminescence from the Reaction 100 eV $He^+ + I_2 \rightarrow He + I^+ + I + Energy$

λ_o (nm)	$\Delta\lambda_o$ (nm)	σ ($cm^2 \times 10^{18}$)	X	Transition Assignment			λ_T (nm)	$\lambda_T - \lambda_o$ (nm)	ΔH (eV)
				Lower State	←	Upper State			
489.50	0.50	1.6	I (I)	$6s\ ^4P_{5/2}$	←	$7p\ ^4S^o_{3/2}$	489.809	0.309	-3.28
			M I (I)	$6s[2]_{5/2}$	←	$7p[2]^o_{3/2}$	489.811	0.311	-3.28
			I (II)	$6p'\ ^3F_3$	←	$8s\ ^5S^o_2$	489.759	0.259	3.89
				$6p'\ ^1P_1$	←	$6d'\ 4^o_0$	489.640	0.140	4.06
				$6p''\ ^3D_3$	←	$6d''\ 41^o_2$	489.348	-0.152	6.00
					←	$6d''\ 41^o_3$	489.348	-0.152	6.00
				$6p''\ ^3P_2$	←	$6d''\ 43^o_1$	489.087	-0.413	6.04
					←	$6d''\ 43^o_2$	489.087	-0.413	6.04
				$7p\ ^3P_2$	←	$6d''\ 26^o_3$	489.093	-0.407	5.63
				$7s\ ^3S^o_1$	←	$7p'\ ^3P_0$	489.256	-0.244	4.82
491.60	0.50	4.6	I (I)	$6s\ ^4P_{5/2}$	←	$7p\ ^4P^o_{5/2}$	491.828	0.228	-3.29
				$6s\ ^4P_{1/2}$	←	$6f\ 5^o_{1/2}$	491.890	0.290	-2.51
					←	$6f\ 6^o_{3/2}$	491.857	0.257	-2.51

Table XVII (continued)

Luminescence from the Reaction 100 eV $He^+ + I_2 \rightarrow He + I^+ + I$ + Energy

λ_o (nm)	$\Delta\lambda_o$ (nm)	σ ($cm^2 \times 10^{18}$)	X	Transition Assignment Lower State	←	Upper State	λ_T (nm)	$\lambda_T - \lambda_o$ (nm)	ΔH (eV)
			I (I)	$6s[2]_{5/2}$	←	$7p[2]^o_{5/2}$	491.832	0.232	-3.29
				$6s''[0]_{1/2}$	←	$6f[1]^o_{3/2}$	491.859	0.259	-2.51
					←	$6f[1]^o_{1/2}$	491.892	0.292	-2.51
			I (II)	$6p'\ ^1F_3$	←	$7d\ ^5D^o_4$	491.517	-0.083	4.10
				$6p'\ ^3P_1$	←	$6d'\ 6^o_1$	491.195	-0.405	4.34
					←	$6d'\ 6^o_2$	491.195	-0.405	4.34
				$6p''\ ^3S_1$	←	$6d''\ 38^o_1$	491.744	0.144	5.88
				$7p\ ^5P_1$	←	$7g\ ^5G^o_2$	491.603	0.003	5.43
				$7p\ ^5P_3$	←	$6d''\ 20^o_2$	491.298	-0.302	5.50
				$7p\ ^3P_1$	←	$11s\ ^5S^o_2$	491.605	0.005	5.59
					←	$11s\ ^3S^o_1$	491.318	-0.282	5.59
				$5d'\ ^1P^o_1$	←	$5f\ ^5F_2$	492.025	0.425	4.18
					←	$5f\ ^5F_1$	491.538	-0.062	4.19
				$5d''\ ^3F^o_3$	←	$6f\ ^3F_4$	491.779	0.179	4.97

Table XVII (continued)

Luminescence from the Reaction 100 eV $He^+ + I_2 \rightarrow He + I^+ + I$ + Energy

λ_o (nm)	$\Delta\lambda_o$ (nm)	σ ($cm^2 \times 10^{18}$)	X	Transition Assignment Lower State	←	Upper State	λ_T (nm)	$\lambda_T - \lambda_o$ (nm)	ΔH (eV)
512.00	0.50	2.7	I (I)	$6s\ ^2P_{3/2}$	←	$7p\ ^4P^o_{3/2}$	512.071	0.071	-3.20
			M I (I)	$6s[2]_{3/2}$	←	$7p[1]^o_{3/2}$	512.071	0.071	-3.20
			I (II)	$6p''\ ^3D_1$	←	$7s''\ ^3P^o_0$	511.602	-0.398	5.16
				$6p''\ ^3P_1$	←	$8s'\ ^3D^o_2$	512.414	0.414	5.36
				$6p''\ ^3S_1$	←	$6d''\ 35^o_2$	512.393	0.393	5.78
				$6p''\ ^1P_1$	←	$6d''\ 45^o_1$	512.269	0.269	6.06
					←	$6d''\ 45^o_2$	512.269	0.269	6.06
					←	$6d''\ 46^o_2$	511.728	-0.272	6.06
				$6d\ ^3D^o_3$	←	$7f\ ^3F_3$	512.244	0.244	5.37
516.20	0.50	1.6	I (I)	$6s\ ^4P_{3/2}$	←	$6f\ 1^o_{5/2}$	515.847	-0.353	-2.51
			M I (I)	$6s'[1]_{3/2}$	←	$6f[3]^o_{5/2}$	515.846	-0.354	-2.51
				$6s'[1]_{1/2}$	←	$8f[2]^o_{3/2}$	515.977	-0.223	-2.34
					←	$8f[1]^o_{3/2}$	515.868	-0.332	-2.34

Table XVII (continued)

Luminescence from the Reaction 100 eV $He^+ + I_2 \rightarrow He + I^+ + I$ + Energy

λ_o (nm)	$\Delta\lambda_o$ (nm)	σ ($cm^2 \times 10^{18}$)	X	Transition Assignment Lower State	←	Upper State	λ_T (nm)	$\lambda_T - \lambda_o$ (nm)	ΔH (eV)
			I (II)	$6p\ ^5P_1$	←	$7s\ ^5S^o_2$	515.784	-0.416	2.13
				$6s\ ^5S^o_2$	←	$6p\ ^5P_3$	516.263	0.063	-0.13
				$6p''\ ^3D_2$	←	$9d\ ^5D^o_3$	516.380	0.180	5.35
				$4f\ ^3F_3$	←	$9d\ ^5D^o_3$	516.506	0.306	5.35
					←	$9d\ ^5D^o_4$	516.411	0.211	5.35
				$6d\ ^3D^o_2$	←	$7f\ ^5F_3$	515.921	-0.279	5.35
520.50	0.50	1.3	I (I)	$6s\ ^2P_{3/2}$	←	$7p\ ^4P^o_{1/2}$	520.555	0.055	-3.24
			M I (I)	$6s[2]_{3/2}$	←	$7p[1]^o_{1/2}$	520.559	0.059	-3.24
			I (II)	$6p\ ^3P_2$	←	$6d\ ^5D^o_2$	520.694	0.194	2.52
				$6p'\ ^3P_2$	←	$6d'\ ^5S^o_1$	520.684	0.184	4.15
				$6p''\ ^3S_1$	←	$6d''\ 32^o_1$	520.034	-0.466	5.74
				$6p''\ ^3D_3$	←	$6d''\ 37^o_2$	520.152	-0.348	5.85
				$7p\ ^5P_3$	←	$8s'\ ^3D^o_2$	520.998	0.498	5.36
				$6d\ ^5D^o_1$	←	$6f\ ^3F_2$	520.091	-0.409	4.96

Table XVII (continued)

Luminescence from the Reaction 100 eV $He^+ + I_2 \rightarrow He + I^+ + I + Energy$

λ_o (nm)	$\Delta\lambda_o$ (nm)	σ ($cm^2 \times 10^{18}$)	X	Transition Assignment Lower State	←	Upper State	λ_T (nm)	$\lambda_T - \lambda_o$ (nm)	ΔH (eV)
523.60	0.50	2.1	I (I)	$6s\ ^2P_{3/2}$	←	$7p\ ^2D^o_{5/2}$	523.602	0.002	-3.26
			M I (I)	$6s[2]_{3/2}$	←	$7p[3]^o_{5/2}$	523.602	0.002	-3.26
			I (II)	$6p'\ ^3D_3$	←	$7d\ ^5D^o_2$	523.514	-0.086	4.08
				$6p'\ ^3F_4$	←	$7d\ ^5D^o_3$	523.896	0.296	4.09
				$6p''\ ^3P_2$	←	$9g\ ^5G^o_3$	524.060	0.460	5.88
					←	$9g\ ^5G^o_2$	523.966	0.366	5.88
					←	$9g\ ^3G^o_3$	523.941	0.341	5.88
				$7p\ ^5P_2$	←	$10s\ ^3S^o_1$	523.616	0.016	5.30
				$7p\ ^5P_3$	←	$9d\ ^5D^o_3$	523.443	-0.157	5.35
					←	$9d\ ^5D^o_4$	523.345	-0.255	5.35
				$4f\ ^3F_4$	←	$9d\ ^5D^o_3$	523.267	-0.333	5.35
					←	$9d\ ^5D^o_4$	523.169	-0.431	5.35
				$4f\ ^3F_2$	←	$8s'\ ^3D^o_1$	523.101	-0.499	5.35
				$7p\ ^3P_0$	←	$6d''\ 21^o_1$	523.285	-0.315	5.56

Table XVII (continued)

Luminescence from the Reaction 100 eV $He^+ + I_2 \rightarrow He + I^+ + I + Energy$

λ_o (nm)	$\Delta\lambda_o$ (nm)	σ ($cm^2 \times 10^{18}$)	X	Transition Assignment Lower State	←	Upper State	λ_T (nm)	$\lambda_T - \lambda_o$ (nm)	ΔH (eV)
			I (II)	$5d'' \ ^3D_1^o$	←	$7p' \ ^1D_2$	523.190	-0.410	4.80
				$5d'' \ ^1P_1^o$	←	$5f' \ 2_2$	524.033	0.433	5.64
534.50	0.70	0.9	I (II)	$6p \ ^5P_1$	←	$5d'' \ ^3P_2^o$	534.308	-0.192	2.04
				$6s' \ ^3D_2$	←	$6p' \ ^3F_3$	533.969	-0.531	1.36
				$6p' \ ^3D_3$	←	$6d' \ 2_3^o$	535.112	0.612	4.03
				$6s' \ ^3D_3^o$	←	$6p' \ ^3F_4$	534.662	0.162	1.72
				$6p' \ ^3P_2$	←	$7d \ ^5D_3^o$	533.810	-0.690	4.09
				$5d' \ ^3F_2^o$	←	$7p \ ^3P_1$	534.070	-0.430	3.07
				$6d \ ^5D_3^o$	←	$4f' \ ^1D_2$	534.360	-0.140	4.84
				$5d'' \ ^3P_2^o$	←	$7p' \ ^3P_1$	534.062	-0.438	4.36
				$5d'' \ ^3F_3^o$	←	$7p' \ ^3F_2$	534.308	-0.192	4.77
				$5d'' \ ^3F_2^o$	←	$6f \ ^3F_2$	534.968	0.468	4.96

Table XVII (continued)

Luminescence from the Reaction 100 eV $He^+ + I_2 \rightarrow He + I^+ + I + Energy$

λ_o (nm)	$\Delta\lambda_o$ (nm)	σ ($cm^2 \times 10^{18}$)	X	Transition Assignment Lower State	←	Upper State	λ_T (nm)	$\lambda_T - \lambda_o$ (nm)	ΔH (eV)
540.80	0.50	1.0	I (I)	$6s\ ^2P_{1/2}$	←	$nd\ 30_{1/2}$	541.151	0.351	-2.45
			I (II)	$5p^5\ ^3P^o_2$	←	$6p\ ^5P_3$	540.691	-0.109	-0.13
				$6s'\ ^3D^o_2$	←	$6p'\ ^3D_2$	540.887	0.087	1.33
				$4f\ ^3F_2$	←	$10s\ ^5S^o_2$	540.569	-0.231	5.28
				$5d''\ ^3F^o_3$	←	$4f'\ ^3G_3$	540.667	-0.133	4.74
543.90	0.50	0.7	I (II)	$5p^5\ ^3P^o_1$	←	$6p\ ^3P_2$	543.734	-0.166	0.14
				$6s'\ ^1D^o_2$	←	$6p'\ ^3P_1$	543.950	0.050	1.81
				$6p''\ ^3D_3$	←	$6d''\ 33^o_3$	543.689	-0.211	5.75
				$6d\ ^5D^o_3$	←	$7p'\ ^1F_3$	543.913	0.013	4.80
				$6d\ ^5D^o_2$	←	$7p'\ ^1D_2$	544.347	0.447	4.80
546.60	0.50	2.0	I (I)	$6s\ ^4P_{1/2}$	←	$8p\ ^4P^o_{1/2}$	546.244	-0.356	-2.76
				$6s\ ^4P_{3/2}$	←	$np\ 4^o_{5/2}$	546.276	-0.324	-2.65

Table XVII (continued)

Luminescence from the Reaction 100 eV $He^+ + I_2 \rightarrow He + I^+ + I + Energy$

λ_o (nm)	$\Delta\lambda_o$ (nm)	σ ($cm^2 \times 10^{18}$)	X	Transition Assignment Lower State	←	Upper State	λ_T (nm)	$\lambda_T - \lambda_o$ (nm)	ΔH (eV)
			M I (I)	$6s'[1]_{3/2}$	←	$(^1D_2)6p[2]^o_{5/2}$	546.278	-0.322	-2.65
			I (II)	$6s\ ^5S^o_2$	←	$6p\ ^5P_2$	546.614	0.014	-0.27
				$5d\ ^3D^o_3$	←	$6p'\ ^3F_2$	546.683	0.083	1.22
				$6p'\ ^3D_3$	←	$7s'\ ^3D^o_3$	546.965	0.365	3.98
				$6p'\ ^3P_1$	←	$7d\ ^5D^o_2$	546.906	0.306	4.08
				$6p''\ ^3P_2$	←	$6d''\ 35^o_2$	546.249	-0.351	5.78
					←	$6d''\ 35^o_3$	546.249	-0.351	5.78
				$7p\ ^5P_1$	←	$7s''\ ^3P^o_1$	546.580	-0.020	5.18
				$5d''\ ^3F^o_3$	←	$4f'\ ^3F_4$	546.329	-0.271	4.72
				$6d\ ^5D^o_4$	←	$7p'\ ^3F_4$	546.987	0.387	4.79
				$5d''\ ^3F^o_2$	←	$6f\ ^5F_3$	546.371	-0.229	4.91
549.60	0.60	1.1	M I (I)	$6p[2]^o_{5/2}$	←	$12d[4]_{7/2}$	549.595	-0.005	-2.28

Table XVII (continued)

Luminescence from the Reaction 100 eV $He^+ + I_2 \rightarrow He + I^+ + I + Energy$

λ_o (nm)	$\Delta\lambda_o$ (nm)	σ ($cm^2 \times 10^{18}$)	X	Transition Assignment			λ_T (nm)	$\lambda_T - \lambda_o$ (nm)	ΔH (eV)
				Lower State	←	Upper State			
			I (II)	$6s\ ^5S_2^o$	←	$6p\ ^5P_1$	549.846	0.246	-0.28
				$6p\ ^5P_3$	←	$7s\ ^5S_2^o$	549.303	-0.297	2.13
				$6p'\ ^3F_3$	←	$7s'\ ^3D_2^o$	549.495	-0.105	3.61
				$5d'\ ^3D_2^o$	←	$6p'\ ^3D_3$	549.918	0.318	1.71
				$6p'\ ^3F_4$	←	$7s'\ ^3D_3^o$	549.553	-0.047	3.98
				$5d'\ ^3P_0^o$	←	$6p'\ ^3P_1$	549.740	0.140	1.81
				$6p''\ ^3P_2$	←	$6d''\ 34_2^o$	549.004	-0.596	5.77
				$6p''\ ^1D_2$	←	$12d\ ^3D_3^o$	549.457	-0.143	5.97
				$7p\ ^3P_2$	←	$9d\ ^5D_3^o$	549.946	0.346	5.35
				$7s'\ ^3D_1^o$	←	$5f'\ 5_2$	549.004	-0.596	5.87
				$7s'\ ^3D_2^o$	←	$5f'\ 5_2$	549.075	-0.525	5.87
					←	$5f'\ 5_3$	549.075	-0.525	5.87

Table XVII (continued)

Luminescence from the Reaction 100 eV $He^+ + I_2 \rightarrow He + I^+ + I$ + Energy

λ_o (nm)	$\Delta\lambda_o$ (nm)	σ ($cm^2 \times 10^{18}$)	X	Transition Assignment Lower State	←	Upper State	λ_T (nm)	$\lambda_T - \lambda_o$ (nm)	ΔH (eV)
562.60	0.50	0.9	I (II)	$6s\ ^3S^o_1$	←	$6p\ ^3P_2$	562.726	0.126	0.14
				$5d''\ ^3D^o_3$	←	$6p''\ ^1D_2$	562.160	-0.440	3.72
				$7p\ ^3P_2$	←	$10s\ ^3S^o_1$	562.489	-0.111	5.30
				$7p\ ^3P_1$	←	$10s\ ^5S^o_2$	562.187	-0.413	5.28
				$5d''\ ^3P^o_2$	←	$5f\ ^3F_2$	562.101	-0.499	4.25
				$5d''\ ^3F^o_2$	←	$4f'\ ^1P_1$	562.359	-0.241	4.85
574.00	0.50	0.7	I (I)	$6p\ ^4S^o_{3/2}$	←	$nd\ 36_{5/2}$	574.461	0.461	-2.36
					←	$nd\ 36.1_{1/2}$	573.504	-0.496	-2.36
			M I (I)	$6p[3]^o_{7/2}$	←	$12d[4]_{9/2}$	573.728	-0.272	-2.28
					←	$12d[4]_{7/2}$	573.673	-0.327	-2.28
				$6s'[1]_{1/2}$	←	$9p[2]^o_{3/2}$	573.744	-0.256	-2.59
				$6p[2]^o_{3/2}$	←	$6d''[2]_{5/2}$	574.465	0.465	-2.36
					←	$6d''[2]_{3/2}$	573.505	-0.495	-2.36

Table XVII (continued)

Luminescence from the Reaction 100 eV $He^+ + I_2 \rightarrow He + I^+ + I$ + Energy

λ_o (nm)	$\Delta\lambda_o$ (nm)	σ ($cm^2 \times 10^{18}$)	X	Transition Assignment Lower State	←	Upper State	λ_T (nm)	$\lambda_T - \lambda_o$ (nm)	ΔH (eV)
			I (II)	$5p^5\ ^3P^o_2$	←	$6p\ ^5P_2$	574.076	0.076	-0.26
				$5p^5\ ^3P^o_1$	←	$6p\ ^3P_1$	573.986	-0.014	0.02
				$6s''\ ^3P^o_1$	←	$6p''\ ^3D_1$	574.137	0.137	2.73
				$6p''\ ^3D_3$	←	$6d''\ 26^o_3$	574.089	0.089	5.63
				$6p''\ ^1D_2$	←	$9g\ ^5G^o_3$	574.387	0.387	5.88
					←	$9g\ ^5G^o_2$	574.274	0.274	5.88
					←	$9g\ ^3G^o_3$	574.244	0.244	5.88
				$5d''\ ^3P^o_2$	←	$5f\ ^3F_3$	574.475	0.475	4.20
				$7s\ ^5S^o_2$	←	$8p\ ^5P_2$	573.502	-0.498	4.29
				$5d''\ ^3F^o_2$	←	$7p'\ ^1D_2$	574.351	0.351	4.80
				$8s\ ^5S^o_2$	←	$5f'\text{-}11_3$	574.249	0.249	6.05
591.60	0.50	0.8	I (I)	$6p\ ^4D^o_{7/2}$	←	$nd\ 38.1_{5/2}$	591.206	-0.394	-2.34
				$6s\ ^4P_{3/2}$	←	$8p\ ^4P^o_{5/2}$	591.279	-0.321	-2.82

Table XVII (continued)

Luminescence from the Reaction 100 eV $He^+ + I_2 \rightarrow He + I^+ + I$ + Energy

λ_o (nm)	$\Delta\lambda_o$ (nm)	σ ($cm^2 \times 10^{18}$)	X	Transition Assignment Lower State	←	Upper State	λ_T (nm)	$\lambda_T - \lambda_o$ (nm)	ΔH (eV)
			M I (I)	$6p[3]^o_{7/2}$	←	$12s[2]_{5/2}$	591.206	-0.394	-2.34
				$6s'[1]_{3/2}$	←	$8p[2]^o_{5/2}$	591.280	-0.320	-2.82
				$5d[3]_{7/2}$	←	$9f[5]^o_{9/2}$	591.168	-0.432	-2.30
					←	$9f[4]^o_{9/2}$	591.360	-0.240	-2.30
					←	$9f[4]^o_{7/2}$	591.341	-0.259	-2.30
				$5d[3]_{5/2}$	←	$9f[4]^o_{7/2}$	591.532	-0.068	-2.30
				$5d[3]_{7/2}$	←	$9f[3]^o_{5/2}$	591.312	-0.288	-2.30
				$5d[3]_{5/2}$	←	$9f[3]^o_{5/2}$	591.504	-0.096	-2.30
					←	$9f[3]^o_{3/2}$	591.369	-0.231	-2.30
					←	$9f[1]^o_{3/2}$	591.219	-0.381	-2.30
			I (II)	$5d\ ^5D^o_3$	←	$6p\ ^3P_2$	592.223	0.623	0.14
				$6p\ ^3P_0$	←	$7s\ ^3S^o_1$	592.251	0.651	2.28
				$6p''\ ^1D_2$	←	$12s\ ^3S^o_1$	591.390	-0.210	5.81
				$5d''\ ^3F^o_2$	←	$4f'\ ^3G_3$	591.263	-0.337	4.74
				$5d''\ ^1F^o_3$	←	$4f'\ ^1D_2$	591.286	-0.314	4.84

Table XVII (continued)

Luminescence from the Reaction 100 eV $He^+ + I_2 \rightarrow He + I^+ + I + Energy$

λ_o (nm)	$\Delta\lambda_o$ (nm)	σ ($cm^2 \times 10^{18}$)	X	Transition Assignment Lower State	←	Upper State	λ_T (nm)	$\lambda_T - \lambda_o$ (nm)	ΔH (eV)
595.50	0.50	1.4	I (I)	$6p\ ^4P^o_{5/2}$	←	$8d\ ^4D_{7/2}$	595.852	0.352	-2.45
					←	$8d\ ^4P_{5/2}$	595.603	0.103	-2.45
					←	$nd\ 31.1_{3/2}$	595.669	0.169	-2.45
				$6s\ ^2P_{3/2}$	←	$np\ 1^o_{3/2}$	595.846	0.346	-3.54
			M I (I)	$6p[3]^o_{5/2}$	←	$6d''[2]_{3/2}$	595.871	0.371	-2.36
				$6p[2]^o_{5/2}$	←	$9d[3]_{7/2}$	595.851	0.351	-2.45
					←	$9d[3]_{5/2}$	595.603	0.103	-2.45
					←	$9d[2]_{3/2}$	595.667	0.167	-2.45
				$6p[1]^o_{1/2}$	←	$nd\ C_{1/2}$	595.798	0.298	-2.33
					←	$nd\ C_{3/2}$	595.798	0.298	-2.33
			I (II)	$6s\ ^3S^o_1$	←	$6p\ ^3P_1$	595.191	-0.309	0.02
				$6p'\ ^1P_1$	←	$7s'\ ^3D^o_1$	595.152	-0.348	3.61
					←	$7s'\ ^3D^o_2$	595.068	-0.432	3.61
				$6p''\ ^3D_2$	←	$6g\ ^5G^o_3$	595.213	-0.287	5.03

Table XVII (continued)

Luminescence from the Reaction 100 eV $He^+ + I_2 \rightarrow He + I^+ + I + Energy$

λ_o (nm)	$\Delta\lambda_o$ (nm)	σ ($cm^2 \times 10^{18}$)	X	Transition Assignment Lower State	←	Upper State	λ_T (nm)	$\lambda_T - \lambda_o$ (nm)	ΔH (eV)
			I (II)	$6p''\ ^3P_2$	←	$11s\ ^5S^o_2$	595.072	-0.428	5.59
				$4f\ ^3F_3$	←	$6g\ ^5G^o_4$	595.533	0.033	5.03
					←	$6g\ ^5G^o_3$	595.380	-0.120	5.03
					←	$6g\ ^3G^o_4$	595.376	-0.124	5.03
				$5f\ ^5F_3$	←	$6d''\ 50^o_3$	595.975	0.475	6.25
					←	$6d''\ 50^o_4$	595.975	0.475	6.25
				$5d''\ ^1F^o_3$	←	$7p'\ ^3F_3$	595.099	-0.401	4.82
				$6d\ ^3D^o_2$	←	$7p'\ ^3D_2$	595.511	0.011	5.03
604.40	0.50	1.2	M I (I)	$5d[3]_{7/2}$	←	$8f[5]^o_{9/2}$	604.161	-0.239	-2.34
					←	$8f[4]^o_{9/2}$	604.438	0.038	-2.34
					←	$8f[4]^o_{7/2}$	604.410	0.010	-2.34
				$5d[3]_{5/2}$	←	$8f[4]^o_{7/2}$	604.610	0.210	-2.34
				$5d[3]_{7/2}$	←	$8f[3]^o_{5/2}$	604.364	-0.036	-2.34

Table XVII (continued)

Luminescence from the Reaction 100 eV $He^+ + I_2 \rightarrow He + I^+ + I$ + Energy

λ_o (nm)	$\Delta\lambda_o$ (nm)	σ ($cm^2 \times 10^{18}$)	Transition Assignment X	Lower State	←	Upper State	λ_T (nm)	$\lambda_T - \lambda_o$ (nm)	ΔH (eV)
			M I (I)	$5d[3]_{5/2}$	←	$8f[3]^o_{5/2}$	604.563	0.163	-2.34
				$5d[3]_{7/2}$	←	$8f[2]^o_{5/2}$	604.091	-0.309	-2.34
				$5d[3]_{5/2}$	←	$8f[2]^o_{5/2}$	604.291	-0.109	-2.34
					←	$8f[2]^o_{3/2}$	604.340	-0.060	-2.34
					←	$8f[1]^o_{3/2}$	604.190	-0.210	-2.34
			I (II)	5d' $^1P^o_1$	←	6p'' $^1D_2$	604.330	-0.070	3.72
				6p'' $^1D_2$	←	6d'' 34^o_2	604.490	0.090	5.77
				5d' $^1D^o_2$	←	7p $^5P_2$	604.346	-0.054	2.93
				7p $^5P_2$	←	8d $^3D^o_3$	604.233	-0.167	4.98
				7p $^5P_3$	←	6g $^5G^o_4$	604.774	0.374	5.03
					←	6g $^5G^o_3$	604.616	0.216	5.03
					←	6g $^5G^o_2$	604.221	-0.179	5.03
					←	6g $^3G^o_4$	604.612	0.212	5.03
					←	6g $^3G^o_3$	604.170	-0.230	5.03

Table XVII (continued)

Luminescence from the Reaction 100 eV $He^+ + I_2 \rightarrow He + I^+ + I$ + Energy

λ_o (nm)	$\Delta\lambda_o$ (nm)	σ ($cm^2 \times 10^{18}$)	Transition Assignment X	Lower State	←	Upper State	λ_T (nm)	$\lambda_T - \lambda_o$ (nm)	ΔH (eV)
			I (II)	$4f\ ^3F_4$	←	$6g\ ^5G^o_5$	604.546	0.146	5.03
					←	$6g\ ^5G^o_4$	604.539	0.139	5.03
					←	$6g\ ^5G^o_3$	604.382	-0.018	5.03
					←	$6g\ ^3G^o_5$	604.100	-0.300	5.03
					←	$6g\ ^3G^o_4$	604.377	-0.023	5.03
					←	$6g\ ^3G^o_3$	603.935	-0.465	5.03
608.50	0.60	1.5	I (I)	$6p\ ^2D^o_{5/2}$	←	$11s\ ^4P_{5/2}$	608.657	0.157	-2.40
				$6s\ ^2P_{3/2}$	←	$6p\ ^4D^o_{5/2}$	608.410	-0.090	-3.59
			M I (I)	$6p[3]^o_{5/2}$	←	$11s[2]_{5/2}$	608.656	0.156	-2.40
					←	$11s[2]_{3/2}$	607.928	-0.572	-2.40
				$6s[2]_{3/2}$	←	$6p'[2]^o_{5/2}$	608.410	-0.090	-3.59
			I (II)	$5d\ ^5D^o_2$	←	$6p\ ^3P_2$	607.952	-0.548	0.14
				$6p\ ^3P_1$	←	$5d'\ ^3P^o_I$	608.647	0.147	2.06

Table XVII (continued)

Luminescence from the Reaction 100 eV $He^+ + I_2 \rightarrow He + I^+ + I$ + Energy

λ_o (nm)	$\Delta\lambda_o$ (nm)	σ ($cm^2 \times 10^{18}$)	X	Transition Assignment Lower State	←	Upper State	λ_T (nm)	$\lambda_T - \lambda_o$ (nm)	ΔH (eV)
			I (II)	$6p''\ ^3D_1$	←	$9s\ ^5S^o_2$	608.376	-0.124	4.77
				$6p''\ ^1P_1$	←	$6d''\ 30^o_2$	609.106	0.606	5.68
				$6p''\ ^1D_2$	←	$6d''\ 33.5^o_1$	609.040	0.540	5.75
				$7p\ ^5P_2$	←	$8d\ ^3D^o_1$	608.415	-0.085	4.97
				$5d''\ ^3F^o_3$	←	$4f'\ ^3P_2$	608.074	-0.426	4.48
				$7s'\ ^3D^o_2$	←	$8f\ ^3F_3$	608.395	-0.105	5.65
619.10	0.70	1.0	I (I)	$6p\ ^4P^o_{5/2}$	←	$nd\ 28.2_{3/2}$	618.575	-0.525	2.53
			M I (I)	$6p[3]^o_{5/2}$	←	$9d[4]_{7/2}$	619.359	0.259	-2.44
				$6p[2]^o_{5/2}$	←	$(^1D_2)5d[1]_{3/2}$	618.572	-0.528	-2.53
			I (II)	$4f\ ^5F_5$	←	$8d\ ^5D^o_4$	619.292	0.192	4.89
				$4f\ ^5F_3$	←	$8d\ ^5D^o_2$	618.861	-0.239	4.89
					←	$8d\ ^5D^o_3$	618.532	-0.568	4.89
				$7p\ ^5P_3$	←	$8d\ ^3D^o_3$	619.168	0.068	4.98

Table XVII (continued)

Luminescence from the Reaction 100 eV $He^+ + I_2 \rightarrow He + I^+ + I + Energy$

λ_o (nm)	$\Delta\lambda_o$ (nm)	σ ($cm^2 \times 10^{18}$)	X	Transition Assignment Lower State	←	Upper State	λ_T (nm)	$\lambda_T - \lambda_o$ (nm)	ΔH (eV)
			I (II)	$4f\ ^3F_4$	←	$8d\ ^3D_3^o$	618.921	-0.179	4.98
				$7s\ ^3S_1^o$	←	$8p\ ^5P_2$	618.984	-0.116	4.29
				$8p\ ^5P_2$	←	$6d''\ 51_1^o$	619.014	-0.086	6.29
					←	$6d''\ 51_2^o$	619.014	-0.086	6.29
					←	$6d''\ 51_3^o$	619.014	-0.086	6.29
				$5d''\ ^1F_3^o$	←	$4f'\ ^1G_4$	619.613	0.513	4.74
				$5d''\ ^3F_3^o$	←	$7p'\ ^3D_3$	618.631	-0.469	4.45
				$6d\ ^3D_2^o$	←	$6f\ ^3F_3$	619.164	0.064	4.95
				$8s\ ^5S_2^o$	←	$5f'\ 6_2$	619.768	0.668	5.89
					←	$5f'\ 6_3$	619.768	0.668	5.89
				$7d\ ^5D_4^o$	←	$5f'\ 13_3$	619.360	0.260	6.10

Table XVII (continued)

Luminescence from the Reaction 100 eV $He^+ + I_2 \rightarrow He + I^+ + I$ + Energy

λ_o (nm)	$\Delta\lambda_o$ (nm)	σ ($cm^2 \times 10^{18}$)	X	Transition Assignment Lower State	←	Upper State	λ_T (nm)	$\lambda_T - \lambda_o$ (nm)	ΔH (eV)
621.40	0.60	1.2	I (I)	$6p\ ^4S^o_{3/2}$	←	$nd\ 28.2_{3/2}$	621.793	0.393	-2.53
				$6p\ ^2D^o_{5/2}$	←	$nd\ 32_{3/2}$	621.390	-0.010	-2.45
				$6p\ ^4D^o_{7/2}$	←	$8d\ ^4F_{9/2}$	621.482	0.082	-2.44
			M I (I)	$6p[3]^o_{7/2}$	←	$9d[4]_{9/2}$	621.482	0.082	-2.44
				$6p[3]^o_{5/2}$	←	$9d[1]_{3/2}$	621.386	-0.014	-2.44
				$6p[2]^o_{3/2}$	←	$(^1D_2)5d[1]_{3/2}$	621.791	0.391	-2.53
			I (II)	$6p''\ ^3S_1$	←	$8s'\ ^3D^o_1$	621.960	0.560	5.35
				$4f\ ^5F_2$	←	$8d\ ^5D^o_1$	620.955	-0.445	4.89
					←	$8d\ ^5D^o_2$	621.602	0.202	4.89
					←	$8d\ ^5D^o_3$	621.270	-0.130	4.89
				$4f'\ ^3F_3$	←	$6d''\ 51^o_2$	621.033	-0.367	6.29
					←	$6d''\ 51^o_3$	621.033	-0.367	6.29
				$5d''\ ^3P^o_1$	←	$5f'\ 5_2$	621.307	-0.093	5.87
				$7d\ ^5D^o_1$	←	$5f'\ 13_2$	621.073	-0.327	6.10

Table XVII (continued)

Luminescence from the Reaction 100 eV $He^+ + I_2 \rightarrow He + I^+ + I + Energy$

λ_o (nm)	$\Delta\lambda_o$ (nm)	σ ($cm^2 \times 10^{18}$)	X	Transition Assignment Lower State	←	Upper State	λ_T (nm)	$\lambda_T - \lambda_o$ (nm)	ΔH (eV)
624.60	0.50	2.7	I (I)	$6p\ ^2D^o_{5/2}$	←	$nd\ 31_{3/2}$	625.088	0.488	-2.46
				$6p\ ^4D^o_{7/2}$	←	$8d\ ^4D_{7/2}$	624.258	-0.342	-2.45
				$(^1D)6s\ ^2D_{5/2}$	←	$7p\ ^4D^o_{5/2}$	624.486	-0.114	-2.41
				$6s\ ^2P_{1/2}$	←	$8p\ ^4P^o_{1/2}$	624.362	-0.238	-2.76
				$(^1D)6s\ ^2D_{5/2}$	←	$10p\ ^4D^o_{7/2}$	624.440	-0.160	-2.41
					←	$7f\ 1^o_{5/2}$	624.783	0.183	-2.41
					←	$7f\ 2^o_{7/2}$	624.621	0.021	-2.41
			M I (I)	$6p[3]^o_{7/2}$	←	$9d[3]_{7/2}$	624.257	-0.343	-2.45
				$6p[3]^o_{5/2}$	←	$9d[2]_{5/2}$	625.087	0.487	-2.46
					←	$nd\ B_{3/2}$	624.166	-0.434	-2.45
				$5d[3]_{7/2}$	←	$7f[5]^o_{9/2}$	624.179	-0.421	-2.41
					←	$7f[4]^o_{9/2}$	624.621	0.021	-2.41
					←	$7f[4]^o_{7/2}$	624.573	-0.027	-2.41
				$5d[3]_{5/2}$	←	$7f[4]^o_{7/2}$	624.786	0.186	-2.41

Table XVII (continued)

Luminescence from the Reaction 100 eV $He^+ + I_2 \rightarrow He + I^+ + I + Energy$

λ_o (nm)	$\Delta\lambda_o$ (nm)	σ ($cm^2 \times 10^{18}$)	X	Transition Assignment Lower State	←	Upper State	λ_T (nm)	$\lambda_T - \lambda_o$ (nm)	ΔH (eV)
			M I (I)	$5d[3]_{7/2}$	←	$7f[3]^o_{7/2}$	624.442	-0.158	-2.41
				$5d[3]_{5/2}$	←	$7f[3]^o_{7/2}$	624.655	0.055	-2.41
				$5d[3]_{7/2}$	←	$7f[3]^o_{5/2}$	624.496	-0.104	-2.41
				$5d[3]_{5/2}$	←	$7f[3]^o_{5/2}$	624.709	0.109	-2.41
					←	$7f[2]^o_{3/2}$	624.490	-0.110	-2.41
			I (II)	$5d'\ ^3F^o_2$	←	$6p''\ ^3D_1$	624.650	0.050	2.73
				$4f\ ^5F_1$	←	$8d\ ^5D^o_0$	624.155	-0.445	4.88
				$5d''\ ^3D^o_2$	←	$5f\ ^3F_3$	624.161	-0.439	4.20
				$5f\ ^3F_2$	←	$6d''\ 49^o_1$	624.291	-0.309	6.23
					←	$6d''\ 49^o_2$	624.291	-0.309	6.23
				$8p\ ^5P_3$	←	$6d''\ 51^o_2$	624.931	0.331	6.29
					←	$6d''\ 51^o_3$	624.931	0.331	6.29

Table XVII (continued)

Luminescence from the Reaction 100 eV $He^+ + I_2 \rightarrow He + I^+ + I + Energy$

λ_o (nm)	$\Delta\lambda_o$ (nm)	σ ($cm^2 \times 10^{18}$)	X	Transition Assignment Lower State	←	Upper State	λ_T (nm)	$\lambda_T - \lambda_o$ (nm)	ΔH (eV)
634.10	0.50	3.7	He I	$2p\ ^3P^o_1$	←	$3s\ ^1S_0$	633.794	-0.306	10.34
			I (I)	$6p\ ^4P^o_{5/2}$	←	$7d\ ^4D_{7/2}$	634.122	0.022	-2.58
					←	$7d\ ^4D_{5/2}$	633.963	-0.137	-2.58
			M I (I)	$6p[2]^o_{5/2}$	←	$8d[3]_{7/2}$	634.121	0.021	-2.58
					←	$8d[3]_{5/2}$	633.962	-0.138	-2.58
			I (II)	$6s'\ ^3D^o_3$	←	$6p'\ ^3F_3$	634.176	0.076	1.36
				$5d'\ ^3F^o_3$	←	$6p'\ ^3P_2$	634.302	0.202	1.77
				$5d''\ ^3D^o_3$	←	$6p''\ ^3D_3$	633.910	-0.190	3.47
				$6p''\ ^1P_1$	←	$11s\ ^3S^o_1$	634.343	0.243	5.59
				$6s''\ ^3P^o_2$	←	$7p\ ^3P_1$	633.835	-0.265	3.07
				$7d\ ^5D^o_3$	←	$5f'\ 10_2$	633.795	-0.305	6.04
					←	$5f'\ 10_3$	633.795	-0.305	6.04
				$7d\ ^4D^o_0$	←	$5f'\ 12_1$	633.791	-0.309	6.05

Table XVII (continued)

Luminescence from the Reaction 100 eV $He^+ + I_2 \rightarrow He + I^+ + I + Energy$

λ_o (nm)	$\Delta\lambda_o$ (nm)	σ ($cm^2 \times 10^{18}$)	X	Transition Assignment Lower State	←	Upper State	λ_T (nm)	$\lambda_T - \lambda_o$ (nm)	ΔH (eV)
637.30	0.60	1.3	I (I)	$6p\ ^4S^o_{3/2}$	←	$7d\ ^4P_{5/2}$	637.344	0.044	-2.58
					←	$nd\ 26_{3/2}$	636.903	-0.397	-2.58
					←	$nd\ 26.1_{1/2}$	636.781	-0.519	-2.58
				$(^1D)6s\ ^2D_{3/2}$	←	$7p\ ^4D^o_{5/2}$	637.812	0.512	-2.41
				$(^1D)6s\ ^2D_{5/2}$	←	$7p\ ^4D^o_{3/2}$	636.848	-0.452	-2.45
					←	$10p\ ^4P^o_{5/2}$	637.881	0.581	-2.45
			M I (I)	$6p[2]^o_{3/2}$	←	$8d[3]_{5/2}$	637.344	0.044	-2.58
					←	$8d[1]_{3/2}$	636.905	-0.395	-2.58
					←	$8d[1]_{1/2}$	636.782	-0.518	-2.58
				$5d[3]_{5/2}$	←	$7p''[1]^o_{3/2}$	636.845	-0.455	-2.45
				$5d[3]_{7/2}$	←	$10p[3]^o_{7/2}$	637.662	0.362	-2.45
					←	$10p[3]^o_{5/2}$	637.776	0.476	-2.45
				$5d[3]_{5/2}$	←	$10p[3]^o_{7/2}$	637.884	0.584	-2.45

Table XVII (continued)

Luminescence from the Reaction 100 eV $He^+ + I_2 \rightarrow He + I^+ + I + Energy$

λ_o (nm)	$\Delta\lambda_o$ (nm)	σ ($cm^2 \times 10^{18}$)	Transition Assignment X	Lower State	←	Upper State	λ_T (nm)	$\lambda_T - \lambda_o$ (nm)	ΔH (eV)
			M I (I)	$5d[1]_{3/2}$	←	$7f[1]^o_{3/2}$	637.337	0.037	-2.41
					←	$7f[2]^o_{3/2}$	637.819	0.519	-2.41
			I (II)	$6p\ ^5P_1$	←	$5d'\ ^1P^o_1$	637.844	0.544	1.67
				$6p''\ ^3P_1$	←	$8d\ ^5D^o_0$	636.885	-0.415	4.88
				$6p''\ ^1D_2$	←	$10d\ ^3D^o_2$	637.055	-0.245	5.66
				$8p\ ^5P_2$	←	$6d''\ 49^o_1$	636.954	-0.346	6.23
					←	$6d''\ 49^o_2$	636.954	-0.346	6.23
				$6d\ ^5D^o_0$	←	$4f'\ ^3P_1$	637.295	-0.005	4.45
				$7d\ ^3D^o_2$	←	$5f'\ 13_2$	637.432	0.132	6.10
					←	$5f'\ 13_3$	637.432	0.132	6.10
				$8s\ ^5S^o_2$	←	$9f\ ^5F_3$	637.664	0.364	5.83

Table XVII (continued)

Luminescence from the Reaction 100 eV $He^+ + I_2 \rightarrow He + I^+ + I + Energy$

λ_o (nm)	$\Delta\lambda_o$ (nm)	σ ($cm^2 \times 10^{18}$)	Transition Assignment X	Lower State	←	Upper State	λ_T (nm)	$\lambda_T - \lambda_o$ (nm)	ΔH (eV)
656.70	0.50	2.7	I (I)	$6p\ ^2D^o_{5/2}$	←	$nd\ 28_{7/2}$	656.833	0.133	-2.55
					←	$nd\ 28.1_{5/2}$	656.255	-0.445	-2.55
				$6s\ ^2P_{1/2}$	←	$(^1D)6p\ ^2P^o_{3/2}$	656.659	-0.041	-2.86
			M I (I)	$6p[3]^o_{5/2}$	←	$8d[4]_{7/2}$	656.829	0.129	-2.55
					←	$8d[2]_{5/2}$	656.263	-0.437	-2.55
				$6s'[1]_{1/2}$	←	$(^1D_2)6p[1]^o_{3/2}$	656.663	-0.037	-2.86
			I (II)	$7p\ ^3P_2$	←	$8d\ ^3D^o_3$	656.596	-0.104	4.98
				$7p\ ^3P_1$	←	$8d\ ^3D^o_2$	656.717	0.017	4.96
				$6s''\ ^1P^o_1$	←	$7p\ ^3P_o$	657.016	0.316	3.19
				$5f\ ^5F_3$	←	$6d''\ 46^o_2$	656.681	-0.019	6.06
				$4f'\ ^3F_2$	←	$6d''\ 49^o_1$	657.156	0.456	6.23
					←	$6d''\ 49^o_2$	657.156	0.456	6.23
				$6d\ ^5D^o_3$	←	$4f'\ ^3D_2$	656.340	-0.360	4.41
				$6d\ ^3D^o_1$	←	$4f'\ ^1P_1$	656.965	0.265	4.85

Table XVII (continued)

Luminescence from the Reaction 100 eV $He^+ + I_2 \rightarrow He + I^+ + I + Energy$

λ_o (nm)	$\Delta\lambda_o$ (nm)	σ ($cm^2 \times 10^{18}$)	X	Transition Assignment Lower State	←	Upper State	λ_T (nm)	$\lambda_T - \lambda_o$ (nm)	ΔH (eV)
			I (II)	$8p\ ^3P_2$	←	$6d''\ 50^o_3$	657.152	0.452	6.25
658.50	0.50	6.4	I (I)	$6p\ ^2D^o_{5/2}$	←	$nd\ 27.1_{5/2}$	658.711	0.211	-2.56
				$(^1D)6s\ ^2D_{5/2}$	←	$6f\ 1^o_{5/2}$	658.555	0.055	-2.51
					←	$6f\ 2^o_{7/2}$	658.472	-0.028	-2.51
					←	$6f\ 3^o_{3/2}$	658.063	-0.437	-2.51
			M I (I)	$6p[3]^o_{5/2}$	←	$nd\ A_{3/2}$	658.714	0.214	-2.56
				$5d[3]_{7/2}$	←	$6f[4]^o_{9/2}$	658.556	0.056	-2.51
					←	$6f[4]^o_{7/2}$	658.473	-0.027	-2.51
					←	$6f[3]^o_{7/2}$	658.236	-0.264	-2.51
					←	$6f[3]^o_{5/2}$	658.311	-0.189	-2.51
				$5d[3]_{5/2}$	←	$6f[4]^o_{7/2}$	658.710	0.210	-2.51
					←	$6f[3]^o_{7/2}$	658.473	-0.027	-2.51
					←	$6f[3]^o_{5/2}$	658.549	0.049	-2.51
					←	$6f[2]^o_{3/2}$	658.060	-0.440	-2.51

Table XVII (continued)

Luminescence from the Reaction 100 eV $He^+ + I_2 \rightarrow He + I^+ + I + Energy$

λ_o (nm)	$\Delta\lambda_o$ (nm)	σ ($cm^2 \times 10^{18}$)	X	Transition Assignment			λ_T (nm)	$\lambda_T - \lambda_o$ (nm)	ΔH (eV)
				Lower State	←	Upper State			
			I (II)	6s' $^3D_1^o$	←	6p' $^3D_1$	658.702	0.202	1.06
				5d" $^1D_2^o$	←	6p" $^3S_1$	658.105	-0.395	3.36
				6p" $^3P_2$	←	9d $^3D_3^o$	658.235	-0.265	5.39
				4f $^5F_2$	←	9s $^5S_2^o$	658.989	0.489	4.77
				7p $^5P_1$	←	9s $^3S_1^o$	658.990	0.490	4.79
				5d' $^1S_0^o$	←	7p $^3P_1$	658.031	-0.469	3.07
				5f $^5F_4$	←	6d" 44_3^o	658.625	0.125	6.06
				5f $^5F_3$	←	6d" 44_2^o	658.519	0.019	6.06
					←	6d" 44_3^o	658.519	0.019	6.06
				6d $^5D_2^o$	←	4f' $^3D_2$	658.081	-0.419	4.41
				4f' $^3D_2$	←	6d" 51_1^o	658.559	0.059	6.29
					←	6d" 51_2^o	658.559	0.059	6.29
					←	6d" 51_3^o	658.559	0.059	6.29

Table XVII (continued)

Luminescence from the Reaction 100 eV $He^+ + I_2 \rightarrow He + I^+ + I + Energy$

λ_o (nm)	$\Delta\lambda_o$ (nm)	σ ($cm^2 \times 10^{18}$)	X	Transition Assignment Lower State	←	Upper State	λ_T (nm)	$\lambda_T - \lambda_o$ (nm)	ΔH (eV)
662.10	0.50	2.7	I (I)	$6p\ ^4P^o_{3/2}$	←	$nd\ 34_{1/2}$	662.358	0.258	-2.39
				$6p\ ^4D^o_{7/2}$	←	$7d\ ^4F_{9/2}$	662.149	0.049	-2.57
			M I (I)	$6p[3]^o_{7/2}$	←	$8d[4]_{9/2}$	662.149	0.049	-2.57
				$6p[1]^o_{3/2}$	←	$6d'[1]_{3/2}$	662.353	0.253	-2.39
			I (II)	$5p^5\ ^3P^o_1$	←	$6p\ ^5P_2$	662.035	-0.065	-0.27
				$5d'\ ^3D^o_2$	←	$6p'\ ^3D_2$	662.419	0.319	1.33
				$5f\ ^5F_2$	←	$6d''\ 44^o_2$	662.141	0.041	6.06
					←	$6d''\ 44^o_3$	662.141	0.041	6.06
				$5f\ ^5F_1$	←	$6d''\ 45^o_1$	662.065	-0.035	6.06
					←	$6d''\ 45^o_2$	662.065	-0.035	6.06
				$4f'\ ^3G_4$	←	$14d\ ^3D^o_3$	662.171	0.071	6.16
				$4f'\ ^3F_3$	←	$14d\ ^3D^o_3$	662.462	0.362	6.16
				$6d\ ^3D^o_3$	←	$4f'\ ^1F_3$	662.298	0.198	4.83
					←	$7p'\ ^3F_3$	662.442	0.342	4.82

Table XVII (continued)

Luminescence from the Reaction 100 eV $He^+ + I_2 \rightarrow He + I^+ + I + Energy$

λ_o (nm)	$\Delta\lambda_o$ (nm)	σ ($cm^2 \times 10^{18}$)	Transition Assignment X	Lower State	←	Upper State	λ_T (nm)	$\lambda_T - \lambda_o$ (nm)	ΔH (eV)
			I (II)	$8s\ ^5S^o_2$	←	$5f'\ 3_2$	662.024	-0.076	5.76
					←	$5f'\ 3_3$	662.024	-0.076	5.76
				$7s'\ ^3D^o_3$	←	$5f'\ 4_3$	662.450	0.350	5.85
					←	$5f'\ 4_4$	662.450	0.350	5.85
666.30	0.50	2.0	I (I)	$6p\ ^4P^o_{5/2}$	←	$9s\ ^4P_{5/2}$	666.296	-0.004	-2.67
				$6p\ ^4P^o_{3/2}$	←	$11s\ ^4P_{5/2}$	666.135	-0.165	-2.40
				$6p\ ^4S^o_{3/2}$	←	$nd\ 25.1_{1/2}$	666.136	-0.164	-2.66
				$6p\ ^4D^o_{7/2}$	←	$7p\ ^4D_{7/2}$	666.393	0.093	-2.58
					←	$7d\ ^4P_{5/2}$	666.217	-0.083	-2.58
			M I (I)	$6p[3]^o_{7/2}$	←	$8d[3]_{7/2}$	666.392	0.092	-2.58
					←	$8d[3]_{5/2}$	666.217	-0.083	-2.58
				$6p[2]^o_{5/2}$	←	$9s[2]_{5/2}$	666.295	-0.005	-2.67
				$6p[1]^o_{3/2}$	←	$11s[2]_{5/2}$	666.132	-0.168	-2.40

Table XVII (continued)

Luminescence from the Reaction 100 eV $He^+ + I_2 \rightarrow He + I^+ + I + Energy$

λ_o (nm)	$\Delta\lambda_o$ (nm)	σ ($cm^2 \times 10^{18}$)	X	Transition Assignment Lower State	←	Upper State	λ_T (nm)	$\lambda_T - \lambda_o$ (nm)	ΔH (eV)
			I (II)	$5p^5\ ^3P^o_1$	←	$6p\ ^5P_1$	666.781	0.481	-0.28
				$6p''\ ^1P_1$	←	$6d''\ 20^o_1$	666.100	-0.200	5.50
					←	$6d''\ 20^o_2$	666.100	-0.200	5.50
				$7p\ ^5P_1$	←	$9s\ ^5S^o_2$	666.355	0.055	4.77
				$5f\ ^5F_2$	←	$5f'\ 10_2$	666.751	0.451	6.04
					←	$5f'\ 10_3$	666.751	0.451	6.04
					←	$6d''\ 43^o_1$	666.780	0.480	6.04
					←	$6d''\ 43^o_2$	666.780	0.480	6.04
				$5f\ ^3F_3$	←	$6d''\ 45^o_2$	666.516	0.216	6.06
				$5d''\ ^3F^o_3$	←	$8p\ ^5P_3$	666.592	0.292	4.31
				$6d\ ^3D^o_2$	←	$7p'\ ^1P_1$	666.335	0.035	4.81
				$7d\ ^5D^o_2$	←	$5f'\ 8_1$	666.776	0.476	5.94
					←	$5f'\ 8_2$	666.776	0.476	5.94

Table XVII (continued)

Luminescence from the Reaction 100 eV $He^+ + I_2 \rightarrow He + I^+ + I + Energy$

λ_o (nm)	$\Delta\lambda_o$ (nm)	σ ($cm^2 \times 10^{18}$)	X	Transition Assignment Lower State ← Upper State	λ_T (nm)	$\lambda_T - \lambda_o$ (nm)	ΔH (eV)
670.00	0.50	1.6	I (I)	$6p\ {}^4P^o_{5/2} \leftarrow 5f\ 1^o_{3/2}$	669.851	-0.149	-2.68
				$6p\ {}^4P^o_{1/2} \leftarrow nd\ 27_{3/2}$	669.993	-0.007	-2.56
				$6p\ {}^4S^o_{3/2} \leftarrow 9s\ {}^4P_{5/2}$	670.032	0.032	-2.67
				$({}^1D)6s\ {}^2D_{5/2} \leftarrow 9p\ {}^4D^o_{7/2}$	670.026	0.026	-2.54
				$nd\ 1_{3/2} \leftarrow np\ 6^o_{5/2}$	670.439	0.439	-2.39
				$6s\ {}^4P_{3/2} \leftarrow nd\ 20_{1/2}$	669.919	-0.081	-3.06
			M I (I)	$6p[2]^o_{3/2} \leftarrow 9s[2]_{5/2}$	670.031	0.031	-2.67
				$6p[1]^o_{1/2} \leftarrow 8d[2]_{3/2}$	669.994	-0.006	-2.56
			I (II)	$4f\ {}^5F_3 \leftarrow 6d'\ 14^o_3$	670.145	0.145	4.73
				$5f\ {}^3F_4 \leftarrow 13d\ {}^3D^o_3$	670.065	0.065	6.09
				$6d\ {}^5D^o_4 \leftarrow 4f'\ {}^3H_5$	669.960	-0.040	4.38
				$6d\ {}^3D^o_2 \leftarrow 7p'\ {}^1F_3$	670.415	0.415	4.80
				$6d\ {}^3D^o_1 \leftarrow 7p'\ {}^1P_1$	670.423	0.423	4.81
				$6d\ {}^5D^o_3 \leftarrow 8p\ {}^3P_2$	670.141	0.141	4.37

Table XVII (continued)

Luminescence from the Reaction 100 eV $He^+ + I_2 \rightarrow He + I^+ + I + Energy$

λ_o (nm)	$\Delta\lambda_o$ (nm)	σ ($cm^2 \times 10^{18}$)	Transition Assignment X	Lower State	←	Upper State	λ_T (nm)	$\lambda_T - \lambda_o$ (nm)	ΔH (eV)
			I (II)	$7s'\ ^1D^o_2$	←	$5f'\ 6_2$	669.557	-0.443	5.89
					←	$5f'\ 6_3$	669.557	-0.443	5.89
				$7d\ ^5D^o_3$	←	$5f'\ 8_2$	670.001	0.001	5.94
673.80	0.60	1.7	He I	$3s\ ^3S_1$	←	$22d\ ^3P^o_2$	673.582	-0.218	11.98
					←	$22d\ ^3P^o_1$	673.582	-0.218	11.98
					←	$22d\ ^3P^o_0$	673.582	-0.218	11.98
			I (I)	$6p\ ^4P^o_{1/2}$	←	$nd\ 26_{3/2}$	674.126	0.326	-2.58
					←	$nd\ 26.1_{1/2}$	673.989	0.189	-2.58
				$(^1D)6s\ ^2D_{3/2}$	←	$6f\ 1^o_{5/2}$	673.393	-0.407	-2.51
			M I (I)	$6p[1]^o_{1/2}$	←	$8d[1]_{3/2}$	674.128	0.328	-2.58
					←	$8d[1]_{1/2}$	673.990	0.190	-2.58
				$5d[1]_{3/2}$	←	$6f[3]^o_{5/2}$	673.388	-0.412	-2.51

Table XVII (continued)

Luminescence from the Reaction 100 eV $He^+ + I_2 \rightarrow He + I^+ + I + Energy$

λ_o (nm)	$\Delta\lambda_o$ (nm)	σ ($cm^2 \times 10^{18}$)	Transition Assignment X	Lower State	←	Upper State	λ_T (nm)	$\lambda_T - \lambda_o$ (nm)	ΔH (eV)
			M I (I)	$5d[4]_{9/2}$	←	$8f[5]^o_{11/2}$	673.839	0.039	-2.34
					←	$8f[5]^o_{9/2}$	673.830	0.030	-2.34
					←	$8f[4]^o_{9/2}$	674.176	0.376	-2.34
					←	$8f[4]^o_{7/2}$	674.140	0.340	-2.34
			I (II)	$6p''\ ^3D_1$	←	$6d'\ 11^o_0$	673.703	-0.097	4.57
				$6p''\ ^1D_2$	←	$6d''\ 21^o_1$	673.524	-0.276	5.56
				$4f\ ^5F_3$	←	$6d'\ 13^o_2$	673.863	0.063	4.72
				$4f\ ^5F_2$	←	$6d'\ 14^o_3$	673.360	-0.440	4.73
				$5d''\ ^3F^o_3$	←	$8p\ ^5P_2$	673.459	-0.341	4.29
				$6d\ ^5D^o_2$	←	$7p'\ ^3P_1$	673.800	0.000	4.36
				$7p'\ ^3D_3$	←	$6d''\ 51^o_2$	673.913	0.113	6.29
					←	$6d''\ 51^o_3$	673.913	0.113	6.29
				$6d\ ^3D^o_1$	←	$7p'\ ^1D_2$	673.389	-0.411	4.80
				$7d\ ^5D^o_2$	←	$5f'\ 7_2$	674.066	0.266	5.92
					←	$5f'\ 7_3$	674.066	0.266	5.92

Table XVII (continued)

Luminescence from the Reaction 100 eV $He^+ + I_2 \rightarrow He + I^+ + I + Energy$

λ_o (nm)	$\Delta\lambda_o$ (nm)	σ ($cm^2 \times 10^{18}$)	X	Transition Assignment Lower State	←	Upper State	λ_T (nm)	$\lambda_T - \lambda_o$ (nm)	ΔH (eV)
699.10	0.50	1.4	He I	$3s\ ^3S_1$	←	$12p\ ^3P^o_2$	699.139	0.039	11.91
					←	$12p\ ^3P^o_1$	699.139	0.039	11.91
					←	$12p\ ^3P^o_0$	699.139	0.039	11.91
					←	$12f\ ^3F^o_2$	698.721	-0.379	11.91
					←	$12p\ ^1P^o_1$	698.643	-0.457	11.91
			I (I)	$6p\ ^4P^o_{3/2}$	←	$nd\ 29_{3/2}$	698.703	-0.397	-2.49
				$6p\ ^4S^o_{3/2}$	←	$7s\ ^2P_{1/2}$	699.533	0.433	-2.75
				$6p\ ^2D^o_{5/2}$	←	$9s\ ^2P_{3/2}$	699.168	0.068	-2.67
				$nd\ 2_{3/2}$	←	$nd\ 40_{5/2}$	699.247	0.147	-2.31
			M I (I)	$6p[3]^o_{5/2}$	←	$9s[2]_{3/2}$	699.170	0.070	-2.67
				$6p[2]^o_{3/2}$	←	$7s[1]_{1/2}$	699.534	0.434	-2.75
				$6p[1]^o_{3/2}$	←	$10s[2]_{3/2}$	698.703	-0.397	-2.49
				$5d[1]_{1/2}$	←	$7p''[1]^o_{1/2}$	698.983	-0.117	-2.46
				$5d[1]_{3/2}$	←	$9p[3]^o_{5/2}$	699.109	0.009	-2.58

Table XVII (continued)

Luminescence from the Reaction 100 eV $He^+ + I_2 \rightarrow He + I^+ + I + Energy$

λ_o (nm)	$\Delta\lambda_o$ (nm)	σ ($cm^2 \times 10^{18}$)	X	Transition Assignment Lower State	←	Upper State	λ_T (nm)	$\lambda_T - \lambda_o$ (nm)	ΔH (eV)
			M I (I)	$5d[4]_{9/2}$	←	$7f[5]^o_{11/2}$	698.843	-0.257	-2.41
					←	$7f[5]^o_{9/2}$	698.828	-0.272	-2.41
					←	$7f[4]^o_{9/2}$	699.381	0.281	-2.41
					←	$7f[4]^o_{7/2}$	699.321	0.221	-2.41
					←	$7f[3]^o_{7/2}$	699.157	0.057	-2.41
			I (II)	$5f\ ^3F_3$	←	$12d\ ^3D^o_3$	699.209	0.109	5.97
				$8p\ ^5P_2$	←	$6d''\ 45^o_1$	699.218	0.118	6.06
					←	$6d''\ 45^o_2$	699.218	0.118	6.06
				$6d\ ^5D^o_3$	←	$4f'\ ^3G_4$	698.724	-0.376	4.29
706.50	0.50	1.6	He I	$2p\ ^3P^o_2$	←	$3s\ ^3S_1$	706.712	0.212	10.14
				$2p\ ^3P^o_1$	←	$3s\ ^3S_1$	706.716	0.216	10.14
				$2p\ ^3P^o_0$	←	$3s\ ^3S_1$	706.766	0.266	10.14

Table XVII (continued)

Luminescence from the Reaction 100 eV $He^+ + I_2 \rightarrow He + I^+ + I + Energy$

λ_o (nm)	$\Delta\lambda_o$ (nm)	σ ($cm^2 \times 10^{18}$)	X	Transition Assignment Lower State	←	Upper State	λ_T (nm)	$\lambda_T - \lambda_o$ (nm)	ΔH (eV)
			He I	$3s\ ^3S_1$	←	$11p\ ^3P^o_2$	706.423	-0.077	11.89
					←	$11p\ ^3P^o_1$	706.423	-0.077	11.89
					←	$11p\ ^3P^o_0$	706.423	-0.077	11.89
			I (I)	$6p\ ^4P^o_{1/2}$	←	$nd\ 25.1_{1/2}$	706.964	0.464	-2.66
				$6s\ ^4P_{1/2}$	←	$7p\ ^4S^o_{3/2}$	706.549	0.049	-3.27
			M I (I)	$6s''[0]_{1/2}$	←	$7p[2]^o_{3/2}$	706.551	0.051	-3.27
			I (II)	$6p\ ^5P_1$	←	$5d''\ ^1D^o_2$	706.795	0.295	1.48
				$7p\ ^5P_3$	←	$6d''\ 14^o_3$	706.686	0.186	4.73
				$4f\ ^3F_4$	←	$6d'\ 14^o_3$	706.365	-0.135	4.73
				$5d''\ ^3D^o_1$	←	$5f\ ^5F_2$	706.922	0.422	4.18
				$5d''\ ^3F^o_3$	←	$5f\ ^3F_3$	706.862	0.362	4.20
				$8p\ ^5P_3$	←	$6d''\ 45^o_2$	706.777	0.277	6.06
				$4f'\ ^3D_3$	←	$6d''\ 44^o_2$	706.467	-0.033	6.06
					←	$6d''\ 44^o_3$	706.467	-0.033	6.06

Table XVII (continued)

Luminescence from the Reaction 100 eV $He^+ + I_2 \rightarrow He + I^+ + I + Energy$

λ_o (nm)	$\Delta\lambda_o$ (nm)	σ ($cm^2 \times 10^{18}$)	Transition Assignment X	Lower State	←	Upper State	λ_T (nm)	$\lambda_T - \lambda_o$ (nm)	ΔH (eV)
			I (II)	$7p'\ ^3D_1$	←	$6d''\ 46^o_2$	706.346	-0.154	6.06
				$5d''\ ^1P^o_1$	←	$7p'\ ^3D_2$	706.735	0.235	5.03
				$7d\ ^5D^o_2$	←	$9f\ ^5F_3$	706.716	0.216	5.83
712.30	0.50	4.4	I (I)	$6p\ ^4P^o_{5/2}$	←	$6d\ ^4P_{5/2}$	712.401	0.101	-2.79
				$6p\ ^4S^o_{3/2}$	←	$nd\ 22_{3/2}$	712.201	-0.099	-2.78
				$nd\ 3_{5/2}$	←	$np\ 7^o_{3/2}$	712.868	0.568	-2.34
			M I (I)	$6p[2]^o_{5/2}$	←	$7d[3]_{5/2}$	712.401	0.101	-2.79
				$6p[2]^o_{3/2}$	←	$7d[1]_{3/2}$	712.202	-0.098	-2.78
			I (II)	$6p\ ^5P_2$	←	$5d''\ ^1D^o_2$	712.208	-0.092	1.48
				$6p'\ ^3F_2$	←	$6d\ ^3D^o_1$	712.204	-0.096	2.96
				$7d\ ^3D^o_1$	←	$5f'\ 10_2$	712.623	0.323	6.04
				$5g\ ^5G^o_3$	←	$5f'\ 13_2$	712.519	0.219	6.10
					←	$5f'\ 13_3$	712.519	0.219	6.10
				$5g\ ^3G^o_4$	←	$5f'\ 13_3$	711.605	-0.695	6.10

Table XVII (continued)

Luminescence from the Reaction 100 eV $He^+ + I_2 \rightarrow He + I^+ + I + Energy$

λ_o (nm)	$\Delta\lambda_o$ (nm)	σ ($cm^2 \times 10^{18}$)	X	Transition Assignment Lower State	←	Upper State	λ_T (nm)	$\lambda_T - \lambda_o$ (nm)	ΔH (eV)
714.40	0.50	5.6	I (I)	$6p\ ^4P^o_{5/2}$	←	$6d\ ^4D_{7/2}$	714.403	0.003	-2.80
				$nd\ ^4_{3/2}$	←	$np\ 7^o_{3/2}$	714.091	-0.309	-2.34
				$nd\ 4.1_{3/2}$	←	$np\ 7^o_{3/2}$	714.286	-0.114	-2.34
			M I (I)	$6p[2]^o_{5/2}$	←	$7d[3]_{7/2}$	714.402	0.002	-2.80
				$5d[0]_{1/2}$	←	$7p'[1]^o_{1/2}$	714.286	-0.114	-2.34
				$5d[4]_{7/2}$	←	$8f[5]^o_{9/2}$	713.909	-0.491	-2.34
					←	$8f[4]^o_{9/2}$	714.296	-0.104	-2.34
					←	$8f[4]^o_{7/2}$	714.257	-0.143	-2.34
					←	$8f[3]^o_{5/2}$	714.192	-0.208	-2.34
			I (II)	$6p'\ ^3F_2$	←	$6d\ ^3D^o_3$	714.786	0.386	2.95
				$5d'\ ^3D^o_3$	←	$6p'\ ^3D_2$	714.095	-0.305	1.33
				$6p''\ ^1P_1$	←	$9d\ ^3D^o_2$	713.927	-0.473	5.38
				$6p''\ ^1S_0$	←	$12s\ ^3S^o_1$	714.756	0.356	5.81

Table XVII (continued)

Luminescence from the Reaction 100 ev $He^+ + I_2 \rightarrow He + I^+ + I + Energy$

λ_o (nm)	$\Delta\lambda_o$ (nm)	σ ($cm^2 \times 10^{18}$)	Transition Assignment X	Lower State	←	Upper State	λ_T (nm)	$\lambda_T - \lambda_o$ (nm)	ΔH (eV)
716.60	.0.60	2.5	He I	$3s\ ^3S_1$	←	$10p\ ^3P^o_2$	716.258	-0.342	11.87
					←	$10p\ ^3P^o_1$	716.258	-0.342	11.87
					←	$10p\ ^3P^o_0$	716.258	-0.342	11.87
			I (I)	$6p\ ^4S^o_{3/2}$	←	$6d\ ^4P_{5/2}$	716.673	0.073	-2.79
			M I (I)	$6p[2]^o_{3/2}$	←	$7d[3]_{5/2}$	716.674	0.074	-2.79
				$5d[0]_{1/2}$	←	$8f[2]^o_{3/2}$	716.758	0.158	-2.34
					←	$8f[1]^o_{3/2}$	716.547	-0.053	-2.34
			I (II)	$6p'\ ^3F_2$	←	$6d\ ^3D^o_2$	716.876	0.276	2.95
				$5d''\ ^3F^o_3$	←	$5f\ ^5F_4$	717.083	0.483	4.17
				$5f\ ^3F_4$	←	$12d\ ^3D^o_3$	716.312	-0.288	5.97
				$6d\ ^5D^o_3$	←	$5f\ ^3F_2$	716.975	0.375	4.25
				$8p\ ^5P_2$	←	$6d''\ 42^o_2$	716.400	-0.200	6.02
				$4f'\ ^3F_2$	←	$6d''\ 47^o_1$	716.364	-0.236	6.08
					←	$6d''\ 47^o_2$	716.364	-0.236	6.08

Table XVII (continued)

Luminescence from the Reaction 100 eV $He^+ + I_2 \rightarrow He + I^+ + I$ + Energy

λ_o (nm)	$\Delta\lambda_o$ (nm)	σ ($cm^2 \times 10^{18}$)	X	Transition Assignment			λ_T (nm)	$\lambda_T - \lambda_o$ (nm)	ΔH (eV)
				Lower State	←	Upper State			
			I (II)	$4f'\ ^3P_0$	←	$6d''\ 51^o_1$	716.200	-0.400	6.29
				$6d\ ^5D^o_1$	←	$7p'\ ^3D_1$	716.042	-0.558	4.31
				$8p\ ^3P_1$	←	$6d''\ 46^o_2$	716.427	-0.173	6.06
719.30	0.60	1.8	I (I)	$6p\ ^4S^o_{3/2}$	←	$7s\ ^4P_{3/2}$	719.365	0.065	-2.80
					←	$nd\ 21.2_{1/2}$	719.451	0.151	-2.80
				$nd\ 1_{3/2}$	←	$6f\ 1^o_{5/2}$	719.065	-0.235	-2.51
			M I (I)	$6p[2]^o_{3/2}$	←	$7s'[1]_{3/2}$	719.365	0.065	-2.80
				$6p[2]^o_{3/2}$	←	$7d[1]_{1/2}$	719.451	0.151	-2.80
			I (II)	$5d\ ^5D^o_1$	←	$6p\ ^3P_1$	718.900	-0.400	0.02
				$5d'\ ^1S^o_0$	←	$7p\ ^5P_1$	718.811	-0.489	2.91
				$7p\ ^5P_2$	←	$6d'\ 12^o_1$	719.760	0.460	4.65
				$6d\ ^5D^o_3$	←	$5f\ ^3F_4$	719.127	-0.173	4.24
				$6d\ ^5D^o_2$	←	$5f\ ^3F_2$	719.054	-0.246	4.25

Table XVII (continued)

Luminescence from the Reaction 100 eV $He^+ + I_2 \rightarrow He + I^+ + I + Energy$

λ_o (nm)	$\Delta\lambda_o$ (nm)	σ ($cm^2 \times 10^{18}$)	X	Transition Assignment Lower State	←	Upper State	λ_T (nm)	$\lambda_T - \lambda_o$ (nm)	ΔH (eV)
			I (II)	$4f'\ ^3F_3$	←	$6d''\ 42^o_2$	719.105	-0.195	6.02
				$4f'\ ^3H_5$	←	$11g\ ^5G^o_6$	719.041	-0.259	6.10
				$8p\ ^3P_2$	←	$6d''\ 48^o_1$	719.765	0.465	6.09
					←	$6d''\ 48^o_2$	719.765	0.465	6.09
					←	$13d\ ^3D^o_3$	719.040	-0.260	6.09
				$7s'\ ^1D^o_2$	←	$5f'\ 3_2$	719.147	-0.153	5.76
					←	$5f'\ 3_3$	719.147	-0.153	5.76
723.80	0.50	11.5	I (I)	$6p\ ^4P^o_{3/2}$	←	$nd\ 28.1_{5/2}$	723.571	-0.229	-2.55
				$nd\ 4_{3/2}$	←	$7p\ ^2D^o_{3/2}$	724.000	0.200	-2.36
				$nd\ 4.1_{3/2}$	←	$7p\ ^2D^o_{3/2}$	724.200	0.400	-2.36
				$nd\ 4_{3/2}$	←	$7p\ ^2P^o_{3/2}$	723.632	-0.168	-2.36
				$nd\ 4.1_{3/2}$	←	$7p\ ^2P^o_{3/2}$	723.832	-0.032	-2.36

Table XVII (continued)

Luminescence from the Reaction 100 eV $He^+ + I_2 \rightarrow He + I^+ + I + Energy$

λ_o (nm)	$\Delta\lambda_o$ (nm)	σ ($cm^2 \times 10^{18}$)	Transition Assignment X	Lower State	←	Upper State	λ_T (nm)	$\lambda_T - \lambda_o$ (nm)	ΔH (eV)
			I (I)	$(^1D)6s\ ^2D_{5/2}$	←	$5f\ 1^o_{3/2}$	723.883	0.083	-2.68
					←	$5f\ 3^o_{5/2}$	723.383	-0.417	-2.68
			M I (I)	$6p[1]^o_{3/2}$	←	$8d[2]_{5/2}$	723.579	-0.221	-2.55
				$5d[0]_{1/2}$	←	$7p'[2]^o_{3/2}$	723.830	0.030	-2.36
					←	$7p'[1]^o_{3/2}$	724.197	0.397	-2.36
				$5d[3]_{7/2}$	←	$5f[4]^o_{9/2}$	723.877	0.077	-2.68
					←	$5f[4]^o_{7/2}$	723.698	-0.102	-2.68
					←	$5f[2]^o_{5/2}$	723.321	-0.479	-2.68
				$5d[3]_{5/2}$	←	$5f[4]^o_{7/2}$	723.985	0.185	-2.68
					←	$5f[3]^o_{5/2}$	723.380	-0.420	-2.68
					←	$5f[2]^o_{5/2}$	723.607	-0.193	-2.68
					←	$5f[2]^o_{3/2}$	723.881	0.081	-2.68
			I (II)	$6p''\ ^3P_1$	←	$6d'\ 12^o_1$	723.807	0.007	4.65
				$6p''\ ^1P_1$	←	$8s'\ ^3D^o_1$	723.780	-0.020	5.35

Table XVII (continued)

Luminescence from the Reaction 100 eV $He^+ + I_2 \rightarrow He + I^+ + I$ + Energy

λ_o (nm)	$\Delta\lambda_o$ (nm)	σ ($cm^2 \times 10^{18}$)	X	Transition Assignment Lower State	←	Upper State	λ_T (nm)	$\lambda_T - \lambda_o$ (nm)	ΔH (eV)
			I (II)	$8p\ ^5P_2$	←	$6d''\ 41^o_1$	723.465	-0.335	6.00
					←	$6d''\ 41^o_2$	723.465	-0.335	6.00
					←	$6d''\ 41^o_3$	723.465	-0.335	6.00
				$4f'\ ^3F_2$	←	$6d''\ 45^o_1$	723.638	-0.162	6.06
					←	$6d''\ 45^o_2$	723.638	-0.162	6.06
				$7p'\ ^3P_2$	←	$14d\ ^3D^o_3$	723.645	-0.155	6.16
				$8p\ ^3P_1$	←	$6d''\ 43^o_1$	724.083	0.283	6.04
					←	$6d''\ 43^o_2$	724.083	0.283	6.04
740.40	0.50	8.6	I (I)	$6p\ ^2D^o_{5/2}$	←	$nd\ 23_{7/2}$	740.408	0.008	-2.77
				$nd\ 1_{3/2}$	←	$9p\ ^2D^o_{5/2}$	740.768	0.368	-2.56
			M I (I)	$6p[3]^o_{5/2}$	←	$7d[4]_{7/2}$	740.408	0.008	-2.77
				$5d[1]_{1/2}$	←	$9p[1]^o_{3/2}$	740.771	0.371	-2.56

Table XVII (continued)

Luminescence from the Reaction 100 eV $He^+ + I_2 \rightarrow He + I^+ + I + Energy$

λ_o (nm)	$\Delta\lambda_o$ (nm)	σ ($cm^2 \times 10^{18}$)	Transition Assignment X	Lower State	←	Upper State	λ_T (nm)	$\lambda_T - \lambda_o$ (nm)	ΔH (eV)
			I (II)	$5d''\ ^3P^o_2$	←	$6p''\ ^1D_2$	740.232	-0.168	3.72
				$6p''\ ^1S_0$	←	$6d''\ 33.5^o_1$	740.699	0.299	5.75
				$5f\ ^3F_3$	←	$9g\ ^5G^o_4$	740.162	-0.238	5.88
					←	$9g\ ^5G^o_3$	740.086	-0.314	5.88
					←	$9g\ ^3G^o_4$	740.097	-0.303	5.88
				$4f'\ ^3P_0$	←	$6d''\ 49^o_1$	740.325	-0.075	6.23
				$7d\ ^5D^o_3$	←	$5f'\ 3_2$	740.701	0.301	5.76
					←	$5f'\ 3_3$	740.701	0.301	5.76
				$7s'\ ^3D^o_3$	←	$8f\ ^3F_3$	740.536	0.136	5.65
741.40	0.50	8.1	I (I)	$6p\ ^4D^o_{7/2}$	←	$nd\ 23_{7/2}$	741.809	0.409	-2.77
				$6s\ ^4P_{3/2}$	←	$7p\ ^4P^o_{1/2}$	741.657	0.257	-3.24
				$nd\ 2_{3/2}$	←	$7p\ ^4D^o_{5/2}$	741.618	0.218	-2.41

Table XVII (continued)

Luminescence from the Reaction 100 eV $He^+ + I_2 \rightarrow He + I^+ + I + Energy$

λ_o (nm)	$\Delta\lambda_o$ (nm)	σ ($cm^2 \times 10^{18}$)	X	Transition Assignment Lower State	← Upper State	λ_T (nm)	$\lambda_T - \lambda_o$ (nm)	ΔH (eV)
			I (I)	$(^1D)6s\ ^2D_{3/2}$	← $5f\ 1^o_{3/2}$	741.850	0.450	-2.68
					← $5f\ 2^o_{1/2}$	741.564	0.164	-2.68
					← $5f\ 3^o_{5/2}$	741.324	-0.076	-.268
			M I (I)	$6p[3]^o_{7/2}$	← $7d[4]_{7/2}$	741.808	0.408	-2.77
				$6s'[1]_{3/2}$	← $7p[1]^o_{1/2}$	741.661	0.261	-3.24
				$5d[1]_{3/2}$	← $5f[3]^o_{5/2}$	741.324	-0.076	-2.68
					← $5f[2]^o_{5/2}$	741.563	0.163	-2.68
					← $5f[2]^o_{3/2}$	741.850	0.450	-2.68
				$5d[4]_{9/2}$	← $6f[5]^o_{11/2}$	741.254	-0.146	-2.51
					← $6f[5]^o_{9/2}$	741.228	-0.172	-2.51
					← $6f[3]^o_{7/2}$	741.797	0.397	-2.51
				$(^1D_2)6s[2]_{3/2}$	← $7f[2]^o_{3/2}$	741.631	0.231	-2.41
					← $7f[1]^o_{3/2}$	740.980	-0.420	-2.41

Table XVII (continued)

Luminescence from the Reaction 100 eV $He^+ + I_2 \rightarrow He + I^+ + I$ + Energy

λ_o (nm)	$\Delta\lambda_o$ (nm)	σ ($cm^2 \times 10^{18}$)	Transition Assignment X	Lower State	←	Upper State	λ_T (nm)	$\lambda_T - \lambda_o$ (nm)	ΔH (eV)
			I (II)	$5f\ ^5F_2$	←	$11d\ ^3D^o_3$	741.880	0.480	5.86
				$6d\ ^5D^o_1$	←	$5f\ ^3F_2$	741.717	0.317	4.25
				$6d'\ 8^o_4$	←	$5f'\ 10_3$	741.495	0.095	6.04
747.00	0.50	5.1	I (I)	$6p\ ^2D^o_{5/2}$	←	$nd\ 22_{3/2}$	747.021	0.021	-2.78
				$6p\ ^4D^o_{7/2}$	←	$6d\ ^4F_{9/2}$	747.104	0.104	-2.78
			M I (I)	$6p[3]^o_{7/2}$	←	$7d[4]_{9/2}$	747.104	0.104	-2.78
				$6p[3]^o_{5/2}$	←	$7d[1]_{3/2}$	747.022	0.022	-2.78
			I (II)	$6p''\ ^1D_2$	←	$9d\ ^3D^o_2$	746.975	-0.025	5.38
				$4f'\ ^3G_4$	←	$6d''\ 40^o_3$	746.771	-0.229	5.95
				$4f'\ ^3F_3$	←	$6d''\ 40^o_3$	747.142	0.142	5.95
				$5d''\ ^3F^o_2$	←	$4f'\ ^3D_3$	746.779	-0.221	4.30
				$7d\ ^5D^o_1$	←	$5f'\ 3_2$	746.519	-0.481	5.76

Table XVII (continued)

Luminescence from the Reaction 100 eV $He^+ + I_2 \rightarrow He + I^+ + I + Energy$

λ_o (nm)	$\Delta\lambda_o$ (nm)	σ ($cm^2 \times 10^{18}$)	Transition Assignment X	Lower State	←	Upper State	λ_T (nm)	$\lambda_T - \lambda_o$ (nm)	ΔH (eV)
			I (II)	$7d\ ^3D^o_3$	←	$5f'\ 6_2$	746.973	-0.027	5.89
					←	$5f'\ 6_3$	746.973	-0.027	5.89
					←	$5f'\ 6_4$	746.973	-0.027	5.89
				$7s'\ ^3D^o_3$	←	$8f\ ^5F_4$	746.964	-0.036	5.64
					←	$8f\ ^5F_3$	747.165	0.165	5.64
755.60	0.50	4.6	I (I)	$6p\ ^4D^o_{7/2}$	←	$6d\ ^4D_{7/2}$	755.627	0.027	-2.80
				$6s\ ^4P_{3/2}$	←	$7p\ ^4S^o_{3/2}$	755.872	0.272	-3.28
			M I (I)	$6p[3]^o_{7/2}$	←	$7d[3]_{7/2}$	755.627	0.027	-2.80
				$6s[1]_{3/2}$	←	$7p[2]^o_{3/2}$	755.873	0.273	-3.28
			I (II)	$6p''\ ^1D_2$	←	$8s'\ ^3D^o_2$	755.700	0.100	5.36
				$7p\ ^5P_2$	←	$6d'\ 10^o_2$	755.734	0.134	4.57
				$7p\ ^3P_2$	←	$6d'\ 14^o_3$	755.863	0.263	4.73
				$7p'\ ^3D_3$	←	$6d''\ 48^o_2$	755.647	0.047	6.09
				$7p'\ ^3P_2$	←	$13d\ ^3D^o_3$	755.576	-0.024	6.09

AD-A034 035 AIR FORCE INST OF TECH WRIGHT-PATTERSON AFB OHIO SCH--ETC F/G 20/8
EMISSION CROSS-SECTION MEASUREMENTS OF LOW ENERGY HE(+) IONS WI--ETC(U)
SEP 76 K E SIEGENTHALER

UNCLASSIFIED DS/PH/76-2 NL

4 OF 4
AD
A034035

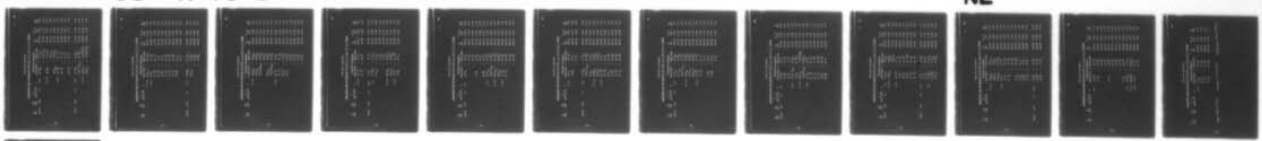

END

DATE
FILMED
2-77

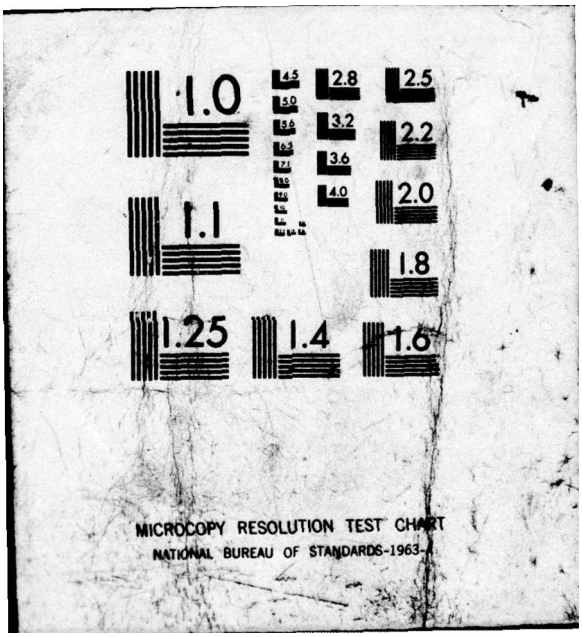
1.0
1.1
1.25
1.4
1.6
1.8
2.0
2.2
2.5
2.8
3.2
3.6
4.0
4.5
5.0
5.6
6.3
7.1
MICROCOPY RESOLUTION TEST CHART
NATIONAL BUREAU OF STANDARDS-1963-A

Table XVII (continued)

Luminescence from the Reaction 100 eV $He^+ + I_2 \rightarrow He + I^+ + I + Energy$

λ_o (nm)	$\Delta\lambda_o$ (nm)	σ ($cm^2 \times 10^{18}$)	X	Transition Assignment Lower State	←	Upper State	λ_T (nm)	$\lambda_T - \lambda_o$ (nm)	ΔH (eV)
767.20	0.60	1.8	I (I)	$6p\ ^4P^o_{3/2}$	←	$7s\ ^4P_{3/2}$	767.212	0.012	-2.80
					←	$nd\ 21.2_{1/2}$	767.310	0.110	-2.80
			M I (I)	$6p[1]^o_{1/2}$	←	$7s'[1]_{3/2}$	767.213	0.013	-2.80
					←	$7d[1]_{1/2}$	767.311	0.111	-2.80
				$5d[2]_{5/2}$	←	$10f[4]^o_{7/2}$	767.124	-0.076	-2.27
			I (II)	$5d'\ ^3F^o_4$	←	$6p'\ ^3F_3$	766.779	-0.421	1.36
				$6p''\ ^3D_1$	←	$6d'\ 7^o_1$	766.809	-0.391	4.35
					←	$6d'\ 7^o_2$	766.809	-0.391	4.35
				$5d''\ ^1D^o_2$	←	$7p\ ^3P_2$	767.096	-0.104	3.09
770.10	0.50	2.2	I (I)	$6p\ ^4P^o_{3/2}$	←	$np\ 3^o_{3/2}$	770.545	0.445	-2.66
				$(^1D)6s\ ^2D_{5/2}$	←	$8p\ ^4D^o_{7/2}$	770.234	0.134	-2.79
			M I (I)	$5d[3]_{7/2}$	←	$(^1D_2)6p[3]^o_{7/2}$	769.906	-0.194	-2.79
				$5d[3]_{5/2}$	←	$(^1D_2)6p[3]^o_{7/2}$	770.230	0.130	-2.79

Table XVII (continued)

Luminescence from the Reaction 100 eV $He^+ + I_2 \rightarrow He + I^+ + I$ + Energy

λ_o (nm)	$\Delta\lambda_o$ (nm)	σ ($cm^2 \times 10^{18}$)	X	Transition Assignment Lower State	←	Upper State	λ_T (nm)	$\lambda_T - \lambda_o$ (nm)	ΔH (eV)
			M I (I)	$5d[0]_{1/2}$	←	$7p''[1]^o_{1/2}$	769.877	-0.223	-2.46
			I (II)	$6p\ ^5P_3$	←	$5d'\ ^1F^o_3$	769.808	-0.292	1.48
				$6s''\ ^3P^o_1$	←	$6p'\ ^1D_2$	770.446	0.346	2.18
				$6s''\ ^1P^o_1$	←	$7p\ ^5P_1$	769.862	-0.238	2.91
				$6d\ ^5D^o_1$	←	$5f\ ^5F_2$	770.535	0.435	4.18
				$4f'\ ^3D_2$	←	$6d''\ 42^o_2$	769.904	-0.196	6.02
				$7p'\ ^3D_3$	←	$6d''\ 45^o_2$	770.079	-0.021	6.06
				$7p'\ ^3P_2$	←	$6d''\ 46^o_2$	769.613	-0.487	6.06
				$7d\ ^3D^o_2$	←	$5f'\ 3_2$	770.280	0.180	5.76
					←	$5f'\ 3_3$	770.280	0.180	5.76
789.90	0.70	2.0	I (I)	$6p\ ^4P^o_{5/2}$	←	$8s\ ^2P_{3/2}$	790.549	0.649	-2.96
				$nd\ 2_{3/2}$	←	$6f\ 1^o_{5/2}$	790.163	0.263	-2.51
					←	$6f\ 3^o_{3/2}$	789.454	-0.446	-2.51
					←	$6f\ 4^o_{5/2}$	789.295	-0.605	-2.51

Table XVII (continued)

Luminescence from the Reaction 100 eV $He^+ + I_2 \rightarrow He + I^+ + I + Energy$

λ_o (nm)	$\Delta\lambda_o$ (nm)	σ ($cm^2 \times 10^{18}$)	Transition Assignment X	Lower State	←	Upper State	λ_T (nm)	$\lambda_T - \lambda_o$ (nm)	ΔH (eV)
			M I (I)	$6p[2]^o_{5/2}$	←	$8s[2]_{3/2}$	790.546	0.646	-2.96
				$5d[4]_{7/2}$	←	$6f[5]^o_{9/2}$	790.015	0.115	-2.51
				$(^1D_2)6s[2]_{3/2}$	←	$6f[3]^o_{5/2}$	790.162	0.262	-2.51
					←	$6f[2]^o_{5/2}$	789.303	-0.597	-2.51
				$5d[4]_{7/2}$	←	$6f[2]^o_{5/2}$	789.912	0.012	-2.51
				$(^1D_2)6s[2]_{3/2}$	←	$6f[2]^o_{3/2}$	789.459	-0.441	-2.51
			I (II)	$6p''\ ^3D_1$	←	$7d\ ^3D^o_1$	789.497	-0.403	4.30
				$6p''\ ^1S_0$	←	$6d''\ 29^o_1$	790.065	0.165	5.65
				$8p\ ^5P_2$	←	$11d\ ^3D^o_3$	790.103	0.203	5.86
				$8p\ ^5P_3$	←	$9g\ ^5G^o_4$	790.145	0.245	5.87
					←	$9g\ ^5G^o_3$	790.057	0.157	5.88
					←	$9g\ ^5G^o_2$	789.843	-0.057	5.88
					←	$9g\ ^3G^o_4$	790.070	0.170	5.88
					←	$9g\ ^3G^o_3$	789.786	-0.114	5.88

Table XVII (continued)

Luminescence from the Reaction 100 eV $He^+ + I_2 \rightarrow He + I^+ + I + Energy$

λ_o (nm)	$\Delta\lambda_o$ (nm)	σ ($cm^2 \times 10^{18}$)	Transition Assignment X	Lower State	←	Upper State	λ_T (nm)	$\lambda_T - \lambda_o$ (nm)	ΔH (eV)
			I (II)	$5d''\ ^1P^o_1$	←	$4f'\ ^1P_1$	789.247	-0.653	4.85
				$7p'\ ^3D_1$	←	$9g\ ^5G^o_2$	790.593	0.693	5.88
797.20	0.60	3.1	He I	$3s\ ^1S_0$	←	$11p\ ^1P^o_1$	797.381	0.181	11.89
			I (I)	$6p\ ^4P^o_{5/2}$	←	$8s\ ^4P_{5/2}$	797.167	-0.033	-2.98
				$nd\ 1_{3/2}$	←	$5f\ 1^o_{3/2}$	797.666	0.466	-2.68
					←	$5f\ 2^o_{1/2}$	797.335	0.135	-2.68
					←	$5f\ 3^o_{5/2}$	797.059	-0.141	-2.68
			M I (I)	$6p[2]^o_{5/2}$	←	$8s[2]_{5/2}$	797.167	-0.033	-2.98
				$5d[1]_{1/2}$	←	$5f[2]^o_{3/2}$	797.666	0.466	-2.68
			I (II)	$5f\ ^5F_1$	←	$6d''\ 32^o_1$	796.752	-0.448	5.74
				$7d\ ^5D^o_4$	←	$8f\ ^3F_3$	796.693	-0.507	5.65

Table XVII (continued)

Luminescence from the Reaction 100 eV $He^+ + I_2 \rightarrow He + I^+ + I + Energy$

λ_o (nm)	$\Delta\lambda_o$ (nm)	σ ($cm^2 \times 10^{18}$)	X	Transition Assignment: Lower State	←	Upper State	λ_T (nm)	$\lambda_T - \lambda_o$ (nm)	ΔH (eV)
800.40	0.60	1.9	He I	$3p\ ^3P_2^o$	←	$21d\ ^3D_3$	800.151	-0.249	11.98
					←	$21d\ ^3D_2$	800.151	-0.249	11.98
					←	$21d\ ^3D_1$	800.151	-0.249	11.98
				$3p\ ^3P_1^o$	←	$21d\ ^3D_2$	800.152	-0.248	11.98
					←	$21d\ ^3D_1$	800.152	-0.248	11.98
				$3p\ ^3P_0^o$	←	$21d\ ^3D_1$	800.169	-0.231	11.98
			I (I)	$6s\ ^4P_{1/2}$	←	$6p\ ^4D_{1/2}^o$	800.582	0.182	-3.48
				$(^1D)6s\ ^2D_{3/2}$	←	$8p\ ^2D_{5/2}^o$	800.022	-0.378	-2.80
			M I (I)	$6s''[0]_{1/2}$	←	$6p'[1]_{1/2}^o$	800.582	0.182	-3.48
				$5d[1]_{3/2}$	←	$8p[3]_{5/2}^o$	800.021	-0.379	-2.80
			I (II)	$4f'\ ^3D_3$	←	$6d''\ 37_2^o$	800.816	0.416	5.85
				$7p'\ ^3P_2$	←	$6d''\ 41_1^o$	800.411	0.011	6.00
					←	$6d''\ 41_2^o$	800.411	0.011	6.00
					←	$6d''\ 41_3^o$	800.411	0.011	6.00

Table XVII (continued)

Luminescence from the Reaction 100 eV $He^+ + I_2 \rightarrow He + I^+ + I$ + Energy

λ_o (nm)	$\Delta\lambda_o$ (nm)	σ ($cm^2 \times 10^{18}$)	Transition Assignment X	Lower State	←	Upper State	λ_T (nm)	$\lambda_T - \lambda_o$ (nm)	ΔH (eV)
			I (II)	$8p\ ^3P_1$	←	$6d''\ 38^o_1$	800.611	0.211	5.88
				$7d\ ^5D^o_3$	←	$8f\ ^5F_4$	800.233	-0.167	5.64
					←	$8f\ ^5F_3$	800.464	0.064	5.64
802.50	0.50	1.7	I (I)	$6p\ ^4S^o_{3/2}$	←	$8s\ ^4P_{5/2}$	802.520	0.020	-2.98
				$(^1D)6s\ ^2D_{3/2}$	←	$8p\ ^4S^o_{3/2}$	802.542	0.042	-2.81
				$nd\ 5_{5/2}$	←	$np\ 7^o_{3/2}$	802.277	-0.223	-2.34
			M I (I)	$6p[2]^o_{3/2}$	←	$8s[2]_{5/2}$	802.521	0.021	-2.98
				$5d[1]_{3/2}$	←	$8p[2]^o_{3/2}$	802.546	0.046	-2.81
			I (II)	$5d''\ ^3F^o_2$	←	$5f\ ^5F_1$	802.349	-0.151	4.19
				$5d''\ ^1F^o_3$	←	$8p\ ^5P_2$	802.294	-0.206	4.29
				$8p\ ^5P_3$	←	$6d''\ 37^o_2$	802.621	0.121	5.85
				$4f'\ ^3H_4$	←	$6d''\ 39^o_4$	802.311	-0.189	5.93
				$4f'\ ^3D_2$	←	$6d''\ 40^o_3$	802.131	-0.369	5.95
				$4f'\ ^3G_5$	←	$6d''\ 50^o_4$	802.051	-0.449	6.25

Table XVII (continued)

Luminescence from the Reaction 100 eV $He^+ + I_2 \rightarrow He + I^+ + I + Energy$

λ_o (nm)	$\Delta\lambda_o$ (nm)	σ ($cm^2 \times 10^{18}$)	X	Transition Assignment Lower State	←	Upper State	λ_T (nm)	$\lambda_T - \lambda_o$ (nm)	ΔH (eV)
804.50	0.50	5.9	I (I)	$6s\ ^4P_{5/2}$	←	$6p\ ^4P^o_{3/2}$	804.592	0.092	-4.27
				$6s\ ^2P_{1/2}$	←	$7p\ ^4P^o_{3/2}$	804.204	-0.296	-3.20
				$(^1D)6s\ ^2D_{3/2}$	←	$7p\ ^2P^o_{1/2}$	804.840	0.340	-2.81
			M I (I)	$6s[2]_{5/2}$	←	$6p[1]^o_{3/2}$	804.594	0.094	-4.27
				$6s'[1]_{1/2}$	←	$7p[1]^o_{3/2}$	804.204	-0.296	-3.20
				$5d[1]_{3/2}$	←	$8p[1]^o_{1/2}$	804.830	0.330	-2.81
			I (II)	$5d''\ ^1P^o_1$	←	$7p'\ ^3P_0$	804.006	-0.494	4.82
				$7s'\ ^1D^o_2$	←	$5f'\ 1_2$	804.934	0.434	5.58
					←	$5f'\ 1_3$	804.934	0.434	5.58
				$7d\ ^5D^o_1$	←	$5f'\ 2_2$	804.760	0.260	5.64
				$7d\ ^5D^o_4$	←	$8f\ ^5F_4$	804.138	-0.362	5.64
					←	$8f\ ^5F_3$	804.371	-0.129	5.64

Table XVII (continued)

Luminescence from the Reaction 100 eV $He^+ + I_2 \rightarrow He + I^+ + I$ + Energy

λ_o (nm)	$\Delta\lambda_o$ (nm)	σ ($cm^2 \times 10^{18}$)	X	Transition Assignment Lower State	←	Upper State	λ_T (nm)	$\lambda_T - \lambda_o$ (nm)	ΔH (eV)
816.90	0.50	2.5	He I	$3p\ ^3P^o_2$	←	$15s\ ^3S_1$	817.096	0.196	11.94
				$3p\ ^3P^o_1$	←	$15s\ ^3S_1$	817.097	0.197	11.94
				$3p\ ^3P^o_0$	←	$15s\ ^3S_1$	817.115	0.215	11.94
			I (I)	$(^1D)6s\ ^2D_{3/2}$	←	$np\ 2^o_{3/2}$	817.158	0.258	-2.84
				$nd\ 2_{3/2}$	←	$9p\ ^2D^o_{5/2}$	816.448	-0.452	-2.56
			M I (I)	$5d[1]_{3/2}$	←	$(^1D_2)6p[3]^o_{5/2}$	817.164	0.264	-2.84
				$(^1D_2)6s[2]_{3/2}$	←	$9p[1]^o_{3/2}$	816.458	-0.442	-2.56
			I (II)	$6p'\ ^3D_1$	←	$6d\ ^5D^o_1$	817.202	0.302	2.58
				$5d'\ ^3F^o_3$	←	$6p'\ ^3D_2$	817.234	0.334	1.33
				$6p''\ ^1P_1$	←	$7s''\ ^3P^o_0$	816.846	-0.054	5.16
				$7p'\ ^3P_1$	←	$6d''\ 38^o_1$	817.056	0.156	5.88
				$8p\ ^3P_1$	←	$6d''\ 37^o_2$	816.462	-0.438	5.85
				$5g\ ^3G^o_4$	←	$5f'\ 5_3$	817.349	0.449	5.87

Table XVII (continued)

Luminescence from the Reaction 100 eV $He^+ + I_2 \rightarrow He + I^+ + I + Energy$

λ_o (nm)	$\Delta\lambda_o$ (nm)	σ ($cm^2 \times 10^{18}$)	X	Transition Assignment Lower State	←	Upper State	λ_T (nm)	$\lambda_T - \lambda_o$ (nm)	ΔH (eV)
824.10	0.50	8.4	I (I)	nd $^3_{5/2}$	←	9p $^4S^o_{3/2}$	824.209	0.109	-2.57
			M I (I)	5d[4]$_{9/2}$	←	5f[5]$^o_{9/2}$	824.189	0.089	-2.68
					←	5f[5]$^o_{11/2}$	824.231	0.131	-2.68
			I (II)	5d' $^1F^o_3$	←	4f $^3F_2$	824.292	0.192	2.98
				7p $^3P_1$	←	6d' 11^o_0	824.527	0.427	4.57
				5f $^3F_4$	←	6d" 33^o_3	823.720	-0.380	5.75
				5f $^3F_2$	←	6d" 33.5^o_1	823.849	-0.251	5.75
				4f' $^3D_3$	←	6d" 36^o_2	823.846	-0.254	5.81
				4f' $^3F_2$	←	6d" 37^o_2	824.436	0.336	5.85
839.50	0.50	3.8	He I	3d $^3D_2$	←	19p $^1P^o_1$	839.943	0.443	11.97
				3d $^3D_1$	←	19p $^1P^o_1$	839.947	0.447	11.97
			I (I)	6p $^4S^o_{3/2}$	←	nd $21_{5/2}$	839.400	-0.100	-3.05
				6p $^2D^o_{5/2}$	←	8s $^2P_{3/2}$	839.540	0.040	-2.96
				6s $^4P_{1/2}$	←	6p $^2D^o_{3/2}$	839.564	0.064	-3.55

Table XVII (continued)

Luminescence from the Reaction 100 eV $He^+ + I_2 \rightarrow He + I^+ + I + Energy$

λ_o (nm)	$\Delta\lambda_o$ (nm)	σ ($cm^2 \times 10^{18}$)	X	Transition Assignment Lower State	←	Upper State	λ_T (nm)	$\lambda_T - \lambda_o$ (nm)	ΔH (eV)
			M I (I)	$6p[3]^o_{5/2}$	←	$8s[2]_{3/2}$	839.538	0.038	-2.96
				$6p[2]^o_{3/2}$	←	$6d[2]_{5/2}$	839.402	-0.098	-3.05
				$6s''[0]_{1/2}$	←	$6p'[2]^o_{3/2}$	839.567	0.067	-3.55
			I (II)	$4f\ ^5F_4$	←	$5g\ ^3G^o_4$	839.521	0.021	4.36
				$7p\ ^3P_2$	←	$6d'\ 10^o_2$	839.466	-0.034	4.57
				$4f'\ ^3D_3$	←	$6d''\ 35^o_2$	839.612	0.112	5.78
					←	$6d''\ 35^o_3$	839.612	0.112	5.78
				$7p'\ ^3D_3$	←	$6d''\ 39^o_4$	839.925	0.425	5.93
				$7d\ ^5D^o_1$	←	$5f'\ 1_2$	839.383	-0.117	5.58
				$5g\ ^3G^o_4$	←	$9f\ ^5F_4$	839.055	-0.445	5.83
				$5g\ ^5G^o_3$	←	$9f\ ^5F_3$	839.906	0.406	5.83
848.70	0.50	2.5	He I	$3p\ ^3P^o_2$	←	$11s\ ^3S_1$	848.303	-0.397	11.89
				$3p\ ^3P^o_1$	←	$11s\ ^3S_1$	848.305	-0.395	11.89
				$3p\ ^3P^o_0$	←	$11s\ ^3S_1$	848.324	-0.376	11.89

Table XVII (continued)

Luminescence from the Reaction 100 eV $He^+ + I_2 \rightarrow He + I^+ + I + Energy$

λ_o (nm)	$\Delta\lambda_o$ (nm)	σ ($cm^2 \times 10^{18}$)	X	Transition Assignment Lower State	←	Upper State	λ_T (nm)	$\lambda_T - \lambda_o$ (nm)	ΔH (eV)
			He I	$3d\ ^3D^o_3$	←	$16p\ ^3P^o_2$	849.109	0.409	11.95
				$3d\ ^3D_2$	←	$16p\ ^3P^o_2$	849.110	0.410	11.95
					←	$16p\ ^3P^o_1$	849.110	0.410	11.95
					←	$16p\ ^1P^o_1$	848.812	0.112	11.95
				$3d\ ^3D_1$	←	$16p\ ^3P^o_2$	849.113	0.413	11.95
					←	$16p\ ^3P^o_1$	849.113	0.413	11.95
					←	$16p\ ^3P^o_0$	849.113	0.413	11.95
					←	$16p\ ^1P^o_1$	848.815	0.115	11.95
				$3d\ ^1D_2$	←	$16p\ ^1P^o_1$	849.058	0.358	11.95
			I (I)	$6p\ ^4D^o_{7/2}$	←	$8s\ ^4P_{5/2}$	848.842	0.142	-2.98
			M I (I)	$6p[3]^o_{7/2}$	←	$8s[2]_{5/2}$	848.842	0.142	-2.98
			I (II)	$4f\ ^5F_2$	←	$6d'\ 7^o_1$	848.997	0.297	4.35
					←	$6d'\ 7^o_2$	848.997	0.297	4.35

Table XVII (continued)

Luminescence from the Reaction 100 eV $He^+ + I_2 \rightarrow He + I^+ + I + Energy$

λ_o (nm)	$\Delta\lambda_o$ (nm)	σ ($cm^2 \times 10^{18}$)	X	Transition Assignment Lower State	←	Upper State	λ_T (nm)	$\lambda_T - \lambda_o$ (nm)	ΔH (eV)
			I (II)	$5f\ ^5F_1$	←	$6d''\ 29^o_1$	848.992	0.292	5.65
				$8p\ ^5P_2$	←	$6d''\ 33^o_3$	848.907	0.207	5.75
				$4f'\ ^3F_2$	←	$6d''\ 36^o_2$	848.865	0.165	5.81
				$7p'\ ^3D_1$	←	$6d''\ 34^o_2$	849.018	0.318	5.77

$\sigma_{TOTAL} = 1592.4 \times 10^{-18}\ cm^2$ $\sigma_{VUV\ TOTAL} = 1437.3 \times 10^{-18}\ cm^2$ $\sigma_{VISIBLE\ TOTAL} = 155.1 \times 10^{-18}\ cm^2$

Vita

Kenneth Eugene Siegenthaler, son of Paul Alfred and Ruth Elizabeth Siegenthaler, was born 10 March 1939 in Huron, South Dakota. In 1957 he was appointed to the United States Military Academy where in 1961 he was graduated and was commissioned in the United States Air Force. He received a Bachelor of Science Degree in Physics from the University of Utah in 1962 and was elected to Sigma Pi Sigma. In 1963 he was graduated from aircraft navigator training. From 1963 to 1971 he flew over 6000 hours as a Military Airlift Command Navigator in C-124 and C-133 aircraft. He entered the Air Force Institute of Technology in 1971, where he was elected to Tau Beta Pi. In 1973 he was graduated from the Air Force Institute of Technology Resident School and awarded the Master of Science Degree in Engineering Physics. He then entered the AFIT Resident School Doctoral Program. Following completion of the academic portion of this program in 1974, he was assigned to the Aerospace Research Laboratories Gaseous Excitation and Ionization Processes Group as a laser research engineer. In 1975 with the disestablishment of the Aerospace Research Laboratories, he was assigned to the Air Force Materials Laboratory as a laser development engineer.

Permanent address: 1421 East Pecan Street
Gainesville, Texas 76240

Unclassified

SECURITY CLASSIFICATION OF THIS PAGE (When Data Entered)

REPORT DOCUMENTATION PAGE		READ INSTRUCTIONS BEFORE COMPLETING FORM
1. REPORT NUMBER DS/PH/76-2	2. GOVT ACCESSION NO.	3. RECIPIENT'S CATALOG NUMBER
4. TITLE (and Subtitle) EMISSION CROSS-SECTION MEASUREMENTS OF LOW ENERGY He^+ IONS WITH Cl_2, Br_2, I_2 REACTIONS		5. TYPE OF REPORT & PERIOD COVERED Dissertation 6. PERFORMING ORG. REPORT NUMBER
7. AUTHOR(s) Kenneth E. Siegenthaler Major USAF		8. CONTRACT OR GRANT NUMBER(s)
9. PERFORMING ORGANIZATION NAME AND ADDRESS Air Force Institute of Technology (AU) Wright-Patterson AFB OH 45433		10. PROGRAM ELEMENT, PROJECT, TASK AREA & WORK UNIT NUMBERS
11. CONTROLLING OFFICE NAME AND ADDRESS		12. REPORT DATE September 1976 13. NUMBER OF PAGES 285
14. MONITORING AGENCY NAME & ADDRESS(if different from Controlling Office)		15. SECURITY CLASS. (of this report) Unclassified 15a. DECLASSIFICATION/DOWNGRADING SCHEDULE

16. DISTRIBUTION STATEMENT (of this Report)

Approved for public release; distribution unlimited.

17. DISTRIBUTION STATEMENT (of the abstract entered in Block 20, if different from Report)

18. SUPPLEMENTARY NOTES

Approved for public release IAW AFR 190-17.

JERRAL F. GUESS, Capt, USAF
Director of Information
Air Force Institute of Tech.

19. KEY WORDS (Continue on reverse side if necessary and identify by block number)

Charge Transfer, Charge Exchange, Atomic Spectroscopy, Ultraviolet Spectroscopy, Low Energy Ion-Neutral Collisions, Low Energy Ion Beam Experiment, Helium Ion/Halogen Reactions, Helium Ion/Chlorine Molecule Collisions, Helium Ion/Bromine Molecule Collisions,
(continued on reverse)

20. ABSTRACT (Continue on reverse side if necessary and identify by block number)

The cross sections for production of emission lines in the 60 nm to 870 nm region were measured for the collision of 100 eV He^+ ions with Cl_2, Br_2, and I_2. These cross section measurements were made with an ion beam apparatus. Only emissions from

DD FORM 1 JAN 73 1473 EDITION OF 1 NOV 65 IS OBSOLETE

Unclassified

SECURITY CLASSIFICATION OF THIS PAGE (When Data Entered)

transitions from excited electronic states with lifetimes shorter than a μsec were measured. The dependence of the cross sections on the kinetic energy of the He^+ ions between 2 to 170 eV was determined by use of the more intense emission lines. The total cross section obtained for emissions between 90 nm and 870 nm for chlorine is 5.0Å; of this, 3.8 A^2 is for emissions in the VUV region. Emissions from excited neutral chlorine atoms account for at least 85% of the total cross section. Of the cross section for production of emission from excited neutral chlorine atoms, 80% is caused by direct excitation with the remainder resulting from cascading. The total cross section obtained for emissions between 80 nm and 870 nm for bromine is 14.9 A^2; of this, 11.9 A^2 is for emissions in the VUV region. Emissions from excited neutral bromine atoms account for at least 85% of the total cross section. Of the cross section for production of emission from excited neutral bromine atoms, 75% is caused by direct excitation with the remainder resulting from cascading. The total cross section obtained for emissions between 100 nm and 870 nm for iodine is 15.9 A^2; of this, 14.4 A^2 is for emissions in the VUV region. The proportion of the total cross section for the production of emissions from singly-ionized iodine atoms is much larger than for either the chlorine or bromine reactions.

Item 19 Continued: Helium Ion/Iodine Molecule Collisions, Emission Cross Sections, Chlorine, Bromine, Iodine, VUV Emissions, Visible Emissions, Near IR Emissions, Halogens